Molecular Dynamics Investigation on the Aggregation of Polyaromatic Compounds in Water and Organic Solvents

by

Cuiying Jian

A thesis submitted in partial fulfillment of the requirements for the degree of

Doctor of Philosophy

Department of Mechanical Engineering
University of Alberta

Abstract

Aggregation of polyaromatic (PA) compounds has drawn great interest due to their wide impacts in areas such as petroleum processing. Despite the extensive studies on PA compounds, fundamental knowledge of their aggregation behaviors is still missing at atomistic level. For instance, it's still unclear how the properties of the solvent can lead to different aggregation mechanisms and hence affect the aggregated structures of PA molecules.

In this dissertation, a series of molecular dynamics (MD) simulations have been performed to investigate the effect of solute chemical structures as well as solvents on the aggregation of PA compounds. The PA molecules studied here possess the same PA core structure but have systematically varied side-chain lengths. We started with simulating a single type of PA compounds in water. Inside the aggregated structures, while some PA core stacking was observed, most of the PA molecules are simply entangled together without preferred orientations. More interestingly, it was found that side-chain length has a non-monotonic effect on the size of the aggregates, with intermediate side-chain length leading to smaller aggregates. In contrast, regardless of the side-chain length, these PA molecules aggregated into ordered structures in toluene and n-heptane, which mainly consist of stacked PA cores. On the other hand, the ranges of stacking of PA cores in these two organic solvents are different, thus resulting in distinct aggregated geometries. Following the above studies which involve only a single type of PA compounds as the solute, we explored the aggregation of mixed PA compounds of different types in toluene, n-heptane and heptol (toluene/n-heptane mixture). It was found that the inhomogeneity in solutes can enhance the stacking of PA cores, leading to the long-range stacking of PA cores. Furthermore, the existence of this long-range stacking of PA cores is insensitive to the solvents employed. Through detailed analysis of the aggregated

structures, the aggregation mechanisms of different kinds of solutes were clarified. This dissertation provided insights for the aggregation of PA compounds from atomic level, and shed lights on controlling their aggregated structures.

Preface

Chapters 1 and 2 of this thesis were adapted from a book chapter submitted by Jian, C. and Tang, T. to *"New Frontiers in Oil and Gas Exploration"* Jin, C. Ed.; Springer. I was responsible for collecting literature resources and writing the manuscript. Dr. T. Tang was the supervisory author who checked the accuracy and revised the manuscript.

A version of Chapter 3 of this thesis has been published as Jian, C.; Tang, T.; Bhattacharjee, S. Probing the Effect of Side-Chain Length on the Aggregation of a Model Asphaltene Using Molecular Dynamics Simulations. *Energy Fuels* **2013,** *27,* 2057-2067. I was responsible for conducting numerical simulations, data analysis and writing the manuscript. Dr. T. Tang and Dr. S. Bhattacharjee were the supervisory authors who contributed to concept formation, checked results and revised the manuscript.

A version of Chapter 4 of this thesis has been published as Jian, C.; Tang, T.; Bhattacharjee, S. Molecular Dynamics Investigation on the Aggregation of Violanthrone78-Based Model Asphaltenes in Toluene. *Energy Fuels* **2014,** *28,* 3604–3613. I was responsible for conducting numerical simulations, data analysis and writing the manuscript. Dr. T. Tang and Dr. S. Bhattacharjee were the supervisory authors who contributed to concept formation, checked results and revised the manuscript.

A version of Chapter 5 of this thesis has been published as Jian, C.; Tang, T. One-Dimensional Self-Assembly of Polyaromatic Compounds Revealed by Molecular Dynamics Simulations. *J. Phys. Chem. B* **2014,** *118,* 12772–12780. I was responsible for conducting numerical simulations, data analysis and writing the manuscript. Dr. T. Tang was the supervisory author who contributed to concept formation, checked results and revised the manuscript.

A version of Chapter 6 of this thesis has been published as Jian, C.; Tang, T. Molecular Dynamics Simulations Reveal Inhomogeneity-Enhanced Stacking of Violanthrone-78-Based Polyaromatic Compounds in *n*-Heptane–Toluene Mixtures. *J. Phys. Chem. B* **2015,** *119,* 8660–8668. I was responsible for conducting numerical simulations, data analysis and writing the manuscript. Dr. T. Tang was the supervisory authors who contributed to concept formation, checked results and revised the manuscript.

A version of Chapter 7 of this thesis has been published as Jian, C.; Tang, T.; Bhattacharjee, S. A Dimension Map for Molecular Aggregates. *J. Mol. Graphics Modell.* **2015,** *58,* 10-15. I was responsible for conducting numerical simulations, data analysis and writing the manuscript. Dr. T. Tang and Dr. S. Bhattacharjee were the supervisory authors who contributed to concept formation, checked results and revised the manuscript.

This page was intentionally left blank.

Acknowledgements

From the bottom of my heart, I would like to take this opportunity to formally appreciate the help I have received during the past four years.

First and foremost, my sincere gratitude to my supervisor Dr. Tian Tang. Without her academic and personal guidance, I would not be able to accomplish this challenging journey. Her style as a supervisor, instructor, and collaborator has been, and will remain to be, the role model for my professional career.

Many thanks to my former co-supervisor Dr. Subir Bhattacharjee for his fantastic insights and inspiring trusts. All of these greatly broaden my view in science, instill the research interest in me, and build my confidence, which will be life-long assets for me.

Special thanks to Dr. Peter Schiavone and Dr. Ben Jar for their generous help and recognition. When difficulties come, they have always been there offering their efforts. These nice interactions encourage me to try my best in my academic life.

My grateful thanks are extended to finanical support from scholarships, particularly, the support from University of Alberta Doctoral Recruitment Scholarship, Jacob H Masliyah Graduate Award in Oil Sands Engineering, and Alberta Innovates Graduate Student Scholarship.

To the end of my PhD journey, I have been, diligently or indolently, pursuing my goals years after years, and paying no attention to my family. I am indebted, forever, to my parents and brother, for their understanding and support before and after.

Finally, to all the friends and colleagues, thanks for the companionship to make life colorful. Hereafter we may make different choices and I believe our best times are yet ahead.

Till then,

Cuiying

Table of Contents

List of Tables

List of Figures

List of Abbreviations

1D:	One-dimensional
AFM:	Atomic force microscopy
CCC:	Critical cluster concentration
CMC:	Critical micelle concentration
CN:	Cumulative number
CNAC:	Critical nanoaggregation concentration
COG:	Center of geometry
CPA-EoS:	Cubic-Plus-Association EoS
DPS:	Direct parallel stacking
EoS:	Equation of state
HBC:	Hexabenzocoronene
LJ:	Lennard-Jones
L^2MS:	Laser desorption/laser ionization mass spectrometry
MD:	Molecular dynamics
MIN:	Minimum
MM:	Molecular mechanics
m-MDPS:	Multiple-molecule direct parallel stacking
m-MPS:	Multiple-molecule parallel stacking
MW:	Molecular weight
NMR:	Nuclear magnetic resonance
PA:	Polyaromatic
PC-SAFT EoS:	Perturbed-Chain SAFT-EoS

PDF:	Probability distribution function
PMF:	Potential of mean force
PR-EoS :	Peng-Robinson EoS
PS:	Parallel stacking
PTCDI:	Perylene tetracarboxylic diimide
QM:	Quantum mechanics
RDF:	Radial distribution function
Rg:	Radius of gyration
RICO:	Ruthenium-ion-catalyzed oxidation
SAFT EoS:	Statistical Associating Fluid Theory EoS
SAFT-VR EoS:	SAFT-EoS for potentials of variable range
SARA:	Saturate, aromatic, resin, and asphaltene
sc-CO_2:	Supercritical carbon dioxide
SEM:	Scanning electron microscopy
SPS:	Shift parallel stacking
TEM:	Transmission electron microscopy
VO-78:	Violanthrone-78
VPO:	Vapor pressure osmometry
XANES:	X-ray absorption near edge structure
XPS:	X-ray photoelectron spectroscopy

Chapter 1: Introduction*

Petroleum resources are of great importance to daily life and economy all over the world.[1] To optimize petroleum processing and utilization, it's thus of great interest to understand the behaviors of petroleum components.[2-4] Crude oil can be categorized into saturate, aromatic, resin, and asphaltene (SARA) fraction groups.[5,6] Asphaltenes, as the heaviest and most aromatic component, are operationally defined as a solubility class that are insoluble in n-alkanes but soluble in aromatic solvents.[7-9] They are known to be the "cholesterol" of petroleum due to their deleterious effects on oil processing, from extraction to refinery.[10] For instance, asphaltenes clog rock pores and production facilities, form deposit during transportation and storage, and deactivate catalysts, thus generating a large cost in petroleum industry.[11-15] Most of these serious problems can be traced to asphaltene aggregation and precipitation.[16-18] Therefore a considerable amount of effort, based on experimental or theoretical approaches, has been dedicated to investigating asphaltene aggregation and precipitation dynamics as well as the associated mechanisms and resultant structures. Recently, with the development of computational techniques, asphaltene investigations from simulation aspects have been emerging quickly.

Motivated from above, a thorough review on the study of asphaltene behaviors was first given in Chapter 2 of this dissertation. As will be shown in Chapter 2, significant discrepancies exist regarding the aggregated structures of asphaltene-like compounds and the mechanisms driving aggregation. Hence this dissertation is developed to provide a systematic study on how the molecular structure of asphaltene-like compounds, along with the type solvents, may influence their aggregation activities. For this purpose, a series of molecular models were first developed based on Violanthrone-78 (VO-78), which is a polyaromatic (PA) compound and

*This chapter is adapted from a book chapter submitted by Jian, C. and Tang, T. to *"New Frontiers in Oil and Gas Exploration"* Jin, C. Ed.; Springer.

possesses some common features people believe to exist in asphaltene molecules.[19] This sequence of models, with variations in functional groups, was then simulated in different solvents. Our ultimate objective is to clarify, from atomic level, the aggregation kinetics, driving forces, and resultant structures of asphaltene-like compounds in water and common organic solvents. The details of our simulations are presented in subsequent chapters.

Chapters 3 and 4 present the investigations on our model compounds in water and toluene, which allow us to compare the effect of asphaltene molecular structure on their aggregation behaviors in different solvents. Chapter 5 presents the study of these model compounds in n-heptane where a particularly interesting structure, namely a one-dimensional (1D) rod-like structure, was found from the aggregation. Although this study was motivated by asphaltene aggregation, it was found that such 1D structures are also of impacts in the design of optical and electronic devices. For instance, aggregates of 1D geometry, formed by PA compounds which have similar structure as our molecular models, have promising applications in organic photovoltaics, sensors, nanophotonics, and nanoelectronics.[20] This motivated us to further explore the favorable conditions for the formation of 1D rod-like aggregates. Therefore, in Chapter 6 we introduced mixed toluene and n-heptane (heptol) as the solvent and systematically varied its composition. In addition, a mixture of molecules with different structures was introduced as the solute. The optimal solvent condition and beneficial effect of solute mixture were demonstrated from our simulations. During the analysis of simulation data in Chapters 3 to 6, we have developed a dimension map which presents a simple yet effective method to characterize the aggregated shapes of the solute compounds. This dimension map not only is useful for the study of ashpaltene aggregation, but also can be applied to a much broader class of problems involving molecular aggregates. It is with this purpose that we present in

Chapter 7 the general concept of our dimension map, and demonstrate its usage through studying several different types of molecules.

Chapters 3 to 7 have been published. Their structures are thus maintained, i.e. each chapter has its own introduction, method, results, discussion, conclusion, and bibliography. An overall conclusion together with future perspectives is given in Chapter 8. A bibliography listing all sources used is also presented at the end of the thesis where each reference is numbered according to the chapter in which it is cited and the corresponding citation number in that chapter. For example, reference 3.5 is the 5th reference in Chapter 3.

Bibliography

(1) Hall, C. A.; Day Jr, J. W. Revisiting the Limits to Growth After Peak Oil. *Am. Sci.* **2009,** *97,* 230-237.

(2) Speight, J. G. *The Chemistry and Technology of Petroleum,* 4th ed.; CRC Press: Boca Raton, 2006.

(3) Hemmingsen, P.; Kim, S.; Pettersen, H. E.; Rodgers, R. P.; Sjöblom, J.; Marshall, A. G. Structural Characterization and Interfacial Behavior of Acidic Compounds Extracted from a North Sea Oil. *Energy Fuels* **2006,** *20,* 1980–1987.

(4) Mansoori, G. A. Modeling of Asphaltene and Other Heavy organic Depositions. *J. Pet. Sci. Eng.* **1997,** *17,* 101-111.

(5) Gaspar, A.; Zellermann, E.; Lababidi, S.; Reece, J.; Schrader, W. Characterization of Saturates, Aromatics, Resins, and Asphaltenes Heavy Crude Oil Fractions by Atmospheric Pressure Laser Ionization Fourier Transform Ion Cyclotron Resonance Mass Spectrometry. *Energy Fuels* **2012,** *26,* 3481-3487.

(6) Jewell, D.; Weber, J.; Bunger, J.; Plancher, H.; Latham, D. Ion-Exchange, Coordination, and

Adsorption Chromatographic Separation of Heavy-End Petroleum Distillates. *Anal. Chem.* **1972,** *44,* 1391-1395.

(7) Mitchell, D. L.; Speight, J. G. The Solubility of Asphaltenes in Hydrocarbon Solvents. *Fuel* **1973,** *52,* 149-152.

(8) Permsukarome, P.; Chang, C.; Fogler, H. S. Kinetic Study of Asphaltene Dissolution in Amphiphile/Alkane Solutions. *Ind. Eng. Chem. Res.* **1997,** *36,* 3960-3967.

(9) Speight, J. G.; Long, R. B.; Trowbridge, T. D.; Linden, N. On the Definition of Asphaltenes. *Am. Chem. Soc., Div. Pet. Chem., Prepr.* **1982,** *27,* 268-275.

(10) Kokal, S. L.; Sayegh, S. G. Asphaltenes: The Cholesterol of Petroleum. Presented at SPE Middle East Oil Show, Manama, Bahrain, March 11−14, 1995; Paper SPE 29787.

(11) Mendoza de la Cruz, José L; Argüelles-Vivas, F. J.; Matías-Pérez, V.; Durán-Valencia, Cecilia de los A; López-Ramírez, S. Asphaltene-Induced Precipitation and Deposition During Pressure Depletion on a Porous Medium: An Experimental Investigation and Modeling Approach. *Energy Fuels* **2009,** *23,* 5611-5625.

(12) Vafaie-Sefti, M.; Mousavi-Dehghani, S. Application of Association Theory to the Prediction of Asphaltene Deposition: Deposition due to Natural Depletion and Miscible Gas Injection Processes in Petroleum Reservoirs. *Fluid Phase Equilib.* **2006,** *247,* 182-189.

(13) Cosultchi, A.; Rossbach, P.; Hernández-Calderon, I. XPS Analysis of Petroleum Well Tubing Adherence. *Surf. Interface Anal.* **2003,** *35,* 239-245.

(14) Bartholomew, C. H. Mechanisms of Catalyst Deactivation. *Appl. Catal. A* **2001,** *212, 17-60.*

(15) Gawel, I.; Bociarska, D.; Biskupski, P. Effect of Asphaltenes on Hydroprocessing of Heavy Oils and Residua. *Appl. Catal. A* **2005,** *295,* 89-94.

(16) Park, S. J.; Ali Mansoori, G. Aggregation and Deposition of Heavy Organics in Petroleum

Crudes. *Energy Sources* **1988,** *10,* 109-125.

(17) Andersen, S. I.; Birdi, K. S. Aggregation of Asphaltenes as Determined by Calorimetry. *J. Colloid Interface Sci.* **1991,** *142,* 497-502.

(18) Leon, O.; Rogel, E.; Espidel, J.; Torres, G. Asphaltenes: Structural Characterization, Self Association, and Stability Behavior. *Energy Fuels* **2000,** *14,* 6-10.

(19) Breure, B.; Subramanian, D.; Leys, J.; Peters, C. J.; Anisimov, M. A. Modeling Asphaltene Aggregation with a Single Compound. *Energy Fuels* **2012,** *27*, 172-176.

(20) Kim, F. S.; Ren, G.; Jenekhe, S. A. One-Dimensional Nanostructures of π-Conjugated Molecular Systems: Assembly, Properties, and Applications from Photovoltaics, Sensors, and Nanophotonics to Nanoelectronics. *Chem. Mater.* **2010,** *23,* 682-732.

Chapter 2: Literature Review*

Many detailed reviews exist for experimental studies, such as the works of Speight et al.,[1] Strausz et al.,[2,3] and Mullins et al.[4] However, there is a lack of review on theoretical and computational studies of asphaltenes. These studies are very useful in that they provide fundamental explanations to asphaltenes' behaviors observed in experiments. Therefore, this chapter aims at reviewing theoretical and computational works performed on asphaltenes. As these studies have been motivated by experimental observations, a brief summary on experimental studies will be first given. This is followed by a detailed review on theoretical and computational works performed on asphaltene aggregation and precipitation. Finally, a summary will be provided.

2.1. Experimental Studies

The behaviors of asphaltenes are strongly related to their chemical structures. Hence significant amount of experimental work has been performed on probing the molecular structures and functional groups of asphaltenes. Two types of molecular structures (island vs. archipelago, see a schematic representation in Figure 2.1) have been proposed in literature for various asphaltene samples investigated, each supported by different experimental observations. Island-type, or continental-type, models were proposed to possess a center that has a large number of fused aromatic cores and a periphery characterized by aliphatic chains, while archipelago-type structures were believed to have small aromatic regions interconnected by aliphatic chains.[5-7]

In the 1960s, Dickie and Yen[6] examined the molecular weight (MW) of asphaltene using a range of techniques including X-ray diffraction and scattering, mass spectrometer, gel

*This chapter is adapted from a book chapter submitted by Cuiying Jian and Tian Tang to *"New Frontiers in Oil and Gas Exploration"* Jin, C. Ed.; Springer.

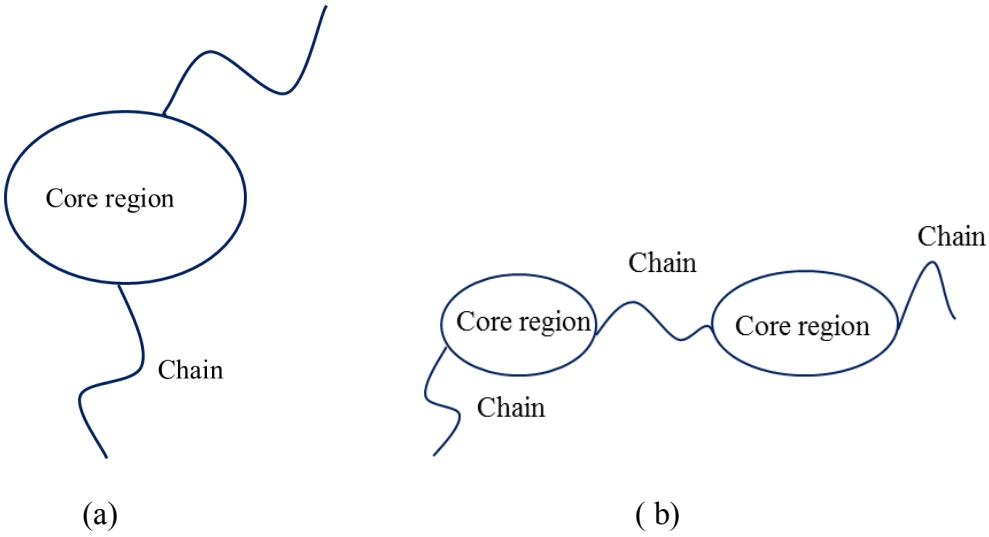

Figure 2.1: Schematic representation of (a) island-type and (b) archipelago-type molecular structures.

permeation chromatography, VPO, ultracentrifugation, and electron microscope. Through investigating the results of MW measurements, the individual asphaltene molecules were inferred to consist of condensed aromatic rings and peripheral aliphatic chains. Later on, various conceptual island-type models constructed from experimental data have been reported. For instance, structural parameters calculated for asphaltene extracted from a Lagunillas crude oil agreed well in most cases with the constructed hypothetical island molecular model; León et al.[8] determined the average molecular parameters (e.g. MW and number of aromatic rings) for four asphaltene samples using LECO CHNS 244 elemental analyzer model, Knauer VPO, as well as nuclear magnetic resonance (NMR) spectra. Based on these data, the average molecular models constructed all possessed a single condensed core.

More recently, in the work of Sabbah et al.[9] using laser desorption/laser ionization mass spectrometry (L^2MS), the spectra of 1, 3, 6, 8-tetradecyl pyrene which possesses one PA core shared similarities with those of asphaltenes, suggesting the existence of island-type asphaltene molecules. Through L^2MS, Zare and co-workers[10] compared the fragmentation behaviors of 23

model compounds with 2 petroleum asphaltene samples extracted from Middle Eastern black oils. The results showed that all model compounds which have one aromatic core, with or without pendant alkyl groups, exhibited similar behaviors to what was observed for the two asphaltene samples; whereas all model compounds which have more than one aromatic core showed energy-dependent fragmentation, different from the two asphaltene samples. Further, a series of work done by Mullins and co-workers, using mass spectral methods,[11] diffusion measurements,[12-14] and X-ray Raman,[15] has widely popularized the island-type asphaltene molecular structure. This model was also supported by a sequence of work using other methods. For instance, the MW distribution of asphaltenes was measured by Pinkston et al.[16] through analyzing laser-induced acoustic desorption/electron ionization mass spectra, and by Qian et al.[17] using field desorption mass spectrometry and electrospray ionization mass spectrometry; the size of asphaltene monomers was determined by Lisitza et al.[18] through NMR diffusion measurements, and by Bouhadda et al.[19] employing Raman spectrometry and X-ray diffraction. These studies all provided evidence for the island-type asphaltene model.

The archipelago-type structure, on the other hand, was supported by other experimental evidences. Strausz and co-workers[20-22] showed that the mild thermolysis products of Athabasca asphaltenes mainly contained mono- to pentacyclic condensed aromatic molecules, which could not be formed from the cracking and rearrangement of large aromatic clusters under mild thermal cracking conditions. Therefore they proposed that small aromatic fragments should be present in the asphaltenes. Similarly, in the work of Calemma et al.,[23] the asphaltenes from different feedstocks (i.e. vacuum residue, atmospheric residue and crude oil) were investigated by pyrolysis−gas chromatography/mass spectrometry, and through comparison with thermolysis reactions of model compounds, the asphaltene samples were considered to be of archipelago-

type molecular structures. For asphaltene fraction of a Venezuela residue examined by Ferris et al.,[24] as MW increased, the aromaticity calculated from NMR data only slightly increased, suggesting that asphaltene molecules were consisting of small units of similar aromatic-to-saturate ratios. Analysis based on ruthenium-ion-catalyzed oxidation (RICO) reaction of asphaltenes was also shown to support the existence of archipelago-type molecular structure. For instance, Su et al.[25] investigated the RICO products of an asphaltene sample from a vacuum residue of Arabian crude mixture, and the resolved aliphatic di- and polycarboxylic acids suggested the presence of aliphatic linkages in a single asphaltene molecule connecting more than two aromatic rings or hydroaromatics; RICO used in Murgich et al.,[26] for Athabasca sand oil, and in Artok et al.,[27] for Arabian crude mixture, also confirmed the existence of sulfide links among fused rings within asphaltene molecules. Furthermore, Siskin et al.,[28] characterized asphaltenes from several shot-coke- and sponge-coke-producing vacuum residue feeds by a combination of solid-state 13C NMR, X-ray photoelectron spectroscopy (XPS), and elemental abundance techniques, and their average chemical structures were shown to have aliphatic bridges among fused rings within the molecular structure. This is consistent with the work of Gray and co-workers,[29,30] where it was proposed that to be consistent with ashpaltene pyrolysis and coking behaviors, asphaltene chemical structures must consist of a variety of aromatic groups joined by bridges and substituted by aliphatic groups. Regarding the island-type structure concluded by Mullins et al.,[12,13,31-34] Strausz et al.[2] commented that the fluorescence decay and depolarization kinetic time measurements used in their studies[12,13,31-34] were erroneous, which is still being debated.[35]

While great controversy exists in the molecular architectures of asphaltenes, it is generally agreed that these molecules[13,36-39] contain heteroatoms such as nitrogen, oxygen, sulfur,

as well as various metals, e.g. iron, nickel, and vanadium, associated with different functional groups. For instance, Strausz and co-workers[5] proposed the presence of thiolane, thiane, thiophene, pyridine, carboxylic esters, and vanadium porphyrins in asphaltene samples from Alberta; X-ray absorption near edge structure (XANES) spectroscopy and XPS by Mullins and co-workers[40,41] as well as Kelemen et al.[42] showed that sulfur forms thiophene, sulfide and sulfoxide in asphaltene molecules. Furthermore, XANES spectra also confirmed the existence of nitrogen in pyrrolic and pyridine.[43] In the work of Desando et al.,[44] using NMR spectroscopy, two-types of oxygen containing functionality (hydroxyl and carboxyl) have been detected for Athabasca oil sand asphaltene. Speight and co-workers,[45] using infrared spectroscopy, inferred that for the asphaltene fraction of Athabasca bitumen, oxygen could also exist as sulfur-oxygen functions, or carbonyl groups, i.e. ketones, quinones, and ethers. The presence of carbonyl functional groups were also proposed by Ignasiak et al.[46] using the same technique. For metals, the fluorescence absorption spectra of asphaltenes, measured using CARY 500 UV−visible−NIR spectrometer by Groenzin et al.,[13] showed similarity with octaethyl porphyrin, suggesting the asphaltene porphyrins were of the β-octa-alkyl type.

The complexity of asphaltene molecular structures has greatly impeded the clear understanding of asphaltene aggregation, leaving this as a highly debated area to date. The most populated theory to describe asphaltene aggregation is perhaps the Yen-Mullins model[4,7,47,48] proposed by Yen and co-workers[48] and later advanced by Mullins and co-workers.[25,64] In this model (shown in Figure 2.2), it was proposed that when the concentration of asphaltenes reaches the critical nanoaggregation concentration (CNAC, 50-150 mg/L), they first form nanoaggregates through the stacking of a small number (≤ 10) of PA cores, surrounded by side-chains. These nanoaggregates further form clusters at the critical cluster concentration (CCC, 2-5

g/L), each containing less than 10 nanoaggregates. Within this hierarchical description for asphaltene aggregation, the individual asphaltene molecules were proposed to be of island-type architectures. In good solvents such as toluene, this theory was supported by the CNAC and CCC detected using high-Q ultrasonic spectroscopy, direct-current electrical conductivity and fluorescence measurements.[49,50] However, there are still ongoing debates even regarding the existence of CNAC and CCC, or the general critical micelle concentration (CMC) for asphaltenes in good solvents. Shown by Andersen et al.,[51] no CMC was detected by calorimetric titration method for heptane-precipitated asphaltenes in pure toluene. Evdokimov et al.[52,53] investigated the aggregation behaviors of aspahltene from Tatarstan virgin crude oils using UV/visible spectroscopy. In toluene, a gradual aggregation process was observed for these asphaltenes, and asphaltene monomers were only abundant when the concentrations were below 1-5 mg/L. These observations were distinct from the two-step aggregation process as described in the Yen-Mullins model[4,7,47,48]. Similarly, in the work of Hoepfner et al.,[54] as asphaltenes were diluted from 5 vol. % to 0.00125 vol. % (15 mg/L) in toluene, dissociation of asphaltene nanoaggregates was observed to occur gradually, and aggregates even persisted down to asphaltene concentrations as low as 15 mg/L. Very different aggregated structures of asphaltenes have also been reported. For instance, using the same technique of small angle neutron scattering, studies have reported different morphologies, ranging from prolate ellipsoid[55] and oblate cylinders[56] to thin discs.[57]

Other components, especially resins, can also have strong effect on the stability of asphaltene monomers and aggregates in crude oil, and hence their final precipitation. There are two views on the effect of resins: the first proposes that resins form an adsorption layer around asphaltene particles which are responsible for the asphaltene stabilization;[58,59] the second

proposes resins and other crude oil components to act as a solvent which may solvate asphaltenes.[60-62] Each of these two views is supported by different experimental observations. For instance, the peptizing role of resins was suggested in the work of Soorghali et al.[75] using wettability measurements, while the latter view was supported by DC conductivity measurements in the work of Sedghi et al.[79]

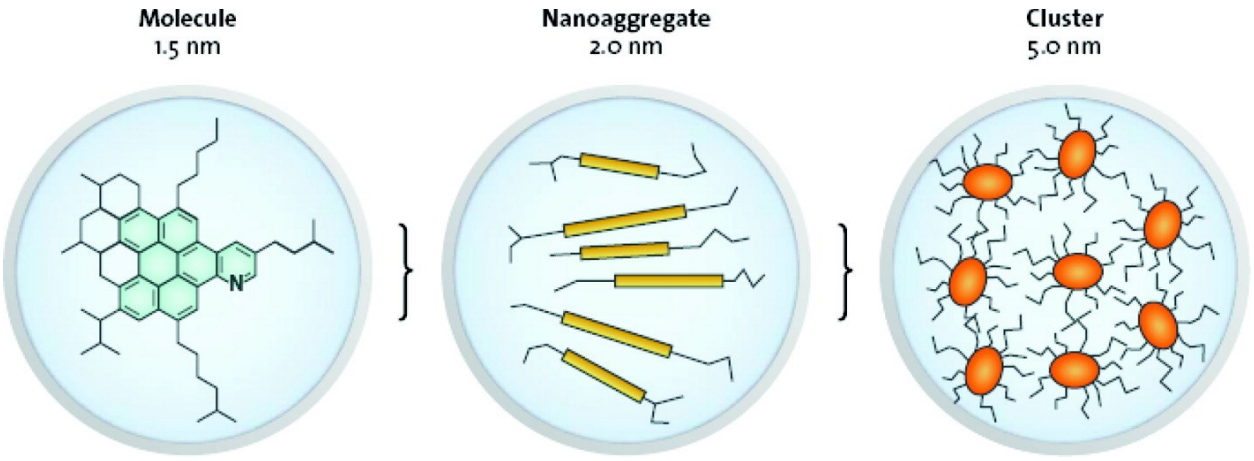

Figure 2.2: Yen-Mullins model[4,7,47,48] for asphaltene aggregation. Asphaltene molecules are proposed to be of island-type structures. When their concentration reaches CNAC, asphaltene molecules form nanoaggregates. At higher concentrations (above CCC), nanoaggregates further form clusters. Reprinted with permission from Mullins, O. C.; Sabbah, H.; Eyssautier, J.; Pomerantz, A. E.; Barré, L.; Andrews, A. B.; Ruiz-Morales, Y.; Mostowfi, F.; McFarlane, R.; Goual, L., et al. Advances in asphaltene science and the Yen–Mullins model. *Energy Fuels* **2012**, *26,* 3986-4003. Copyright 2012 American Chemical Society.

Despite the existing debates on the asphaltene aggregation and precipitation, it is generally accepted that the interaction between PA cores (so-called $\pi - \pi$ interaction) is an important contributor to aggregation,[4,29,63,64] and hence precipitation. The stacking of PA cores has been widely observed,[4,29,63,64] although whether $\pi - \pi$ interaction was the dominating driving force for asphaltene aggregation is still under debate.[65-68] In this context, theoretical and the

emerging computational approaches, based on the available experimental observation, can help with the prediction of asphaltene behaviors under given conditions, provide atomic/molecular information for the system studied, and further shed lights on resolving the existing debates.

2.2. Theoretical Studies

In this section, we will provide a detailed review of the theoretical approaches used for investigating asphaltene aggregation and precipitation.

2.2.1. Theoretical Modeling of Asphaltene Aggregation

Based on Yen's model that describes asphaltene aggregates as stacked aromatic sheets surrounded by aliphatic side chains,[4,7,47] Rogel[69] first proposed a molecular thermodynamic approach that predicted asphaltene aggregation behaviors in different solvents. An analytical expression was developed for the free energy of aggregation in benzene, toluene, cyclohexane, and n-decylbenzene, which included contributions from (1) transferring of the PA rings from the solvent into the aromatic core stacks, (2) mixing of the aliphatic chains with the solvent, (3) deformation of the aliphatic chains, (4) steric repulsion among the aliphatic chains, and (5) the interaction between the aggregated core and solvent. The calculated free energy curves from the five contributions showed that the aggregation was mostly affected by the free energy of transferring the PA rings of asphaltenes from the solvent into the stacking structure. Later, Rogel[70] applied the same approach to compare the free energy of aggregation for asphaltene aggregates of different shapes in benzene, toluene, 1-methyl naphthalene, nitrobenzene, quinoline, and 1,2 dichlorobenzene. It was showed that cylindrical shape containing stacked aromatic cores was preferred over spherical shape and disks. According to this model, the existence of CMC for asphaltene solutions depended on the characteristics of the PA ring: asphaltenes with low aromaticities and aromatic condensations did not have an operational

CMC. These results suggested[69,70] that the interaction between PA cores was the main driving forces for asphaltene aggregation. The same approach was also applied by Rogel[71] to study the effect of resins on asphaltene aggregation. Resins were considered to be of similar chemical structures with asphaltenes but have a smaller PA core area. Consistent with experiments, Rogel's model predicted[71] that resins decreased the size of asphaltene aggregates and increased the CMC of the asphaltene solutions in toluene. This series of models proposed by Rogel were based on assuming island-type molecular structure for the asphaltenes. Contrarily, Agrawala et al.[72] proposed an asphaltene association model analogous to linear polymerization, where asphaltene molecules were assumed to contain multiple active sites capable of linking with each other. This oligomerization-like asphaltene association model was consistent with archipelago-type asphaltene molecular structure, and well fitted experimental molar mass data for asphaltenes in different solvents at different temperatures.

While the above works focused on a one-step aggregation scenario, several studies considered the aggregation process to be of multiple steps. In the work of Zhang et al.,[73] a hindered stepwise aggregation model was developed to simulate asphaltene aggregation. In this model, it was assumed that the effective interaction/collision among asphaltene monomers promoted the initial aggregation, and the sequential collisions of monomers with smaller aggregates resulted in larger aggregates. The results showed that asphaltene molecules formed polymer aggregates, and the size of the aggregates increased significantly with its concentration in solution. Later, this model was used by the same group[74] to infer the aggregation morphologies of asphaltenes, and it was shown that the dominant aggregates were of 2 to 8 monomers with stacked aromatic cores. Acevedo et al.[75] investigated asphaltene aggregation using a mathematical model based on two consecutive equilibrium steps: $nA \overset{K_1}{\leftrightarrow} A_n$ and $mA + A_n$

$\overset{K_2}{\leftrightarrow} A_{n+m}$, where n and m were number of moles; A, A_n and A_{n+m} represented single molecules, n aggregates and $n+m$ aggregates of A, respectively; K_1 and K_2 were equilibrium constants. The results suggested that in toluene nanoaggregates were first formed by asphaltene fraction of extremely low solubility; asphaltene fraction of higher solubility would then keep the aggregates in solution and prevent phase separation.

2.2.2. Theoretical Modeling of Asphaltene Precipitation

Tremendous theoretical efforts have been spent on predicting asphaltene's precipitation behaviors. Depending on the way asphaltenes are assumed to be stabilized in crude oils, two types of theories have been developed, namely colloidal and solubility theories.[76] According to the colloidal theory, asphaltenes form insoluble solid particles in crude oil, which are stabilized by the presence of resins adsorbed onto their surface (see Figure 2.3); detachment of the resins from the asphaltene particles leads to their aggregation and final precipitation.[76] Contrarily, the solubility theory adopts the view that asphaltene molecules are soluble in crude oil and precipitation will occur if its concentration is beyond the solubility limit.[77]

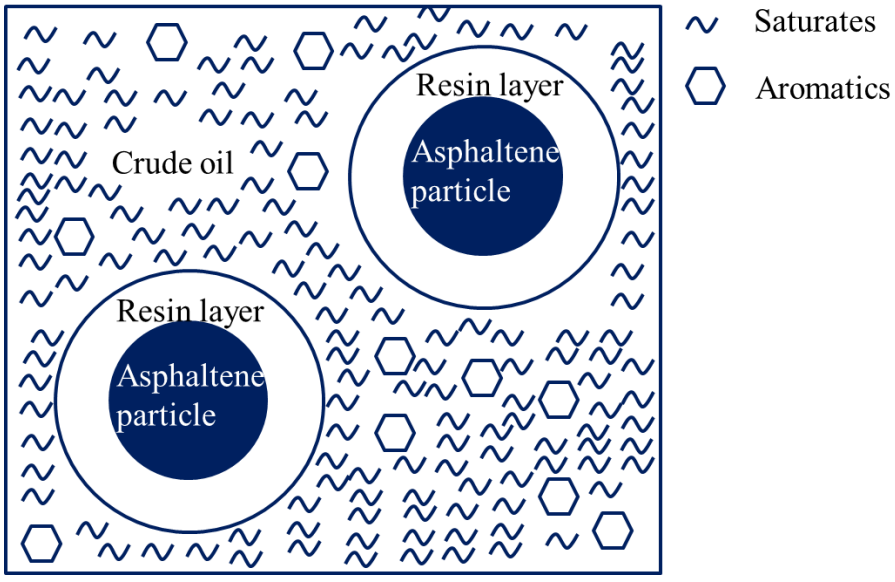

Figure 2.3: Schematic representation of crude oil system based on colloidal theory.

2.2.2.1. Models based on Colloidal Theory. In 1987, Leontaritis and Mansoori proposed[78] a thermodynamic model for asphaltene precipitation based on colloidal theory. In this model, it was assumed that resin molecules were adsorbed onto asphaltene particles and the repulsive forces between these resins kept asphaltene aggregates from precipitation. The amount of adsorbed resin depended on its concentration in the crude oil phase. Therefore the concentration must be maintained above certain critical values to keep asphaltene particles stabilized. The corresponding critical resin chemical potential was calculated based on the Flory-Huggins statistical thermodynamic theory of polymer solutions.[79,80] Adding precipitants affected resin concentration as well as its chemical potential. The amount of precipitants, needed to bring the resin chemical potential to its critical values, was calculated and defined as the onset condition for asphaltene precipitation. It was shown that the predicted onset agreed well with experimental ones. Later on, Firoozabadi and co-workers[81,82] incorporated asphaltene aggregation model into precipitation. In their model, resins adhered to the surface of the asphaltene colloidal particles, and stabilized these particles in a way analogous to that of surfactant amphiphilic molecules in the theories of solubilization.[83] In their first work,[81] the Gibbs free energy of micellization was derived by mainly considering lyophobic contributions gained from transferring asphaltene molecule from an infinitely diluted crude to a micelle. Adding a precipitant would change the concentration of asphaltene monomers and the associated chemical potential, hence the Gibbs free energy of micellization, leading to a new equilibrium. The monomeric asphaltene concentration in the crude oil phase at this new equilibrium state was calculated using the Peng-Robinson equation of state (PR-EoS),[84] which in turn determined the amount of precipitated asphaltenes. This model predicted that the amounts of asphaltenes precipitate decreased with increasing the chain length of n-alkanes added to the crude, which agreed well with experimental

data. In their subsequent work, Pan and Firoozabadi[82] evaluated the total Gibbs free energy of a system consisting of a bulk liquid phase and a precipitated phase, the latter assumed to be an ideal solid mixture of asphaltenes and resins. Then, the composition of the precipitated phase was determined by minimizing the total Gibbs free energy subject to mass balance equations. It was shown that[82] the predicted amount of precipitated asphaltenes by adding precipitants n-pentane, n-heptane, and n-decane was in good agreement with the experimentally measured data. Furthermore, when n-alkanes of short chains, such as propane and ethane were added to the crude, co-precipitation of asphaltenes and resins were predicted in this model.[82] Consistent with the work of Rogel et al.,[71] it was also revealed that[82] for precipitant n-heptane and n-decane, increasing the resin concentration decreased the amount of precipitated asphaltenes. The performance of this model was also examined in the work of Assoori et al.,[85] in which the effect of each micellization parameter on the asphaltene precipitation was demonstrated.

Also based on colloidal theory, Wu et al.[86] used pseudo-pure components to represent asphaltenes and resins, while all other components in the crude oil were modeled as a continuous solvent medium that affected interactions among asphaltene and resin molecules. While it was assumed that asphaltene molecules were stabilized by resins molecules in the crude oil, the precipitated asphaltene-rich phase was considered a liquid phase. At equilibrium, the chemical potentials and the osmotic pressures for each species (asphaltene or resins) were the same in both liquid (oil and precipitated) phases, and they were calculated from the Helmholtz free energy derived by a perturbation theory. Together with mass balance equations, the compositions of each liquid phase were obtained. The predicted fraction of precipitated asphaltenes was compared with experiments to study the effect of precipitants. It was shown that[86] when a large amount of precipitants were added, the calculated results were in line with the experiments. To

address the effect of geometries on the solubilization of asphaltene particles, Victorov et al.[87] formulated a thermodynamic model which explicitly considered the shapes of resin molecules as well as the deformation of the resin layer adsorbed onto the asphaltene aggregates. By incorporating the PR-EoS, the proposed model was applied to predict the amounts of asphaltene precipitates.[87,88]

2.2.2.2. Models Based on Solubility Theory. In this category, two main types of models have emerged for investigating the phase separation of asphaltenes, which is based on either regular solution theory or EoS methods. The works reviewed in this section are summarized in Figure 2.4.

2.2.2.2.1. Models Based on Regular Solution Theory. Regular solution theory was first applied by Hirschberg et al.[77] to model asphaltene precipitation. Crude oil was described as a quasi-binary mixture of two pseudo-components with asphaltene as the solute and the remainder as the mixed solvent. Asphaltene precipitation occurred when its concentration exceeded the solubility limit. At equilibrium, the chemical potentials for each pseudocomponent must be the same in both the precipitated phase P and solvated phase S:

$$\mu_a^P = \mu_a^S \,, \tag{2.1}$$

$$\mu_m^P = \mu_m^S \,, \tag{2.2}$$

where subscripts a and m represent asphaltene and the mixed solvent, respectively. Following the Flory-Huggins theory,[79,80] the chemical potential for each of the two components is given by:

$$\frac{\mu_a - (\mu_a)_{ref}}{RT} = \ln \varphi_a + 1 - \frac{V_a}{V} + \chi_a, \tag{2.3}$$

$$\frac{\mu_m - (\mu_m)_{ref}}{RT} = \ln \varphi_m + 1 - \frac{V_m}{V} + \chi_m, \tag{2.4}$$

where R is the universal gas constant; T is the absolute temperature; $(\mu_a)_{ref}$ and $(\mu_m)_{ref}$ were, respectively, the chemical potentials for pure liquids a and m (the reference state); χ_a and χ_m are

the interaction parameters for a and m; φ_a and φ_m were the volume fractions of a and m in the crude oil; and V_a and V_m were the molar volumes for a and m. Volume fractions and molar volumes are related by:

$$\varphi_a = \frac{x_a V_a}{V}, \tag{2.5}$$

$$\varphi_m = \frac{x_m V_m}{V}. \tag{2.6}$$

Here, x_a and x_m are the mole factions of components a and m. The molar volume, V, of the crude oil and the interaction parameter χ were calculated by using Hildebrand's approximation:[89]

$$V = x_a V_a + x_m V_m, \tag{2.7}$$

and

$$\chi_a = \frac{V_a}{RT} (\delta - \delta_a)^2, \tag{2.8}$$

$$\chi_m = \frac{V_m}{RT} (\delta - \delta_m)^2, \tag{2.9}$$

where δ_a and δ_m are the solubility parameters for components a and m, estimated by fitting the cohesive energy density to experimental data using EoS. The solubility parameter δ for the crude oil was given by

$$\delta = \varphi_a \delta_a + \varphi_m \delta_m \tag{2.10}$$

Hirschberg et al.[77] assumed that the precipitation phase was pure asphaltenes and the volume fraction of asphaltene in the solvate phase $({\varphi_a}^S) \ll 1$. Therefore combing eqs. (2.1), (2.3) and (2.8), the maximum volume fraction, $({\varphi_a}^S)_{max}$, of asphaltenes soluble in the crude was given by:

$$({\varphi_a}^S)_{max} = \exp(-1 + \frac{V_a}{V_m} - \frac{V_a}{RT} (\delta_a - \delta_m)^2) \tag{2.11}$$

Because of its simplicity, this model has been widely adopted in the oil industry, and many adaptations have been performed.

Correra and Donaggio[90] simplified the model proposed by Hirschberg et al.[77] by using the interaction parameter χ to predict whether asphaltene precipitation occurred or not. This new model was based on the assumption that asphaltene precipitation was ruled by the overall solvent power of the crude oil toward asphaltenes, which in turn could be predicted by the interaction parameters χ defined in eqs. (2.8) and (2.9) as functions of the solubility parameters. According to this model, precipitation occurred when χ exceeded certain critical value χ_C. Correra et al.[91] showed that χ_C =1 when asphaltenes were considered to be at infinite dilution. In their subsequent work[92], the authors presented a detailed discussion on the determination of the parameters used in the proposed model.

While Hirschberg et al.[77] assumed asphaltene to be a homogenous component of petroleum crude, Burke et al.[93] applied this approach to predict the effect of composition on precipitate formation. As the model was only able to qualitatively match the experimental precipitation data, it was suggested that the aggregation of asphaltenes in crude oil might affect the performance of this model. Novosad and Costain[94] adopted a modified Hirschberg's model[77,95] to study asphaltene precipitation, which incorporated both asphaltene aggregation and asphaltene-resin association through introducing equilibrium association constants. Correspondingly, the crude oil was described to consist of three components: asphaltene, resin, and solvent (oil components that were neither asphaltene nor resin). It was shown that the precipitation model, qualitatively and to some degree quantitatively, reproduced the trends in asphaltene behaviors.

Kawanaka et al.[96] applied the Scott-Magat[97] heterogeneous polymer solution theory, developed based on Flory-Huggins theory, to predict the onset point and amount of asphaltene precipitation from petroleum crude under the influence of precipitants. They considered

asphaltenes to be a mixture of many similar polymeric molecules and used a continuous model in which a MW-distribution was assumed. For precipitants n-pentane, n-heptane, and n-decane, the predicted onset point and amount of precipitates were shown to be in good agreement with experimental data. The Scott-Magat[97] heterogeneous polymer solution theory was also used in the work of Manshad et al.,[98] where equilibrium conditions were established by minimizing the total Gibbs free energy. In this work, Manshad et al.[98] compared the performance of three distribution functions for asphaltene MW, namely, Gamma, Schultz-Zimm and fractal distribution functions. It was shown that for predicting the amount of asphaltene precipitation, fractal distribution function had the lowest average absolute deviation and the best rate of convergence. To include the intermolecular interaction, Browarzik et al.[99] described the crude oils using continuous distribution functions for the solubility parameter. The crude oil was considered to consist of maltenes and asphaltenes, each described by a separate distribution function. The calculated precipitation point was found to be in excellent agreement with the experimental results. Later on, Browarzik et al.[100] proposed that the association of the asphaltenes led to a great number of aggregates with different size. Therefore a continuous size distribution function was used to describe asphaltenes to improve the performance of the proposed model for crude oils of high ashphaltene content.[100,101]

Yarranton et al.[102] combined the material balance equation with the Flory-Huggins equation to predict the amount of asphaltene precipitated, similar to the approach developed by Nor-Azian and Adewumi.[103] In this model, the activity coefficients of asphaltene and solvent were used to develop the criterion for thermodynamic equilibrium, which were related to the change of the chemical potentials expressed in eqs. (2.3) and (2.4). The asphaltenes were considered as a class of PA hydrocarbons with randomly distributed functional groups. Their

molar mass distribution was determined from experiments, and their molar volume as well as solubility parameter was correlated to the molar mass. The proposed method was tested on asphaltenes solvated in toluene with hexane being the precipitant. The predicted onset point and the amount of precipitate were shown to be in good agreement with experimental data. Alboudwarej et al.[104] extended this method to study the precipitation of asphaltene from mixtures of Western Canadian bitumen by n-alkanes. The bitumen was separated into SARA pseudo-fractions, and the molar mass distribution of asphaltenes was assumed to follow a Schultz-Zimm distribution function. Later, Akbarzadeh et al.[105] further tested this model on four international bitumen and heavy oil samples. It was shown that the predicted onset and amount of precipitation were in good agreement with the experiments in all cases. The same model was also applied by Wiehe et al.[106] to study the effect of n -alkane size on its amount to cause precipitation. From n-pentane to n-hexadecane, it was demonstrated that the model quantitatively described the precipitation of asphaltenes from the onset to full precipitation. In addition, application of this model to asphaltene precipitation from live oils was available.[107]

While Hirschberg et al.[77] assumed that only asphaltene partitioned into the precipitated phase, in the model of Cimino et al.[108], the precipitated phase consisted of asphaltene and nonasphaltene components but the oil phase was free of asphaltene. To remove these two assumptions, Buckley and co-worker[109] used refractive indices to estimate solubility parameters of asphaltenes and solvents. This was based on their earlier work,[110] where London dispersion forces were proposed to dominate aggregation and precipitation of asphaltenes. It was suggested[110] that the solubility parameter, hence the interaction parameter χ in eqs. (2.8) and (2.9), could be described by the refractive indices of asphaltene and the solvent. This approach was then adopted to develop a new asphaltene solubility model.[109] It was shown[109] that this model

produces fairly good matches to experimental data for the onset conditions of asphaltene precipitation from seven crude oils using precipitants from pentane to pentadecane. Also in order to remove the two assumptions on the oil and precipitated phases, Mohammadi et al.[111] proposed a different approach, namely a monodisperse thermodynamic model, in which a distribution of asphaltenes and nonasphaltene components in the oil and precipitated phases was considered. It was further shown that the models developed by Hirschberg et al.[77] and Cimino et al.[108] were special cases of this new model. Later on, asphaltene aggregation was taken into account by assuming that the asphaltenes existed in solution in the form of linear hydrogen-like bonded polymers.[112] Compared with the case where the aggregation was ignored, the model provided a better agreement with experimental data.

In the original model of Hirschberg et al.,[77] the solute-solvent interaction was captured through the solubility parameters derived from pure liquids, and there was no other adjustable parameters. To improve accuracy, Pazuki et al.[113] introduced an adjustable interaction parameter λ_{PS} to eqs. (2.3) and (2.4). λ_{PS} was defined to depend on the ratio of MW of asphaltene and solvent, and was obtained by optimization of an objective function on mass fractions of asphaltene precipitates. With this parameter, the model provided a good match with experimental data on asphaltene precipitation when precipitants n-pentane, n-hexane and n-heptane were added to the crude oil sample from south west of Iran. Following a similar approach, in the work by Mofidi et al.,[114] an adjustable interaction parameter was added to eqs. (2.3) and (2.4) to calculate the activity coefficients, which was subsequently used to determine the change of Gibbs free energy. At thermodynamic equilibrium, the change of Gibbs free energy was zero. Therefore, the solubility parameters δ_a and δ_m were obtained through solving equilibrium equations instead of being quantities that must be prescribed a priori for asphaltene precipitation

calculation. The adjustable interaction parameter depended on MW of asphaltene and solvent, and a tuning procedure was used to determine its value. The predicted onset precipitation was shown to agree well with experimental data. In the work of Nourbakhsh et al.,[115] this adjustable interaction parameter was further modified to take solvent ratio (volume of the solvent divided by the mass of the oil) into account. These above models did not separate precipitants from the crude oil and considered them as a single-phase solvent. In the work of Orangi et al.,[116] a three-component system of asphaltene + solvent + precipitant was proposed. The predicted fractional precipitation agreed well with experimental data for the n-alkanes at high dilution ratios.

While majority of the above models focused on investigating asphaltene precipitation upon the addition of precipitants, the original model proposed by Hirschberg et al.[77] addressed the influence of temperature and pressure on asphaltene precipitation. Therefore theoretical models have also been developed to predict the effect of temperature and pressure. For instance, Orangi et al.[116] obtained a spinodal diagram (phase stability limits) of temperature (T) versus the volume faction of asphaltenes in the crude oil (φ_a), based on solving the phase stability limit (spinodal curve) equation:

$$\frac{\partial \mu_a}{\partial \varphi_a} = 0, \tag{2.12}$$

where μ_a was obtained using Flory-Huggins theory as in eqs. (2.3) and (2.4). Mousavi-Dehghani et al.[117] adopted Miller's combinatory entropy[118] to modify Flory-Huggins theory, and predicted the amount of asphaltene precipitation versus pressure and temperature. Furthermore, theoretical models developed based on the Flory-Huggins theory have also been employed to predict asphaltene precipitation when gas was injected, such as in the works of Hirschberg et al.,[77] Mousavi-Dehghani et al.[117] and Yang et al.[119]

2.2.2.2.2. Models Based on EoS Methods. Traditional cubic EoS has been used to investigate the phase separations of crude oils where asphaltene precipitation occurs. In addition to providing critical parameters such as molar volumes and solubility parameter to other prediction models,[77,111,120] they have also been used to directly predict the onset conditions of asphaltene precipitation and the amount of precipitates.

Du and Zhang[121] developed a thermodynamic model to predict asphaltene precipitation conditions, in which the PR-EoS was used to calculate the component fugacity coefficient and the phase compressibility. Asphaltene association was taking into account by adding a chemical contribution[122-124] (resulted from treating aggregates as "new chemical species") to the expression of fugacity coefficients, similar to the approach adopted in the work of Vafaie-Sefti et al.[125] It was shown that the proposed model provided satisfactory predictions of asphaltene precipitation such as the onset point temperature of asphaltene precipitation with n-heptane injection. Assuming equilibrium between a primary liquid phase and a second dense asphaltene phase, Yarranton and co-workers[126] applied the PR-EoS to calculate the fugacity and K-values of each phase and further determine their composition. The bitumens and heavy oils were separated into four pseudo-components corresponding to the SARA fractions. To incorporate the effects of asphaltene self-association, asphaltenes were divided into 30 pseudo-component fractions of different molar mass based on a gamma distribution function. The model was tested on three Western Canadian oils (Athabasca, Cold Lake, and Lloydminster) and four other oils (Venezuela 1 and 2, Russia, and Indonesia). In all cases, the model successfully matched asphaltene yields for n-alkane diluted bitumens at temperatures from 0 to 100 °C and pressures up to 7 MPa. Later on, an Advanced PR-EoS was used by Yarranton and co-workers[127] to model asphaltene precipitation, in which a volume translation correction to better describe liquid densities was

included. In this model, to fit both the saturation pressure and asphaltene onset condition, a temperature dependent correlation was developed for the binary interaction parameters between solvent and bitumen pseudo-components.

Even though the above works considered asphaltene self-association, the cross association between asphaltenes and aromatics/resins were not included. To do so, Li et al.[128] applied a Cubic-Plus-Association EoS (CPA-EoS) model[129] to study asphaltene precipitation due to the injection of n-alkanes from model solution (asphaltene + toluene), and real heavy oils and bitumens (characterized by three pseudo-components: saturates, aromatics/resins, and asphaltenes). In this model, the excess Helmholtz free energy A^{ex} was assumed to consist of two parts: the physical (non-associating) part describing molecular interactions such as short-range repulsions and dispersion attractions; and the association part describing the polar−polar cross-association of asphaltene and toluene (or aromatic/resin) molecules as well as self-association of asphatlenes. The physical and association contributions were respectively described by the PR-EoS and Wertheim thermodynamic perturbation theory.[130-135] It was shown that the proposed model reproduced most of the experiment results on the amount of asphaltene precipitation by different n-alkanes over a wide range of temperatures, pressures and compositions. In their subsequent work,[136] the application of this CPA-EoS was extended to seven live oils. Similarly, in the work of Saeedi Dehaghani et al.,[137] a CPA-EoS was used to predict asphaltene deposition during gas injection. However, in this work, the physical compressibility factor was obtained from Soave-Redlich-Kwong EoS and the chemical part was from the generalized Anderko's model[122] that included the cross association between different components of a mixture.

Recently developed Statistical Associating Fluid Theory (SAFT) EoS by Chapman et al.,[138,139] in terms of residual Helmholtz free energy, has also been employed in predicting

asphaltene phase behaviors. The original SAFT EoS modeled each molecule as a chain of freely-jointed spherical segments connected through covalent bonds, and aggregates were formed by the association of chain-like molecules. Therefore, the residual Helmholtz free energy A^{res} of a mixture was described as:

$$A^{res} = A^{seg} + A^{chain} + A^{assoc}, \quad (2.13)$$

where A^{seg}, A^{chain} and A^{assoc}, respectively, represent contributions from the segment-segment interaction, i.e. Lennard-Jones (LJ) interaction, chain-forming covalent bonds, and the site-site specific interactions among segments, for example, hydrogen bonding interactions. A^{seg} was assumed to be composed of two parts that, respectively, corresponded to the repulsive (hard sphere, A^{hs}) and attractive (dispersion, A^{disp}) parts of the potential:

$$A^{seg} = A^{hs} + A^{disp}. \quad (2.14)$$

In 2003, Chapman and co-workers[140] modeled asphaltene phase behavior with the Perturbed-Chain SAFT (PC-SAFT) EoS,[141] in which the dispersion term was derived by applying a perturbation theory of Barker and Henderson[142,143] to a hard-chain reference fluid. Molecular size and non-polar van der Waals interactions were assumed to dominate asphaltene phase behaviors. Therefore, the SAFT association term (A^{assoc}), due to the presence of site-site specific interactions, was not considered. Three parameters were required by PC-SAFT EoS for each non-associating component of the mixture: the temperature-independent diameter of each molecular segment (σ), the number of segments per molecule (m), and the segment−segment dispersion energy (ε/k; ε is an LJ energy, and k is Boltzmann constant.). The PC-SAFT parameters for asphaltenes were obtained by fitting EoS results to experimental data from oil titrations with n-alkanes at ambient condition, while those for other subfractions in the live oil liquid phase (i.e. saturates, aromatics and resins) were obtained from correlations with MW for

each class of compound. It was shown[144,145] that the PC-SAFT EoS properly predicted the effect of temperature, pressure and composition on asphaltene precipitation behaviors. In the subsequent work of Chapman and co-workers,[146] 3D asphaltene phase plots between pressure, temperature, and gas content were generated.

In a few of the works by Chapman and co-workers[140,144,146] reviewed above, asphaltenes were assumed to be monodisperse. In a separate work, the same research group[147] investigated the case where asphaltenes were considered as a polydisperse class of compounds with resins as their lower MW subfraction. Polydisperse asphaltenes were represented by four pseudo-components in SAFT: $n-C_{15+}$, $n-C_{7-15}$, $n-C_{5-7}$, and the $n-C_{3-5}$ n-alkane insoluble subfraction which corresponded to the resins subfraction. The SAFT parameters for each subfraction were obtained by fitting the experimental onset data at ambient conditions. In their recent work,[148] a detailed approach was presented to reduce the number of fitting parameters when adopting the polydisperse asphaltene model. The analysis showed[147,148] that the largest pseudo-component ($n-C_{15+}$ insoluble fraction) precipitated first, followed by the precipitation of smaller pseudo-components. Compared with monodisperse asphaltene model, the amount of asphaltenes precipitated increased more gradually with precipitant (n-alkane) addition; as well polydisperse asphaltenes re-dissolution started at lower precipitant volume fractions and with a higher re-dissolution amount. Adopting the gamma molar mass distribution function reported in the work of Sabbagh et al.,[126] Zúñiga-Hinojosa et al.[149] considered polydisperse asphaltenes by dividing them into 30 subfractions To determine the PC-SAFT parameter, empirical correlations were proposed for σ, m, and ε/k as functions of the molar mass of each subfraction. In addition, unlike in the work of Chapman and co-workers[140,144-148] where binary interaction parameters between different fractions in crude oil mixtures were assumed to be constants, Zúñiga-Hinojosa

et al.[149] estimated the parameters for asphaltene-n-alkane binary interaction as a function of the n-alkane mass fraction. The results obtained showed[149] that the PC-SAFT EoS was able to predict the amount of asphaltene precipitates from n-alkane diluted heavy oils and bitumens at different temperatures and pressures.

The SAFT EoS for potentials of variable range (SAFT-VR)[150] is the other emerging approach within the SAFT framework that has been used to model apshaltene precipitation behavior. Compared with the original SAFT model, the attractive potentials, hence A^{disp} in eq. (2.14), are allowed to have variable widths. Artola et al.[151] applied SAFT-VR EoS to investigate their model oil system, where asphaltenes were represented by polystyrene oligomers with similar MW and the lighter components in the crude oil by alkanes. The square-well (SW) potential was used to model segment-segment interaction in eq. (2.13), and similar to the works of Chapman et al.,[140,144-148] A^{assoc} was not considered when calculating the residual Helmholtz free energy. Using this simplified approach, Artola et al.[151] generated constant-composition pressure –Temperature phase diagrams that incorporated both the bubble curve and the asphaltene precipitation boundary. Their analysis supported the view that asphaltene precipitation was initiated by a thermodynamic instability leading to liquid–liquid phase separation. SAFT-VR EoS has also been applied in the case[152-154] where resins were believed to play important roles for asphaltene stabilization in crude oil, and its effect was taken into account by explicitly calculating A^{assoc}. However, unlike traditional colloidal theory for asphaltenes, these works[152-154] described asphaltene precipitation from crude oil solution as a liquid–liquid equilibrium process. Actually, the A^{assoc} calculated here was obtained from the Wertheim thermodynamic perturbation theory[130-135] as used in the original SAFT EoS[138,139] and was similar to the one in the work of Li et al.[128,136] where CPA-EoS was applied.

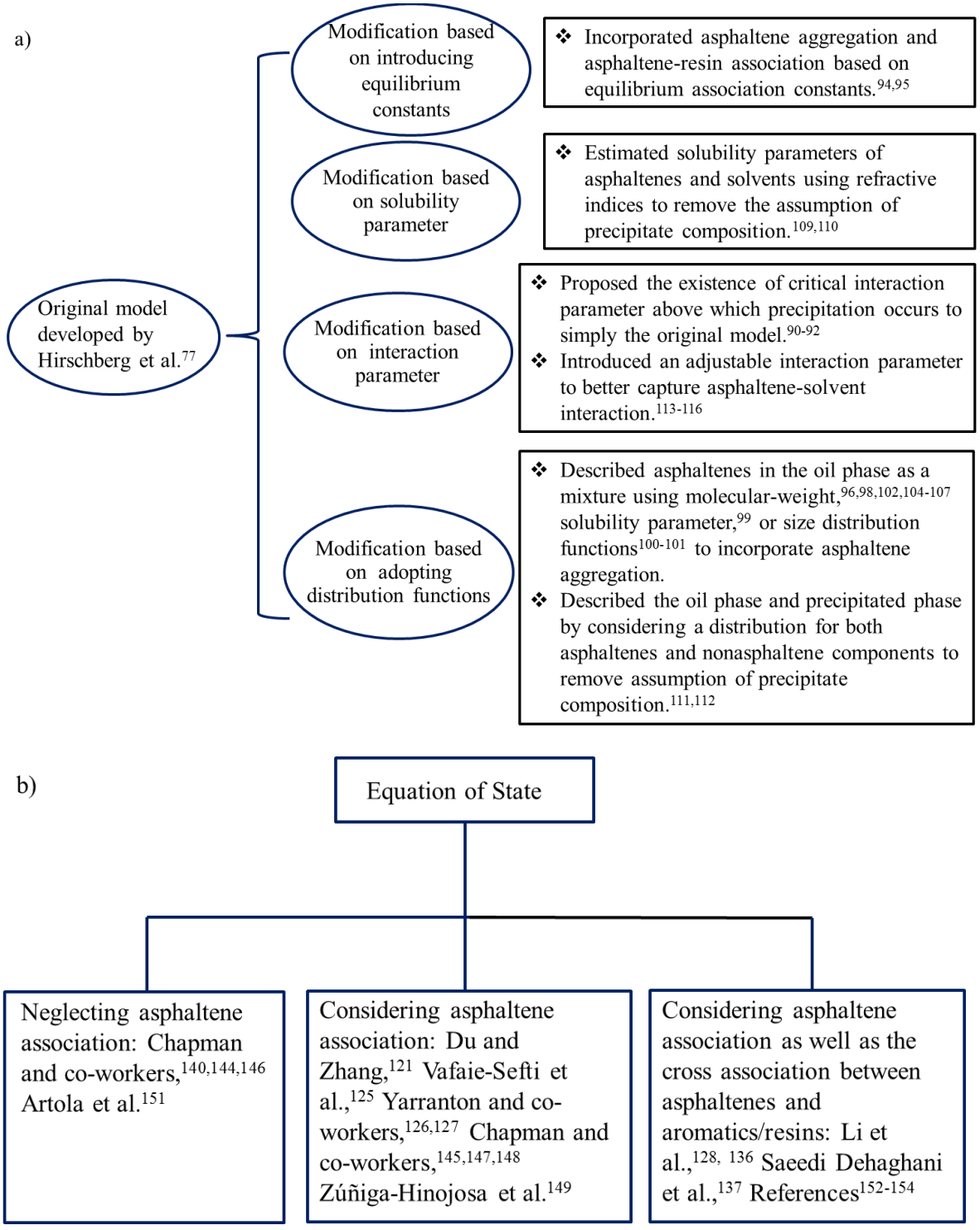

Figure 2.4: Summary of theoretical works based on (a) regular solution theory and (b) EoS.

Besides the colloidal and solubility models reviewed above, other approaches, such as the scaling equation,[155-157] integral equation theory,[158] and artificial neural network algorithm,[159] support vector regression[160], have also been applied to predict asphaltene precipitation.

2.3. Computational Studies

While most theoretical works have been focusing on predicting asphaltene precipitation behaviors at macroscopic level, a large amount of computational studies aim at, from microscopic level, understanding the forces driving asphaltene aggregation as well as probing the aggregated structures. One of the major motivations behind these studies is that the extent of aggregation determines whether precipitation will occur. Furthermore, these computational studies can shed lights on the existing debates on the mechanisms and structures of asphaltene aggregation. Because these computational studies require knowledge of the exact chemical structures of simulated molecules, they were all based on model compounds as surrogates for real asphaltenes. According to the methods used, these works can be categorized into three groups: (1) studies using quantum mechanics (QM) approach; (2) studies using molecular mechanics (MM) and molecular dynamics (MD) approaches; and (3) studies using mesoscopic simulation techniques. The computational works reviewed here are listed in Table 2.1.

2.3.1. Studies Using QM Approach

QM calculations provide numerical solutions to the Schrödinger equation and thus can accurately determine the interaction energy among atoms/molecules and further evaluate the stability of the formed structure.

Density functional theory (DFT) calculation has been used to investigate the driving forces and structure of asphaltene aggregation. Alvarez-Ramirez et al.[161] used two DFT approaches, namely Harris functional[162] with the Vosko, Wilk, Nusair exchange-correlation

potential[163] and GGA Perdew-Wang 91 functional,[164] to calculate the isotropic intermolecular potentials between asphaltene dimers in a vacuum, and a double numerical basis set[165] was adopted in both cases. In this work, the Groenzin−Mullins molecular model[12,13] was used as asphaltene surrogates; the interaction energy curves for different configurations of model asphaltene dimers, namely T-shaped, face-to-face, and edge-edge (see a schematic representation in Figure 2.5), were obtained by varying the minimum atomic distance between two asphaltene dimers. The results[161] showed that among the different configurations studied, the face-to-face orientation had the lowest energy, suggesting it as the most preferred configuration. Moreira da Costa et al.[166] compared the accuracy of different DFT approaches with respect to the highly accurate spin component scaled Møller–Plesset second-order perturbation theory,[167,168] and the results obtained using DFT with ωB97X-D functional[169,170] was shown to be in the closest agreement with those from the highly accurate method. Therefore this functional[171] with 6-31+G(d,p) basis set[172] was employed to evaluate the strength of $\pi-\pi$ interaction for stacked di-, tri-, tetra-, and pentamer aggregates of fused polycyclic aromatic hydrocarbons, such as naphthalene, anthracene, phenanthrene, tetracene, pyrene, coronene and benzene, in chloroform, and the solvent effect was taking into account using the conductor-like polarizable continuum model.[173,174] The results suggested that[166] the polycyclic aromatic hydrocarbons containing more than four fused benzene rings would spontaneously form aggregates at 298 K while those containing fewer rings couldn't, confirming the importance of aromatic rings for the aggregation of asphaltene-like compounds.

Gray and co-workers[175] applied DFT with the ωB97Xd functional[176] and 6-31G(d,p) basis set[172] to investigate contributions of $\pi-\pi$ stacking and hydrogen-bonding interactions to the homodimerization of their 10 asphaltene model compounds in chloroform, which was modeled

using the polarizable continuum solvation method.[177] These model compounds contained a 2,2'-bipyridine moiety which was bonded to one (monosubstituted) or two (disubstituted) aromatic hydrocarbon moieties (phenyl, naphthyl, anthracyl, phenanthryl, and pyrenyl) through ethylene tethers. Consistent with the work[178] of the same authors performed on 4,4'-bis(2-pyren-1-yl-ethyl)-2,2'-bipyridine, it was shown that because of $\pi-\pi$ stacking interactions, the homodimers of both mono- and disubstituted compounds were stable and had a negative Gibbs free energy change upon aggregation, demonstrating that aggregation was a spontaneous process. To explore the effect of water which may be present in solvents, one explicit water molecule was added to the simulated system. After optimization, this water molecule was found to form a bridge between the 2,2'-bipyridine moieties, and the Gibbs free energy of homodimers decreased, suggesting that hydrogen bonding to water might bring additional stability to the aggregates formed by the asphaltene molecules. On the other hand, Carauta et al.,[179] adopting a hybrid

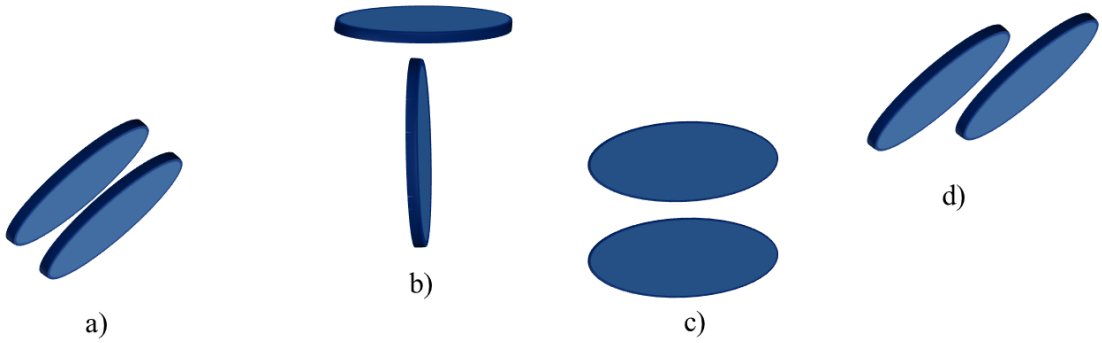

Figure 2.5: A schematic representation of the possible aggregated geometries formed by two PA cores: (a) face-to-face stacking (PA cores parallel to each other with one directly on top of the other), (b) T-shaped stacking (PA cores perpendicular to each other), (c) edge-edge stacking (PA cores co-planar), and (d) offset stacking (PA cores parallel with the two cores shifted laterally from directly on top of each other). Face-to-face stacking and offset stacking together define parallel stacking.

methodology (QM:MM), did not observe the formation of intermolecular hydrogen bonds between their asphaltene dimers of island-type molecules in vacuum.

Regarding the effect of resins on asphaltene aggregation, DFT calculations have been applied to evaluate the interaction energy between resins and asphaltenes, which showed that stable structures of stacked PA cores were formed between model resin and asphaltene molecules.[161,180]

2.3.2. Studies Using MM and MD Approaches

MM and MD approaches are based on classical mechanics and thus less time consuming compared with QM approaches. In MM and MD calculations, the potential energy of the system studied is defined by a force field, which is a set of equations describing the bonded as well as nonbonded interactions between atoms. After an initial configuration is specified, MM adjusts the atomic positions through an iterative procedure until the minimum energy configuration is obtained. MD, on the other hand, evaluates forces on every atom and updates its velocity and position through the integration of Newton's equation of motion. Therefore standard MM and MD can provide energetic and structural information regarding the configurations and dynamic behaviors of asphaltene aggregation.

2.3.2.1. Studies Using MM Approach

Brandt et al.[181] assumed an island-type model structure for asphaltene molecules and constructed a dimer from two optimized unit sheets. The conformational search using MM calculations showed that the minimum energy structure was formed by parallel stacked PA cores. Ortega-Rodriguez et al.[182] applied MM to calculate the interaction energy in vacuum between two model asphaltene molecules as a function of their relative distance. These two molecules have an identical chemical structure, which consists of 630 atoms with an extended aromatic region and

long aliphatic side chains. Similar to the work of Brandt et al.,[181] they found that given the distance between the PA cores, the most stable molecular configuration of the dimers was of parallel stacked PA cores with opposite-oriented aliphatic chains. The interaction curve between the dimmers was then constructed for this relative orientation at different PA core separations, and the potential well was shown to be at ~0.52 nm, corresponding to the equilibrium distance between two parallel stacked PA cores. A stable aggregate of several stacking sheets was observed in the work of Pacheco-Sánchez et al.,[183,184] who investigated the aggregated structures of four island-type asphaltene molecular models in vacuum. However, T-shaped stacking was also reported.[184]

MM calculations have also been performed to probe the effect of resins and solvents on asphaltene aggregation. For instance, in the work of Ortega-Rodriguez et al.[182] reviewed above, by adopting a representative molecular model for resins, the potential curve for asphaltene-resin interaction was constructed, and the potential well was shown to be at ~0.36 nm for the separation of aromatic regions of asphaltenes and resins. In the same work.[182] the effect of the surrounding medium (heptane + pyridine) was taken into account by a mean-field approximation, where the Coulomb and London interaction terms of the asphaltene-asphaltene and asphaltene-resin potentials were scaled. It was shown that as the molar fraction of pyridine in the medium was increased, the equilibrium separations in both cases (asphaltene-asphaltene and asphaltene-resin) shifted to a larger distance and the depths of the potential wells decreased, indicating that pyridine tended to lower the dimer binding energy and enhance asphaltene solubility. Murgich et al.[185] applied MM to study the interaction of two archipelago-type asphaltene molecules with a water molecule in toluene solution. Different initial configurations were constructed, each of which was energy minimized through MM calculations. It was shown that the strength of water-

mediated hydrogen bonding between the two asphaltene molecules depended on the heteroatoms involved, and water molecules might generate additional mechanisms for aggregation of asphaltenes in toluene, similar to the observation of Gray and co-workers.[175,178]

Murgich and co-workers[26,186-188] have also done a series of work to investigate asphaltene aggregation using MM calculations together with short MD simulations. For a specified starting configuration, the general procedure was to first do a minimization to relax any initial strain, followed by an MD equilibration period. Then MM minimization was performed again for the conformation obtained from MD. For island-type asphaltene molecules, it was found that the most stable configurations for asphaltene dimers, trimers, and tetramer were of parallel stacked aromatic cores; and the growth of aggregates was limited by the presence of alkyl and cycloalkyls groups in asphaltenes.[186] Analysis of the different molecular interactions confirmed the dominant role of $\pi - \pi$ interaction for asphaltene aggregates while the alkyl and cycloalkyls groups introduced steric interference to the aggregation.[186] However, for archipelago-type asphaltene molecules, the aggregates had more complex configurations, and Hydrogen bonding and bridging were proposed to be additional mechanisms driving aggregation.[188] Compared with n-octane and toluene, resins showed higher affinities to model asphaltenes constructed from the same oil.[26,186-188]Also, resins showed selectivity for the adsorption sites of the asphaltene, i.e. given the overall shape of asphaltene molecules and aggregates, only certain resins were allowed to be adsorbed.[26,186-188] Using similar procedure (coupled MM and MD simulation), Rogel[189] built initial monomers and further constructed dimers for their model asphaltenes (island-type). It was shown in vacuum, dimers were mainly stabilized by the van der Waals interaction, i.e. $\pi - \pi$ interaction, which depended on the asphaltene structure. Adding solvents may only dissociate the asphaltene dimers of weak van der Waals interaction.

With the further development of computational capacities and MD efficiency, nowadays a more general application of MM method in studying asphaltene aggregation behaviors is to provide energy-minimized initial configurations for the subsequent MD runs.

2.3.2.2. Studies Using MD Approach. The emerging MD techniques have been widely used in probing the aggregation behaviors of asphaltenes in vacuum, organic and inorganic solvents.

Pacheco-Sánchez et al.[190] investigated the aggregation behaviors of the model asphaltene proposed by Groenzin and Mullins[12,13] in vacuum. Initially, 96 identical model asphaltene molecules were set into an array with the neighboring sulfur-sulfur separation of ~4 nm. After energy minimization, MD simulations were conducted under 5 different temperatures: 298, 310, 340, 370, and 400 K. The final MD configurations showed that many aggregates were not in the stacking form and remained irregular shapes; for the stacked molecules, face-to-face, T-shaped and offset π-stacked geometries formed by PA cores were all observed (see Figure 2.5). Furthermore, as the temperature increased, dissociation of large aggregates into smaller ones was observed. Temperature-induced dissociation was also observed in the work of Takanohashi et al.,[191] in which a mixture of asphaltene molecular models were adopted. These models included 2 island-type and 1 archipelago-type structures. A simulation cell containing 3 molecules, each representing one asphaltene molecular model, was constructed and simulated at 300, 523, and 673 K. It was shown that the hydrogen bond between asphaltene molecules dissociated at 523 K, while aromatic−aromatic stacking interactions, i.e. $\pi - \pi$ interactions, appeared to be stable at the same temperature. In addition, it was reported[191] that the removal of all aliphatic side chains and the replacement of heteroatoms with carbon atoms decreased the stability of stacking in the aggregates.

As asphaltenes are a solubility class which is soluble in aromatic solvents but insoluble in n-alkanes,[192-194] aggregation behaviors of asphaltenes in toluene (representing aromatic solvents) and heptane (representing n-alkanes) have been extensively studied using MD approach. Boek, Headen and co-workers[195] investigated the aggregation of 6 island-type model asphaltene molecules in toluene and heptane at 7 wt%. In both solvents, no stable dimers living longer than roughly 10 ns were observed. It was suggested that in heptane, the preferred configuration between two nearest asphaltene molecules were parallel stacking, although non-parallel stacked PA cores were also reported, and in toluene, the preference of parallel stacking was less. For mixed heptane and toluene (heptol), Rogel[196] monitored the interaction energy between two island-type asphaltene monomers along the MD simulation course. The results showed the dimer formation in pure heptane, but not in heptol or in pure toluene.

In a separate work of Headen et al.,[197] both island-type and archipelago structures were adopted, generated using a Monte Carlo method, and simulated in toluene and heptane, again at 7 wt%. Although similar to their previous study,[195] no stable dimers/trimers were observed, aggregates lived longer in heptane. In addition, it was shown[197] that higher temperature decreased the average aggregation time. For the aggregated structures, offset stacking was reported to be the prevalent conformation in both solvents. Ungerer et al.[198] studied the aggregation behaviors of three model asphaltenes, two island types and one archipelago type, in toluene and heptane. In both solvents, significant aggregation was observed for larger island-type molecules while for smaller island-type molecules, the aggregation was stronger in heptane than in toluene. On the other hand, it was shown that the archipelago-type molecules did not evidently aggregate in heptane or toluene. Their results suggested that small island-type molecules could represent the average structures of real asphaltenes. Aggregation of a mixture of archipelago-type and island-

type asphaltene molecules in toluene and heptane were studied by Kuznicki et al.[199] In their work, an ordered array of 12 island-type and 12 archipelago-type molecules were packed into a cubic box of edge 6.5 nm, followed by solvation. After 10 ns simulation, all 24 molecules formed a single aggregate in both solvents, and the stacking of PA cores was evident in both cases, suggesting the importance of $\pi - \pi$ interaction for aggregation. Furthermore, the stacking behaviors were reported[199] to be more pronounced in heptane compared with those in toluene. Sedghi et al.[200] investigated the aggregation behaviors of 8 types of asphaltene-like compounds (island-type) in heptane. The concentrations of asphaltenes were kept constant at 7 wt% in all the simulations. Stable aggregates of different sizes were observed. It was proposed that T-shape configuration was predominant in the nanoaggregates formed by model asphaltene molecules without aliphatic chains while model compounds with several short aliphatic side chains could only form nanoaggregates with parallel configuration due to the steric hindrance between the side chains. Furthermore, the presence of hydroxyl groups in the aliphatic side chains was suggested[200] to help aggregation.

The effect of hydroxyl groups, present in carboxylic acid, on asphaltene aggregation was discussed in the work of Teklebrhan et al.,[201] who studied the aggregation of 5 synthesized PA compounds in toluene and heptane. These 5 island-type models were of the same PA cores and differentiated by the structures of the substituent side chains. Twenty-four molecules of a single type of model compounds were dispersed in a cubic box of dimension $12\,\text{nm} \times 12\,\text{nm} \times 12\,\text{nm}$, and solvated by toluene or heptane. After 20 ns MD simulations, depending on the nature of the side chains attached, aggregation extents were shown to be different and aggregates of various configurations were observed including PA core parallel stacking, T-shaped stacking, and tail-tail association. For instance, the change from -COOH to -$COOCH_3$ functionality

enhanced the nanoaggregate formation in toluene. Generally, it was shown that the toluene hindered the molecular association of model asphaltenes through weakening $\pi - \pi$ stacking, and aggregates grew to a much larger size in heptane than in toluene.

Besides toluene and heptane, the effects of other organic solvents have also been studied in literature. For instance, in the work of Carauta et al.[202], the effects of n-butane and isobutane on the dissociation of asphaltene dimers were compared with those of toluene and heptane, where model asphaltenes were of island-type architectures. It was shown that the ability of n-butane and isobutane to break asphaltene dimers fell in between that of toluene (most effective) and heptane (least effective). In contrast to the work of Headen et al.,[197] increasing temperature did not lower the stability of asphaltene dimers in n-butane, isobutene, and toluene. Frigerio et al.[203] investigated the aggregation behaviors of their island-type asphaltenes in four solvents: toluene, tetrahydrofuran, pentane and heptane. A high concentration (20-30 wt%) was used, and the parallel stacking of PA cores were reported in all cases. Particularly, a decamer of parallel stacked PA cores were observed for model asphaltene in pentane. In the work of Takanohashi et al.,[204] the effects of solvent on the stability of the asphaltene aggregates were studied at 573 K. They observed that quinolone could disrupt some stacking interactions of model asphaltenes while 1-methylnaphthalene, having a similar structure to toluene, could not. On the other hand, Pacheco-Sánchez et al.[205] showed that toluene could intrigue the dissociation of asphaltenes while pentane could not.

In addition to these organic solvents, the aggregation behaviors of asphaltenes in inorganic solvents were also probed. Adopting previous simulation procedure,[195,197] Headen and Boek[206] studied the aggregation of asphaltenes in supercritical carbon dioxide (sc-CO_2) with and without limonene. At all temperatures (300, 350 and 400 K) and all pressures (100, 150 and 200

bar), an aggregate of six molecules, mainly by stacking of the aromatic cores, was quickly formed in pure sc-CO_2 with some structural fluctuations. The presence of limonene considerably decreased the size and stability of the aggregate, confirming the role of limonene as a dispersant. Hu et al.[207] investigated the effect of CO_2 on the interaction in asphaltene aggregates, and showed that pure CO_2 would enhance the hydrogen bond and the dipolar interaction between asphaltene molecules.

Using MD simulations, Zhang et al.[208] investigated the molecular orientation of asphaltenes in asphalt mixtures, consisting of asphaltenes, resins and maltenes. In this work, two island-type models were adopted as asphaltene surrogates, and the resin and maltene were respectively represented by 1,7-Dimethylnaphthalene and linear alkane n-C_{22}. It was shown that the relative orientation between two nearest asphaltene molecules was affected by their chemical structures and temperatures. For model asphaltene molecules with long aliphatic side chains, the PA cores preferred to be almost parallel at high temperature but perpendicular at low temperature, and at intermediate temperatures, the most probable relative orientation between the cores was near 40°. This was attributed to the combination of $\pi - \pi$ interaction from aromatic rings, $\pi - \theta$ interactions between the aromatic ring and aliphatic chains, and $\theta - \theta$ interaction between aliphatic chains. However for highly aromatic asphaltene molecules (with short aliphatic side chains), because of the dominant $\pi - \pi$ interaction, they preferred to stay almost parallel to each other at low temperatures and almost perpendicular at high temperatures.

MD simulations have also been conducted to calculate solubility parameters (δ) which are of great importance in solubility theory. In MD simulations, the cohesive energy E_{coh}, used to define solubility parameters, is calculated as the energy difference between per mole of materials in their condensed phase and in the ideal gas phase where all intermolecular

interactions are eliminated. Then the solubility parameter δ is calculated using the following equation:

$$\delta = (\frac{E_{coh}}{V})^{0.5}, \quad (2.15)$$

where V is the molar volume. Rogel[196] calculated the solubility parameters for the monomer, dimer, trimer, and tetramer of their model asphaltenes, each of which was treated as a "single molecule". It was showed[196] that aggregate of more molecules had a lower solubility parameter. Diallo et al.[209] investigated the effect of temperature on the solubility parameters of model asphaltenes and observed a linear decrease in δ as temperature increased. Aray et al.[210] investigated the solubility parameters of 13 island-type and 2 archipelago-type asphaltenes. In general, δ became larger as the number of aromatic rings forming the asphaltene cores increased or as the number and length of aliphatic chains decreased. In addition, the solubilities of these model asphaltenes in toluene, heptane, and amphiphiles (resins) were also studied using the Scatchard-Hildebrand and the Hansen sphere methodologies.[211] According to these theories, the maximum of solubility was observed when the solubility parameters of asphaltenes and solvents were identical. Aray et al.[210] showed that the increase of aromatic ring number decreased the asphaltene solubility in toluene and heptane. Further, archipelago-type models were observed to have a large solubility in amphiphiles containing large aliphatic tails and no aromatic rings while island-type models showed high solubility in those containing aromatic rings and small aliphatic chains.[210]

Recently, MD techniques have been used to calculate the free energy of asphaltene association, which was defined as the difference in the potential of mean force (PMF) at infinite and equilibrium separations. Headen and co-workers[197] calculated the aspaltene-asphaltene PMF using two approaches: unconstrained and constraint MD simulations. In the unconstrained

simulations, radial distribution function (RDF) was used to calculate the PMF. In the constrained simulation, the center of mass distance between two molecules were restrained at specific distances from 0.5 to 1.5 nm with an interval of 0.1 nm; the force needed to keep molecules at a specific distance was then calculated and the PMF profile was obtained by integration of the force-distance curve. These two methods yielded similar results: values for free energy of dimer formation were very close in both toluene and heptane. This was a surprising result, as asphaltenes do exhibit very different solubility behaviors in these two solvents. A completely different result was reported by Sedghi et al.,[200] where the umbrella sampling method was applied to calculate the dimerization free energy of 8 island-type asphaltenes. Their results suggested that due to the $\pi - \pi$ interaction between toluene and asphaltene, the association free energy (absolute value) of asphaltene was lower in toluene than in heptane. In addition, $\pi - \pi$ interaction was shown to be the driving force for asphaltene association, which was dependent on both the number of aromatic rings and the presence of heteroatoms in the aromatic core.

The time and length scales of the systems studied in MM and MD simulations are restricted by available computational capacity. The application of mesoscopic simulation techniques, as reviewed below, allows the study of larger and more complex systems.

2.3.3. Studies Using Mesoscopic Simulation Techniques

Compared with MM and MD simulations, mesoscopic simulation techniques adopt coarse-grained models to describe molecular structures, instead of considering all the atomic details inside each molecule. These techniques include coarse-grained Monte Carlo (CGMC), coarse-grained molecule dynamics (CGMD), and dissipative particle dynamics (DPD) methods.

Aguilera-Mercado et al.[212] modeled resin molecule as a single sphere and described asphaltene molecule as a central sphere surrounded by a ring of spheres. The intermolecular

potential function for each type of spheres was obtained using the method from the work of Ortega-Rodriguez et al,[182] Moreover, the surrounding crude oil medium was modeled as a continuum, characterized by a screening factor. CGMC simulations were performed to investigate the effect of temperatures as well as asphaltene and resin concentrations on aggregation. It was shown that aggregation was affected by temperature and asphaltene concentration but was insensitive to resin concentration.

Based on the method from previous work,[182] Ortega-Rodriguez et al.[213] obtained intermolecular potential functions for asphaltene-asphaltene, asphaltene-resin, and resin-resin molecules, which were subsequently used in their CGMD studies. Inside each system, asphaltene and resin molecules were modeled as dots and the solvent was taking into account using a mean-field approximation. Their results suggested that among the different interactions, asphaltene-asphaltene affinity was the strongest followed by asphaltene-resin and then resin-resin affinities. Therefore it was proposed that resins could stabilize asphaltene aggregates. Regarding the effect of solvent, heptane was shown to have a poor screening effect on the long-range interactions of asphaltenes and thus promote aggregation; pyridine were observed to have the largest screening effect and prevent aggregation.

Zhang et al.[214] implemented a rotational algorithm into the DPD program to evolve the motion of rigid bodies and investigated the aggregation of asphaltenes in model heavy crude oil consisting of SARA components and additional light fractions. For the island-type models studied, three typical aggregated structures were observed: face-to-face stacking, offset π-stacking and T-shaped stacking (see Figure 2.5). In their subsequent work[215], three rotational algorithms were compared, and the results confirmed the superiority of the Quaternion method. Therefore the aggregation of island-type asphaltenes in heavy oil and very diluted toluene was

investigated by performing DPD simulation integrated with Quaternion method. It was shown that in the system of model heavy oil, although both offset π-stacking and T-shaped stacking were observed, as many as five molecules could concurrently form a well-ordered face-to-face stacking geometry. For asphaltenes in very diluted toluene (model asphaltene concentration: 0.47 g/L-1.7 g/L), the coexistence of monomers and aggregates were confirmed and aggregates were suggested to undergo the dynamics of forming, breaking-up and reforming. In the most recent work[216] of the same group, the above method was implemented on graphics processing units, which speeded up the simulations by more than ten folds. It was shown that the determined diffusion coefficients of island-type asphaltenes in toluene were similar to those obtained in experimental studies.

2.4. Summary

In this chapter, we provided a detailed review on the theoretical and computational works performed on asphaltene aggregation and precipitation, together with the key results from relevant experimental studies. As can be seen from section 2.1, great discrepancies exist regarding the molecular structure of asphaltenes found from experimental studies. Several reasons that may contribute to the existence of the discrepancies are: the usage of diverse samples from different sources, the employment of various techniques, as well as the different conditions under which the experiments were performed. These discrepancies have impeded the clear understanding of asphaltene aggregation and precipitation, and prevented the development of unified theoretical models for predicting asphaltene behaviors. As reviewed in section 2.2, calibrated by different experimental data, almost all the reviewed theoretical works have been shown to agree well with the experimental observations on the specific asphaltene sample used. However, none of these models has been able to reproduce the experimental results for all the

Table 2.1: Summary of Computational Works on Aggregation: (a) QM Studies, (b) MM Studies, (c) MD Studies, and (d) Mesoscopic studies[a]

[a]In each table, for the works listed in the first column, the systems investigated are given in the second column, and the last 3 columns describe the key findings. Empty cells in the last 3 columns indicate no discussion on the corresponding topic from the cited work.

a) QM studies (DFT approach)

References	Systems	Forces driving aggregations	Favorite configurations	Effect of solvent and/or external conditions
Alvarez-Ramirez et al.[161]	Island-type asphaltene dimers in vacuum	$\pi - \pi$ interaction	Face-to-face stacking of PA cores	
Moreira da Costa et al.[166]	Stacked di-, tri-, tetra-, and pentamer aggregates of island-type molecules in chloroform	$\pi - \pi$ interaction	Parallel stacking of PA cores	Chloroform weakened the stacking interaction, especially for the compounds with small PA cores.
Gray and co-workers[175,178]	Archipelago-type dimers in chloroform	$\pi - \pi$ interaction	Parallel stacking of PA cores	
	One water molecule added to the above system	Hydrogen bonding to water introduced additional stability to the asphaltene aggregates.	Parallel stacking of PA cores	Water enhanced the aggregation of model asphaltenes.
Carauta et al.[179]	Asphaltene dimers of island-type molecules in vacuum	No intermolecular hydrogen bond formed	Parallel stacking of PA cores	

b) MM studies

References	Systems	Forces driving aggregations	Favorite configurations	Effect of solvent and/or external conditions
Brandt et al.[181]	Island-type asphaltene dimer in vacuum	$\pi - \pi$ interaction	Parallel stacking of PA cores	
Ortega-Rodriguez et al.[182]	Island-type asphaltene dimer in vacuum		Parallel stacking of PA cores	
	Island-type asphaltene dimer in mixture of heptane + pyridine		Parallel stacking of PA cores	Solvency power: pyridine > heptane
Pacheco-Sánchez et al.[183,184]	Island-type asphaltene molecules in vacuum	$\pi - \pi$ interaction, which was influenced by the steric hindrance of the side chains	Face-to-face, offset π-stacking and T-shaped stacking of PA cores	
Murgich and co-workers[26,186-188]	Island-type asphaltene molecules	$\pi - \pi$ interaction	Parallel stacking of PA cores	Solvency power: resin > toluene, n-octane
	Archipelago-type asphaltene molecules	Hydrogen bonding and bridging provided additional mechanisms driving aggregation.	Complex shape including parallel stacking of PA cores, molecular tangling and inter aggregate links	Solvency power: resin > toluene, n-octane
Rogel[189]	Island-type asphaltene dimer in vacuum	$\pi - \pi$ interaction	Parallel stacking of PA cores	

c) MD studies

References	Systems	Forces driving aggregations	Favorite configurations	Effect of solvent and/or external conditions
Pacheco-Sánchez et al.[190]	Ninety-six island-type asphaltene molecules in vacuum		Face-to-face, T-shaped and offset π-stacking of PA cores	High temperature could dissociate larger aggregates.
Takanohashi et al.[191]	Two island-type and 1 archipelago-type molecules in vacuum	$\pi-\pi$ interaction as well as hydrogen bond		Compared with $\pi-\pi$ interactions, hydrogen bond between molecules was easily dissociated at high temperature.
Takanohashi et al.[207]	Asphaltene aggregates in quinolone and toluene			Solvency power: quinolone > toluene
Boek, Headen and co-workers[195]	Six island-type asphaltene molecules in toluene or heptane		Parallel stacking of PA cores in heptane; less preference of parallel stacking in toluene	
Headen et al.[197]	Archipelago-type and island-type structures in toluene and heptane		Offset stacking	Solvency power: toluene > heptane. High temperature decreased the average aggregation time.
	PMF calculations of asphaltene dimers in toluene and heptane			Similar values of free energy for dimer formation in toluene and heptane
Headen and Boek[209]	Asphaltene molecules in sc-CO_2 with and without limonene		Parallel stacking of PA cores	Adding limonene considerably decreased the size and stability of the aggregate.
Rogel[196]	Two island-type molecules in mixed heptane and toluene		Parallel stacking of PA cores	Solvency power: toluene > heptane
Ungerer et al.[198]	Two island-type and one archipelago-type model asphaltenes in toluene and heptane		Significant parallel stacking of PA cores was observed for island-type molecules.	Solvency power: toluene > heptane

Kuznicki et al.[199]	A mixture of archipelago-type and island-type asphaltene molecules in toluene and heptane	$\pi-\pi$ interaction	Parallel stacking of PA cores	Solvency power: toluene > heptane
Sedghi et al.[200]	Island-type molecules in heptane	$\pi-\pi$ interaction and additional aggregation driving forces introduced by hydroxyl groups in the aliphatic side chains	T-shaped configuration was predominant in the nanoaggregates formed by model asphaltene molecules without aliphatic chains while model compounds with several short side chains could only form parallel stacking configuration.	Solvency power: toluene > heptane
	PMF calculations of asphaltene dimers in toluene and heptane	$\pi-\pi$ interaction		Lower association free energy (absolute value) of asphaltene in toluene compared with that in heptane
Teklebrhan et al.[201]	Island-type molecules in toluene and heptane	$\pi-\pi$ interaction, which was greatly influenced by the steric hindrance and polarity of the substituted side chains	PA core parallel stacking, T-shaped stacking, and tail-tail association	Solvency power: toluene > heptane
Carauta et al.[202]	Island-type asphaltene dimers in n-butane, isobutene, toluene and n-heptane	$\pi-\pi$ interaction	Parallel stacking of PA cores	Solvency power: toluene > butane, isobutene >heptane. High temperature did not lower the stability of asphaltene dimers.
Frigerio et al.[203]	Island-type asphaltenes in toluene, tetrahydrofurane, pentane and heptane,	$\pi-\pi$ interaction	Parallel stacking of PA cores	Solvency power: toluene, tetrahydrofurane > pentane and heptane

Pacheco-Sánchez et al.[205]	Asphaltene aggregates in toluene and pentane		Face-to-face stacking, offset π-stacking and T-shaped stacking of PA cores were all observed with offset π-stacking being the most common geometry.	Solvency power: toluene > pentane
Hu et al.[207]	Asphaltene aggregates in CO_2	Pure CO_2 enhanced the hydrogen bond and the dipolar interaction between asphaltene molecules.	Face-to-face stacking of PA cores in pure CO_2	CO_2 injection could enhance asphaltene aggregation in methane, ethane, and octane.
Zhang et al.[208]	Model asphaltenes in asphalt mixtures	Core-core interaction, core-tail interaction, and tail-tail interaction for model asphaltenes with long aliphatic side chains	Parallel stacking at high temperature but perpendicular at low temperature; at intermediate temperatures, the most probable relative orientation between the cores near 40°	
		$\pi - \pi$ interaction for highly aromatic asphaltene molecules (with short aliphatic side chains)	Parallel stacking at low temperature and almost perpendicular at high temperature	
Aray et al.[210]	Solubility parameter calculation for asphaltenes and amphiphiles	$\pi - \pi$ interaction	Parallel stacking of PA cores in vacuum	Archipelago-type models had a large solubility in amphiphiles containing large aliphatic tails and no aromatic rings; island-type models showed high solubility in those containing aromatic rings and small aliphatic chains.

d) Mesoscopic studies

References	Systems	Forces driving aggregations	Favorite configurations	Effect of solvent and/or external conditions
Aguilera-Mercado et al.[212]	Asphaltene in crude oil mixture studied by CGMC method			Temperature and asphaltene concentration affected aggregation while resin concentration did not.
Ortega-Rodriguez et al.[213]	Asphaltene in crude oil mixture studied by CGMD method			Solvency power: pyridine > heptane. Resins had stabilizing effect on asphaltene aggregates.
Zhang et al.[214,215]	Asphaltene in crude oil mixture studied by DPD program integrated with a rotational algorithm[217]		Face-to-face stacking, offset π-stacking and T-shaped stacking of PA cores	
	Asphaltene in crude oil mixture studied by DPD program integrated with Quaternion method[218]		Face-to-face stacking, offset π-stacking and T-shaped stacking of PA cores	

available samples in literature. Compared with theoretical works, computational studies, as reviewed in section 2.3, require explicit molecular models as surrogates for real asphaltenes, thus leading to model-dependent conclusions (shown in Table 2.1). For instance, for the aggregated structures, parallel stacking and T-shaped stacking of PA cores as well as tail-tail association were all reported to be the favorite configurations. Moreover, computational results are restricted by the time and length dimensions of the systems studied. Hence caution must be taken in drawing generalized conclusions from specific studies.

Despite the discrepancies, theoretical efforts have clearly demonstrated the possibility of developing predictive models for asphaltene aggregation and precipitation. These models can be very helpful in the cases where experimental operations are extremely difficult and costly. On the other hand, with the development of computational capacities, complex and large systems that correspond to real crude oil mixtures may be simulated to generate a comprehensive picture for asphaltene aggregation from microscopic level. All these studies, although may be sample-related, can help with probing the underlying mechanisms and proposing suitable ways to prevent, and further utilize, asphaltene aggregation and precipitation.

Bibliography

(1) Speight, J.; Wernick, D.; Gould, K.; Overfield, R.; Rao, B. Molecular Weight and Association of Asphaltenes: A Critical Review. *Rev. Inst. Fr. Pet.* **1985,** *40*, 51-61.

(2) Strausz, O. P.; Safarik, I.; Lown, E.; Morales-Izquierdo, A. A Critique of Asphaltene Fluorescence Decay and Depolarization-Based Claims about Molecular Weight and Molecular Architecture. *Energy Fuels* **2008,** *22*, 1156-1166.

(3) Strausz, O. P.; Mojelsky, T. W.; Faraji, F.; Lown, E. M.; Peng, P. Additional Structural Details on Athabasca Asphaltene and Their Ramifications. *Energy Fuels* **1999,** *13*, 207-

227.

(4) Mullins, O. C.; Sabbah, H.; Eyssautier, J.; Pomerantz, A. E.; Barré, L.; Andrews, A. B.; Ruiz-Morales, Y.; Mostowfi, F.; McFarlane, R.; Goual, L., et al. Advances in Asphaltene Science and the Yen–Mullins Model. *Energy Fuels* **2012,** *26*, 3986-4003.

(5) Strausz, O. P.; Mojelsky, T. W.; Lown, E. M. The Molecular Structure of Asphaltene: an Unfolding Story. *Fuel* **1992,** *71*, 1355-1363.

(6) Dickie, J. P.; Yen, T. F. Macrostructures of the Asphaltic Fractions by Various Instrumental Methods. *Anal. Chem.* **1967,** *39*, 1847-1852.

(7) Mullins, O. C. The Asphaltenes. *Annu. Rev. Anal. Chem.* **2011,** *4*, 393-418.

(8) Leon, O.; Rogel, E.; Espidel, J.; Torres, G. Asphaltenes: Structural Characterization, Self-Association, and Stability Behavior. *Energy Fuels* **2000,** *14*, 6-10.

(9) Sabbah, H.; Morrow, A. L.; Pomerantz, A. E.; Mullins, O. C.; Tan, X.; Gray, M. R.; Azyat, K.; Tykwinski, R. R.; Zare, R. N. Comparing Laser Desorption/Laser Ionization Mass Spectra of Asphaltenes and Model Compounds. *Energy Fuels* **2010,** *24*, 3589-3594.

(10) Sabbah, H.; Morrow, A. L.; Pomerantz, A. E.; Zare, R. N. Evidence for Island Structures as the Dominant Architecture of Asphaltenes. *Energy Fuels* **2011,** *25*, 1597-1604.

(11) Hortal, A. R.; Hurtado, P.; Martínez-Haya, B.; Mullins, O. C. Molecular-Weight Distributions of Coal and Petroleum Asphaltenes from Laser Desorption/Ionization Experiments. *Energy Fuels* **2007,** *21*, 2863-2868.

(12) Groenzin, H.; Mullins, O. C. Asphaltene Molecular size and Structure. *J. Phys. Chem. A* **1999,** *103*, 11237-11245.

(13) Groenzin, H.; Mullins, O. C. Molecular Size and Structure of Asphaltenes from Various Sources. *Energy Fuels* **2000,** *14*, 677-684.

(14) Andrews, A. B.; Guerra, R. E.; Mullins, O. C.; Sen, P. N. Diffusivity of Asphaltene Molecules by Fluorescence Correlation Spectroscopy. *J. Phys. Chem. A* **2006,** *110*, 8093-8097.

(15) Bergmann, U.; Groenzin, H.; Mullins, O. C.; Glatzel, P.; Fetzer, J.; Cramer, S. Carbon K-Edge X-ray Raman Spectroscopy Supports Simple, yet Powerful Description of Aromatic Hydrocarbons and Asphaltenes. *Chem. Phys. Lett.* **2003,** *369*, 184-191.

(16) Pinkston, D. S.; Duan, P.; Gallardo, V. A.; Habicht, S. C.; Tan, X.; Qian, K.; Gray, M.; Mullen, K.; Kenttamaa, H. I. Analysis of Asphaltenes and Asphaltene Model Compounds by Laser-Induced Acoustic Desorption/Fourier Transform Ion Cyclotron Resonance Mass Spectrometry. *Energy Fuels* **2009,** *23*, 5564-5570.

(17) Qian, K.; Edwards, K. E.; Siskin, M.; Olmstead, W. N.; Mennito, A. S.; Dechert, G. J.; Hoosain, N. E. Desorption and Ionization of Heavy Petroleum Molecules and Measurement of Molecular Weight Distributions. *Energy Fuels* **2007,** *21*, 1042-1047.

(18) Lisitza, N. V.; Freed, D. E.; Sen, P. N.; Song, Y. Study of Asphaltene Nanoaggregation by Nuclear Magnetic Resonance (NMR). *Energy Fuels* **2009,** *23*, 1189-1193.

(19) Bouhadda, Y.; Bormann, D.; Sheu, E.; Bendedouch, D.; Krallafa, A.; Daaou, M. Characterization of Algerian Hassi-Messaoud Asphaltene Structure Using Raman Spectrometry and X-ray Diffraction. *Fuel* **2007,** *86*, 1855-1864.

(20) Payzant, J.; Rubinstein, I.; Hogg, A.; Strausz, O. Field-Ionization Mass Spectrometry: Application to Geochemical Analysis. *Geochim. Cosmochim. Acta* **1979,** *43*, 1187-1193.

(21) Rubinstein, I.; Strausz, O. Thermal Treatment of the Athabasca Oil Sand Bitumen and

Its Component Parts. *Geochim. Cosmochim. Acta* **1979,** *43*, 1887-1893.

(22) Rubinstein, I.; Spyckerelle, C.; Strausz, O. Pyrolysis of Asphaltenes: A Source of Geochemical Information. *Geochim. Cosmochim. Acta* **1979,** *43*, 1-6.

(23) Calemma, V.; Rausa, R.; D'Anton, P.; Montanari, L. Characterization of Asphaltenes Molecular Structure. *Energy Fuels* **1998,** *12*, 422-428.

(24) Ferris, S.; Black, E.; Clelland, J. Aromatic Structure in Asphalt Fractions. *Ind. Eng. Chem. Prod. Res. Dev.* **1967,** *6*, 127-132.

(25) Su, Y.; Artok, L.; Murata, S.; Nomura, M. Structural Analysis of the Asphaltene Fraction of an Arabian Mixture by a Ruthenium-Ion-Catalyzed Oxidation Reaction. *Energy Fuels* **1998,** *12*, 1265-1271.

(26) Murgich, J.; Abanero, J. A.; Strausz, O. P. Molecular Recognition in Aggregates Formed by Asphaltene and Resin Molecules from the Athabasca Oil Sand. *Energy Fuels* **1999,** *13*, 278-286.

(27) Artok, L.; Su, Y.; Hirose, Y.; Hosokawa, M.; Murata, S.; Nomura, M. Structure and Reactivity of Petroleum-Derived Asphaltene. *Energy Fuels* **1999,** *13*, 287-296.

(28) Siskin, M.; Kelemen, S.; Eppig, C.; Brown, L.; Afeworki, M. Asphaltene Molecular Structure and Chemical Influences on the Morphology of Coke Produced in Delayed Coking. *Energy Fuels* **2006,** *20*, 1227-1234.

(29) Gray, M. R. Consistency of Asphaltene Chemical Structures with Pyrolysis and Coking Behavior. *Energy Fuels* **2003,** *17*, 1566-1569.

(30) Karimi, A.; Qian, K.; Olmstead, W. N.; Freund, H.; Yung, C.; Gray, M. R. Quantitative Evidence for Bridged Structures in Asphaltenes by Thin Film Pyrolysis. *Energy Fuels* **2011,** *25*, 3581-3589.

(31) Ralston, C. Y.; Mitra-Kirtley, S.; Mullins, O. C. Small Population of One to Three Fused-Aromatic Ring Moieties in Asphaltenes. *Energy Fuels* **1996,** *10*, 623-630.

(32) Buenrostro-Gonzalez, E.; Groenzin, H.; Lira-Galeana, C.; Mullins, O. C. The Overriding Chemical Principles that Define Asphaltenes. *Energy Fuels* **2001,** *15*, 972-978.

(33) Groenzin, H.; Mullins, O. C.; Eser, S.; Mathews, J.; Yang, M.; Jones, D. Molecular Size of Asphaltene Solubility Fractions. *Energy Fuels* **2003,** *17*, 498-503.

(34) Badre, S.; Carla Goncalves, C.; Norinaga, K.; Gustavson, G.; Mullins, O. C. Molecular Size and Weight of Asphaltene and Asphaltene Solubility Fractions from Coals, Crude Oils and Bitumen. *Fuel* **2006,** *85*, 1-11.

(35) Mullins, O. C. Rebuttal to Strausz et al. Regarding Time-Resolved Fluorescence Depolarization of Asphaltenes. *Energy Fuels* **2009,** *23*, 2845-2854.

(36) Nalwaya, V.; Tantayakom, V.; Piumsomboon, P.; Fogler, S. Studies on Asphaltenes Through Analysis of Polar Fractions. *Ind. Eng. Chem. Res.* **1999,** *38*, 964-972.

(37) Kaminski, T. J.; Fogler, H. S.; Wolf, N.; Wattana, P.; Mairal, A. Classification of Asphaltenes via Fractionation and the Effect of Heteroatom Content on Dissolution Kinetics. *Energy Fuels* **2000,** *14*, 25-30.

(38) Fish, R. H.; Komlenic, J. J.; Wines, B. K. Characterization and Comparison of Vanadyl and Nickel Compounds in Heavy Crude Petroleums and Asphaltenes by Reverse-Phase and Size- Exclusion Liquid Chromatography/Graphite Furnace Atomic Absorption Spectrometry. *Anal. Chem.* **1984,** *56*, 2452-2460.

(39) Ancheyta, J.; Centeno, G.; Trejo, F.; Marroquin, G.; Garcia, J.; Tenorio, E.; Torres, A. Extraction and Characterization of Asphaltenes from Different Crude Oils and Solvents.

Energy Fuels **2002,** *16*, 1121-1127.

(40) George, G. N.; Gorbaty, M. L. Sulfur K-Edge X-ray Absorption Spectroscopy of Petroleum Asphaltenes and Model Compounds. *J. Am. Chem. Soc.* **1989,** *111*, 3182-3186.

(41) Waldo, G. S.; Mullins, O. C.; Penner-Hahn, J. E.; Cramer, S. Determination of the Chemical Environment of Sulphur in Petroleum Asphaltenes by X-ray Absorption Spectroscopy. *Fuel* **1992,** *71*, 53-57.

(42) Kelemen, S.; George, G.; Gorbaty, M. Direct Determination and Quantification of Sulphur Forms in Heavy Petroleum and Coals: 1. The X-ray Photoelectron Spectroscopy (XPS) Approach. *Fuel* **1990,** *69*, 939-944.

(43) Mitra-Kirtley, S.; Mullins, O. C.; Van Elp, J.; George, S. J.; Chen, J.; Cramer, S. P. Determination of the Nitrogen Chemical Structures in Petroleum Asphaltenes Using XANES Spectroscopy. *J. Am. Chem. Soc.* **1993,** *115*, 252-258.

(44) Desando, M. A.; Ripmeester, J. A. Chemical Derivatization of Athabasca Oil Sand Asphaltene for Analysis of Hydroxyl and Carboxyl Groups via Nuclear magnetic Resonance Spectroscopy. *Fuel* **2002,** *81*, 1305-1319.

(45) Moschopedis, S. E.; Speight, J. G. Oxygen Functions in Asphaltenes. *Fuel* **1976,** *55*, 334-336.

(46) Ignasiak, T.; Strausz, O. P.; Montgomery, D. S. Oxygen Distribution and Hydrogen Bonding in Athabasca Asphaltene. *Fuel* **1977,** *56*, 359-365.

(47) Mullins, O. C. The Modified Yen Model. *Energy Fuels* **2010,** *24*, 2179-2207.

(48) Yen, T. Structure of Petroleum Asphaltene and Its Significance. *Energy Sources* **1974,** *1*, 447-463.

(49) Andreatta, G.; Goncalves, C. C.; Buffin, G.; Bostrom, N.; Quintella, C. M.; Arteaga-Larios, F.; Pérez, E.; Mullins, O. C. Nanoaggregates and Structure−Function Relations in Asphaltenes. *Energy Fuels* **2005,** *19*, 1282-1289.

(50) Zeng, H.; Song, Y.; Johnson, D. L.; Mullins, O. C. Critical Nanoaggregate Concentration of Asphaltenes by Direct-Current (DC) Electrical Conductivity. *Energy Fuels* **2009,** *23*, 1201-1208.

(51) Andersen, S. I.; del Rio, J. M.; Khvostitchenko, D.; Shakir, S.; Lira-Galeana, C. Interaction and Solubilization of Water by Petroleum Asphaltenes in Organic Solution. *Langmuir* **2001,** *17*, 307-313.

(52) Evdokimov, I.; Eliseev, N. Y.; Akhmetov, B. Assembly of Asphaltene Molecular as Studied by Near-UV/Visible Spectroscopy Aggregates, I. Structure of the Absorbance Spectrum. *J. Petrol. Sci. Eng.* **2003,** *37*, 135-143.

(53) Evdokimov, I.; Eliseev, N. Y.; Akhmetov, B. Assembly of Asphaltene Molecular Aggregates as Studied by Near-UV/Visible Spectroscopy: II. Concentration Dependencies of Absorptivities. *J. Pet. Sci. Eng.* **2003,** *37*, 145-152.

(54) Hoepfner, M. P.; Fogler, H. S. Multiscale Scattering Investigations of Asphaltene Cluster Breakup, Nanoaggregate Dissociation, and Molecular Ordering. *Langmuir* **2013,** *29*, 15423-15432.

(55) Tanaka, R.; Hunt, J. E.; Winans, R. E.; Thiyagarajan, P.; Sato, S.; Takanohashi, T. Aggregates Structure Analysis of Petroleum Asphaltenes with Small-Angle Neutron Scattering. *Energy Fuels* **2003,** *17*, 127-134.

(56) Gawrys, K. L.; Kilpatrick, P. K. Asphaltenic Aggregates are Polydisperse Oblate Cylinders. *J. Colloid Interface Sci.* **2005,** *288*, 325-334.

(57) Eyssautier, J.; Levitz, P.; Espinat, D.; Jestin, J.; Gummel, J.; Grillo, I.; Barré, L. Insight into Asphaltene Nanoaggregate Structure Inferred by Small Angle Neutron and X-ray Scattering. *J. Phys. Chem. B* **2011,** *115*, 6827-6837.

(58) Seki, H.; Kumata, F. Structural Change of Petroleum Asphaltenes and Resins by Hydrodemetallization. *Energy Fuels* **2000,** *14*, 980-985.

(59) Soorghali, F.; Zolghadr, A.; Ayatollahi, S. Effect of Resins on Asphaltene Deposition and the Changes of Surface Properties at Different Pressures: A Microstructure Study. *Energy Fuels* **2014,** *28*, 2415-2421.

(60) González, G.; Neves, G. B.; Saraiva, S. M.; Lucas, E. F.; dos Anjos de Sousa, M. Electrokinetic Characterization of Asphaltenes and the Asphaltenes−Resins Interaction. *Energy Fuels* **2003,** *17*, 879-886.

(61) Mullins, O. C.; Betancourt, S. S.; Cribbs, M. E.; Dubost, F. X.; Creek, J. L.; Andrews, A. B.; Venkataramanan, L. The Colloidal Structure of Crude Oil and the Structure of Oil Reservoirs. *Energy Fuels* **2007,** *21*, 2785-2794.

(62) Sedghi, M.; Goual, L. Role of Resins on Asphaltene Stability. *Energy Fuels* **2009,** *24*, 2275- 2280.

(63) Breure, B.; Subramanian, D.; Leys, J.; Peters, C. J.; Anisimov, M. A. Modeling Asphaltene Aggregation with a Single Compound. *Energy Fuels* **2012,** *27*, 172-176.

(64) Tan, X.; Fenniri, H.; Gray, M. R. Pyrene Derivatives of 2, 2′-Bipyridine as Models for Asphaltenes: Synthesis, Characterization, and Supramolecular Organization. *Energy Fuels* **2007,** *22*, 715-720.

(65) Gray, M. R.; Tykwinski, R. R.; Stryker, J. M.; Tan, X. Supramolecular Assembly Model for Aggregation of Petroleum Asphaltenes. *Energy Fuels* **2011,** *25*, 3125-3134.

(66) Murgich, J. Intermolecular Forces in Aggregates of Asphaltenes and Resins. *Petrol. Sci. Technol.* **2002,** *20*, 983-997.

(67) Tan, X.; Fenniri, H.; Gray, M. R. Water Enhances the Aggregation of Model Asphaltenes in Solution via Hydrogen Bonding. *Energy Fuels* **2009,** *23*, 3687-3693.

(68) Stoyanov, S. R.; Yin, C.; Gray, M. R.; Stryker, J. M.; Gusarov, S.; Kovalenko, A. Computational and Experimental Study of the Structure, Binding Preferences, and Spectroscopy of Nickel(II) and Vanadyl Porphyrins in Petroleum. *J. Phys. Chem. B* **2010,** *114*, 2180-2188.

(69) Rogel, E. Asphaltene Aggregation: A Molecular Thermodynamic Approach. *Langmuir* **2002,** *18*, 1928-1937.

(70) Rogel, E. Thermodynamic Modeling of Asphaltene Aggregation. *Langmuir* **2004,** *20*, 1003-1012.

(71) Rogel, E. Molecular Thermodynamic Approach to the Formation of Mixed Asphaltene-Resin Aggregates. *Energy Fuels* **2008,** *22*, 3922-3929.

(72) Agrawala, M.; Yarranton, H. W. An Asphaltene Association Model Analogous to Linear Polymerization. *Ind. Eng. Chem. Res.* **2001,** *40*, 4664-4672.

(73) Zhang, L.; Shi, Q.; Zhao, C.; Zhang, N.; Chung, K. H.; Xu, C.; Zhao, S. Hindered Stepwise Aggregation Model for Molecular Weight Determination of Heavy Petroleum Fractions by Vapor Pressure Osmometry (VPO). *Energy Fuels* **2013,** *27*, 1331-1336.

(74) Zhang, L.; Zhao, S.; Xu, Z.; Chung, K. H.; Zhao, C.; Zhang, N.; Xu, C.; Shi, Q. Molecular Weight and Aggregation of Heavy Petroleum Fractions Measured by Vapor Pressure Osmometry and Hindered Stepwise Aggregation Model. *Energy Fuels* **2014,** *28,* 6179-6187.

(75) Acevedo, S.; Caetano, M.; Ranaudo, M. A.; Jaimes, B. Simulation of Asphaltene Aggregation and Related Properties Using an Equilibrium-Based Mathematical Model. *Energy Fuels* **2011,** *25*, 3544-3551.

(76) Andersen, S. I.; Speight, J. G. Thermodynamic Models for Asphaltene Solubility and Precipitation. *J. Pet. Sci. Eng.* **1999,** *22*, 53-66.

(77) Hirschberg, A.; DeJong, L.; Schipper, B.; Meijer, J. Influence of Temperature and Pressure on Asphaltene Flocculation. *Soc. Pet. Eng. J.* **1984,** *24*, 283-293.

(78) Leontaritis, K.; Mansoori, G. Asphaltene Flocculation During Oil Production and Processing: A Thermodynamic Colloidal model. Presented at the SPE International Symposium on Oil field Chemistry, San Antonio, TX, Feb. 4–6, 1987; Paper SPE 16258.

(79) Flory, P. J. Thermodynamics of High Polymer Solutions. *J. Chem. Phys.* **1942,** *10*, 51-61.

(80) Huggins, M. L. Solutions of Long Chain Compounds. *J. Chem. Phys.* **1941,** *9*, 440-440.

(81) Victorov, A. I.; Firoozabadi, A. Thermodynamic Micellization Model of Asphaltene Precipitation from Petroleum Fluids. *AIChE J.* **1996,** *42*, 1753-1764.

(82) Pan, H.; Firoozabadi, A. Thermodynamic Micellization Model for Asphaltene Aggregation and Precipitation in Petroleum Fluids. *SPE Prod. Facil.* **1998,** *13*, 118-127.

(83) Hinze, W. L.; Pramauro, E. A Critical Review of Surfactant-Mediated Phase Separations (Cloud-Point Extractions): Theory and Applications. *Crit. Rev. Anal. Chem.* **1993,** *24*, 133-177.

(84) Peng, D.; Robinson, D. B. A New Two-Constant Equation of State. *Ind. Eng. Chem. Fundam.* **1976,** *15*, 59-64.

(85) Ashoori, S.; Shahsavani, B.; Ahmadi, M. A.; Rezaei, A. Developing Thermodynamic

Micellization Approach to Model Asphaltene Precipitation Behavior. *J. Dispersion Sci. Technol.* **2013**, *35,* 1325-1338.

(86) Wu, J.; Prausnitz, J. M.; Firoozabadi, A. Molecular-Thermodynamic Framework for Asphaltene-Oil Equilibria. *AIChE J.* **1998,** *44*, 1188-1199.

(87) Victorov, A. I.; Smirnova, N. A. Thermodynamic Model of Petroleum Fluids Containing Polydisperse Asphaltene Aggregates. *Ind. Eng. Chem. Res.* **1998,** *37*, 3242-3251.

(88) Victorov, A. I.; Smirnova, N. A. Description of Asphaltene Polydispersity and Precipitation by Means of Thermodynamic Model of Self-Assembly. *Fluid Phase Equilib.* **1999,** *158*, 471-480.

(89) Hildebrand, J.; Scott, R. *Solubility of Nonelectrolytes;* Reinhold Pub. Corp.: New York 1950.

(90) Correra, S.; Donaggio, F. OCCAM: Onset-Constrained Colloidal Asphaltene Model. Presented at the SPE International Symposium on Formation Damage, Lafayette, LA, Feb. 23-24, 2000; Paper SPE 58724.

(91) Correra, S.; Merino-Garcia, D. Simplifying the Thermodynamic Modeling of Asphaltenes in Upstream Operations. *Energy Fuels* **2007,** *21*, 1243-1247.

(92) Merino-Garcia, D.; Correra, S. A Shortcut Application of a Flory-Like Model to Asphaltene Precipitation. *J. Dispersion Sci. Technol.* **2007,** *28*, 339-347.

(93) Burke, N. E.; Hobbs, R. E.; Kashou, S. F. Measurement and Modeling of Asphaltene Precipitation (includes associated paper 23831). *J. Pet. Technol.* **1990,** *42*, 1,440-1,446.

(94) Novosad, Z.; Costain, T. G. Experimental and Modeling Studies of Asphaltene Equilibria for a Reservoir Under CO_2 Injection. Presented at the Annual Technical

Conference and Exhibition of the Society of Petroleum Engineers, New Orleans, LA, Sept. 23-26, 1990; Paper SPE 20530.

(95) Hirschberg, A.; Hermans, L. Hirschberg, A.; Hermans, L. Asphaltene Phase Behavior: A Molecular Thermodynamic Model. Characterization of Heavy Crude Oils and Petroleum Residues, Symposium Internationale, Lyon June 25−27, 1984; Editions Technip, 492-497.

(96) Kawanaka, S.; Park, S.; Mansoori, G. A. Organic Deposition from Reservoir Fluids: A Thermodynamic Predictive. *SPE Reservoir Eng.* **1991,** *6*, 185-192.

(97) Scott, R. L.; Magat, M. The Thermodynamics of High-Polymer Solutions: I. The Free Energy of Mixing of Solvents and Polymers of Heterogeneous Distribution. *J. Chem. Phys.* **1945,** *13*, 172-177.

(98) Manshad, A. K.; Edalat, M. Application of Continuous Polydisperse Molecular Thermodynamics for Modeling Asphaltene Precipitation in Crude Oil Systems. *Energy Fuels* **2008,** *22*, 2678-2686.

(99) Browarzik, D.; Laux, H.; Rahimian, I. Asphaltene Flocculation in Crude Oil Systems. *Fluid Phase Equilib.* **1999,** *154*, 285-300.

(100) Browarzik, C.; Browarzik, D. Modeling the Onset of Asphaltene Flocculation at High Pressure by an Association Model. *Pet. Sci. Technol.* **2005,** *23*, 795-810.

(101) Browarzik, D.; Kabatek, R.; Kahl, H.; Laux, H. Flocculation of Asphaltenes at High Pressure. II. Calculation of the Onset of Flocculation. *Pet. Sci. Technol.* **2002,** *20*, 233-249.

(102) Yarranton, H. W.; Masliyah, J. H. Molar Mass Distribution and Solubility Modeling of Asphaltenes. *AIChE J.* **1996,** *42*, 3533-3543.

(103) Nor-Azlan, N.; Adewumi, M. Development of Asphaltene Phase Equilibria Predictive Model. Present at SPE Eastern Regional Meeting: Pittsburgh, PA, 2−4 Nov. 1993; Paper SPE 26905.

(104) Alboudwarej, H.; Akbarzadeh, K.; Beck, J.; Svrcek, W. Y.; Yarranton, H. W. Regular Solution Model for Asphaltene Precipitation from Bitumens and Solvents. *AIChE J.* **2003,** *49*, 2948-2956.

(105) Akbarzadeh, K.; Dhillon, A.; Svrcek, W. Y.; Yarranton, H. W. Methodology for the Characterization and Modeling of Asphaltene Precipitation from Heavy Oils Diluted with n-Alkanes. *Energy Fuels* **2004,** *18*, 1434-1441.

(106) Wiehe, I. A.; Yarranton, H. W.; Akbarzadeh, K.; Rahimi, P. M.; Teclemariam, A. The Paradox of Asphaltene Precipitation with Normal Paraffins. *Energy Fuels* **2005,** *19*, 1261-1267.

(107) Tharanivasan, A. K.; Yarranton, H. W.; Taylor, S. D. Application of a Regular Solution-Based Model to Asphaltene Precipitation from Live Oils. *Energy Fuels* **2010,** *25*, 528-538.

(108) Cimino, R.; Correra, S.; Sacomani, P. A.; Carniani, C. Thermodynamic Modelling for Prediction of Asphaltene Deposition in Live Oils. Presented at the SPE International Symposium on Oilfield Chemistry, San Antonio, TX, Feb. 14–17, 1995; Paper SPE 28993.

(109) Wang, J.; Buckley, J. A Two-Component Solubility Model of the Onset of Asphaltene Flocculation in Crude Oils. *Energy Fuels* **2001,** *15*, 1004-1012.

(110) Buckley, J.; Hirasaki, G.; Liu, Y.; Von Drasek, S.; Wang, J.; Gill, B. Asphaltene Precipitation and Solvent Properties of Crude oils. *Pet. Sci. Technol.* **1998,** *16*, 251-

285.

(111) Mohammadi, A. H.; Richon, D. A Monodisperse Thermodynamic Model for Estimating Asphaltene Precipitation. *AIChE J.* **2007,** *53*, 2940-2947.

(112) Mohammadi, A. H.; Eslamimanesh, A.; Richon, D. Monodisperse Thermodynamic Model Based on Chemical Flory–Huggins Polymer Solution Theories for Predicting Asphaltene Precipitation. *Ind. Eng. Chem. Res.* **2012,** *51*, 4041-4055.

(113) Pazuki, G.; Nikookar, M. A Modified Flory-Huggins Model for Prediction of Asphaltenes Precipitation in Crude Oil. *Fuel* **2006,** *85*, 1083-1086.

(114) Mofidi, A. M.; Edalat, M. A Simplified Thermodynamic Modeling Procedure for Predicting Asphaltene Precipitation. *Fuel* **2006,** *85*, 2616-2621.

(115) Nourbakhsh, H.; Yazdizadeh, M.; Esmaeilzadeh, F. Prediction of Asphaltene Precipitation by the Extended Flory–Huggins Model Using the Modified Esmaeilzadeh–Roshanfekr Equation of State. *J. Pet. Sci. Eng.* **2011,** *80*, 61-68.

(116) Orangi, H. S.; Modarress, H.; Fazlali, A.; Namazi, M. Phase Behavior of Binary Mixture of Asphaltene + Solvent and Ternary Mixture of Asphaltene + Solvent + Precipitant. *Fluid Phase Equilib.* **2006,** *245*, 117-124.

(117) Mousavi-Dehghani, S.; Mirzayi, B.; Mousavi, S. M. H.; Fasih, M. An Applied and Efficient Model for Asphaltene Precipitation in Production and Miscible Gas Injection Processes. *Pet. Sci. Technol.* **2010,** *28*, 113-124.

(118) Miller A. R. The Vapor-Pressure Equations of Solutions and the Osmotic Pressure of Rubber. *Proc. Cambridge Philos. Soc.* **1943,** *39*, 131-131.

(119) Yang, Z.; Ma, C.; Lin, X.; Yang, J.; Guo, T. Experimental and Modeling Studies on the Asphaltene Precipitation in Degassed and Gas-Injected Reservoir Oils. *Fluid*

Phase Equilib. **1999,** *157*, 143-158.

(120) Akbarzadeh, K.; Ayatollahi, S.; Moshfeghian, M.; Alboudwarej, H.; Yarranton, H. Estimation of SARA Fraction Properties with the SRK EOS. *J. Can. Pet. Technol.* **2004,** *43*, 31-39.

(121) Du, J. L.; Zhang, D. A Thermodynamic Model for the Prediction of Asphaltene Precipitation. *Pet. Sci. Technol.* **2004,** *22*, 1023-1033.

(122) Anderko, A. Extension of the AEOS Model to Systems Containing Any Number of Associating and Inert Components. *Fluid Phase Equilib.* **1989,** *50*, 21-52.

(123) Ikonomou, G.; Donohue, M. D. Thermodynamics of Hydrogen-Bonded Molecules: The Associated Perturbed Anisotropic Chain theory. *AIChE J.* **1986,** *32*, 1716-1725.

(124) Ikonomou, G. D.; Donohue, M. D. Extension of the Associated Perturbed Anisotropic Chain Theory to Mixtures with More than One Associating Component. *Fluid Phase Equilib.* **1988,** *39*, 129-159.

(125) Vafaie-Sefti, M.; Mousavi-Dehghani, S. A.; Mohammad-Zadeh, M. A Simple Model for Asphaltene Deposition in Petroleum Mixtures. *Fluid Phase Equilib.* **2003,** *206*, 1-11.

(126) Sabbagh, O.; Akbarzadeh, K.; Badamchi-Zadeh, A.; Svrcek, W.; Yarranton, H. Applying the PR-EoS to Asphaltene Precipitation from n-Alkane Diluted Heavy Oils and Bitumens. *Energy Fuels* **2006,** *20*, 625-634.

(127) Agrawal, P.; Schoeggl, F.; Satyro, M.; Taylor, S.; Yarranton, H. Measurement and Modeling of the Phase Behavior of Solvent Diluted Bitumens. *Fluid Phase Equilib.* **2012,** *334*, 51-64.

(128) Li, Z.; Firoozabadi, A. Modeling Asphaltene Precipitation by n-Alkanes from Heavy

Oils and Bitumens Using Cubic-Plus-Association Equation of State. *Energy Fuels* **2010,** *24*, 1106-1113.

(129) Kontogeorgis, G. M.; Voutsas, E. C.; Yakoumis, I. V.; Tassios, D. P. An Equation of State for Associating Fluids. *Ind. Eng. Chem. Res.* **1996,** *35*, 4310-4318.

(130) Wertheim, M. Fluids with Highly Directional Attractive Forces. I. Statistical Thermodynamics. *J. Stat. Phys.* **1984,** *35*, 19-34.

(131) Wertheim, M. Fluids with Highly Directional Attractive Forces. II. Thermodynamic Perturbation Theory and Integral Equations. *J. Stat. Phys.* **1984,** *35*, 35-47.

(132) Wertheim, M. Fluids of Dimerizing Hard Spheres, and Fluid Mixtures of Hard Spheres and Dispheres. *J. Chem. Phys.* **1986,** *85*, 2929-2936.

(133) Wertheim, M. Fluids with Highly Directional Attractive Forces. III. Multiple Attraction Sites. *J. Stat. Phys.***1986,** *42*, 459-476.

(134) Wertheim, M. Fluids with Highly Directional Attractive Forces. IV. Equilibrium Polymerization. *J. Stat. Phys.* **1986,** *42*, 477-492.

(135) Wertheim, M. Thermodynamic Perturbation Theory of Polymerization. *J. Chem. Phys.* **1987,** *87*, 7323-7331.

(136) Li, Z.; Firoozabadi, A. Cubic-Plus-Association Equation of State for Asphaltene Precipitation in Live Oils. *Energy Fuels* **2010,** *24*, 2956-2963.

(137) Saeedi Dehaghani, A.; Sefti, M. V.; Amerighasrodashti, A. The Application of a New Association Equation of State (AEOS) for Prediction of Asphaltenes and Resins Deposition During CO_2 Gas Injection. *Pet. Sci. Technol.* **2012,** *30*, 1548-1561.

(138) Chapman, W. G.; Jackson, G.; Gubbins, K. E. Phase Equilibria of Associating Fluids. Chain Molecules with Multiple Bonding Sites. *Mol. Phys.* **1988,** *65*, 1057-1079.

(139) Chapman, W. G.; Gubbins, K. E.; Jackson, G.; Radosz, M. New Reference Equation of State for Associating Liquids. *Ind. Eng. Chem. Res.* **1990,** *29*, 1709-1721.

(140) David Ting, P.; Hirasaki, G. J.; Chapman, W. G. Modeling of Asphaltene Phase Behavior with the SAFT Equation of State. *Pet. Sci. Technol.* **2003,** *21*, 647-661.

(141) Gross, J.; Sadowski, G. Perturbed-Chain SAFT: An Equation of State Based on a Perturbation Theory for Chain Molecules. *Ind. Eng. Chem. Res.* **2001,** *40*, 1244-1260.

(142) Barker, J. A.; Henderson, D. Perturbation Theory and Equation of State for Fluids: The Square-Well Potential. *J. Chem. Phys.* **1967,** *47*, 2856-2861.

(143) Barker, J. A.; Henderson, D. Perturbation Theory and Equation of State for Fluids. II. A Successful Theory of Liquids. *J. Chem. Phys.* **1967,** *47*, 4714-4721.

(144) Vargas, F. M.; Gonzalez, D. L.; Hirasaki, G. J.; Chapman, W. G. Modeling Asphaltene Phase Behavior in Crude Oil Systems Using the Perturbed Chain Form of the Statistical Associating Fluid Theory (PC-SAFT) Equation of State. *Energy Fuels* **2009,** *23*, 1140-1146.

(145) Panuganti, S. R.; Tavakkoli, M.; Vargas, F. M.; Gonzalez, D. L.; Chapman, W. G. SAFT Model for Upstream Asphaltene Applications. *Fluid Phase Equilib.* **2013,** *359*, 2-16.

(146) Panuganti, S. R.; Vargas, F. M.; Gonzalez, D. L.; Kurup, A. S.; Chapman, W. G. PC-SAFT Characterization of Crude Oils and Modeling of Asphaltene Phase Behavior. *Fuel* **2012,** *93*, 658-669.

(147) Gonzalez, D. L.; Hirasaki, G. J.; Creek, J.; Chapman, W. G. Modeling of Asphaltene Precipitation Due to Changes in Composition Using the Perturbed Chain Statistical Associating Fluid Theory Equation of State. *Energy Fuels* **2007,** *21*, 1231-1242.

(148) Tavakkoli, M.; Panuganti, S. R.; Taghikhani, V.; Pishvaie, M. R.; Chapman, W. G. Understanding the Polydisperse Behavior of Asphaltenes during Precipitation. *Fuel* **2014,** *117*, 206-217.

(149) Zúñiga-Hinojosa, M. A.; Justo-García, D. N.; Aquino-Olivos, M. A.; Román-Ramírez, L. A.; García-Sánchez, F. Modeling of Asphaltene Precipitation from n-Alkane Diluted Heavy Oils and Bitumens Using the PC-SAFT Equation of State. *Fluid Phase Equilib.* **2014,** *376*, 210-224.

(150) Gil-Villegas, A.; Galindo, A.; Whitehead, P. J.; Mills, S. J.; Jackson, G.; Burgess, A. N. Statistical Associating Fluid Theory for Chain Molecules with Attractive Potentials of Variable Range. *J. Chem. Phys.* **1997,** *106*, 4168-4186.

(151) Artola, P.; Pereira, F. E.; Adjiman, C. S.; Galindo, A.; Müller, E. A.; Jackson, G.; Haslam, A. J. Understanding the Fluid Phase Behaviour of Crude Oil: Asphaltene Precipitation. *Fluid Phase Equilib.* **2011,** *306*, 129-136.

(152) Wu, J.; Prausnitz, J. M.; Firoozabadi, A. Molecular Thermodynamics of Asphaltene Precipitation in Reservoir Fluids. *AIChE J.* **2000,** *46*, 197-209.

(153) Buenrostro-Gonzalez, E.; Lira-Galeana, C.; Gil-Villegas, A.; Wu, J. Asphaltene Precipitation in Crude Oils: Theory and Experiments. *AIChE J.* **2004,** *50*, 2552-2570.

(154) Aquino-Olivos, M. A.; Grolier, J. E.; Randzio, S. L.; Aguirre-Gutiérrez, A. J.; García-Sánchez, F. Determination of the Asphaltene Precipitation Envelope and Bubble Point Pressure for a Mexican Crude Oil by Scanning Transitiometry. *Energy Fuels* **2013,** *27*, 1212-1222.

(155) Rassamdana, H.; Dabir, B.; Nematy, M.; Farhani, M.; Sahimi, M. Asphalt Flocculation and Deposition: I. The Onset of Precipitation. *AIChE J.* **1996,** *42*, 10-22.

(156) Rassamdana, H.; Sahimi, M. Asphalt Flocculation and Deposition: II. Formation and Growth of Fractal Aggregates. *AIChE J.* **1996,** *42*, 3318-3332.

(157) Hu, Y.; Chen, G.; Yang, J.; Guo, T. A Study on the Application of Scaling Equation for Asphaltene Precipitation. *Fluid Phase Equilib.* **2000,** *171*, 181-195.

(158) Duda, Y.; Lira-Galeana, C. Thermodynamics of Asphaltene Structure and Aggregation. *Fluid Phase Equilib.* **2006,** *241*, 257-267.

(159) Zahedi, G.; Fazlali, A.; Hosseini, S.; Pazuki, G.; Sheikhattar, L. Prediction of Asphaltene Precipitation in Crude Oil. *J. Pet. Sci. Eng.* **2009,** *68*, 218-222.

(160) Na'imi, S. R.; Gholami, A.; Asoodeh, M. Prediction of Crude Oil Asphaltene Precipitation Using Support Vector Regression. *J. Dispersion Sci. Technol.* **2014,** *35*, 518-523.

(161) Alvarez-Ramirez, F.; Ramirez-Jaramillo, E.; Ruiz-Morales, Y. Calculation of the Interaction Potential Curve between Asphaltene−Asphaltene, Asphaltene−Resin, and Resin−Resin Systems Using Density Functional Theory. *Energy Fuels* **2006,** *20*, 195-204.

(162) Harris, J. Simplified Method for Calculating the Energy of Weakly Interacting Fragments. *Physical Review B* **1985,** *31*, 1770.

(163) Vosko, S.; Wilk, L.; Nusair, M. Accurate Spin-Dependent Electron Liquid Correlation Energies for Local Spin Density Calculations: A Critical Analysis. *Can. J. Phys.* **1980,** *58*, 1200-1211.

(164) Perdew, J. P.; Wang, Y. Accurate and Simple Analytic Representation of the Electron-Gas Correlation Energy. *Phys. Rev. B* **1992,** *45,* 13244– 13249.

(165) Delley, B. An All-Electron Numerical Method for Solving the Local Density

Functional for Polyatomic Molecules. *J. Chem. Phys.* **1990,** *92*, 508-517.

(166) Moreira da Costa, L.; Stoyanov, S. R.; Gusarov, S.; Seidl, P. R.; Walkimar de M. Carneiro, José; Kovalenko, A. Computational Study of the Effect of Dispersion Interactions on the Thermochemistry of Aggregation of Fused Polycyclic Aromatic Hydrocarbons as Model Asphaltene Compounds in Solution. *J. Phys. Chem. A* **2014,** *118*, 896-908.

(167) Grimme, S. Improved Second-Order Møller–Plesset Perturbation Theory by Separate Scaling of Parallel- and Antiparallel-Spin Pair Correlation Energies. *J. Chem. Phys.* **2003,** *118*, 9095-9102.

(168) Takatani, T.; Hohenstein, E. G.; Sherrill, C. D. Improvement of the Coupled-Cluster Singles and Doubles Method via Scaling Same- and Opposite-Spin Components of the Double Excitation Correlation Energy. *J. Chem. Phys.* **2008,** *128*, 124111.

(169) Frisch, M. J.; Head-Gordon, M.; Pople, J. A. A Direct MP2 Gradient Method. *Chem. Phys. Lett.* **1990,** *166*, 275-280.

(170) Head-Gordon, M.; Head-Gordon, T. Analytic MP2 Frequencies without Fifth-Order Storage. Theory and Application to Bifurcated Hydrogen Bonds in the Water Hexamer. *Chem. Phys. Lett.* **1994,** *220*, 122-128.

(171) Frisch, M. J.; Pople, J. A.; Binkley, J. S. Self-Consistent Molecular Orbital Methods 25. Supplementary Functions for Gaussian Basis Sets. *J. Chem. Phys.* **1984,** *80*, 3265-3269.

(172) Rassolov, V. A.; Ratner, M. A.; Pople, J. A.; Redfern, P. C.; Curtiss, L. A. 6-31G* Basis Set for Third-Row Atoms. *J. Comput. Chem.* **2001,** *22*, 976-984.

(173) Barone, V.; Cossi, M. Quantum Calculation of Molecular Energies and Energy Gradients in Solution by a Conductor Solvent Model. *J. Phys. Chem. A* **1998,** *102*,

1995-2001.

(174) Cossi, M.; Rega, N.; Scalmani, G.; Barone, V. Energies, Structures, and Electronic Properties of Molecules in Solution with the C-PCM Solvation Model. *J. Comput. Chem.* **2003,** *24*, 669-681.

(175) da Costa, L. M.; Stoyanov, S. R.; Gusarov, S.; Tan, X.; Gray, M. R.; Stryker, J. M.; Tykwinski, R.; de M. Carneiro, J Walkimar; Seidl, P. R.; Kovalenko, A. Density Functional Theory Investigation of the Contributions of π− π Stacking and Hydrogen-Bonding Interactions to the Aggregation of Model Asphaltene Compounds. *Energy Fuels* **2012,** *26*, 2727-2735.

(176) Chai, J.; Head-Gordon, M. Long-Range Corrected Hybrid Density Functionals with Damped Atom–Atom Dispersion Corrections. *Phys. Chem. Chem. Phys.* **2008,** *10*, 6615-6620.

(177) Tomasi, J.; Mennucci, B.; Cammi, R. Quantum Mechanical Continuum Solvation Models. *Chem. Rev.* **2005,** *105*, 2999-3094.

(178) da Costa, L. M.; Hayaki, S.; Stoyanov, S. R.; Gusarov, S.; Tan, X.; Gray, M. R.; Stryker, J. M.; Tykwinski, R.; Carneiro, J. d. M.; Sato, H. 3D-RISM-KH Molecular Theory of Solvation and Density Functional Theory Investigation of the Role of Water in the Aggregation of Model Asphaltenes. *Phys. Chem. Chem. Phys.* **2012,** *14*, 3922-3934.

(179) Carauta, A. N.; Correia, J. C.; Seidl, P. R.; Silva, D. M. Conformational Search and Dimerization Study of Average Structures of Asphaltenes. *J. Mol. Struct. (Theochem)* **2005,** *755*, 1-8.

(180) Castellano, O.; Gimon, R.; Soscun, H. Theoretical Study of the σ-π and π-π

Interactions in Heteroaromatic Monocyclic Molecular Complexes of Benzene, Pyridine, and Thiophene Dimers: Implications on the Resin Asphaltene Stability in Crude Oil. *Energy Fuels* **2011,** *25*, 2526-2541.

(181) Brandt, H.; Hendriks, E.; Michels, M.; Visser, F. Thermodynamic Modeling of Asphaltene Stacking. *J. Phys. Chem.* **1995,** *99*, 10430-10432.

(182) Ortega-Rodriguez, A.; Lira-Galeana, C.; Ruiz-Morales, Y.; Cruz, S. A. Interaction Energy in Maya-Oil Asphaltenes: A Molecular Mechanics Study. *Pet. Sci. Technol.* **2001,** *19*, 245-256.

(183) Pacheco-Sánchez, J. H.; Alvarez-Ramírez, F.; Martínez-Magadán, J. Aggregate Asphaltene Structural Models. *Prepr. Am. Chem. Soc., Div. Pet. Chem.* **2003,** *48*, 71-73.

(184) Pacheco-Sánchez, J. H.; Alvarez-Ramirez, F.; Martínez-Magadán, J. Morphology of Aggregated Asphaltene Structural Models. *Energy Fuels* **2004,** *18*, 1676-1686.

(185) Murgich, J.; Merino-Garcia, D.; Andersen, S. I.; Manuel del Río, J.; Galeana, C. L. Molecular Mechanics and Microcalorimetric Investigations of the Effects of Molecular Water on the Aggregation of Asphaltenes in Solutions. *Langmuir* **2002,** *18*, 9080-9086.

(186) Murgich, J.; Rodríguez, J.; Aray, Y. Molecular Recognition and Molecular Mechanics of Micelles of Some Model Asphaltenes and Resins. *Energy Fuels* **1996,** *10*, 68-76.

(187) Murgich, J.; Strausz, O. P. Molecular Mechanics of Aggregates of Asphaltenes and Resins of the Athabasca Oil. *Pet. Sci. Technol.* **2001,** *19*, 231-243.

(188) Murgich, J. Molecular Simulation and the Aggregation of the Heavy Fractions in Crude Oils. *Mol. Simul.* **2003,** *29*, 451-461.

(189) Rogel, E. Simulation of Interactions in Asphaltene Aggregates. *Energy Fuels* **2000,** *14*,

566-574.

(190) Pacheco-Sánchez, J. H.; Zaragoza, I.; Martinez-Magadan, J. Asphaltene Aggregation under Vacuum at Different Temperatures by Molecular Dynamics. *Energy Fuels* **2003,** *17*, 1346-1355.

(191) Takanohashi, T.; Sato, S.; Saito, I.; Tanaka, R. Molecular Dynamics Simulation of the Heat-Induced Relaxation of Asphaltene Aggregates. *Energy Fuels* **2003,** *17*, 135-139.

(192) Mitchell, D. L.; Speight, J. G. The Solubility of Asphaltenes in Hydrocarbon Solvents. *Fuel* **1973,** *52*, 149-152.

(193) Permsukarome, P.; Chang, C.; Fogler, H. S. Kinetic Study of Asphaltene Dissolution in Amphiphile/Alkane Solutions. *Ind. Eng. Chem. Res.* **1997,** *36*, 3960-3967.

(194) Speight, J. G.; Long, R. B.; Trowbridge, T. D.; Linden, N. On the Definition of Asphaltenes. *Am. Chem. Soc., Div. Pet. Chem., Prepr.* **1982,** *27*, 268-275.

(195) Boek, E. S.; Yakovlev, D. S.; Headen, T. F. Quantitative Molecular Representation of Asphaltenes and Molecular Dynamics Simulation of Their Aggregation. *Energy Fuels* **2009,** *23*, 1209-1219.

(196) Rogel, E. Studies on Asphaltene Aggregation via Computational Chemistry. *Colloids Surf., A.* **1995,** *104*, 85-93.

(197) Headen, T. F.; Boek, E. S.; Skipper, N. T. Evidence for Asphaltene Nanoaggregation in Toluene and Heptane from Molecular Dynamics Simulations. *Energy Fuels* **2009,** *23*, 1220-1229.

(198) Ungerer, P.; Rigby, D.; Leblanc, B.; Yiannourakou, M. Sensitivity of the Aggregation Behaviour of Asphaltenes to Molecular Weight and Structure Using Molecular Dynamics. *Mol. Simul.* **2014,** *40*, 115-122.

(199) Kuznicki, T.; Masliyah, J. H.; Bhattacharjee, S. Molecular Dynamics Study of Model Molecules Resembling Asphaltene-Like Structures in Aqueous Organic Solvent Systems. *Energy Fuels* **2008,** *22*, 2379-2389.

(200) Sedghi, M.; Goual, L.; Welch, W.; Kubelka, J. Effect of Asphaltene Structure on Association and Aggregation Using Molecular Dynamics. *J. Phys. Chem. B* **2013,** *117*, 5765-5776.

(201) Teklebrhan, R. B.; Ge, L.; Bhattacharjee, S.; Xu, Z.; Sjöblom, J. Probing Structure–Nanoaggregation Relations of Polyaromatic Surfactants: A Molecular Dynamics Simulation and Dynamic Light Scattering Study. *J. Phys. Chem. B* **2012,** *116*, 5907-5918.

(202) Carauta, A. N.; Seidl, P. R.; Chrisman, E. C.; Correia, J. C.; Menechini, P. d. O.; Silva, D. M.; Leal, K. Z.; de Menezes, S. M.; de Souza, W. F.; Teixeira, M. A. Modeling Solvent Effects on Asphaltene Dimers. *Energy Fuels* **2005,** *19*, 1245-1251.

(203) Frigerio, F.; Molinari, D. A Multiscale Approach to the Simulation of Asphaltenes. *Comput. Theor. Chem.* **2011,** *975*, 76-82.

(204) Takanohashi, T.; Sato, S.; Tanaka, R. Molecular Dynamics Simulation of Structural Relaxation of Asphaltene Aggregates. *Pet. Sci. Technol.* **2003,** *21*, 491-505.

(205) Pacheco-Sánchez, J. H.; Zaragoza, I.; Martínez-Magadán, J. Preliminary Study of the Effect of Pressure on Asphaltene Disassociation by Molecular Dynamics. *Pet. Sci. Technol.* **2004,** *22*, 927-942.

(206) Headen, T. F.; Boek, E. S. Molecular Dynamics Simulations of Asphaltene Aggregation in Supercritical Carbon Dioxide with and without Limonene. *Energy Fuels* **2010,** *25*, 503-508.

(207) Hu, M.; Shao, C.; Dong, L.; Zhu, J. Molecular Dynamics Simulation of Asphaltene Deposition During CO_2 Miscible Flooding. *Pet. Sci. Technol.* **2011,** *29*, 1274-1284.

(208) Zhang, L.; Greenfield, M. L. Molecular Orientation in Model Asphalts Using Molecular Simulation. *Energy Fuels* **2007,** *21*, 1102-1111.

(209) Diallo, M. S.; Strachan, A.; Faulon, J.; Goddard III, W. A. Thermodynamic Properties of Asphaltenes Through Computer Assisted Structure Elucidation and Atomistic Simulations. 1. Bulk Arabian Light asphaltenes. *Pet. Sci. Technol.* **2004,** *22*, 877-899.

(210) Aray, Y.; Hernández-Bravo, R.; Parra, J. G.; Rodríguez, J.; Coll, D. S. Exploring the Structure–Solubility Relationship of Asphaltene Models in Toluene, Heptane, and Amphiphiles Using a Molecular Dynamic Atomistic Methodology. *J. Phys. Chem. A* **2011,** *115*, 11495-11507.

(211) Hansen, C. M. *Hansen Solubility Parameters: A User's Handbook;* 2nd ed.; CRC press: Hoboken, 2007.

(212) Aguilera-Mercado, B.; Herdes, C.; Murgich, J.; Müller, E. Mesoscopic Simulation of Aggregation of Asphaltene and Resin Molecules in Crude Oils. *Energy Fuels* **2006,** *20*, 327-338.

(213) Ortega-Rodríguez, A.; Cruz, S. A.; Gil-Villegas, A.; Guevara-Rodriguez, F.; Lira-Galeana, C. Molecular View of the Asphaltene Aggregation Behavior in Asphaltene−Resin Mixtures. *Energy Fuels* **2003,** *17*, 1100-1108.

(214) Zhang, S.; Sun, L. L.; Xu, J.; Wu, H.; Wen, H. Aggregate Structure in Heavy Crude Oil: Using a Dissipative Particle Dynamics Based Mesoscale Platform. *Energy Fuels* **2010,** *24*, 4312-4326.

(215) Zhang, S.; Xu, J.; Wen, H.; Bhattacharjee, S. Integration of Rotational Algorithms into

Dissipative Particle Dynamics: Modeling Polyaromatic Hydrocarbons on the Meso-Scale. *Mol. Phys.* **2011,** *109*, 1873-1888.

(216) Wang, S.; Xu, J.; Wen, H. The Aggregation and Diffusion of Asphaltenes Studied by GPU-Accelerated Dissipative Particle dynamics. *Comput. Phys. Commun.* **2014,** *185*, 3069-3078.

Chapter 3: Probing the Effect of Side-Chain Length on the Aggregation of a Model Asphaltene in Water*

3.1. Introduction

Asphaltenes, which are the heaviest fraction of crude oil and classified as a complex mixture of heavy organic molecules, have drawn great interest because of its serious effect on the processing of petroleum resources from clogging pipelines to reducing oil recovery.[1,2] Most of these problems can be attributed to the aggregation and precipitation behavior of asphaltenes,[3,4] which have been widely observed in experimental studies. For example, VPO,[5,6] interfacial tension measurements,[6] small angle X-ray scattering,[7] small-angle neutron scattering,[5,8] calorimetric titration,[9] photon correlation spectroscopy[10] and NMR[11,12] have all shown the aggregation of asphaltenes. A wide range of experimental studies have been shown[13] to be consistent with the Yen-Mullins model[14,15] where it is proposed[13] that in organic solvents and at sufficient concentration, aspahtlene molecules form nanaoaggregates with aggregation number <10; and at higher concentration, these nanoaggregates form clusters with aggregation number <10. An excellent review of the experimental measurements and comparison with the Yen-Mullins model can be found in the work of Mullins et al.[13]

Due to the complexity and diversity of asphaltenes, different model compounds have been proposed in literature to represent the constituents of asphaltenes. According to their molecular architectures, these model compounds can be categorized into two different types, namely “continental” and “archipelago”. The continental model consists of a dominant PA core

*A version of this chapter has been published. Reprinted with permission from Jian, C.; Tang, T.; Bhattacharjee, S. Probing the Effect of Side-Chain Length on the Aggregation of a Model Asphaltene Using Molecular Dynamics Simulations. *Energy Fuels* **2013,** *27,* 2057-2067. Copyright 2013 American Chemical Society.

bonded to peripheral substituent side chains, while the archipelago model consists of small PA regions interconnected by alkyl chains.[16] The existence of these two types of aspaltenes is supported by different experimental observations. The molecular size of asphaltenes interrogated by time-resolved fluorescence depolarization studies indicated the existence of continental type asphaltenes,[17] while the cracked products of asphaltenes analyzed by Gray and co-works[18] using thin film pyrolysis are consistent with the structures of archipelago type of asphatlenes. Both types of asphaltene models have been used in literature to capture the aggregation behavior of asphaltene. For example, the Yen-Mullins model[14,15] for investigating asphaltene structure-function relationships, such as the structure-solubility relation, can be classified to the continental type. On the contrary, the asphaltene model compounds synthesized by Gray and co-workers[19] in studying asphaltene aggregation belong to the archipelago type.

Because of the difference in the model compounds, diverse kinds of driving forces and mechanisms for asphaltene aggregations have been proposed. Interaction between asphaltene molecules,[5] entropy effect,[12] asphaltene solution concentration,[20,21] solvent property[16,22] and other smaller polar compounds in crude oil (e.g. resins)[23,24] are all reported to affect asphaltene aggregation. It is of importance to mention the effect of solvent property since asphaltenes are defined as a solubility class of compounds that are toluene soluble and n-heptane insoluble.[6,25] Water, as a common inorganic solvent, is a "bad solvent" for asphatlenes. Aggregation of asphaltene in pure water and the enhancement effect of water on asphatlene aggregation in organic solvents have been observed.[16,26] Despite the ubiquitous existence of water in the processing of petroleum resources, its effect on asphaltene aggregation hasn't drawn enough attention.[14,27] The detailed mechanisms and structures of asphaltene aggregation in pure aqueous

environment is unclear in literature. In order to provide fundamental viewpoints for asphaltene aggregation in water, water was adopted as the solvent in our current work.

Among the various factors of asphaltene aggregation, the interactions between PA cores in both continental and archipelago models have generally been considered to be a major contributor to aggregation, even for asphaltenes with very long side chains (e.g. 20 aliphatic carbons in the side chain).[24] Because of such interactions, the preferred aggregated structure for neighboring asphaltene molecules consists of the stacking of their PA cores.[28] Considerable efforts have been spent on investigating the effect of functional groups of model asphaltenes on the interaction between PA cores. Of particular importance is the side chain, which is universal in the continental type of asphaltene molecules. Through investigating the melting points and solubilities of alkyl aromatics, it has been proposed[29] that the alkane chains of alkyl aromatics introduce a steric interference to the interactions between PA cores. The stacking of PA cores in the continental type of asphaltenes, which belongs to such aromatic systems, is believed to be disrupted by the same steric interference. The steric hindrance is further supported by the existence of CNACs of asphaltenes in organic solvents, as well as by the limit of the stacking (nanoaggregate) size detected by low-frequency impedance measurements, high-quality-factor (high-Q) ultrasonic spectroscopy and fluorescence quenching measurements.[20,30] Despite their steric effect, interaction between the side chains has been reported to be responsible for the formation and stabilization of asphaltene aggregates, which is supported by studies on the interactions between n-alkane and asphaltenes using titration calorimetry and inverse chromatography, and by investigations on the interaction energy between asphaltene molecules in vacuum using MD simulation.[31,32] In the latter case, Takanohashi et al.[32] compared the interaction energies between asphaltene molecules with and without aliphatic side chains and

found a decrease in the interaction energy when the aliphatic side chains were removed, leading to reduced stability of the aggregated structure.

Under the influence of side chains, different stacking structures of PA cores were reported in literature using molecular simulations. Pacheco-Sánchez et al.,[33] by simulating four molecular models with different PA core sizes and side-chain lengths (original chemical structures proposed by Groenzin and Mullins,[34] Speight and Moschopedis,[35,36] Zajac et al.,[37] and Murgich et al.[38]) in vacuum, observed face-to-face, as well as offset stacked and T-shaped geometries formed by neighboring PA cores. The type of stacking structure formed was shown to depend on the specific molecular model used.[33] Headen et al.[39] showed that the offset stacked geometry was the most favorable stacking structure for PA cores in toluene and heptane, while close contact between PA core and side chain group was also observed for the continental type of asphaltene models used in their work. Teklebrhan et al.[40] showed that their synthetic PA surfactants with n-alkane side chains preferred T-stacking or tail-to-tail arrangement (i.e. tail-tail contact) in toluene and heptane due to the strong steric interference of the branched side chains. Zhang et al.[41] investigated the effect of the length of the alkane branch on the stacking structure of asphaltenes in asphalt mixtures including asphaltene, resin and maltene model compounds. Two asphaltene molecular models were used in their work, one composed of many fused aromatic rings with very short chains and the other composed of fewer aromatic rings with long side chains. Their results showed that the probability density for the relative orientation between two neighboring PA cores had a peak at around 40° at room temperature (298.15 K) for asphaltene molecules with long alkane branches, whereas asphaltene molecules with short alkane branches preferred to stay almost parallel to one another at the same temperature.[41] These different results imply that the stacking structures of asphaltenes have a strong dependence on

the specific asphaltene molecular structure, especially the length of the side chains relative to the PA cores. To understand the role of side chain on asphaltene aggregation, it is important to investigate the asphaltene aggregation behavior under the influence of the side chain in a consistent manner.

In this chapter, we present the first systematic study that addresses the effect of the aliphatic side chain on asphaltene aggregation in water. In particular, we performed a series of MD simulations based on a commonly used surrogate of continental asphaltenes. The length of the side chain was systematically varied while maintaining a fixed PA core structure, and the dynamics of aggregation and the aggregated structures were analyzed. Our results show that the length of the aliphatic chain has a non-monotonic effect on the extent of the aggregation. The distinct aggregation and stacking structures caused by different side-chain lengths were then systematically analyzed. The remainder of this chapter is organized as follows: the molecular models studied and simulation procedures are described in section 3.2; the aggregation kinetics, mechanisms and aggregated structure are quantified and discussed in section 3.3; conclusions are given in section 3.4.

3.2. Methods

3.2.1. Simulated Systems

The asphaltene model simulated here is based on the polycyclic aromatic hydrocarbon compound, VO-78 ($C_{70}H_{84}O_6$),[42] which possesses some key structural and compositional features of continental asphaltenes with one large PA core region and two long aliphatic side chains per molecule. The VO-78 model does not contain any nitrogen or sulfur atoms, but it has been employed in literature as a standard PA compound to investigate the behaviors of asphaltenes,[43,44] and it is suitable for this study where the focus is to address the effect of the

aliphatic side chain on the aggregation behavior. The original VO-78 model contains 16 interconnected aliphatic hydrocarbons in each of its side chain. Asphaltene models with different side-chain lengths were obtained by decreasing the number of aliphatic hydrocarbons in the side chains to 12, 8 and 4, resulting in a total of four different molecular models. Throughout this chapter, these models will be referred to as VO-16C, VO-12C, VO-8C and VO-4C, respectively and their chemical structures are shown in Figure 3.1. The structure of VO-16C was obtained using Chem3D ultra 10.0 software. The structures of the other three molecular models were then obtained by manually removing certain number of terminal aliphatic hydrocarbons from the side chains of VO-16C.

Four systems were simulated to study the aggregation behavior of asphaltenes with different side-chain lengths, each of which contains 24 molecules of a single type of asphaltene models mentioned above. Each of these systems will be referred to by the name of the asphaltene molecules it contains. For example, the system that contains 24 VO-12C asphaltene molecules will be referred to as system VO-12C. In constructing the initial configuration of each system, the 24 asphaltene molecules were arranged with their PA cores parallel to one another, forming a $2 \times 3 \times 4$ array contained in a cubic box with an edge dimension of 12 nm. Following this, the box was randomly filled with water. These four systems represent a high concentration (~20 g/L) of asphaltene and formation of nanoaggregates is expected. The initial configurations of the simulated systems are available in Appendix A (section A.1).

3.2.2. Simulation Details

The topology for each of the asphaltene models was first generated by supplying the coordinates of the molecule to the GlycoBioChem PRODRG2 server.[45] The CH_2 and CH_3 groups on the aliphatic chains were modeled as united atoms while the carbons in the PA region were modeled

as sp^2 hybridized carbons. The default topology obtained from PRODRG was then modified by manually adjusting the partial charges and charge groups so that they are compatible with the GROMOS96 force field parameter set 53A6,[46] which has been tested to be suitable for probing the dynamics of PA cores.[40] Such an approach[47] was recommended in literature to remove the artifacts existing in the default topology obtained from PRODRG. Detailed information on the development and test of the topology is available in Appendix A (section A.2).

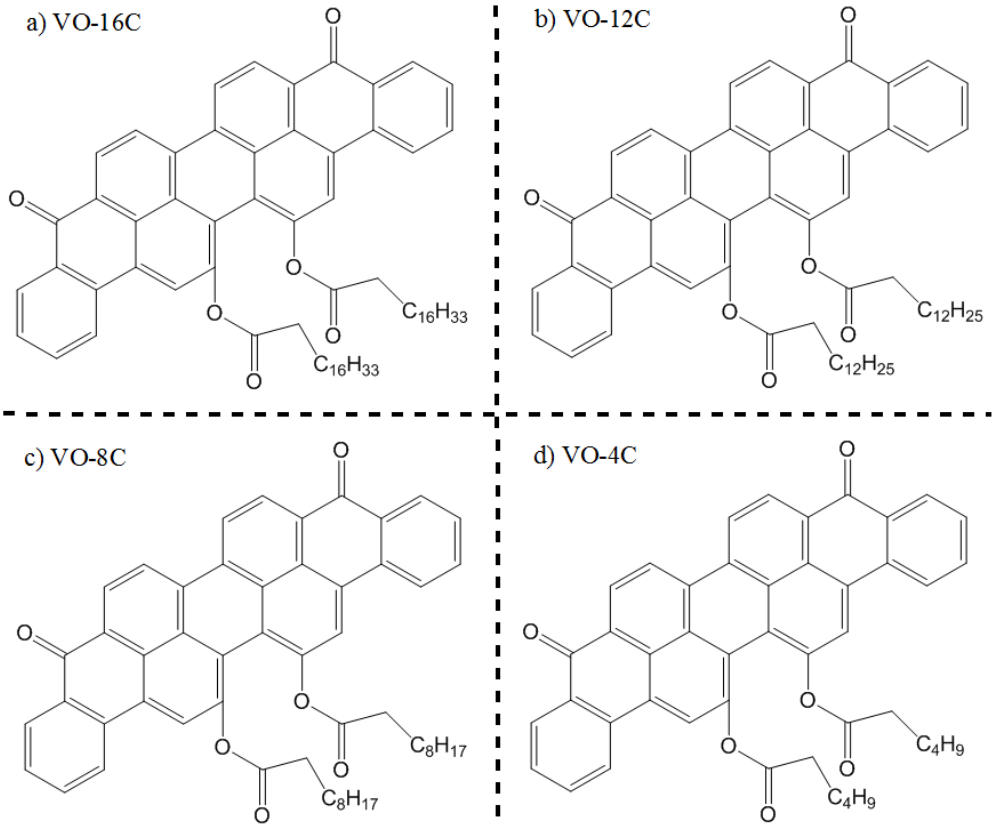

Figure 3.1: Molecular structures employed in the simulations: (a) VO-16C, (b) VO-12C, (c) VO-8C, (d) VO-4C. Molecular models (b), (c) and (d) are identical to model (a) in all aspects except that they have different numbers of aliphatic carbons in their side chains.

All simulations were performed using the MD package GROMACS (version 4.0.7).[48-51] Simple point charge (SPC) water model,[52] periodic boundary conditions, full electrostatics with particle-mesh Ewald method,[53] cutoff distance of 1.4 nm for van der Waals and electrostatics

pairwise calculations, SETTLE algorithm[54] to constrain all bonds for water molecules, LINCS algorithm[55] to constrain all bonds for solute molecules, and a time step of 2 fs were used for all simulations. The SPC water molecule model chosen here has been widely tested in literature and is shown to be suitable, to some extent, for simulating solutes in water.[56,57] Also, previous simulation work done by Kuznickl et al.[16,21] have shown the suitability of SPC water for asphaltene simulations. During each simulation, static structure optimization was first performed to minimize the total potential energy. Then the non-hydrogen atoms of the solutes were restrained with 1000 kJ/(mol·nm^2) harmonic potential while the solvent molecules were allowed to relax around the solutes for 1 ns at 300 K and 1 bar. The restraint was then removed and NPT ensemble simulation was performed for 60 ns for each system. Appropriate post-processing programs available in GROMACS as well as VMD[58] were used for trajectory analysis and visualization.

3.2.3. Acronyms and Definitions

To facilitate the discussion of the simulation results, we introduce the following acronyms and definitions.

As mentioned in section 3.2.1, the four asphaltene models, as well as the four simulated systems that contain them are referred to as VO-16C, VO-12C, VO-8C and VO-4C, respectively. Inside each system, the 24 asphaltene molecules are labeled by number 1-24. To describe the relative position and orientation of two asphaltene molecules in one simulated system, we first approximate each core region by a plane using three carbon atoms located in the PA core (see Appendix A section A.3 for details). We then make use of the distance between the centers of geometry of the two PA planes (COG distance) and the angle between the PA planes (cosine of angle ($cos\,\sigma$), which can be calculated using standard analytical tools in GROMACS. To

quantify the intensity of the interactions between PA cores ($\pi - \pi$ interaction, originated from π electrons[59]), between PA core and aliphatic chain ($\pi - \theta$ interaction) and between aliphatic chains ($\theta - \theta$ interaction), we separate each asphaltene molecule into two groups: one containing the united atoms in the chain region (aliphatic side chain group) and the other containing the 30 heavy (non-hydrogen) atoms in the core region (PA core group). Details of these two groups can be found in Appendix A (section A.3). The minimum distance ("MIN distance") between any two groups is then calculated by the standard analytical tool in GROMACS, in order to compute the number of $\pi - \pi$, $\pi - \theta$ and $\theta - \theta$ contacts. Note that the $\pi - \pi$, $\pi - \theta$ and $\theta - \theta$ interactions quantified in this chapter result from the molecular interactions defined in the force field.[46] Unlike in the work of Hunter and Sanders,[59] no separate potential functions were defined for these interactions.

3.3. Results and Discussions

Figure 3.2 shows snapshots of the four systems at the final stages of the simulations. The first interesting observation from Figure 3.2 is that all of the asphaltene molecules form a single aggregate in systems VO-4C and VO-16C but not in systems VO-8C and VO-12C, suggesting that aggregation is not only driven by the interaction among the PA cores,[31] and large aggregate formation is favored by having very long or very short side chains. Secondly, in all of the four systems, PA cores of adjacent asphaltene molecules in an aggregate tend to be parallel, suggesting that parallel alignment may be the most favored configuration for neighboring PA cores due to the $\pi - \pi$ interaction. In addition, it seems that the parallel alignments in systems VO-4C and VO-8C can extend to a larger number of PA cores than those in systems VO-12C and VO-16C (indicated by the black arrows in Figure 3.2), suggesting that long chains have stronger interference with the $\pi - \pi$ interaction. For clarity, in each subfigure of Figure 3.2 one

axis is indicated by a blue line, along which several parallel PA cores are aligned. Finally, all the side chains are excluded from the regions between parallel PA cores. However, there exist contacts between the PA cores and aliphatic side chains and contacts between aliphatic side chains, suggesting that $\pi - \theta$ interaction and/or $\theta - \theta$ interaction may play a role in the aggregation. To examine these observations in a quantitative manner, we further study the detailed mechanisms and structures of the aggregates in the following.

3.3.1. Aggregation Kinetics

By visually examining the simulation trajectories, we found that the dimers are unlikely to break once they are formed, verifying the previous report[16] that asphaltene aggregates are long-lived in water. To quantitatively show this, in Appendix A, we plotted the MIN distance between adjacent PA cores that became parallel at the final stages of the simulations as a function of simulation time (Figure A.5). For all four systems, the MIN distances decrease with time until they reach their plateau value and remain unchanged afterwards, indicating the permanent existence of dimers in water. Also, the final plateau value of the MIN distance (~0.35 nm) is identical in all four systems and is close to the mean separation between $\pi - \pi$ stacked PA cores,[60] indicating the formation of $\pi - \pi$ stacking between the asphaltene molecules. Long-lived aggregates can be further confirmed by examining the number of asphaltene molecules in the largest aggregate formed as a function of simulation time as shown in Figure 3.3a. It can be seen that for all four systems, the aggregation continues for a period of time evidenced by the growing number of asphaltene molecules in the largest aggregate. For systems VO-8C and VO-12C, the numbers reach their plateau values of 10 and 13 at 28 ns and 22 ns respectively and remain unchanged afterwards. For systems VO-4C and VO-16C, the number of molecules in the largest aggregate reaches 24 at 54 ns in both cases, corresponding to all the asphaltene molecules

forming a single aggregate. The aggregates never break for the remaining time of the simulation, again confirming the high stability of the formed aggregates.

The size of the largest aggregate as calculated above reflects the extent of asphaltene aggregation. The formation of a single aggregate in systems VO-4C and VO-16C but not in systems VO-8C and VO-12C indicates that there is a non-monotonic relation between the extent of asphaltene aggregation in water and the side-chain length; this is shown in Figure 3.3b. Since the aggregation is driven by intermolecular interactions among the molecules, to understand the non-monotonic dependence of aggregation on the side-chain length, it is necessary to examine

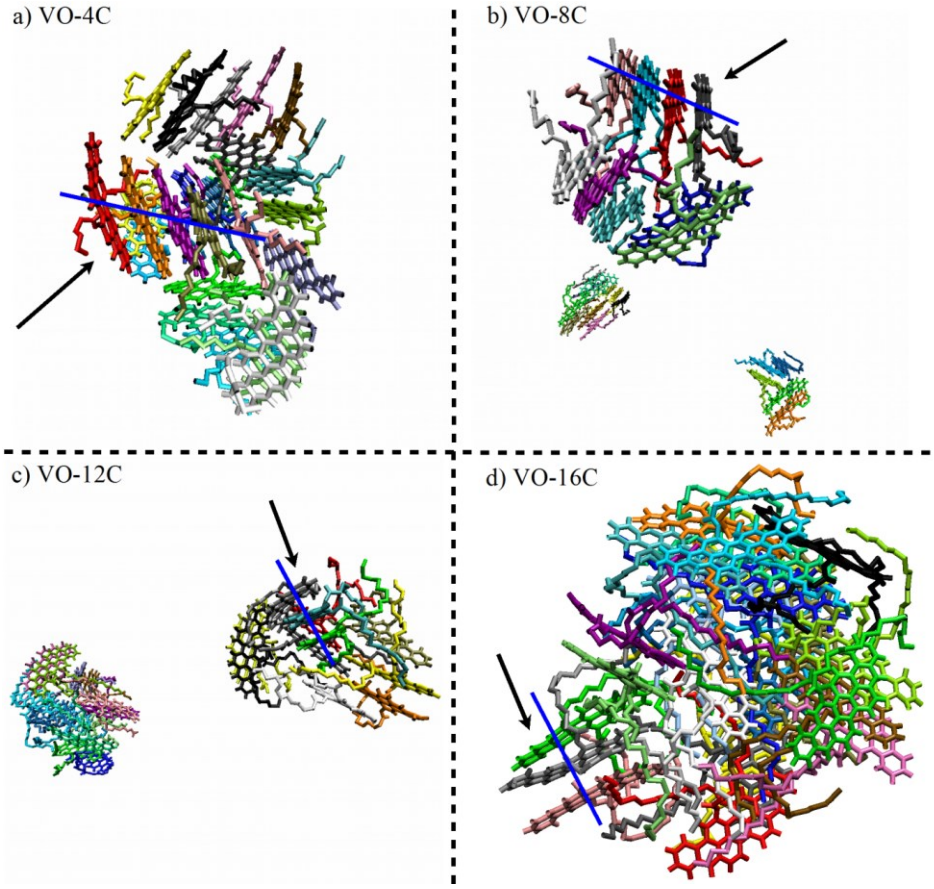

Figure 3.2: Snapshots of the systems at the final simulation stages: (a) VO-4C, (b) VO-8C, (c) VO-12C, (d) VO-16C. The 24 asphaltene molecules in each system are represented by different colors. Water molecules are removed for clarity.

these interactions in detail. The strong interactions among the asphaltene molecules are evidenced by the difference between the diffusion coefficient of a single asphaltene molecule and that of an asphaltene molecule in the aggregate. The diffusion coefficient for a single asphaltene molecule (in the absence of intermolecular interaction with other asphaltene molecules) is predicted by the Stokes-Einstein equation:[61]

$$D_{SE} = \frac{k_B T}{6\pi\mu(0.676 < R^2 >^{1/2})}, \tag{3.1}$$

where k_B is the Boltzmann constant, T is the absolute temperature, μ is solvent viscosity, and $< R^2 >^{1/2}$ is the root mean square radius of gyration of a single molecule, obtained by averaging over all 24 asphaltene molecules at the beginning of the simulation (at ~1 ns) when aggregation

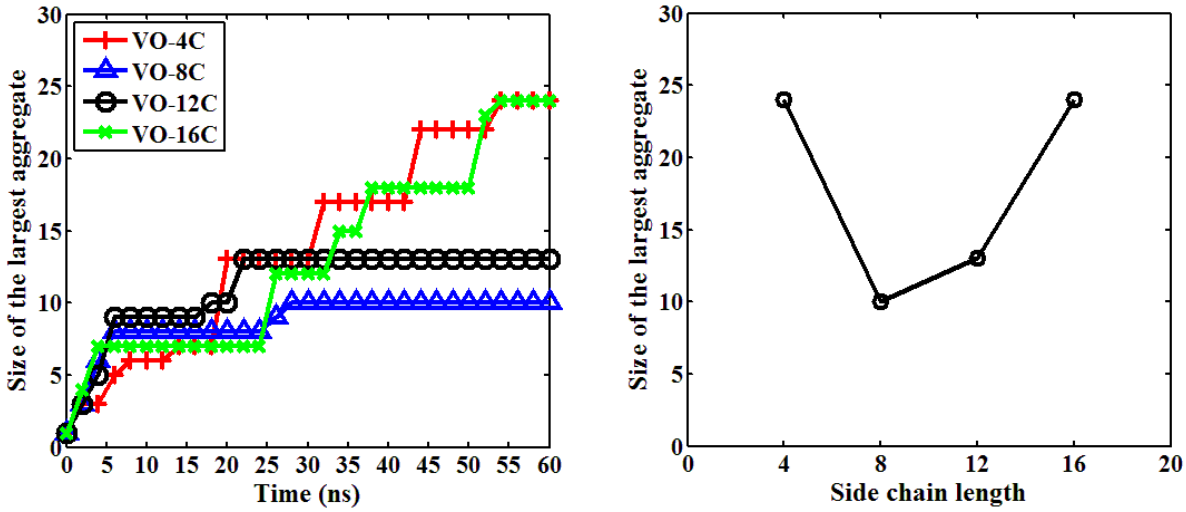

a) Growth of the largest aggregate b) Size of the largest aggregate

Figure 3.3: Size of the largest aggregate quantified by the number of asphaltene molecules in the largest aggregate: (a) Growth of the largest aggregate over simulation time, (b) Size of the largest aggregate formed at the final stage of the simulation as a function of side-chain length (number of carbons in the side chain).

has not started. The diffusion coefficient for an asphaltene molecule in the aggregate is estimated through the Einstein relation for self-diffusion:[62]

$$D_{msd} = \frac{1}{6}\lim_{t\to\infty}\frac{d}{dt}\langle|\vec{r}(t+t_0)-\vec{r}(t_0)|^2\rangle\ , \tag{3.2}$$

where t_0 is a reference time, $\langle|\vec{r}(t+t_0)-\vec{r}(t_0)|^2\rangle$ is the mean square displacement calculated by performing averages over time as well as over all 24 asphaltene molecules. To determine the diffusion coefficient of asphaltene after aggregation starts, the last 10 ns (50-60 ns) was chosen to calculate the mean square displacement, i.e., $t_0 = 50$ ns. The calculated diffusion coefficients by these two methods are listed in Table 3.1. It can be seen that the diffusion coefficient decreases significantly in all four systems as the asphaltene molecules aggregate, demonstrating the existence of strong intermolecular interactions. The values of the diffusion coefficients, however, do not allow us to acquire further information on the nature or magnitude of the intermolecular interactions because the molecules simulated in the four systems have different structures that can affect the diffusion coefficients. In the following section, we make use of the MIN distance defined in section 3.2.3 to examine in detail the intermolecular interactions between the asphaltene molecules.

Table 3.1: Diffusion Coefficients

system	$D_{SE}\ (10^{-10}\ m^2/s)$	$D_{msd}(10^{-10}\ m^2/s)$
VO-4C	8.21	1.76
VO-8C	7.48	1.46
VO-12C	6.97	1.98
VO-16C	6.33	0.828

3.3.2. Aggregation Mechanism

The aggregation of asphaltenes has commonly been attributed to the $\pi-\pi$ interaction between the PA cores, while it has been proposed[20,29,30] that the side chains of continental type of asphaltenes introduce a steric interference for the $\pi-\pi$ interactions. Such an argument would imply that as the side-chain length is increased, there will be increased disruption of the $\pi-\pi$ interactions. However, our simulation results show that very long side chains in VO-16C do not

result in the least aggregated structure. On the contrary, the extent of aggregation in VO-16C is comparable to that in VO-4C where the side chains are the shortest. This indicates that the dominating driving force for the final formation of a single aggregate in VO-16C is unlikely the $\pi - \pi$ interaction. Rather, it may be due to the strong $\pi - \theta$ or $\theta - \theta$ interaction arising from the long side chains, which may compensate for the decrease in the $\pi - \pi$ interaction.

In order to examine these three types of intermolecular interactions for the four systems in a quantitative manner, for each pair of asphaltene molecules, we defined three types of "contacts". For two asphaltene molecules, a $\pi - \pi$ contact is formed if the MIN distance between their PA core groups is within 0.5 nm; a $\pi - \theta$ contact is formed if the MIN distance between the PA core group from one molecule and the aliphatic side chain group from the other molecule is within 0.5 nm; finally a $\theta - \theta$ contact is formed if the MIN distance between their aliphatic side chain groups is within 0.5 nm. Figure 3.4 shows the numbers of $\pi - \pi$, $\pi - \theta$ and $\theta - \theta$ contacts as a function of simulation time for the four systems. These numbers are indicators of the intensity of $\pi - \pi$, $\pi - \theta$ and $\theta - \theta$ interactions. Each subfigure in Figure 3.4 corresponds to one of the four systems and it contains 3 curves that respectively describe the numbers of $\pi - \pi$, $\pi - \theta$ or $\theta - \theta$ contacts in that system. The first observation from Figure 3.4 is that the curves for systems VO-4C and VO-16C keep increasing during the entire course of the simulation, corresponding to the continued growth of the largest aggregate and the final formation of a single aggregate shown in Figure 3.3a. The curves for systems VO-8C and VO-12C have a very similar trend: substantial increase at the initial stage of the simulation and stabilization at the later stage of the simulation.

Detailed inspection of Figure 3.4 shows that at the final stage of the simulation, system VO-4C has the largest number of $\pi - \pi$ contacts (~50), as compared to ~30 in the other three

systems. On the other hand, system VO-4C has the smallest amount of $\theta - \theta$ contacts (~30), compared with systems VO-8C (~40), VO-12C (~50) and VO-16C (~90) which has the largest number of $\theta - \theta$ contacts. For $\pi - \theta$ contacts, systems VO-4C, VO-12C and VO-16C have a similar number (~90), larger than ~50 for system VO-8C. As it has been shown in Figures 3.2 and 3.3 that a single large aggregate is formed in systems VO-4C and VO-16C but not in systems VO-8C and VO-12C, these numbers suggest that it is the strong $\pi - \pi$ interaction that facilitates the complete aggregation in system VO-4C, while it is the strong $\theta - \theta$ interaction that facilitates the complete aggregation in system VO-16C. For system VO-12C, compared with system VO-16C, it has similar numbers of $\pi - \theta$ and $\pi - \pi$ contacts but a smaller number of $\theta - \theta$ contacts. The number of asphaltene molecules involved in the largest aggregate in system VO-12C is also smaller, being 13 compared to 24 in system VO-16C. This further confirms that the final formation of a single aggregate in system VO-16C is promoted mainly by the $\theta - \theta$ interaction. For system VO-8C, the numbers of the three different contacts are very similar over the entire course of the simulation. Its number of $\theta - \theta$ contact is only slightly larger than VO-4C while its numbers of $\pi - \pi$ and $\pi - \theta$ contacts are the smallest among the four systems, leading to the previous observation that its largest aggregate involves the smallest number (10) of asphaltene molecules

Despite the importance of $\pi - \pi$ interaction for asphaltene aggregation, our simulation results suggest that $\pi - \theta$ and $\theta - \theta$ interaction, i.e. the interaction between PA core and aliphatic chain and that between aliphatic chains, can also contribute significantly to asphaltene aggregation in water, provided that the $\pi - \theta$ and $\theta - \theta$ interactions induced by the side chains can compensate for their interference with the $\pi - \pi$ interaction. Of particular importance is the $\theta - \theta$ interaction that arises from the hydrophobic association of the side chains, resulting in the

large extent of aggregation for asphaltene molecules with very long side chains. Asphaltenes with intermediate side-chain length (e.g., VO-8C) are most difficult to aggregate due to the greatly reduced $\pi - \pi$ interaction and insufficient $\pi - \theta$ and $\theta - \theta$ interactions. The different aggregation mechanisms for asphaltene molecules with different side-chain lengths provide an explanation to the observation in section 3.1 that there is a non-monotonic relation between the size of the largest aggregate in water and the length of the side chain.

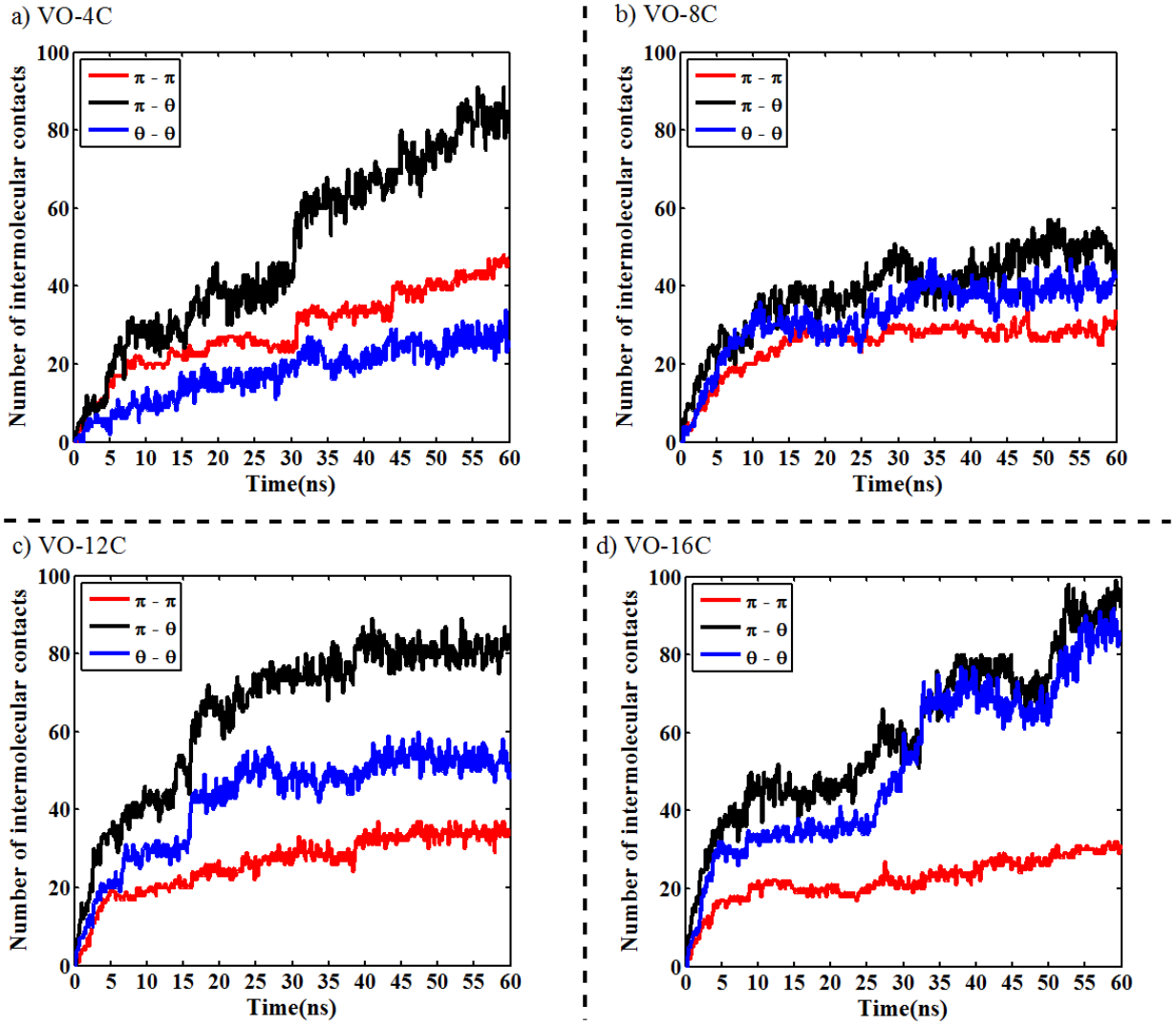

Figure 3.4: Numbers of $\pi - \pi$, $\pi - \theta$ and $\theta - \theta$ contacts for the four systems: (a) VO-4C, (b) VO-8C, (c) VO-12C, and (d) VO-16C.

3.3.3. Stacking Modes

As shown in Figure 3.2, stacking of the PA cores from different asphaltene molecules is universally observed in the aggregates. To examine whether and how the side-chain length may affect the stacking structures, we first plotted the RDF for the COG separation of the PA cores, which is shown in Figure 3.5 for the four systems. It can be clearly seen that the RDF has its first and most prominent peak at ~0.45 nm in all the cases. This is consistent with the MIN separation of ~0.35 nm between adjacent parallel PA cores (see section 3.1 and Appendix A) and indicates again the formation of strong $\pi - \pi$ stacking between the PA cores. Meanwhile, the sharpness of the first peak in the RDF plot shows a monotonic relationship with the chain length: system VO-4C has the sharpest peak, followed by systems VO-8C, VO-12C and VO-16C, demonstrating that progressively longer side chains increasingly interfere with the $\pi - \pi$ interaction.

To further confirm the parallel alignment, at the COG separation of ~0.45 nm, we plotted the PDF for the cosine of the angle ($cos\,\sigma$) between two PA cores, shown in Figure 3.6a. The angle between two PA planes can vary from 0° to 90°; thus $cos\,\sigma$ is in the range of 0 to 1, with $cos\,\sigma = 0$ ($\sigma = 90^{\circ}$) corresponding to two PA cores being perpendicular to each other and $cos\,\sigma = 1$ ($\sigma = 0^{\circ}$) corresponding to two PA cores being parallel. It can be seen that the PDF has its sole and prominent peak at $cos\,\sigma = 0.9{\sim}1$, demonstrating that the favorite orientation between two PA cores at a COG separation of 0.45 nm is parallel. This corresponds to a stacking mode where one PA core is located directly on top of the other. Figure 3.6b shows such a stacking structure, and we shall from now on refer to two asphaltene molecules in such a stacking mode as a direct parallel stacking (DPS) pair, which is quantified by having COG distance ≤ 0.50 nm and $cos\,\sigma \geq 0.90$.

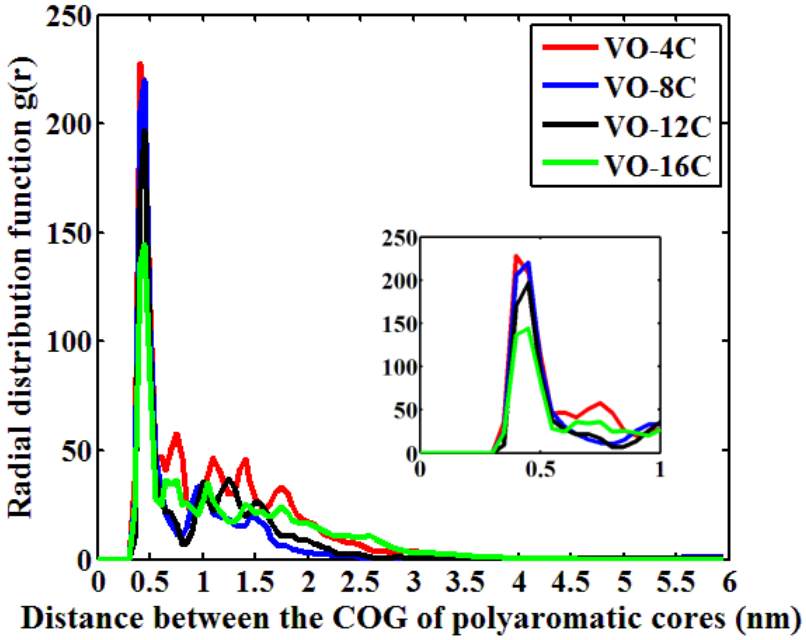

Figure 3.5: RDF for the COG separation of the PA cores. The inset shows the enlarged first peak of the RDF.

Following the first peak in Figure 3.5, the next peak in the RDF is found to be at ~0.75 nm for systems VO-4C and VO-16C and at ~1 nm for systems VO-8C and VO-12C. This indicates that different alignments of the PA cores may exist for asphaltenes with different side-chain length. At the COG separation of ~0.75 nm, we plotted PDF of $cos\,\sigma$ in Figure 3.6c. The most pronounced peak in the PDF is still located at $cos\,\sigma$ = 0.9~1, suggesting that the PA cores are still aligned parallel to each other, but their COG separation (~0.75 nm) is larger than the separation between the two PA planes in a DPS pair ($\pi-\pi$ stacking of COG distance ~0.45 nm). In such stacking structure one PA core lies on top of the other but its COG is laterally shifted, which is shown in Figure 3.6d. We define two asphaltene molecules in this stacking mode, quantified by 0.50 nm < COG distance ≤ 0.75 nm and $cos\,\sigma \geq 0.90$, as a shift parallel stacking (SPS) pair. Compared with Figure 3.6a, the PDF for $\cos(\sigma)$ at ~0.75 nm also has multiple peaks between 0.30 and 0.80, although the heights of these peaks are much smaller.

This indicates that the parallel alignment in the SPS mode is less stable compared with that in the DPS mode. It should be noted that SPS pairs are in fact present in all the four systems. However, the RDF of the COG separation for systems VO-8C and VO-12C do not show peaks at ~0.75 nm (see Figure 3.5). This implies that SPS is a less prominent mode in systems VO-8C and VO-12C compared with other stacking modes represented by the peaks in their RDF (at 0.45 nm, as well as at 1 nm and beyond discussed below).

The DPS and SPS pairs are defined for the stacking of PA cores from two asphaltene molecules. Together they will be referred to as parallel stacking (PS) pairs in this chapter and are present when two PA cores have COG distance ≤ 0.75 nm and $cos\,\sigma \geq 0.90$. As has been seen in Figure 3.2, multiple asphaltene molecules in an aggregate can be concurrently involved in one parallel configuration. Hence, we further define multiple-molecule parallel stacking (m-MPS, where "m" stands for "multiple", which can be replaced by an integer when a particular number of molecules involved in the stacking mode is specified) mode as follows. If molecules 1 and 2 form a PS pair and molecules 2 and 3 form a PS pair, then molecules 1, 2 and 3 are said to be in the 3-molecule parallel stacking (3-MPS) mode, an example of which is shown in Figure 3.7a. Similar definitions hold for 4-molecule and 5-molecule parallel stacking (4-MPS and 5-MPS) modes as shown in Figures 3.7b and c respectively. If only two molecules form a PS pair, they are said to be in the 2-MPS mode. In our simulations, we did not observe parallel stacking of more than 5 PA cores. The existence of multiple-molecule parallel stacking modes can be confirmed by the PDF of $cos\,\sigma$at COG separation of ~ 1 nm for systems VO-8C, VO-12C and VO-16C (see Figure A.6 in Appendix A). At this separation, the most pronounced peak in the PDF occurs at $cos\,\sigma$ = 0.9~1, corresponding to the parallel stacking between two PA cores that have a third PA core sandwiched in between. As can be seen in Figure 3.2, m-MPS mode seems

to be most prominent in system VO-4C. In fact, the RDF for system VO-4C does have its third peak located at ~1.1 nm, where one may expect the PDF of $cos\,\sigma$ to have a pronounced peak at

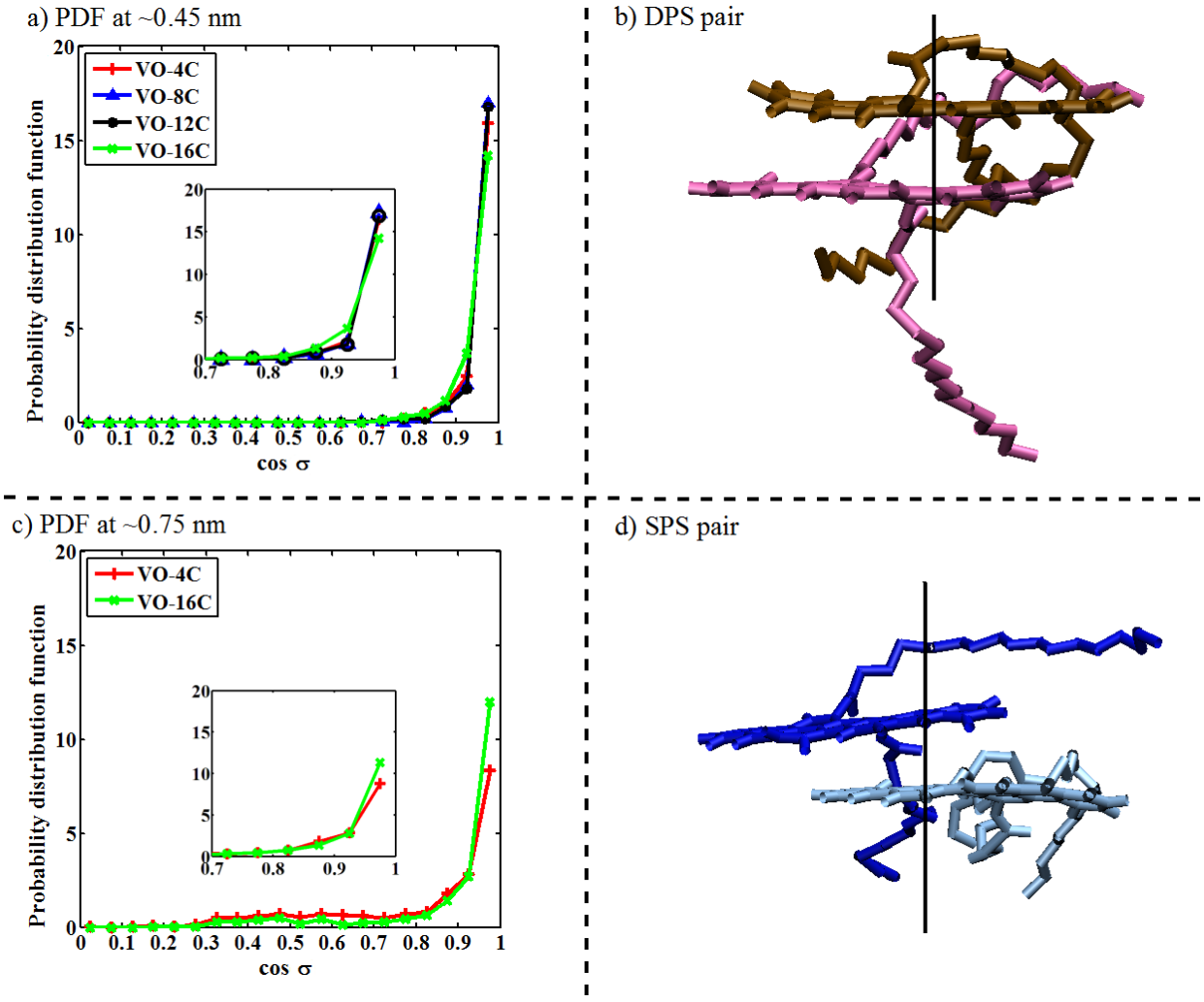

Figure 3.6: PDF of $cos\,\sigma$ at different COG distances and the corresponding stacking structures at the peaks of the PDF curves: (a) PDF at COG distance = ~0.45 nm, (b) DPS pair, (c) PDF at COG distance = ~0.75 nm, (d) SPS pair. The insets in (a) and (c) show the enlarged PDF behaviors around $cos\,\sigma = 0.9 - 1$. The axes along which the PA rings are stacked are depicted in (b) and (d) as solid lines.

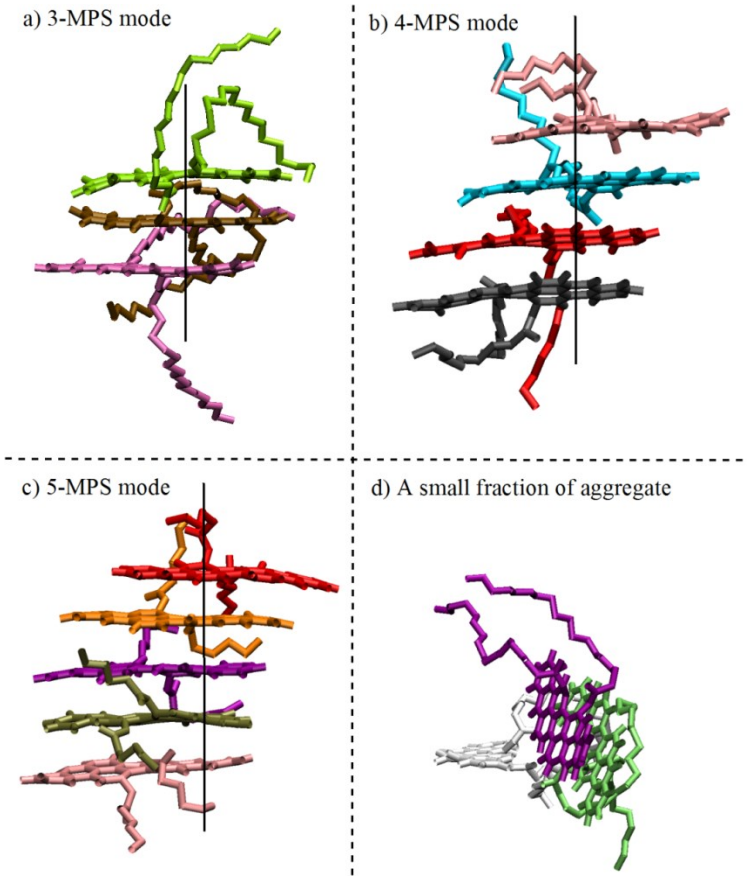

Figure 3.7: Stacking modes: (a) 3-MPS mode, (b) 4-MPS mode, (c) 5-MPS mode, (d) A small fraction of aggregate. We do not consider the perpendicular configurations in (d) formed by molecules in parallel stacking modes (2-MPS mode in this case) and other molecules (the molecule in white color in this case) as T-stacking mode.

$cos\,\sigma$ close to one. However, this was not observed (see Figure A.7 in Appendix A) because the asphaltene molecules in a large aggregate are not all aligned and as a result, the COG distance between non-parallel PA cores may become comparable to the COG distance between two non-neighboring PA cores in an m-MPS mode. This diminishes the possible peaks in the PDF of $cos\,\sigma$near $cos\,\sigma \sim 1$ at large COG distances, especially for system VO-4C in which the aliphatic tails are extremely short.

Each RDF curve in Figure 3.5 also contains peaks beyond 1 nm COG separation. PDF of $cos\,\sigma$ at these peaks are available in Appendix A (Figures A.8-A.11). Most of these curves do not have apparent peaks because at those large COG separations, the relative orientation of two PA cores is more or less random. It should be noted that the PDFs of system VO-16C at COG distance ~1.4 nm (Figure A.9 in Appendix A) and ~1.75 nm (Figure A.11 in the Appendix A) do have noticeable peaks located at $cos\,\sigma = 0.9{\sim}1$ while the PDFs of system VO-4C do not have such peaks at the same COG distances. Because of the strong interference of side chains, these peaks for system VO-16C is unlikely attributed to large m-MPS structures in system VO-16C. Rather, they may be attributed to molecules that are not involved the same m-MPS structure but parallel with one another. As mentioned before, $\pi-\theta$ and $\theta-\theta$ interactions facilitate the formation of a single aggregate in the late stage of the simulation for system VO-16C. In the case of $\pi-\theta$ or $\theta-\theta$ contact formed between two molecules that are involved in two different m-MPS structures, the PA core from one m-MPS structure can be parallel with the PA core from the other m-MPS structure (see Appendix A Figure A.12) but the COG distance between these two PA cores is larger.

To quantitatively compare the parallel structures in the four systems, we summarize the PS pairs formed in the final stage of the simulations in Figure 3.8. In each subfigure, the x-axis and y-axis represent the molecule identification number explained in section 3.3, and each grid point represents one pair that can be potentially formed by two molecules. For example, the grid point with coordinates (x=1, y=2) corresponds to one pair that can be potentially formed by molecules 1 and 2. If a PS pair is in fact formed, the grid point will be marked with a symbol. Due to symmetry, only the upper left half of the grid is utilized. Grid points that represent PS pairs involved in the same m-MPS structure are labeled with the same symbol while a particular

color is used for a specific m, i.e., red is for 2-MPS mode, blue for 3-MPS mode, black for 4-MPS mode and pink for 5-MPS mode. For example, in system VO-4C, there are four pink squares that represent four PS pairs (1-3, 3-11, 5-9, 5-11) involved in the same 5-MPS structure consisting of molecules 1-3-11-5-9. It can be clearly seen that while the largest m-MPS structure that can be formed in system VO-4C is 5-MPS, system VO-8C only has one 4-MPS structure (consisting of molecules 2-1-21-9). Furthermore, 5-MPS and 4-MPS structures are entirely absent in VO-12C and VO-16C and the largest m-MPS structure formed in these two systems is 3-MPS. The decrease in the number of molecules involved in m-MPS mode again demonstrates that long side chains can interfere with the interaction of PA cores in water and verifies that the pronounced peaks of PDF at larger COG separations for system VO-16C are due to the $\pi - \theta$ and $\theta - \theta$ contacts (see Appendix A Figures A.9, A.11 and A.12).

The numbers of DPS pairs, SPS pairs and m-MPS structures are summarized in Table 3.2. It can be seen that DPS is more favorable than SPS in all four systems, again demonstrating the popularity of $\pi - \pi$ interaction for neighboring asphaltene molecules. If we count the total number of molecules involved in 3-MPS, 4-MPS and 5-MPS modes, such number is 19 for system VO-4C, 13 for system VO-8C and 9 for system VO-12C, indicating the general stronger ability of forming larger m-MPS modes for asphaltene with shorter side chains. For system VO-16C, though it has 12 molecules involved in 3-MPS mode compared with 9 in system VO-12C, the total number of asphaltene molecules that are involved in PS pairs are smaller than the other 3 cases. A word of explanation for Table 3.2 is that the total number of PS pairs (DPS+SPS) may be slightly different from the total number of stacking pairs counted from the m-MPS modes. For example, for system VO-4C, if we consider that there is one stacking pair in each 2-MPS mode, two in each 3-MPS mode, three in each 4-MPS mode and four in each 5-MPS mode, the

a) VO-4C

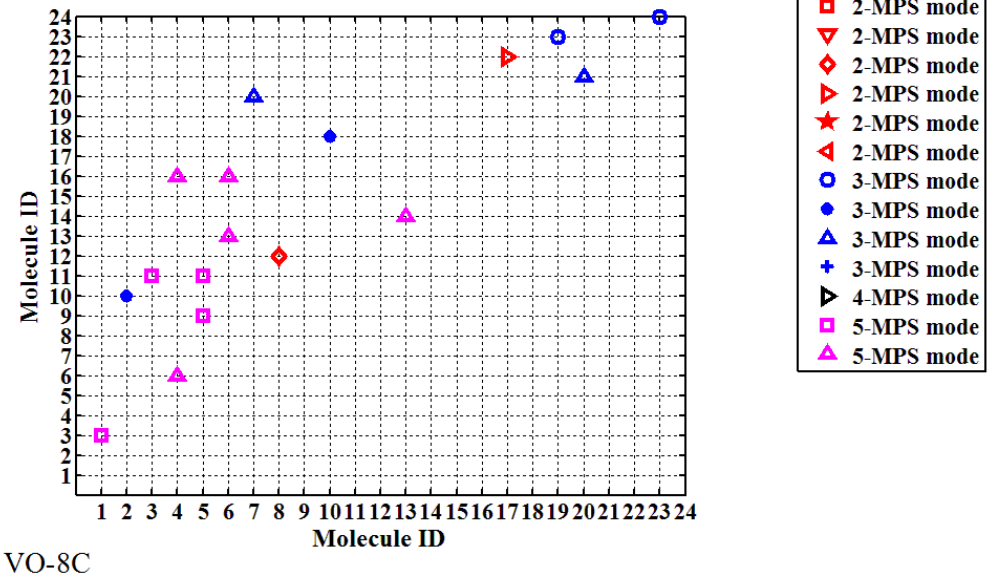
Molecule ID
Molecule ID
2-MPS mode
2-MPS mode
2-MPS mode
2-MPS mode
2-MPS mode
2-MPS mode
3-MPS mode
3-MPS mode
3-MPS mode
3-MPS mode
4-MPS mode
5-MPS mode
5-MPS mode

b) VO-8C

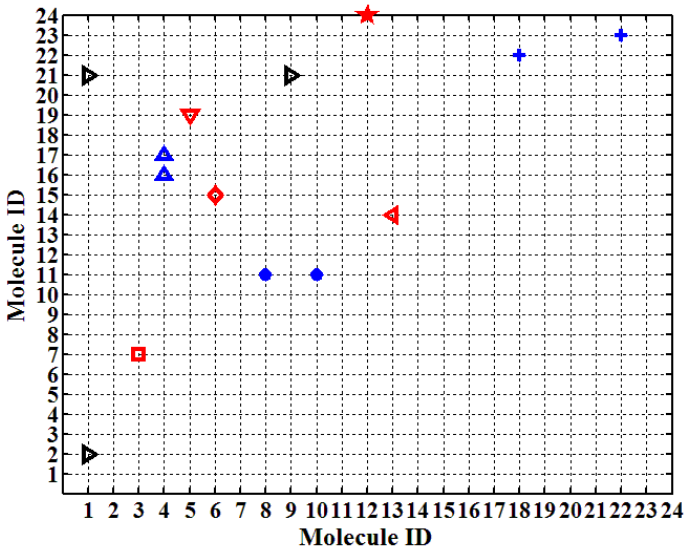
Molecule ID
Molecule ID

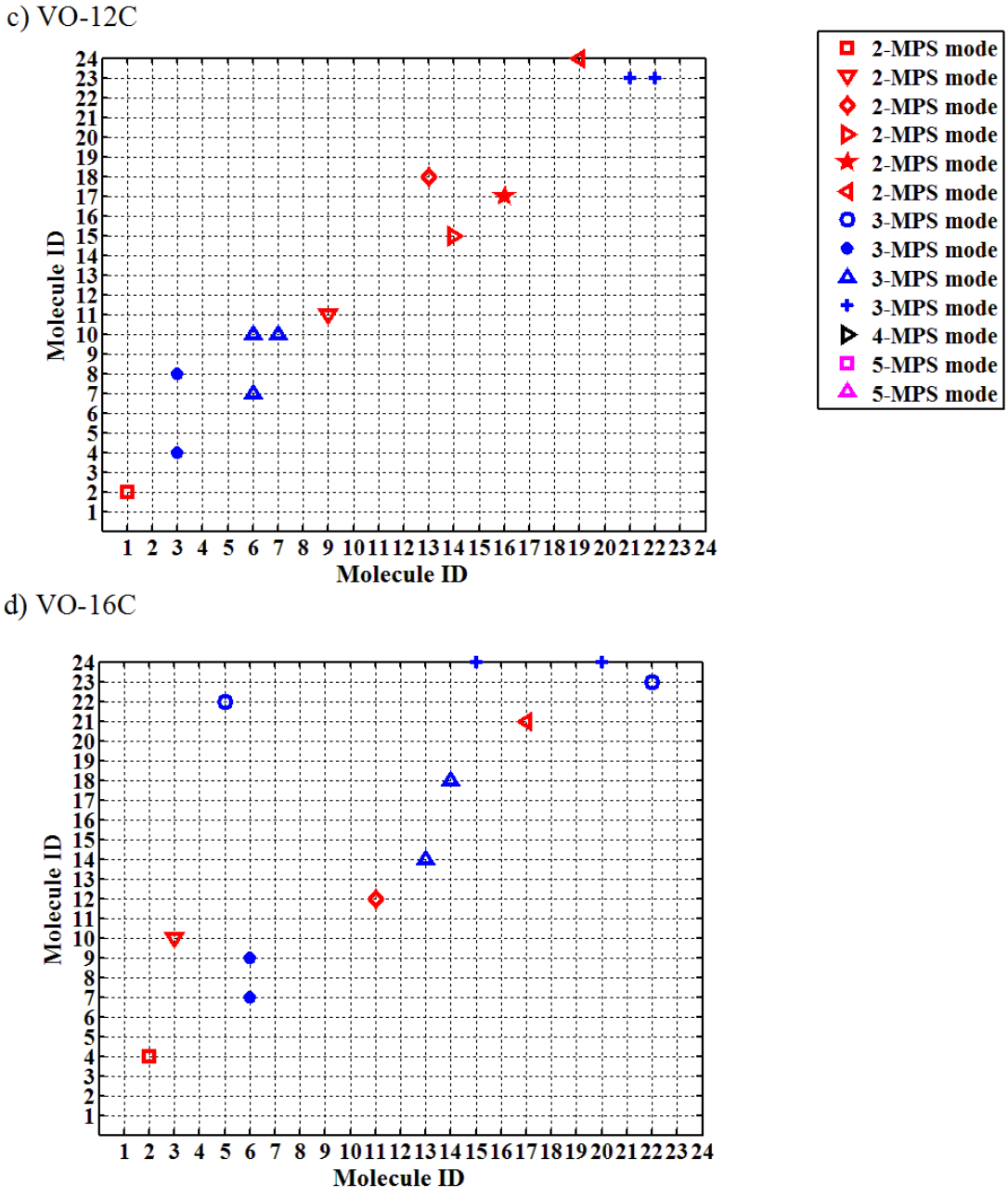

Figure 3.8: PS pairs in the four systems: (a) VO-4C, (b) VO-8C, (c) VO-12C, (d) VO-16C.

stacking pairs counted in this way will be $2 \times 1 + 3 \times 2 + 2 \times 4 = 16$. On the other hand, the sum of DPS and SPS pairs is $11 + 6 = 17$. This is because from the five molecules (4-16-6-13-14) in the 5-MPS mode, molecules 4 and 6 are not adjacent but are separated by a COG distance of less than 0.75 nm. Therefore they are counted as a stacking pair in the calculation.

Table 3.2: Numbers of Parallel Pairs and m-MPS Structures

system	DPS pair	SPS pair	2-MPS structure	3-MPS structure	4-MPS structure	5-MPS structure
VO-4C	11	6	2	3	0	2
VO-8C	10	4	5	3	1	0
VO-12C	10	3	6	3	0	0
VO-16C	8	4	4	4	0	0

At the equilibration stage of the simulation (55ns~60ns), we do not observe T stacking between the PA cores, which has been previously reported.[33,39-41] We do not consider configurations such as shown in Figure 3.7d as T-stacking or at least, we do not consider this structure to be a favorable configuration for neighboring PA cores. This is evidenced by the PDF of $cos\,\sigma$ at COG distance = ~0.45 nm, which shows strict zero possibility for $cos\,\sigma \leq 0.70$ and has only one peak at $cos\,\sigma = 0.9{\sim}1$.

The aggregation mechanisms concluded from this chapter share qualitative similarities with the experiment work on perylene diimide molecules conducted by Balakrishnan et al.,[63] in which the effect of side chain on stacking and aggregation was investigated by UV-vis adsorption, fluorescence, X-ray fraction, and different scanning calorimetries. They proposed that long alkyl side chains possess strong hydrophobic interaction and help molecules assemble cooperatively with $\pi - \pi$ interaction between the cores. At the same time, linear side chains bring in steric hindrance for the stacking of cores. These postulates are well proved by our simulation results, suggesting the broad usage of these encouraging findings in reality.

3.4. Conclusions

We performed a series of MD simulations to study the effect of side-chain length on asphaltene aggregation in water. Consistent with previous literature, regardless of the side-chain length, long-lived asphaltene aggregates are formed in water. Due to the $\pi - \pi$ interaction between neighboring PA cores, parallel stacking is found to be the most favorable configuration for asphaltene molecules at close separation. Two neighboring PA cores can form direct parallel stacking (COG separation of ~0.45 nm) and shifted parallel stacking (COG separation of ~0.75 nm). More than two PA cores can also form a multiple molecule parallel stacking structure, and up to five molecules are found to stack together for asphaltenes with very short side chains (4 interconnected aliphatic hydrocarbons on each chain). Long aliphatic chains introduce an interference with the $\pi - \pi$ interactions, leading to a smaller number of molecules involved in multiple molecule parallel stacking structures. However, this does not imply that the extent of aggregation is necessarily smaller for asphaltenes with long side chains. In fact, our results reveal that the extent of aggregation has a non-monotonic dependence on the side-chain length. Large aggregates are found for asphaltenes with very short or very long side chains for different reasons: short chains have small interference with the $\pi - \pi$ interaction between PA cores, while long side chains promote aggregation via the increased $\theta - \theta$ and $\pi - \theta$ interactions that may compensate for the reduction in the $\pi - \pi$ interaction caused by the long side chains. Because of the general presence of water in the processing of bitumen, the simulation results reported here could provide significant insights regarding the problems caused by asphaltene aggregation in aqueous environments.

Bibliography

(1) Groenzin, H.; Mullins, O. C. Asphaltene Molecular Size and Structure. *J. Phys. Chem. A*

1999, *103*, 11237-11245.

(2) Mansoori, G. A. Modeling of Asphaltene and Other Heavy Organic Depositions. *J. Petr. Sci. Eng.* **1997,** *17*, 101-111.

(3) Escobedo, J.; Mansoori, G. A. Heavy Organic Deposition and Plugging of Wells (Analysis of Mexico's experience). Presented at the SPE Latin America Petroleum Engineering Conference, Caracas, Venezuela, March 8–11, 1992; Paper SPE 23696.

(4) Kokal, S. L.; Sayegh, S. G. Asphaltenes: The Cholesterol of Petroleum. Presented at the SPE Middle East Oil Show, Bahrain, March 11–14, 1995; Paper SPE 29787.

(5) Spiecker, P. M.; Gawrys, K. L.; Kilpatrick, P. K. Aggregation and Solubility Behavior of Asphaltenes and Their Subfractions. *J. Colloid Interface Sci.* **2003,** *267*, 178-193.

(6) Yarranton, H. W.; Alboudwarej, H.; Jakher, R. Investigation of Asphaltene Association with Vapor Pressure Osmometry and Interfacial Tension Measurements. *Ind. Eng. Chem. Res.* **2000,** *39*, 2916-2924.

(7) Ho, B.; Briggs, D. E. Small Angle X-Ray Scattering from Coal-Derived Liquids. *Colloids Surf.* **1982,** *4*, 271-284.

(8) Ravey, J. C.; Ducouret, G.; Espinat, D. Asphaltene Macrostructure by Small Angle Neutron Scattering. *Fuel* **1988,** *67*, 1560-1567.

(9) Andersen, S. I.; Birdi, K. S. Aggregation of Asphaltenes as Determined by Calorimetry. *J. Colloid Interface Sci.* **1991,** *142*, 497-502.

(10) Anisimov, M. A.; Yudin, I. K.; Nikitin, V.; Nikolaenko, G.; Chernoutsan, A.; Toulhoat, H.; Frot, D.; Briolant, Y. Asphaltene Aggregation in Hydrocarbon Solutions Studied by Photon Correlation Spectroscopy. *J. Phys. Chem.* **1995,** *99*, 9576-9580.

(11) Sjöblom, J.; Aske, N.; Auflem, I. H.; Brandal, Ø; Havre, T. E.; Sæther, Ø; Westvik, A.;

Johnsen, E. E.; Kallevik, H. Our current Understanding of Water-in-Crude Oil Emulsions.: Recent Characterization Techniques and High Pressure Performance. *Adv. Colloid Interface Sci.* **2003,** *100-102*, 399-473.

(12) Lisitza, N. V.; Freed, D. E.; Sen, P. N.; Song, Y. Q. Study of Asphaltene Nanoaggregation by Nuclear Magnetic Resonance (NMR). *Energy Fuels* **2009,** *23*, 1189-1193.

(13) Mullins, O. C.; Sabbah, H.; Eyssautier, J.; Pomerantz, A. E.; Barré, L.; Andrews, A. B.; Ruiz-Morales, Y.; Mostowfi, F.; McFarlane, R.; Goual, L., et al. Advances in Asphaltene Science and the Yen–Mullins Model. *Energy Fuels* **2012,** *26*, 3986-4003.

(14) Mullins, O. C. The Modified Yen Model. *Energy Fuels* **2010,** *24*, 2179-2207.

(15) Mullins, O. C. The Asphaltenes. *Annu. Rev. Anal. Chem.* **2011,** *4*, 393-418.

(16) Kuznicki, T.; Masliyah, J. H.; Bhattacharjee, S. Molecular Dynamics Study of Model Molecules Resembling Asphaltene-Like Structures in Aqueous Organic Solvent Systems. *Energy Fuels* **2008,** *22*, 2379-2389.

(17) Badre, S.; Carla Goncalves, C.; Norinaga, K.; Gustavson, G.; Mullins, O. C. Molecular Size and Weight of Asphaltene and Asphaltene Solubility Fractions from Coals, Crude Oils and Bitumen. *Fuel* **2006,** *85*, 1-11.

(18) Karimi, A.; Qian, K.; Olmstead, W. N.; Freund, H.; Yung, C.; Gray, M. R. Quantitative Evidence for Bridged Structures in Asphaltenes by Thin Film Pyrolysis. *Energy Fuels* **2011,** *25*, 3581-3589.

(19) Tan, X.; Fenniri, H.; Gray, M. R. Pyrene Derivatives of 2,2'-Bipyridine as Models for Asphaltenes: Synthesis, Characterization, and Supramolecular Organization. *Energy Fuels* **2008,** *22*, 715-720.

(20) Zeng, H.; Song, Y. Q.; Johnson, D. L.; Mullins, O. C. Critical Nanoaggregate Concentration of Asphaltenes by Direct-Current (DC) Electrical Conductivity. *Energy Fuels* **2009,** *23*, 1201-1208.

(21) Kuznicki, T.; Masliyah, J. H.; Bhattacharjee, S. Aggregation and Partitioning of Model Asphaltenes at Toluene−Water Interfaces: Molecular Dynamics Simulations. *Energy Fuels* **2009,** *23*, 5027-5035.

(22) Aray, Y.; Hernández-Bravo, R.; Parra, J. G.; Rodríguez, J.; Coll, D. S. Exploring the Structure–Solubility Relationship of Asphaltene Models in Toluene, Heptane, and Amphiphiles Using a Molecular Dynamic Atomistic Methodology. *J. Phys. Chem. A* **2011,** *115*, 11495-11507.

(23) Spiecker, P. M.; Gawrys, K. L.; Trail, C. B.; Kilpatrick, P. K. Effects of Petroleum Resins on Asphaltene Aggregation and Water-in-Oil Emulsion Formation. *Colloids Surf. A* **2003,** *220*, 9-27.

(24) Ortega-Rodríguez, A.; Cruz, S. A.; Gil-Villegas, A.; Guevara-Rodríguez, F.; Lira-Galeana, C. Molecular View of the Asphaltene Aggregation Behavior in Asphaltene−Resin Mixtures. *Energy Fuels* **2003,** *17*, 1100-1108.

(25) Speight, J. G.; Long, R. B.; Trowbridge, T. D. Factors Influencing the Separation of Asphaltenes from Heavy Petroleum Feedstocks. *Fuel* **1984,** *63*, 616-620.

(26) Tan, X.; Fenniri, H.; Gray, M. R. Water Enhances the Aggregation of Model Asphaltenes in Solution via Hydrogen Bonding. *Energy Fuels* **2009,** *23*, 3687-3693.

(27) Gray, M. R.; Tykwinski, R. R.; Stryker, J. M.; Tan, X. Supramolecular Assembly Model for Aggregation of Petroleum Asphaltenes. *Energy Fuels* **2011,** *25*, 3125-3134.

(28) Yen, T. F. Structure of Petroleum Asphaltene and its Significance. *Energy Sources*

1974, *1*, 447-463.

(29) Buenrostro-Gonzalez, E.; Groenzin, H.; Lira-Galeana, C.; Mullins, O. C. The Overriding Chemical Principles that Define Asphaltenes. *Energy Fuels* **2001,** *15*, 972-978.

(30) Andreatta, G.; Goncalves, C. C.; Buffin, G.; Bostrom, N.; Quintella, C. M.; Arteaga-Larios, F.; Pérez, E.; Mullins, O. C. Nanoaggregates and Structure−Function Relations in Asphaltenes. *Energy Fuels* **2005,** *19*, 1282-1289.

(31) Stachowiak, C.; Viguié, J. R..; Grolier, J. P. E.; Rogalski, M. Effect of n-Alkanes on Asphaltene Structuring in Petroleum Oils. *Langmuir* **2005,** *21*, 4824-4829.

(32) Takanohashi, T.; Sato, S.; Saito, I.; Tanaka, R. Molecular Dynamics Simulation of the Heat-Induced Relaxation of Asphaltene Aggregates. *Energy Fuels* **2003,** *17*, 135-139.

(33) Pacheco-Sánchez, J. H.; Álvarez-Ramírez, F.; Martínez-Magadán, J. M. Morphology of Aggregated Asphaltene Structural Models. *Energy Fuels* **2004,***18*, 1676-1686.

(34) Groenzin, H.; Mullins, O. C. Molecular Size and Structure of Asphaltenes from Various Sources. *Energy Fuels* **2000,** *14*, 677-684.

(35) Speight, J. G.; Moschopedis, S. E. Some Observations on the Molecular "Nature" of Petroleum Asphaltenes. *Am. Chem. Soc., Div. Pet. Chem. Prepr.* **1979,** *24*, 910-923.

(36) Speight, J. G. *The Chemistry and Technology of Petroleum,* 4th ed.; CRC Press: Boca Raton, 2006.

(37) Zajac, G. W.; Sethi, N. K.; Joseph, J. T.; Thomson, D. J.; Weiss, P. S. Molecular Imaging of Petroleum Asphaltenes by Scanning Tunneling Microscopy: Verification of Structure from ^{13}C and Proton Nuclear Magnetic Resonance Data. *Scanning Microscopy* **1994,** *8*, 463-470.

(38) Murgich, J.; Jesús Rodríguez, M.; Aray, Y. Molecular Recognition and Molecular Mechanics of Micelles of Some Model Asphaltenes and Resins. *Energy Fuels* **1996,** *10*,

68-76.

(39) Headen, T. F.; Boek, E. S.; Skipper, N. T. Evidence for Asphaltene Nanoaggregation in Toluene and Heptane from Molecular Dynamics Simulations. *Energy Fuels* **2009,** *23*, 1220-1229.

(40) Teklebrhan, R. B.; Ge, L.; Bhattacharjee, S.; Xu, Z.; Sjöblom, J. Probing Structure–Nanoaggregation Relations of Polyaromatic Surfactants: A Molecular Dynamics Simulation and Dynamic Light Scattering Study. *J. Phys. Chem. B* **2012,** *116*, 5907-5918.

(41) Zhang, L.; Greendfield, M. L. Molecular Orientation in Model Asphalts Using Molecular Simulation. *Energy Fuels* **2007,** *21*, 1102-1111.

(42) Andrews, A. B.; McClelland, A.; Korkeila, O.; Demidov, A.; Krummel, A.; Mullins, O. C.; Chen, Z. Molecular Orientation of Asphaltenes and PAH Model Compounds in Langmuir−Blodgett Films Using Sum Frequency Generation Spectroscopy. *Langmuir* **2011,** *27*, 6049-6058.

(43) González, M. F.; Stull, C. S.; López-Linares, F.; Pereira-Almao, P. Comparing Asphaltene Adsorption with Model Heavy Molecules over Macroporous Solid Surfaces. *Energy Fuels* **2007,** *21*, 234-241.

(44) Jarne, C.; Cebolla, V. L.; Membrado, L.; Le Mapihan, K.; Giusti, P. High-Performance Thin-Layer Chromatography Using Automated Multiple Development for the Separation of Heavy Petroleum Products According to Their Number of Aromatic Rings. *Energy Fuels* **2011,** *25*, 4586-4594.

(45) Schüttelkopf, A. W.; Van Aalten, D. M. F. PRODRG: A Tool for High-Throughput Crystallography of Protein-Ligand Complexes. *Acta Crystallogr. Sect. D: Biol. Crystallogr.* **2004,** *60*, 1355-1363.

(46) Oostenbrink, C.; Villa, A.; Mark, A. E.; Van Gunsteren, W. F. A Biomolecular Force Field Based on the Free Enthalpy of Hydration and Solvation: The GROMOS Force-Field Parameter Sets 53A5 and 53A6. *J. Comput. Chem.* **2004,** *25*, 1656-1676.

(47) Lemkul, J. A.; Allen, W. J.; Bevan, D. R. Practical Considerations for Building GROMOS-Compatible Small-Molecule Topologies. *J. Chem. Inf. Model.* **2010,** *50*, 2221-2235.

(48) Hess, B.; Kutzner, C.; van der Spoel, D.; Lindahl, E. GROMACS 4: Algorithms for Highly Efficient, Load-Balanced, and Scalable Molecular Simulation. *J. Chem. Theory Comput.* **2008,** *4*, 435-447.

(49) van der Spoel, D.; Lindahl, E.; Hess, B.; Groenhof, G.; Mark, A. E.; Berendsen, H. J. C. GROMACS: Fast, Flexible, and Free. *J. Comput. Chem.* **2005,** *26*, 1701-1718.

(50) Lindahl, E.; Hess, B.; van der Spoel, D. GROMACS 3.0: A Package for Molecular Simulation and Trajectory Analysis. *J. Mol. Model.* **2001,** *7*, 306-317.

(51) Berendsen, H. J. C.; van der Spoel, D.; van Drunen, R. GROMACS: A Message-Passing Parallel Molecular Dynamics Implementation. *Comput. Phys. Commun.* **1995,** *91*, 43-56.

(52) Berendsen, H. J. C.; Postma, J. P. M.; van Gunsteren, W.; Hermans, J. In *Intermolecular Forces;* Pullman, B., Ed.; Reidel: Dordrecht, The Netherlands, 1981.

(53) Essmann, U.; Perera, L.; Berkowitz, M. L.; Darden, T.; Lee, H.; Pedersen, L. G. A Smooth Particle Mesh Ewald Method. *J. Chem. Phys.* **1995,** *103*, 8577-8593.

(54) Miyamoto, S.; Kollman, P. A. Settle: An Analytical Version of the SHAKE and RATTLE Algorithm for Rigid Water Models. *J. Comput. Chem.* **1992,** *13*, 952-962.

(55) Hess, B. P-LINCS: A Parallel Linear Constraint Solver for Molecular Simulation. *J.*

Chem. Theory Comput. **2008,** *4*, 116-122.

(56) van der Spoel, D.; van Maaren, P. J.; Berendsen, H. J. A Systematic Study of Water Models for Molecular Simulation: Derivation of Water Models Optimized for Use with a Reaction Field. *J. Chem. Phys.* **1998,** *108*, 10220-10230.

(57) Zielkiewicz, J. Structural Properties of Water: Comparison of the SPC, SPCE, TIP4P, and TIP5P Models of Water. *J. Chem. Phys.* **2005,** *123*, 104501.

(58) Humphrey, W.; Dalke, A.; Schulten, K. VMD: Visual Molecular Dynamics. *J. Mol. Graphics* **1996,** *14*, 33-38.

(59) Hunter, C. A.; Sanders, J. K. The Nature of π-π Interactions. *J. Am. Chem. Soc.* **1990***, 112*, 5525-5534.

(60) Pisula, W.; Tomović, Ž; Simpson, C.; Kastler, M.; Pakula, T.; Müllen, K. Relationship between Core Size, Side Chain Length, and the Supramolecular Organization of Polycyclic Aromatic Hydrocarbons. *Chem. Mater.* **2005,** *17*, 4296-4303.

(61) Cussler, E. L. *Diffusion: Mass Transfer in Liquid Systems,* 2nd ed.; Cambridge University Press: Cambridge, U.K., 1997.

(62) Frenkel, D.; Smit, B. *Understanding Molecular Simulation: From Algorithms to Applications,*2nd ed.; Academic Press: San Diego, 2002.

(63) Balakrishnan, K.; Datar, A.; Naddo, T.; Huang, J.; Oitker, R.; Yen, M.; Zhao, J.; Zang, L. Effect of Side-Chain Substituents on Self-Assembly of Perylene Diimide Molecules: Morphology Control. *J. Am. Chem. Soc.* **2006,** *128*, 7390-7398.

Chapter 4: Aggregation of Violanthrone-78-Based Model Asphaltenes in Toluene*

4.1. Introduction

Because of their aggregation behaviors, widely observed in experiments,[1-7] asphaltenes have caused many problems during the processing of petroleum compounds, from production to transportation and refinement stages.[8-11] Asphaltenes are polycyclic aromatic hydrocarbon compounds with heteroatoms; the molecules typically consist of PA cores and aliphatic side chains, which can play different roles in their aggregation.[12,13] It is generally believed that the $\pi - \pi$ interaction among PA cores leads to their stacking, which is a critical driving force for asphaltene aggregation.[14-17] The $\pi - \pi$ stacking of PA cores has been widely confirmed in previous work. Mullins et al.[18] probed the structural order of four petroleum asphaltene samples (Ven20, UG8, BG5 and AR) by high-resolution transmission electron microscopy (TEM). The direct imaging of these samples clearly illustrated the stacking of PA cores. X-ray diffraction experiments on asphaltenes and vacuum residua isolated from three different crude oils (Maya, Khafji and Iranian Light) showed that the interlayer distance between neighboring stacked PA cores was approximately 3.5-3.6 Å.[19] The stacking of PA cores has also been observed in MD simulations conducted for asphaltenes.[20-24] In particular, Murgich et al.[25] performed MM minimization and MD sampling of molecular models developed from a residue of a Venezuelan crude. Different initial dimer, trimer and tetramer configurations were adopted, including both perpendicular and parallel configurations. By comparing energy, the most stable final

*A version of this chapter has been published. Reprinted with permission from Jian, C.; Tang, T.; Bhattacharjee, S. Molecular Dynamics Investigation on the Aggregation of Violanthrone78-Based Model Asphaltenes in Toluene. *Energy Fuels* **2014,** *28,* 3604-3613.

configuration was shown to be parallel stacking.

The aliphatic side chains in asphaltenes, on the other hand, have been generally thought to hinder the PA core stacking.[13,20,23] Zhang et al.[26] investigated the relative orientation between two neighboring PA cores and showed that at room temperature (298.15 K) asphaltene molecules with short alkane branches preferred to stay almost parallel to each other whereas those with long alkane branches had a preferred relative orientation of around 40°. Through high–Q ultrasonic spectroscopy and direct-current electrical conductivity measurement, it was found that when asphaltenes from UG8 Kuwait crude oil were mixed with toluene at the concentration range of 100 mg/L - 2 g/L, there existed a maximum size for the structure formed from PA core stacking, which was attributed to the steric hindrance of the side chains.[27,28] Asphaltene structures detected by TEM showed that the removal of alkyl chains during hydroprocessing allowed asphaltenes to rearrange their PA cores, leading to well-ordered stacked layers in solid state.[29] MD simulations conducted for asphaltene-like molecules in toluene and heptane have also shown the existence of non-parallel stacking of PA cores due to the steric hindrance of the side chains.[21,23] On the other hand, works that reported opposite roles of aliphatic side chains also exist in literature. In particular, for model asphaltenes in vacuum, the stacking structures were shown to depend on the specific molecular models used,[30] and aliphatic side chains could increase the stability of asphaltene aggregates.[31] Studies on the interactions between n-alkanes and asphaltenes using titration calorimetry and inverse chromatography also suggested that side-chain interactions were responsible for the formation and stabilization of asphaltene aggregates.[32]

Besides intermolecular interactions among asphaltene molecules, their aggregation behavior also strongly depends on the surrounding solvent. By definition, asphaltenes are toluene soluble but n-heptane insoluble.[33,34] Kuznicki et al.[20] conducted MD simulations for asphaltenes

in water, toluene and heptane. They found that the aggregation rate for asphaltenes in toluene and heptane was smaller compared with that in water. Boek et al.[24] conducted MD simulations for their model asphaltene in toluene and heptane, and found that although asphaltene dimers/trimers could not stay stable for longer than 10 ns in either solvents, the average aggregation time and numbers were larger in heptane than in toluene. To address such difference, studies have been carried out in order to understand the molecular mechanism of asphaltene aggregation in different solvents.

MM calculations by Murgich et al.[35] indicated that asphaltene aggregation may be promoted through water-mediated hydrogen bonding between their heteroatoms. Determined by calorimetric titration, the Gibbs free energy associated with addition of water into asphaltenes/toluene solution was also shown to be in the range of the free energy for hydrogen bonding formation.[36] In our recent MD study, a series of asphaltene models, which had different aliphatic/aromatic ratios, and contained oxygen as the only heteroatom, were simulated.[37] For 24 asphaltene molecules in water, it was found that[37] while asphaltene with very short side chains could fully aggregate through strong PA core interactions, those with very long side chains could also fully aggregate due to the compensation from hydrophobic association among the side chains. Asphaltenes with intermediate side chains were most difficult to aggregate because of the strong interference with $\pi - \pi$ stacking and insufficient side-chain interactions.

For asphaltenes in organic solvents, Wang et al.[38] investigated the interaction energy between asphaltene and heptol, a mixture of heptane and toluene. They showed that the interaction energy between asphaltene and solvent molecules approached that between pure asphaltenes as the volume fraction of toluene increased, indicating relatively similar molecular interactions between asphaltene and toluene compared to the interactions among asphaltenes.

Durand et al.[39] investigated the diffusion coefficients of asphaltenes, from Buzurgan, Athabasca and Maya crudes, in toluene-d_8 using ^{1}H diffusion-ordered spectroscopy and NMR. For each type of asphaltenes, they obtained a constant diffusion coefficient below a certain asphaltene concentration and a continuous decrease in the diffusion coefficient beyond this concentration. These findings indicated that solute-solvent interactions were predominant at low asphaltene concentrations whereas solute-solute interactions were dominant at higher concentrations. Mullins et al.[13] proposed that the interference of aliphatic side chains with the stacking of PA cores was crucial to maintain asphaltene's solubility in toluene, and investigated this hypothesis by studying asphaltenes from different origins using experimental techniques such as fluorescence depolarization and fluorescence emission spectroscopy. They found that to maintain solubility, asphaltene molecules lacking alkane chains could only have small PA cores; while molecules with long chains could have larger PA cores because of the stronger disruption of long chains to core stacking. Despite the above efforts, a clear understanding on the mechanisms driving asphaltenes aggregation in organic solvents is still far from being complete. What are the contributions from the aliphatic and aromatic regions to aggregation? Will the aggregation behavior vary as the relative sizes of PA cores and side chains change? How does the aggregation mechanism in organic solvents differ from that in water? Answers to these questions can provide insights into solubility behaviors of asphaltenes in different environments, which is useful for proposing means to reduce asphaltene aggregation during petroleum processing.

In this chapter, we investigate the aggregation mechanism and aggregated structures of asphaltenes in toluene by simulating four types of molecules with different aliphatic/aromatic ratios (from 0.24 to 0.94). Attractions that may exist between toluene and the aliphatic and aromatic regions of the model asphaltenes are examined. These model molecules were simulated

in our earlier work[37] to investigate their aggregation behaviors in water. Comparison of their different behaviors in toluene and in water provides elucidation on the different driving forces for aggregation in these two solvents. The remainder of this chapter is organized as follows: in section 4.2, the molecular models studied and simulation procedures are described. The aggregation mechanisms and aggregated structures are explained in section 4.3, together with a detailed discussion on the distinct behaviors of model asphaltenes in water and in toluene. Conclusions are given in section 4.4.

4.2. Methods

4.2.1. Asphaltene Models

The asphaltene models simulated here are based on VO-78 ($C_{70}H_{84}O_6$),[40-42] which has been used in our earlier work[37] to probe the aggregation of asphaltenes in water. Asphaltene models with different aliphatic/aromatic ratios, defined as the ratio between the number of interconnected aliphatic hydrocarbons on the side chains and the number of carbons in the PA core, were built using the approach described in our previous work.[37] The chemical structures of these models are shown in Figure 4.1, and their aliphatic/aromatic ratios are respectively 0.94, 0.71, 0.47 and 0.24. Throughout this chapter, they will be referred to as VO-16C, VO-12C, VO-8C and VO-4C, where 16, 12, 8 and 4 correspond to the numbers of interconnected aliphatic hydrocarbons on each side chain. It should be emphasized that the goal of this study is to elucidate the effect of side-chain length on the aggregation of asphaltenes in toluene while keeping the PA core and the types of heteroatoms fixed. Hence, heteroatoms other than oxygen originally present in the VO-78 molecules are not considered. Inclusion of other elements is feasible, but it will make the study of the relative proportion of aromatic and aliphatic contributions to asphaltene aggregation very complicated. Recent work by Breure et al.[17] also justified the approach of employing a

single compound without heteroatoms to investigate asphaltene aggregation. In addition, in our previous work[37] on the aggregation of these four asphaltene models in water, the size of the aggregation showed a non-monotonic dependence on the aliphatic/aromatic ratios. It is therefore interesting to examine whether such a non-monotonic relationship remains in toluene.

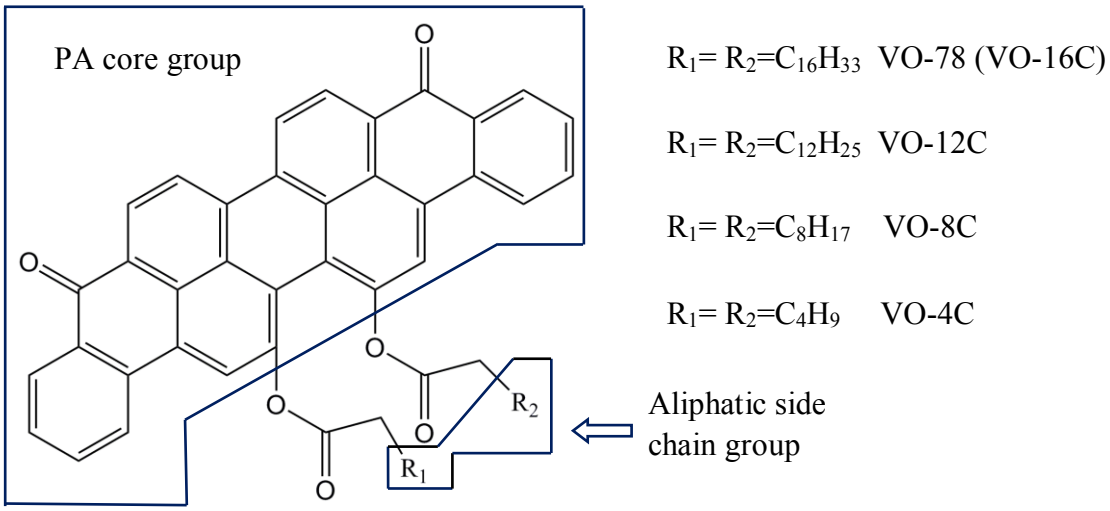

Figure 4.1: Chemical structures of the four asphaltene models employed in this chapter.

4.2.2. Simulation Procedure

Four systems were simulated, each containing 24 molecules of a single type of asphaltene models shown in Figure 4.1, and were named systems VO-16C, VO-12C, VO-8C and VO-4C, respectively. For each system, the initial configuration was constructed in a cubic box with an edge dimension of 12 nm and the 24 molecules formed a 2×3×4 array with their PA cores parallel to one another. The spacing between the mass centers of two neighboring asphaltene molecules is respectively 5.2, 3 and 2.6 nm in the three directions. Then the box was randomly filled with toluene molecules. The details of the four systems are available in Appendix B (section B.1). These four systems represent a high concentration (~20 g/L), far above the CNAC

(50~150 mg/L) and even the CCC (2~5 g/L) for asphaltenes in toluene proposed in literature.[43] Hence, formation of aggregates is expected.

All simulations were performed using the MD package GROMACS (version 4.0.7).[44-47] The topology for each asphaltene model was adopted from our previous work.[37] Partial charges on the molecular models are available in Appendix B (section B.1). The topology for toluene molecular model was generated from phenylalanine amino acid fraction in the GROMOS96 force field parameter set 53A6[48] through the *pdb2gmx* routine in GROMACS.

During each simulation, static structure optimization was first performed to ensure that the maximum force is less than 1000.0 kJ/(mol*nm). Then harmonic potential was applied on the non-hydrogen atoms of the solutes with a spring constant of 1000 kJ/(mol·nm^2) while the solvent molecules were allowed to relax around the solutes for 1 ns. The restraint was then removed and NPT ensemble simulation was performed for 80 ns. Parrinello-Rahman barostat[49] was used to keep the average pressure at 1 bar and a velocity rescaling thermostat[50] was used to keep the average temperature at 300 K. It should be mentioned that the velocity rescaling coupling method used here differs from the isokinetic scheme[51] of maintaining constant temperature. Instead, it is based on correctly producing the probability distribution of kinetic energy under constant temperature, and therefore is an accurate method. In all the simulations, periodic boundary condition was applied; electrostatics was treated with particle-mesh Ewald method;[52] a cutoff distance of 1.4 nm was used for the calculation of non-bonded (van der Waals and electrostatic) interactions; the bonds were constrained through the LINCS[53] algorithm, and a time step of 2 fs was used in the integration. It should be pointed out that the simulation time employed here, 80 ns, is considerably longer compared with most previous works[20,21,23,24,26] on asphaltene aggregation.

4.2.3. Data Analysis

Appropriate post-processing programs available in GROMACS were used for trajectory analysis and VMD[54] used for visualization. Unless otherwise specified, all analysis was based on the last 10 ns of the simulation. Demonstration for the achievement of dynamics equilibrium in the last 10 ns is available in Appendix B (section B.2).

Inside each simulated system, the 24 model asphaltene molecules were labeled by numbers 1 to 24. To quantify the relative position between the PA cores of two model asphaltene molecules, we calculated the distance between the COG of the two PA cores. Similarly, COG distance was also calculated between the PA core of one model asphaltene molecule and the aromatic core of one toluene molecule in order to describe their relative position. The relative orientation between two PA cores or between one PA core and one toluene aromatic core was determined by first approximating the PA core plane or the aromatic core plane of toluene by three aromatic carbons. The cosine of the angle between any two planes ("$\cos\sigma$") was then calculated.

To quantify the intensity of the interactions between PA cores ($\pi-\pi$ interaction), between PA core and aliphatic chain ($\pi-\theta$ interaction) and between aliphatic chains ($\theta-\theta$ interaction), we first separated each model asphaltene molecule into two groups: one containing the united atoms in the chain region, called "aliphatic side chain group" indicated by the bottom right box in Figure 4.1, and the other containing the heavy (non-hydrogen) atoms in the core region, called "PA core group" indicated by the top left box in Figure 4.1. Then the minimum distance ("MIN distance") between any two groups was calculated to compute the numbers of $\pi-\pi$, $\pi-\theta$ and $\theta-\theta$ contacts. For each pair of model asphaltene molecules, a $\pi-\pi$ contact was counted if the MIN distance between their PA core groups was ≤ 0.5 nm; a $\pi-\theta$ contact

was counted if the MIN distance between the PA core group from one molecule and the aliphatic side chain group from the other molecule was ≤ 0.5 nm; a $\theta - \theta$ contact was counted if the MIN distance between their aliphatic side chain groups was ≤ 0.5 nm.

A quantity useful to describe the dynamics of interaction between two molecules is the time correlation coefficient. For example, the coefficient for the correlation between COG distance of PA cores of two model asphaltene molecules at time $t_0 + \Delta t$ and that at time t_0 can be calculated by the Pearson correlation formula:[55,56]

$$\gamma(\Delta t) = \frac{\langle (d(t_0) - \langle d_{t_0} \rangle) * (d(t_0 + \Delta t) - \langle d_{t_0 + \Delta t} \rangle) \rangle}{\{\langle [d(t_0) - \langle d_{t_0} \rangle]^2 \rangle \langle [d(t_0 + \Delta t) - \langle d_{t_0 + \Delta t} \rangle]^2 \rangle\}^{0.5}}, \quad (4.1)$$

where $\gamma(\Delta t)$ is the correlation coefficient for time separation Δt, and $d(t_0)$ and $d(t_0 + \Delta t)$ are the COG distances between PA cores of any two model asphaltene molecules at time t_0 and $t_0 + \Delta t$ respectively. $\langle d_{t_0} \rangle$ and $\langle d_{t_0 + \Delta t} \rangle$ are respectively the average distances between two model asphaltene molecules at time t_0 and $t_0 + \Delta t$. Since in each simulated system, there are 24 model asphaltene molecules, resulting in total $\frac{24 \times 23}{2} = 276$ pairs of distances at any time. Therefore the averages were performed over all 276 pairs as well as over different time origins t_0. According to eq. 1, $\gamma = \pm 1$ implies that there is a perfectly linear relationship between $d(t_0)$ and $d(t_0 + \Delta t)$ whereas $\gamma = 0$ corresponds to the case where the linear correlation between $d(t_0)$ and $d(t_0 + \Delta t)$ is weak. γ always takes the value of 1 at $\Delta t = 0$ and decays as Δt increases. The rate of decay for γ is an indicator for the strength of the correlation.

4.3. Results and Discussion

4.3.1. Basic Characteristics of Aggregation

By visually examining the simulation trajectories, we found that aggregates formed by model asphaltene molecules are very unstable, which can be verified by plotting the number of model

asphaltene molecules in the largest aggregates as a function of simulation time as shown in Figure 4.2. The number of associated molecules is determined by the single-linkage algorithm implemented in GROMACS with a cutoff distance of 0.5 nm. It can be seen that for all four systems, the number of model asphaltene molecules in the largest aggregates fluctuates quite significantly, corresponding to the unstable aggregates formed in toluene. From 70 to 80 ns of the simulations, the largest aggregates in the four systems that do not break during this period contain similar numbers of molecules: 7, 10, 7 and 7 in systems VO-4C, VO-8C, VO-12C and VO-16C respectively. This observation seems to imply that for the model asphaltenes studied here, which have aliphatic/aromatic ratios from 0.24 to 0.94, the overall extent of aggregation has negligible dependence on the actual value of the ratio, and the aliphatic side chains have little contribution to aggregating the asphaltenes.

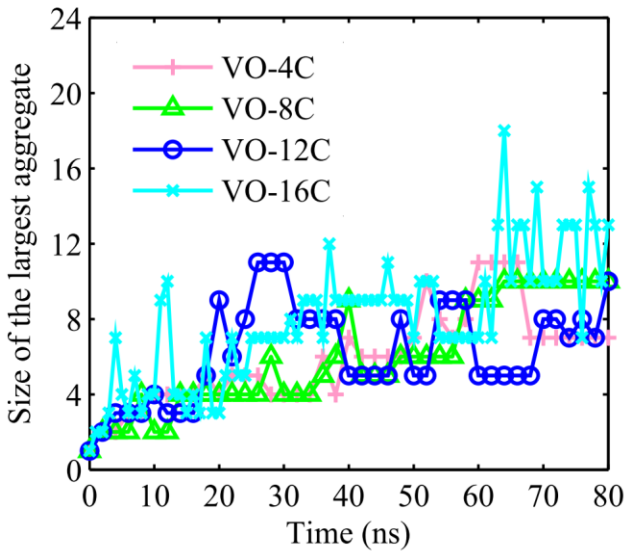

Figure 4.2: Size of the largest aggregate quantified by the number of model asphaltene molecules in the largest aggregate.

Detailed examination on the intermolecular contacts confirms the insensitivity of aggregation to the aliphatic/aromatic ratio. Figure 4.3 shows the numbers of $\pi - \pi$, $\pi - \theta$ and

$\theta - \theta$ contacts as a function of simulation time for the four systems. The first observation from Figure 4.3 is that all three types of contacts are very similar among the four systems. In particular, the number of $\pi - \pi$ contacts is ~20 in all cases. Among the three types of contacts, the number of $\theta - \theta$ contacts is the smallest even for asphaltene with very long side chains. For example, in VO-12C the average number of $\theta - \theta$ contacts is 14 as compared to 22 $\pi - \pi$ contacts and 47 $\pi - \theta$ contacts. This suggests little association among the side chains and insignificant contribution to aggregation from $\theta - \theta$ interactions. More interestingly, it can be seen that VO-12C and VO-16C, which have very long side chains, do not possess greater number of $\pi - \theta$ contacts compared with VO-4C and VO-8C. While in the past, longer side chains were generally believed to have stronger interference with $\pi - \pi$ interaction,[13,23,37] the results here suggest that for asphaltene aggregation in toluene, longer side chains do not introduce more disruptions to the number of $\pi - \pi$ contacts. Nor do they form more contacts with the PA cores compared with shorter chains. This leads us to propose that asphaltene aggregation in toluene is mainly driven by $\pi - \pi$ interaction among the PA cores, and the aliphatic regions of the molecules play negligible roles in causing aggregation. Below, we verify this hypothesis by taking a detailed look at the aggregated structure.

4.3.2. Aggregated Structure

Figure 4.4a shows the RDFs for the COG distance r (nm) between PA cores of model asphaltenes. It can be seen that for all four models the first peak in the RDF is located at COG distance of ~0.45 nm, which is also the most pronounced peak in the RDF. Following the first peak, the next peak is located at ~0.75 nm. There are several peaks afterwards, but they are much smaller compared with the first two, and there are no noticeable peaks beyond 2 nm. Since peaks

in the RDFs may be associated with particular aggregated structure, the first two peaks are examined in detail.

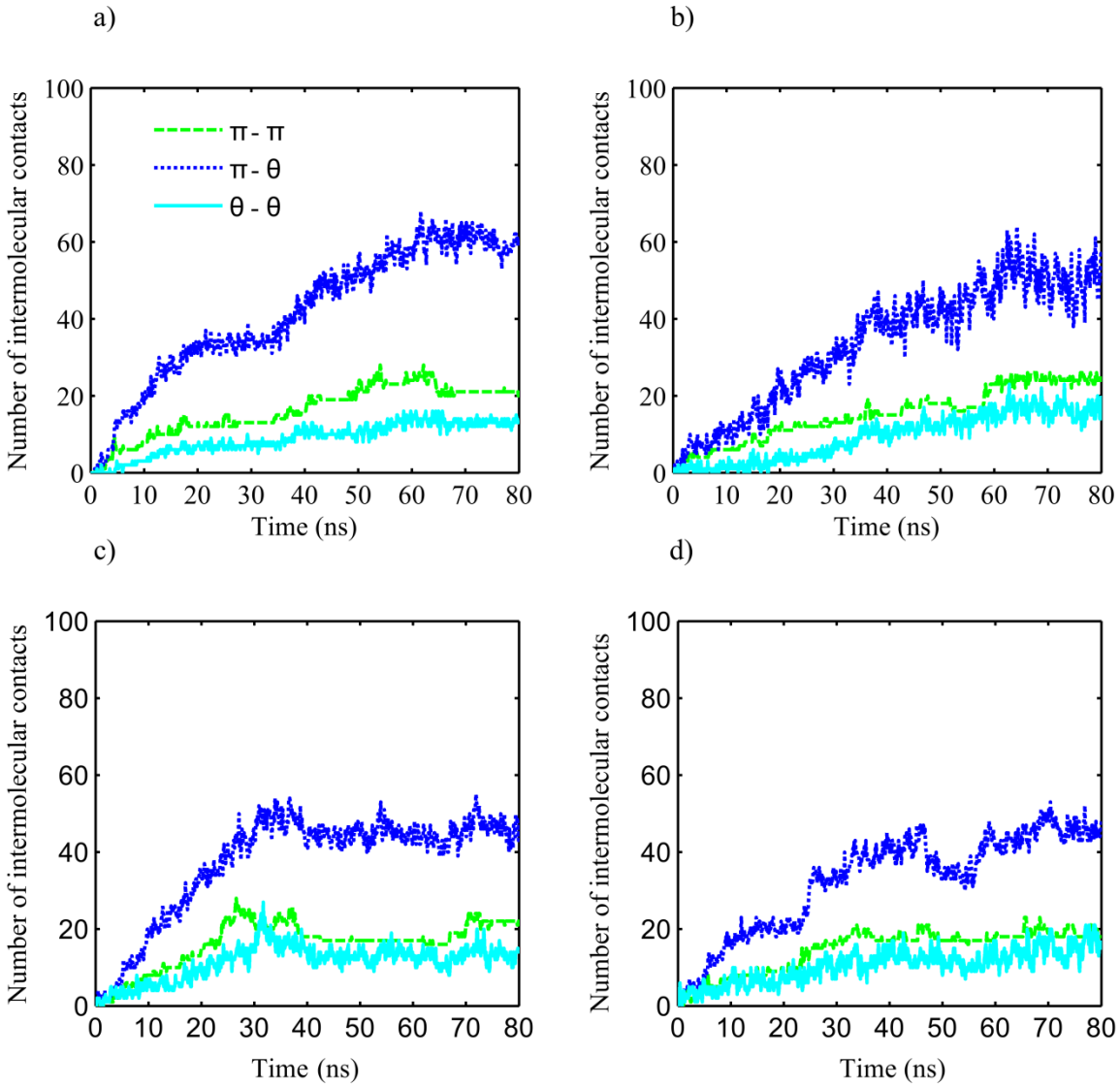

Figure 4.3: Numbers of $\pi - \pi$, $\pi - \theta$ and $\theta - \theta$ contacts for the 4 systems: (a) VO-4C, (b) VO-8C, (c) VO-12C and (d) VO-16C.

Firstly, the location of the first peak, ~0.45 nm, is similar to the COG distance between two $\pi - \pi$ stacked PA cores revealed by our previous work,[37] and is consistent with the minimum interlayer separation between stacked PA cores (~0.35 nm).[19,37,57] To confirm the $\pi - \pi$ stacking structure, the orientation of any two PA cores at COG distance of ~0.45 nm is

determined through the PDF for $\cos\sigma$ at this distance, as shown in Figure 4.4b. It can be seen that the PDF has its sole and significant peak at $\cos\sigma$ close to 1, demonstrating the parallel

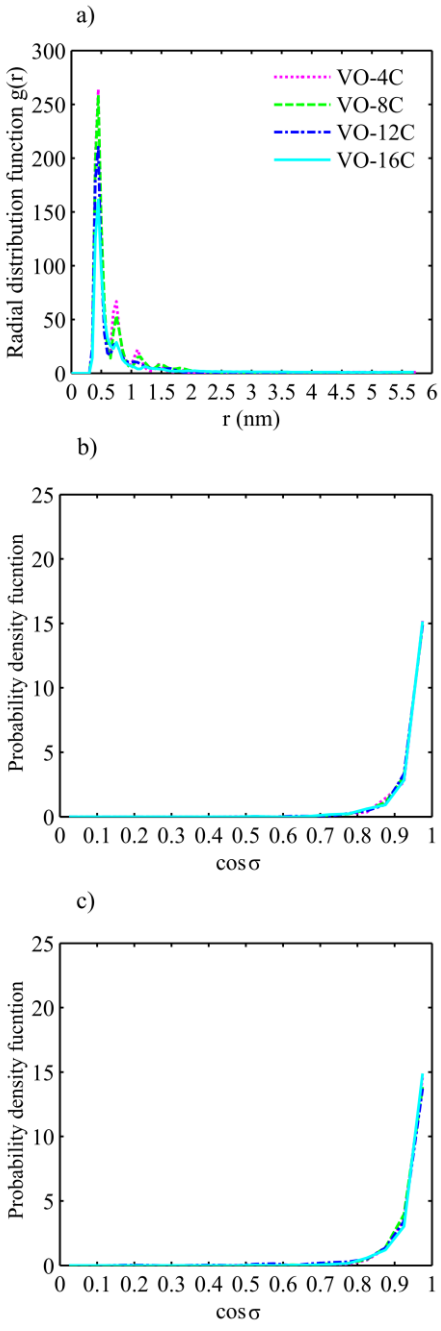

Figure 4.4: (a) RDFs for COG distance r (nm) between PA cores, (b) PDF for $\cos\sigma$ at COG distance of ~0.45 nm and (c) PDF for $\cos\sigma$ at COG distance of ~0.75 nm. σ is the angle between two PA planes.

alignment between the two PA cores. This is a configuration in which the COG of one PA core is directly on top of the other with side chains being excluded from the stacking region. Hereafter such a configuration, which is quantified by two PA cores having COG distance ≤0.5 nm and $\cos\sigma \geq 0.9$, will be referred to as DPS mode. Through the simulations, we found that although the size of the aggregates fluctuates a lot (Figure 4.2), the DPS pairs, once formed, are very stable (see Figure B.2 in Appendix B, Section B.3). Further inspection of Figure 4.4a shows that at COG distance of ~0.45 nm, the peaks of the RDF for the four systems have a clear order: VO-4C>VO-8C>VO-12C>VO-16C, suggesting that model asphaltenes with shorter side chains are more likely to form DPS structure. To explore this in a more quantitative manner, we define m-MDPS mode, where m is an integer and can be replaced by a specific number, as follows. If molecules 1 and 2 form a DPS pair and molecules 2 and 3 form a DPS pair, then molecules 1, 2 and 3 are said to be in a 3-MDPS mode; similar definitions hold for 4-MDPS, 5-MDPS modes, etc. The numbers of DPS pairs and m-DMPS structures formed in the four systems are summarized in Table 4.1. System VO-4C has the largest total number of DPS pairs (14), compared with 13 in VO-8C, 10 in VO-12C and 8 in VO-16C. In addition, the largest m-MDPS structure formed in system VO-4C is 7-MDPS, whereas system VO-8C can only form a 4-MDPS structure, VO-12C has two 3-MDPS structures and only one 3-MDPS structure is found in VO-16C. Clearly with the increase in side- chain length, there is a decreasing trend for both the total number of DPS pairs and the size of the m-MDPS structures. One might attribute this to stronger interference of longer side chains with the number of $\pi - \pi$ contacts. However, in section 4.3.1 the numbers of $\pi - \pi$ and $\pi - \theta$ contacts are found to be comparable in the four system; long side chains in VO-12C and VO-16C do not lead to increased interaction between the PA cores

and the aliphatic chains. To understand this seemly contradiction, it is necessary to look at the second peak in the RDF curve.

Table 4.1: Number of DPS Pairs and m-MDPS Structures for Model Asphaltenes in Toluene

systems	VO-4C	VO-8C	VO-12C	VO-16C
DPS pairs	14	13	10	8
2-MDPS	1		6	6
3-MDPS	2	5	2	1
4-MDPS	1	1		
5-MDPS				
6-MDPS				
7-MDPS	1			

The second peak in the RDF is located at ~0.75 nm, and the associated PDF for $\cos\sigma$ is shown in Figure 4.4c. It can be seen that at this COG distance, the most popular configuration for two PA cores is still parallel. In fact, this is the configuration where one PA core plane is parallel to a second one, but its COG is not directly on top of the other COG. Such a configuration will be referred to as SPS, and quantified by two PA cores having 0.5 nm <COG distance $\leq$ 0.75 nm and $\cos\sigma \geq 0.9$. DPS and SPS together will be defined as PS, and a PS pair is formed when two PA cores have COG distances $\leq$ 0.75 nm and $\cos\sigma \geq 0.9$. Similar to m-MDPS, m-MPS can be defined from the consecutive formation of PS by multiple molecules. The total numbers of PS pairs and m-MPS structures formed in the four systems are summarized in Table 4.2. The largest m-MPS structures for the four systems are respectively 7-MPS in VO-4C, 6-MPS in VO-8C, and 5-MPS in both VO-12C and VO-16C, the difference being much smaller compared with what was seen in Table 4.1. This implies that although when SPS is included, molecules with long side chains can form m-MPS structures that are only slightly smaller, they are much less likely to form large m-MDPS structures. The weaker capability of asphaltenes with long aliphatic side chains to form large m-MDPS structures is not due to interference of the side

chains with the number of $\pi - \pi$ contacts. Rather, it can be attributed to the greater steric hindrance and reduced molecular flexibility caused by the long side chains, which makes it difficult for a large number (> 3) of them to line up in a direct parallel fashion.

Table 4.2: Number of PS Pairs and m-MPS Structures for Model Asphaltenes in Toluene

systems	VO-4C	VO-8C	VO-12C	VO-16C
PS pairs	20	19	16	15
2-MPS			3	5
3-MPS	2	1	4	3
4-MPS	1	2		
5-MPS	1		1	1
6-MPS		2		
7-MPS	1			

In addition, our simulations revealed an interesting structure in the aggregates for VO-8C, VO-12C and VO-16C, namely that several small m-MPS structures in these systems can form a larger aggregate by aligning themselves in a parallel manner, but they are not able to form a larger m-MPS structure. Such a configuration is shown in Figure 4.5 (illustrated for VO-8C and VO-12C), where the black lines represent the axes for the small m-MPS structures. These axes are parallel in the aggregate, but do not coincide with one another. This configuration is not prevalent in system VO-4C, where each aggregate usually consists of a single m-MPS structure, but is quite popular in systems VO-8C, VO-12C and VO-16C. In particular, we calculated cosine of angle θ ("$\cos\theta$") between any two m-MPS structures involved in the largest aggregates during the last 10 ns of the simulation. To do so, we took an arbitrary molecule from one m-MPS structure as a reference molecule and calculated $\cos\theta$ between the PA core of this reference molecule and those of all molecules in the other m-MPS structure. $\theta = 0^{\circ}$ $(\cos\theta = 1)$ corresponds to two m-MPS structures being parallel and $\theta = 90^{\circ}(\cos\theta = 0)$ corresponds to two m-MPS structures being perpendicular. Figure 4.6 shows the PDF of $\cos\theta$ for systems VO-8C,

VO-12C and VO-16C. In all cases, the PDF has the most significant peak at $\cos\theta$ close to 1, suggesting that the m-MPS structures in the aggregates tend to be parallel. Such an aggregated structure provides another reason for the observation that while model asphaltenes with long aliphatic side chains form slightly smaller m-MPS structures and much smaller m-MDPS structures, their overall extent of aggregation is similar to model asphaltenes with shorter side chains.

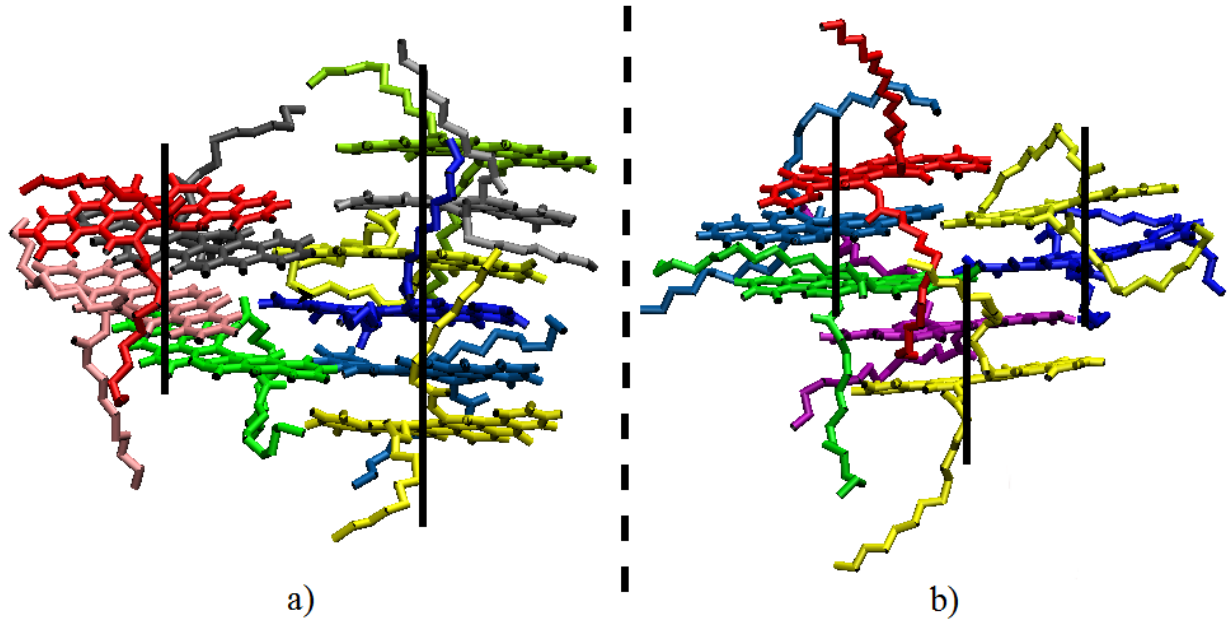

Figure 4.5: Snapshots of the largest aggregates that do not break during the last 10 ns of the simulation in systems: (a) VO-8C and (b) VO-12C.

One of the most accepted models that describe the aggregation behavior of asphaltenes in toluene is the Yen-Mullins model.[43,58,59] In this model, it is proposed that the asphaltene molecules first form nanoaggregates through the stacking of PA cores. Each nanoaggregate involves less than 10 molecules, and it consists of a single cylindrical polycyclic aromatic hydrocarbons stack residing in interior and alkanes in exterior. These nanoaggregates further form clusters each containing less than 10 nanoaggregates. Although limited by simulation time and system size, our results on the aggregated structures showed similarity to the Yen-Mullins

model, especially for systems VO-8C, VO-12C and VO-16C as seen above. Our simulations further allowed us to gain insights into the mechanisms of aggregation for asphaltenes in toluene. In particular, the aggregation is mainly driven by $\pi - \pi$ interaction between the PA cores even though the aliphatic/aromatic ratios were varied from 0.24 to 0.94. The aliphatic side chains have very limited interference with the number of $\pi - \pi$ contacts and the interference does not increase with increasing aliphatic/aromatic ratio. The role of long aliphatic side chains is to introduce steric hindrance which prohibits the formation of DPS of a large (>3) number of molecules. The overall extent of aggregation is insensitive to the actual aliphatic/aromatic ratios.

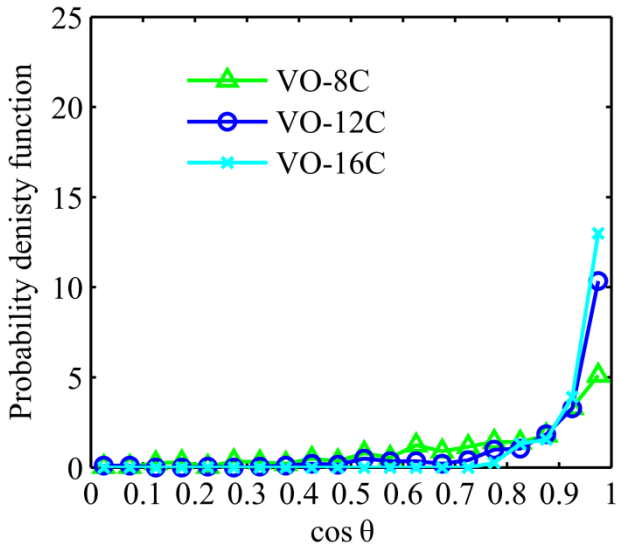

Figure 4.6: PDF for $\cos\theta$ between two m-MPS structures in the largest aggregates during the last 10 ns of the simulations.

Apart from the Yen-Mullins model, aggregation of model asphaltene molecules has also been investigated by MD simulations in literature. For instance, the work performed by Kuznicki et al.[20] on their conceptual asphaltene models also revealed the existence of parallel stacking by the PA cores although detailed examination of the stacking structures was not presented. In the same study, Kuznicki et al.[20] showed that as many as 24 asphaltene molecules could form stable

aggregates in toluene, which may be caused by the extremely high mass concentration used in their work (nearly septupled the value used here). On the contrary, the MD simulations done by Boek et al.[24] showed that no stable asphaltene dimers/trimers could live longer than 10 ns in toluene during their 60 ns simulations. Considering that more than doubled mass concentration was used in their work, the discrepancy may be attributed to the different asphaltene models employed in the simulations. In particular, the model asphaltene molecules simulated by Boek et al.[24] had smaller MW especially a smaller aromatic region, which might have led to weaker stacking interaction. For the aggregated structures, non-parallel stacking of PA cores were also reported in literature[21,23] as highly possible configurations between two adjacent asphaltene molecules, which were not observed here considering the prevalence of parallel stacking. Those simulations were usually conducted for a short period of time (around 10-20 ns) during which dynamic equilibrium may not have been reached.

4.3.3. Comparison with Model Asphaltene Aggregation in Water

Asphaltene is known to be soluble in toluene,[30,31] but not in water. Therefore, the comparison between model asphaltene aggregation in toluene and in water can allows us to address the role of the solvent in affecting the asphaltene-asphaltene interaction. The details for simulations in water are available in Chapter 3 and Appendix B (Section B.1).

For all four asphaltene models, the overall aggregation extent is less in toluene than in water, where all 24 molecules in VO-4C and VO-16C can fully aggregate and the largest aggregates in VO-8C and VO-12C consist of 10 and 13 molecules respectively.[37] Also, the model asphaltene aggregates formed in toluene are much less stable than those in water; in the latter case the aggregates never broke once formed. This suggests that the attraction among model asphaltene molecules is weaker in toluene. This can be confirmed by examining the time

correlation functions for the COG distance between PA cores of model asphaltene molecules in the two solvents, as shown in Figure 4.7. The analysis here was based on the last 10 ns of the simulations in toluene and the last 5 ns of the simulations in water. Although the time correlation functions in toluene still display ~80% correlations after 5 ns, due to the high concentration (~20 g/L) of model asphaltenes, compared with in water they evidently deviate more quickly from 1 as the time separation increases. This suggests that the intermolecular attractions between model asphaltene pairs in toluene are weaker, with the original COG distance maintained for a shorter time.

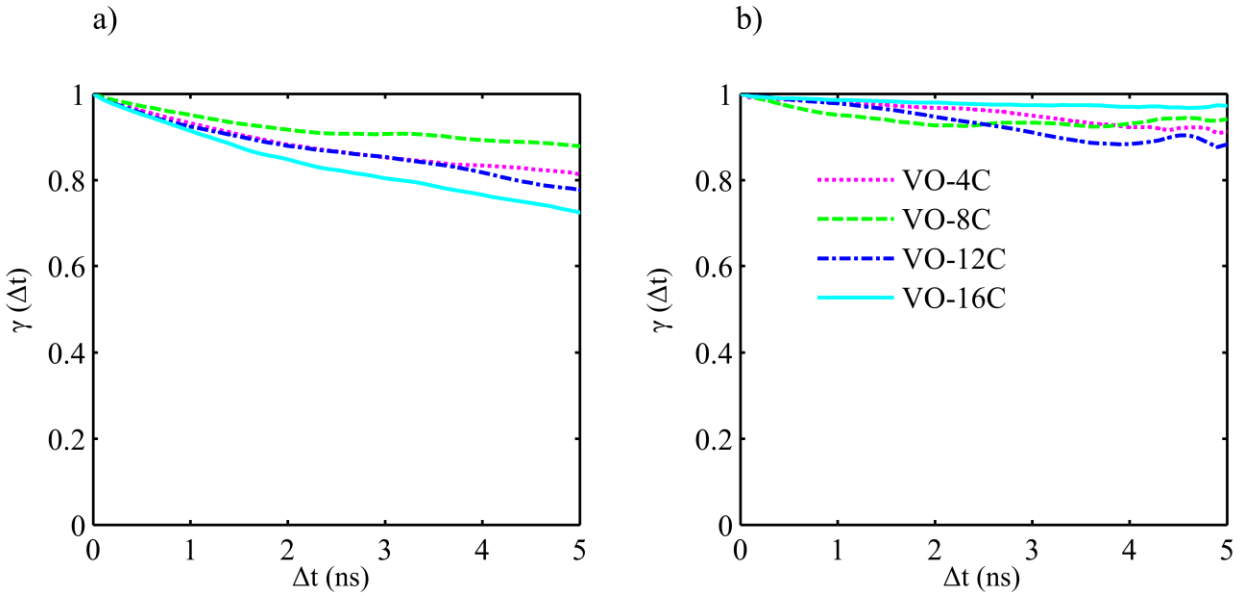

Figure 4.7: Time correlation functions for the COG distance between asphaltenes: a) in toluene and b) in water.

In addition, the mechanisms driving the aggregation are different in these two solvents. Table 4.3 compares the average numbers of $\pi-\pi$, $\pi-\theta$ and $\theta-\theta$ contacts in the two solvents at the final stage of the simulations. Both $\pi-\pi$ and $\pi-\theta$ contacts are higher in water compared to toluene, except for VO-8C, for which the $\pi-\theta$ contacts are identical in both solvents. The $\theta-\theta$ contacts are significantly more prevalent in water, with the ratio of contacts in water to

the contacts in toluene ranging between 2.69 to 5.62 as the aliphatic proportion of the asphaltene is increased (from VO-4C to VO-16 C). This indicates that while the aliphatic chains contribute little to the extent of aggregation in toluene, they play very important roles in promoting aggregation in water. The association among the side chains, due to hydrophobic interactions, provides an additional mechanism for asphaltenes aggregation in water and contributes to the much enhanced stability of the aggregates in water. It is also the side chain association that leads to the non-monotonic dependence of the aggregation size on the aliphatic/aromatic ratio in water and in particular the full aggregation observed for system VO-16C with large aliphatic/aromatic ratio.[37]

Table 4.3: Average Number of Intermolecular Contacts at the End Stage of the Simulation: Comparison between Two Different Solvents (Toluene vs Water)[a]

systems	VO-4C		VO-8C		VO-12C		VO-16C	
	toluene	water	toluene	water	toluene	water	toluene	water
$\pi-\pi$	21	45	24	29	22	35	19	30
$\pi-\pi$ ratio	2.14		1.2		1.59		1.57	
$\pi-\theta$	60	97	50	50	47	97	46	104
$\pi-\theta$ ratio	1.62		1		2.06		2.26	
$\theta-\theta$	13	35	16	45	14	59	16	90
$\theta-\theta$ ratio	2.69		2.81		4.21		5.62	

[a]The rows with "ratio" in the title indicate the ratio of the number of contacts in water to those in toluene.

Further distinctions exist in the aggregated structures in the two solvents. In toluene, because the main driving force for aggregation is the $\pi-\pi$ interaction, a large number of parallel stacking structures are formed, as seen in Table 4.2. In water, on the other hand, due to the increased $\pi-\theta$ and $\theta-\theta$ interactions, the PS pairs that can be formed in water are reduced (see Table 4.4). The number of molecules that can form large m-MPS structure also decreases in water. It should be noted that the total number of $\pi-\pi$ contacts is still larger in water than in

toluene (see Table 4.3). This is because a greater number of molecules aggregate in water, although their PA cores are not able to form as large m-MPS structures as in toluene. In other words, the aggregated structures in toluene involve fewer molecules, but they exhibit more ordered geometry. On the contrary, many molecules aggregate in water and they are densely packed to maximize not only the $\pi - \pi$ interaction, but also the $\pi - \theta$ and $\theta - \theta$ interactions, resulting in a less ordered structure.

Table 4.4: Number of PS Pairs and m-MPS Structures for Model Asphaltenes in Water

systems	VO-4C	VO-8C	VO-12C	VO-16C
PS pairs	17	14	13	12
2-MPS	2	5	6	4
3-MPS	3	3	3	4
4-MPS		1		
5-MPS	2			
6-MPS				
7-MPS				

The reduced intermolecular attractions (especially $\theta - \theta$ attraction) between model asphaltene molecules in toluene and hence better solubility are facilitated by the attraction between the solute (model asphaltene) and solvent (toluene) molecules. The first component of the attraction is between toluene and aliphatic side chains of model asphaltenes. To see this, we plotted in Figure 4.8 the average radius of gyration (R_g) of model asphaltene molecules, which shows the compactness of the molecular structure. In the initial configurations, each model asphaltene molecule has an extended structure as shown in Figure 4.1, where the aliphatic chains are fully solvated in the solvent. As the simulations start, it can be clearly seen that for the four asphaltene models in water, R_g decreases in the first 1 ns, corresponding to the folding of aliphatic side chains due to their hydrophobic nature. After this rapid decrease, R_g begins to slowly increase. This is because aggregates start forming among the solutes and the side chains are excluded from the region where the PA cores stack. On the contrary, for the asphaltene

models in toluene, R_g is almost a constant during the entire simulation course, and there is no apparent folding of the side chains. This suggests that there exists attraction between toluene and the aliphatic side chains, and the side chains remain solvated in toluene.

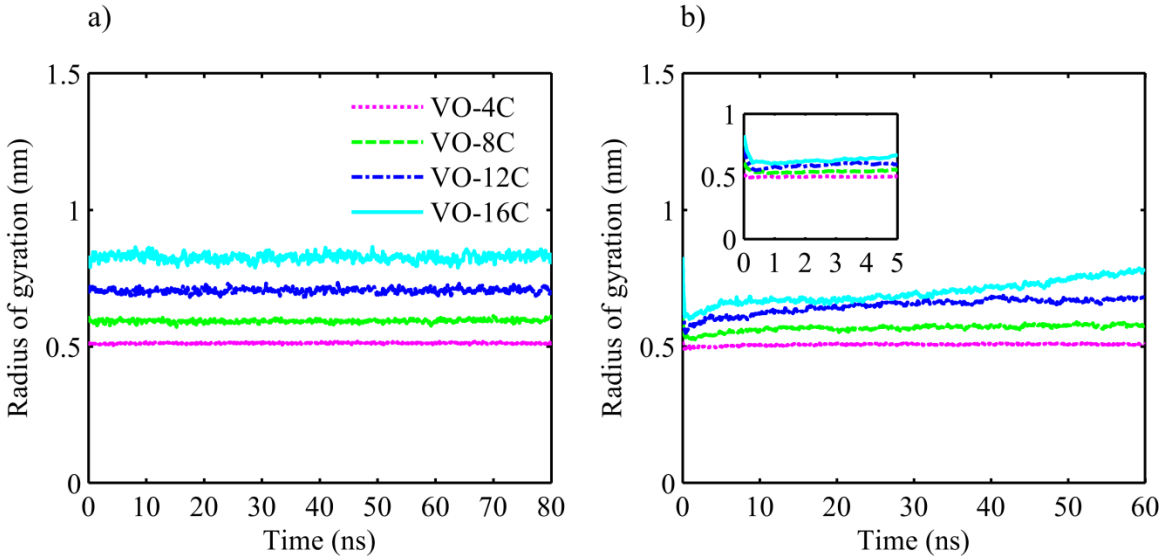

Figure 4.8: Radius of gyration as a function of simulation time for asphaltenes: (a) in toluene and (b) in water. The inset in (b) shows the enlarged initial 5 ns for water. In each subfigure, the curves from bottom to top are respectively for: VO-4C, VO-8C, VO-12C, and VO-16C

The second component of toluene-asphaltene attraction is between the model asphaltene PA cores and the toluene aromatic cores. Because of this structural similarity, it is expected that toluene molecules can have $\pi - \pi$ interaction with model asphaltene molecules. To probe this, we first plot the RDF for the COG distance of toluene aromatic cores from any model asphaltene PA cores, as shown in Figure 4.9a. It can be clearly seen that there is a peak at COG distance of ~0.5 nm, which is close to the COG distance between $\pi - \pi$ stacked aromatic cores. More interestingly, when we plot the PDF for the cosine of the angle ("$\cos\sigma$") between toluene and asphaltene cores at COG distance of ~0.5 nm (Figure 4.9b), it shows a prominent peak at $\cos\sigma \geq 0.9$. This indicates the formation of parallel stacking between toluene aromatic cores

and model asphaltene PA cores at short separations. That is, toluene molecules exhibit a certain degree of order when they are in the vicinity of the PA cores. The attraction of toluene with both aromatic and aliphatic regions of the asphaltene leads to weaker attractive interaction among the model asphaltene molecules, hence smaller and less stable aggregates in toluene compared with water.

Finally, the oxygen atoms present in the model asphaltenes can form hydrogen bonds with water, evidenced by the RDFs of hydrogen and oxygen atoms in water around oxygen atoms in the model asphaltenes (see Appendix B, section B.4). On the other hand, compared with water, toluene is less polar and none of the oxygen atoms in the model asphaltenes are connected to hydrogen. Therefore, we do not expect the formation of hydrogen bonds between model asphaltene and toluene molecules or between model asphaltene molecules.

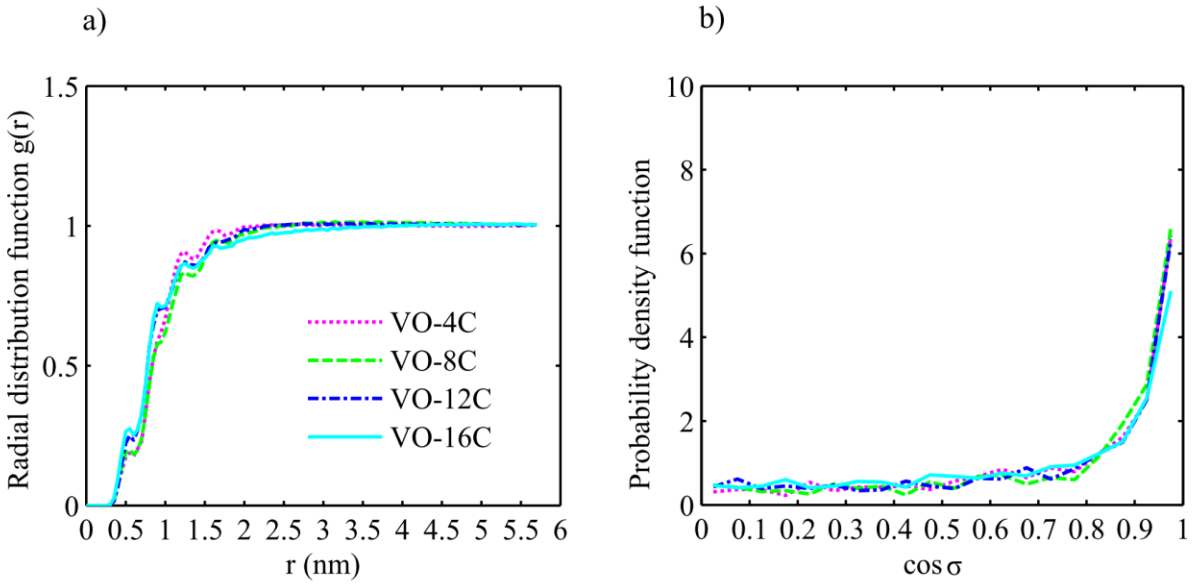

Figure 4.9: (a) RDF for the COG distance between toluene and model asphaltene core planes. (b) PDF for $\cos\sigma$ at COG distance of ~0.5 nm.

It is worth pointing out that the above comparison was made for the aggregation of model asphaltenes in toluene and water as bulk solvents. The situation where a small amount of water is

added to an organic solution of asphaltenes has been investigated, but very different findings were reported in literature. While some proposed that asphaltene aggregation in chloroform or toluene may be promoted by the addition of water,[35,36,60] others reported that the aggregation was not affected by the small amounts of water added.[61] Given that water is ubiquitous during petroleum processing and often co-exists with organic solvents, the role of water is important to study[62] and still needs further exploration.

4.4. Concluding Remarks

Asphaltene, by definition, is toluene-soluble.[33,34] Our MD simulation results show direct evidence for the formation of smaller and less stable aggregation in toluene compared with that in water. The larger solubility is caused by intermolecular attraction between toluene and both the aromatic and aliphatic regions of model asphaltenes. In particular, our results show that toluene can exhibit certain degree of order around the PA cores of model asphaltenes and tend to form parallel stacking with them at short distance (~0.5 nm). Simulations with different aliphatic/aromatic ratios reveal the aggregation mechanism of asphaltenes in toluene. For all aliphatic/aromatic ratios studied here (varying from 0.24 to 0.94), the main driving force for aggregation is the $\pi - \pi$ interaction among the PA cores. The aliphatic side chains do not contribute strongly to aggregation in toluene. Nor do they cause strong interference with the number of $\pi - \pi$ contacts through the formation of $\pi - \theta$ contacts. Instead, long side chains cause larger steric hindrance and less molecular flexibility which prohibits the formation of large direct parallel stacking structures that involve more than 3 molecules. However, asphaltene models with long side chains can aggregate through shifted parallel stacking as well as side-by-side arrangement of several m-MPS structures. The overall extent of aggregation is therefore insensitive to the actual aliphatic/aromatic ratio.

Bibliography

(1) Spiecker, P. M.; Gawrys, K. L.; Kilpatrick, P. K. Aggregation and Solubility Behavior of Asphaltenes and Their Subfractions. *J. Colloid Interface Sci.* **2003,** *267*, 178-193.

(2) Ho, B.; Briggs, D. E. Small Angle X-ray Scattering from Coal-Derived Liquids. *Colloids Surf.* **1982,** *4*, 271-284.

(3) Ravey, J. C.; Ducouret, G.; Espinat, D. Asphaltene Macrostructure by Small Angle Neutron Scattering. *Fuel* **1988,** *67*, 1560-1567.

(4) Andersen, S. I.; Birdi, K. S. Aggregation of Asphaltenes as Determined by Calorimetry. *J. Colloid Interface Sci.* **1991,** *142*, 497-502.

(5) Anisimov, M. A.; Yudin, I. K.; Nikitin, V.; Nikolaenko, G.; Chernoutsan, A.; Toulhoat, H.; Frot, D.; Briolant, Y. Asphaltene Aggregation in Hydrocarbon Solutions Studied by Photon Correlation Spectroscopy. *J. Phys. Chem.* **1995,** *99*, 9576-9580.

(6) Sjöblom, J.; Aske, N.; Auflem, I. H.; Brandal, Ø.; Havre, T. E.; Sæther, Ø.; Westvik, A.; Johnsen, E. E.; Kallevik, H. Our Current Understanding of Water-in-Crude Oil Emulsions.: Recent Characterization Techniques and High Pressure Performance. *Adv. Colloid Interface Sci.* **2003,** *100-102*, 399-473.

(7) Lisitza, N. V.; Freed, D. E.; Sen, P. N.; Song, Y. Study of Asphaltene Nanoaggregation by Nuclear Magnetic Resonance (NMR). *Energy Fuels* **2009,** *23*, 1189-1193.

(8) Groenzin, H.; Mullins, O. C. Asphaltene Molecular Size and Structure. *J. Phys. Chem. A* **1999,** *103*, 11237-11245.

(9) Mansoori, G. A. Modeling of Asphaltene and Other Heavy Organic Depositions. *J. Pet. Sci. Eng.* **1997,** *17*, 101-111.

(10) Escobedo, J.; Mansoori, G. A. Heavy Organic Deposition and Plugging of Wells (Analysis of Mexico's Experience). Presented at the SPE Latin America Petroleum Engineering Conference, Caracas, Venezuela, March 8−11, 1992; Paper SPE 23696.

(11) Kokal, S. L.; Sayegh, S. G. Asphaltenes: The Cholesterol of Petroleum. Presented at the SPE Middle East Oil Show, Bahrain, March 11−14, 1995; Paper SPE 29787.

(12) Ruiz-Morales, Y. HOMO−LUMO Gap as an Index of Molecular Size and Structure for Polycyclic Aromatic Hydrocarbons (PAHs) and Asphaltenes: A Theoretical Study. I. *J. Phys. Chem. A* **2002,** *106*, 11283-11308.

(13) Buenrostro-Gonzalez, E.; Groenzin, H.; Lira-Galeana, C.; Mullins, O. C. The Overriding Chemical Principles that Define Asphaltenes. *Energy Fuels* **2001,** *15*, 972-978.

(14) Dickie, J. P.; Yen, T. F. Macrostructures of the Asphaltic Fractions by Various Instrumental Methods. *Anal. Chem.* **1967,** *39*, 1847-1852.

(15) Yen, T. F. Structure of Petroleum Asphaltene and Its Significance. *Energy Sources* **1974,** *1*, 447-463.

(16) Murgich, J. Intermolecular Forces in Aggregates of Asphaltenes and Resins. *Pet. Sci. Technol.* **2002,** *20*, 983-997.

(17) Breure, B.; Subramanian, D.; Leys, J.; Peters, C. J.; Anisimov, M. A. Modeling Asphaltene Aggregation with a Single Compound. *Energy Fuels* **2012,** *27*, 172-176.

(18) Sharma, A.; Groenzin, H.; Tomita, A.; Mullins, O. C. Probing Order in Asphaltenes and Aromatic Ring Systems by HRTEM. *Energy Fuels* **2002,** *16*, 490-496.

(19) Tanaka, R.; Sato, E.; Hunt, J. E.; Winans, R. E.; Sato, S.; Takanohashi, T. Characterization of Asphaltene Aggregates Using X-ray Diffraction and Small-Angle X-ray Scattering. *Energy Fuels* **2004,** *18*, 1118-1125.

(20) Kuznicki, T.; Masliyah, J. H.; Bhattacharjee, S. Molecular Dynamics Study of Model Molecules Resembling Asphaltene-Like Structures in Aqueous Organic Solvent Systems. *Energy and Fuels* **2008,** *22*, 2379-2389.

(21) Headen, T. F.; Boek, E. S.; Skipper, N. T. Evidence for Asphaltene Nanoaggregation in Toluene and Heptane from Molecular Dynamics Simulations. *Energy and Fuels* **2009,** *23*, 1220-1229.

(22) Kuznicki, T.; Masliyah, J. H.; Bhattacharjee, S. Aggregation and Partitioning of Model Asphaltenes at Toluene−Water Interfaces: Molecular Dynamics Simulations. *Energy Fuels* **2009,** *23*, 5027-5035.

(23) Teklebrhan, R. B.; Ge, L.; Bhattacharjee, S.; Xu, Z.; Sjöblom, J. Probing Structure–Nanoaggregation Relations of Polyaromatic Surfactants: A Molecular Dynamics Simulation and Dynamic Light Scattering Study. *J Phys. Chem. B* **2012,** *116*, 5907-5918.

(24) Boek, E. S.; Yakovlev, D. S.; Headen, T. F. Quantitative Molecular Representation of Asphaltenes and Molecular Dynamics Simulation of Their Aggregation. *Energy Fuels* **2009,** *23*, 1209-1219.

(25) Murgich, J.; Rodríguez, J.; Aray, Y. Molecular Recognition and Molecular Mechanics of Micelles of Some Model Asphaltenes and Resins. *Energy Fuels* **1996,** *10*, 68-76.

(26) Zhang, L.; Greendfield, M. L. Molecular Orientation in Model Asphalts Using Molecular Simulation. *Energy Fuels* **2007,** *21*, 1102-1111.

(27) Andreatta, G.; Goncalves, C. C.; Buffin, G.; Bostrom, N.; Quintella, C. M.; Arteaga-Larios, F.; Pérez, E.; Mullins, O. C. Nanoaggregates and Structure−Function Relations in Asphaltenes. *Energy Fuels* **2005,** *19*, 1282-1289.

(28) Zeng, H.; Song, Y. -.; Johnson, D. L.; Mullins, O. C. Critical Nanoaggregate Concentration of Asphaltenes by Direct-Current (DC) Electrical Conductivity. *Energy Fuels* **2009,** *23*, 1201-1208.

(29) Trejo, F.; Ancheyta, J.; Rana, M. S. Structural Characterization of Asphaltenes Obtained from Hydroprocessed Crude Oils by SEM and TEM. *Energy Fuels* **2009,** *23*, 429-439.

(30) Pacheco-Sánchez, J. H.; Álvarez-Ramírez, F.; Martínez-Magadán, J. M. Morphology of Aggregated Asphaltene Structural Models. *Energy Fuels* **2004,** *18*, 1676-1686.

(31) Takanohashi, T.; Sato, S.; Saito, I.; Tanaka, R. Molecular Dynamics Simulation of the Heat-Induced Relaxation of Asphaltene Aggregates. *Energy Fuels* **2003,** *17*, 135-139.

(32) Stachowiak, C.; Viguie, J. R.; Grolier, J. P. E.; Rogalski, M. Effect of n-Alkanes on Asphaltene Structuring in Petroleum Oils. *Langmuir* **2005***, 21*, 4824-4829.

(33) Yarranton, H. W.; Alboudwarej, H.; Jakher, R. Investigation of Asphaltene Association with Vapor Pressure Osmometry and Interfacial Tension Measurements. *Ind. Eng. Chem. Res.* **2000,** *39*, 2916-2924.

(34) Speight, J. G.; Long, R. B.; Trowbridge, T. D. Factors Iinfluencing the Separation of Asphaltenes from Heavy Petroleum Feedstocks. *Fuel* **1984,** *63*, 616-620.

(35) Murgich, J.; Merino-Garcia, D.; Andersen, S. I.; Manuel del Río, J.; Galeana, C. L. Molecular Mechanics and Microcalorimetric Investigations of the Effects of Molecular Water on the Aggregation of Asphaltenes in Solutions. *Langmuir* **2002,** *18*, 9080-9086.

(36) Andersen, S. I.; del Rio, J. M.; Khvostitchenko, D.; Shakir, S.; Lira-Galeana, C. Interaction and Solubilization of Water by Petroleum Asphaltenes in Organic Solution. *Langmuir.* **2001,** *17*, 307-313.

(37) Jian, C.; Tang, T.; Bhattacharjee, S. Probing the Effect of Side-Chain Length on the Aggregation of a Model Asphaltene Using Molecular Dynamics Simulations. *Energy Fuels* **2013,** *27*, 2057-2067.

(38) Wang, S.; Liu, J.; Zhang, L.; Masliyah, J.; Xu, Z. Interaction Forces between Asphaltene Surfaces in Organic Solvents. *Langmuir* **2009,** *26*, 183-190.

(39) Durand, E.; Clemancey, M.; Lancelin, J.; Verstraete, J.; Espinat, D.; Quoineaud, A. Effect of Chemical Composition on Asphaltenes Aggregation. *Energy Fuels* **2010,** *24*, 1051-1062.

(40) Andrews, A. B.; McClelland, A.; Korkeila, O.; Demidov, A.; Krummel, A.; Mullins, O. C.; Chen, Z. Molecular Orientation of Asphaltenes and PAH Model Compounds in Langmuir−Blodgett Films Using Sum Frequency Generation Spectroscopy. *Langmuir* **2011,** *27*, 6049-6058.

(41) González, M. F.; Stull, C. S.; López-Linares, F.; Pereira-Almao, P. Comparing Asphaltene Adsorption with Model Heavy Molecules over Macroporous Solid Surfaces. *Energy Fuels* **2007,** *21*, 234-241.

(42) Jarne, C.; Cebolla, V. L.; Membrado, L.; Le Mapihan, K.; Giusti, P. High-Performance Thin-Layer Chromatography Using Automated Multiple Development for the Separation of Heavy Petroleum Products According to Their Number of Aromatic Rings. *Energy Fuels* **2011,** *25*, 4586-4594.

(43) Mullins, O. C.; Sabbah, H.; Eyssautier, J.; Pomerantz, A. E.; Barré, L.; Andrews, A. B.; Ruiz-Morales, Y.; Mostowfi, F.; McFarlane, R.; Goual, L, et al. Advances in Asphaltene Science and the Yen–Mullins Model. *Energy Fuels* **2012,** *26*, 3986-4003.

(44) Hess, B.; Kutzner, C.; van der Spoel, D.; Lindahl, E. GROMACS 4: Algorithms for Highly Efficient, Load-Balanced, and Scalable Molecular Simulation. *J. Chem. Theory Comput.* **2008,** *4*, 435-447.

(45) van der Spoel, D.; Lindahl, E.; Hess, B.; Groenhof, G.; Mark, A. E.; Berendsen, H. J. GROMACS: Fast, Flexible, and Free. *J. Comput. Chem.* **2005,** *26*, 1701-1718.

(46) Lindahl, E.; Hess, B.; van der Spoel, D. GROMACS 3.0: A Package for Molecular Simulation and Trajectory Analysis. *J. Mol. Model.* **2001,** *7*, 306-317.

(47) Berendsen, H. J.; van der Spoel, D.; van Drunen, R. GROMACS: A Message-Passing Parallel Molecular Dynamics Implementation. *Comput. Phys. Commun.* **1995,** *91*, 43-56.

(48) Oostenbrink, C.; Villa, A.; Mark, A. E.; Van Gunsteren, W. F. A Biomolecular Force Field Based on the Free Enthalpy of Hydration and Solvation: The GROMOS Force-Field Parameter Sets 53A5 and 53A6. *J. Comput. Chem.* **2004,** *25*, 1656-1676.

(49) Parrinello, M.; Rahman, A. Polymorphic Transitions in Single Crystals: A New Molecular Dynamics Method. *J. Appl. Phys.* **1981,** *52*, 7182-7190.

(50) Bussi, G.; Donadio, D.; Parrinello, M. Canonical Sampling through Velocity Rescaling. *J. Chem. Phys.* **2007,** *126,* 014101.

(51) Evans, D. J.; Morriss, G. P. Non-Newtonian Molecular Dynamics. *Comput. Phys. Rep.* **1984,** *1*, 297-343.

(52) Essmann, U.; Perera, L.; Berkowitz, M. L.; Darden, T.; Lee, H.; Pedersen, L. G. A Smooth Particle Mesh Ewald Method. *J. Chem. Phys.* **1995,** *103*, 8577.

(53) Hess, B. P-LINCS: A Parallel Linear Constraint Solver for Molecular Simulation. *J. Chem. Theory Comput.* **2008,** *4*, 116-122.

(54) Humphrey, W.; Dalke, A.; Schulten, K. VMD: Visual Molecular Dynamics. *J. Mol. Graphics* **1996,** *14*, 33-38.

(55) Gravetter, F. J. *Essentials of Statistics for the Behavioral Sciences,* 7th ed.; Wadsworth, Cengage Learning: Belmont, CA, 2009.

(56) Allen, M. P.; Tildesley, D. J. *Computer Simulation of Liquids;* Oxford university press: New York, 1989.

(57) Pisula, W.; Tomovic, Z.; Simpson, C.; Kastler, M.; Pakula, T.; Müllen, K. Relationship between Core Size, Side Chain Length, and the Supramolecular Organization of Polycyclic Aromatic Hydrocarbons. *Chem. Mater.* **2005,** *17*, 4296-4303.

(58) Mullins, O. C. The Modified Yen Model. *Energy Fuels* **2010,** *24*, 2179-2207.

(59) Mullins, O. C. The Asphaltenes. *Annu. Rev. Anal. Chem.* **2011,** *4*, 393-418.

(60) Tan, X.; Fenniri, H.; Gray, M. R. Water Enhances the Aggregation of Model Asphaltenes in Solution via Hydrogen Bonding. *Energy Fuels* **2009,** *23*, 3687-3693.

(61) Aslan, S.; Firoozabadi, A. Effect of Water on Deposition, Aggregate Size, and Viscosity of Asphaltenes. *Langmuir* **2014,** *30*, 3658-3664.

(62) Gray, M. R.; Tykwinski, R. R.; Stryker, J. M.; Tan, X. Supramolecular Assembly Model for Aggregation of Petroleum Asphaltenes. *Energy Fuels* **2011,** *25*, 3125-3134.

Chapter 5: One-Dimensional Self-Assembly Formed by Polyaromatic Compounds in *n*-Heptane*

5.1. Introduction

PA compounds are a broadly-defined class of condensed homocyclic or heterocyclic aromatic rings.[1] They have pi-conjugated molecular structures and are widely found in a variety of environmental samples including water and soil,[2] as well as in novel functional materials.[3] Industrial PA compounds such as asphaltenes in oil sands usually consist of fused heterocyclic aromatic rings with substituted side chains and heteroatoms, e.g. oxygen, nitrogen, and sulfur.[4] Under certain conditions, PA compounds have been observed to self-associate and form aggregates. The aggregated structures have wide applications such as being used in light harvesting arrays,[5,6] organic thin film transistors,[7,8] liquid crystals,[9,10] laser dyes,[11] and organic solar cells.[12] On the other hand, the highly stable aggregates can also have serious adverse effects on a number of industrial processes, such as upgrading, refinery and recovery, and water treatment in oil sand production.[13-15] Through experimental and theoretical methods, self-association of many natural and synthetic PA compounds have been studied, examples including perylene tetracarboxylic diimide (PTCDI) derivatives,[16] hexabenzocoronene (HBC) derivatives,[16] and pyrene derivatives.[17] For instance, it was revealed,[18-20] by scanning electron microscopy (SEM), TEM and atomic force microscopy (AFM), that vesicles, micelles, or nanocoils could be obtained from self-association of PTCDI or HBC derivatives. Using NMR spectroscopy, steady-state fluorescence spectroscopy, VPO, single crystal X-ray diffraction

*A version of this chapter has been published. Reprinted with permission from Jian, C.; Tang, T. One-Dimensional Self-Assembly of Polyaromatic Compounds Revealed by Molecular Dynamics Simulations. *J. Phys. Chem. B* **2014,** *118,* 12772–12780.

and thermogravimetric analysis, 4,4'-bis-(2-pyren-1-yl-ethyl)-[2,2'] bipyridinyl (PBP) was shown to self-associate in chloroform when the PBP concentration exceeded 6×10^{-6} M and form dimers in toluene when its concentration was beyond 1.5×10^{-5} M.[21] Recently, a series of computational studies at atomic level revealed stacked parallel PA cores for hypothetical PA molecules in water and organic solvents.[22-27]

One particularly interesting category of aggregates formed by PA compounds is a 1D rod-like self-assembly. Such a structure was proposed[28,29] to be formed by face-to-face $\pi - \pi$ stacking of PA cores (see an ideal representation in Figure 5.1), and has promising applications in optical and electronic nanodevices.[28,29] A large amount of experimental work has focused on investigating suitable PA compounds that can efficiently self-assemble into 1D structures. For instance, trialkylphenyl-functionalized PTCDI in methylcyclohexane, at a concentration of 5.0×10^{-3} M, was revealed[18] by VPO measurements to form extended stacks of 9, 7 and 6 molecules at 40 ℃, 50 ℃ and 60 ℃ respectively, which agreed well with the sizes found[18,19] by UV/Vis spectroscopy. Through a surface X-ray diffraction study, it was shown[30] that highly ordered hexa(3,7-dimethyl-octanyl)hexa-*peri*-hexabenzocoronene (HBC-C8,2) films of uniaxially aligned PA cores could be fabricated by crystallization from cyclohexanone solution onto friction-transferred poly (tetrafluoroethylene) layers.

The existence of such a 1D structure appears to strongly depend on the molecular structure of PA compounds. Investigated by AFM, the morphology of aggregates formed by two peptide functionalized PTCDIs in aqueous buffer was revealed[31] to change from chiral nanofibers to spherical shapes, depending on the nature of peptide used in the molecule. Dodecyloxy and thiododecyl substituted PTCDIs were shown by TEM, SEM, and AFM to exhibit different aggregation behaviors in methanol: nanowires were observed for PTCDI

compounds with two dodecyloxy groups while spherical particles were found for PTCDI compounds with two thiododecyl groups.[32] Within the 1D stacked structures, it has been revealed[33] by X-ray scattering that substituents of HBCs, such as alkyl, phenyl alkyl, carboxyl, cyano, or bromo, can tune the packing organization of PA cores.

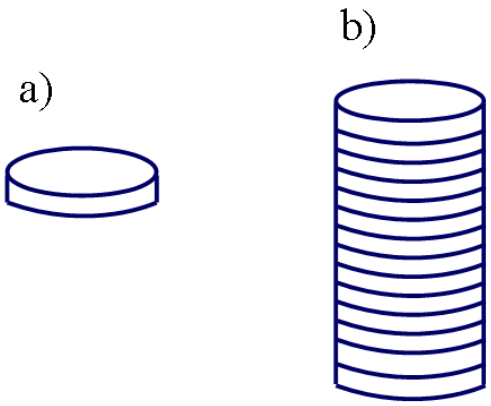

Figure 5.1: Schematic representation of (a) a single PA core, and (b) a 1D structure formed by perfect face-to-face stacking of PA cores. Note that offset stacking can also be found in such a 1D structure but is not shown here.

Property of the solvent is another factor that influences the structure of the aggregates. Alkyl substituted PTCDIs, e.g. PTCDI-C_8, formed a homogenous solution in chloroform (a "good" solvent) at the concentration of 1 g/L, while 1D microstructures were observed by SEM and TEM after an equal amount of methanol (a "poor" solvent) was added to the above solution.[34] In our previous work,[25,27] MD simulations performed on VO-78 based PA models revealed distinct aggregated structures in water and toluene. In water, while some stacking between PA cores was observed, most PA molecules were simply entangled together without apparent order, and the final geometry formed by PA cores was close to a three dimensional sphere. In toluene, however, the largest stable aggregate consisted of less than 11 molecules with their PA cores parallel stacked, thus the interior core region resembling the geometry of a short

cylinder. Such different geometries are caused by different aggregation mechanisms in the two solvents: in water, besides $\pi - \pi$ interaction between the PA cores, additional hydrophobic association exists among the aliphatic side chains to minimize their contact with water, leading to sphere-like aggregates; while in toluene hydrophobic association is absent and $\pi - \pi$ interaction dominates, resulting in aggregates consisting solely of parallel stacked PA molecules.

In addition, even for a given solvent and PA compounds with a certain molecular structure, the geometry of the aggregates can be affected by the concentration of the solution. For instance, as the concentration of propyl substituted PICDIs in water increases from 1×10^{-7} M to 1×10^{-4} M, the UV/Vis spectra indicated a more ordered molecular arrangement inside the aggregate.[35] Characterized by SEM, self-assemblies formed by T-shaped bisphenazine in deuterated chloroform with different concentrations showed morphological transformation from straight strands to nanofiber bundles with substantial coiling and further to flat nanofibers with less bundling and coiling.[36]

n-Heptane, like water, is also considered as a "poor" solvent for PA compounds in petroleum engineering.[37,38] However, n-heptane molecules are apolar compared with water, and it has been suggested[39] in literature that n-hexane (of similar chemical structure with n-heptane) can enhance the $\pi - \pi$ interaction between VO-based PA molecules. Hence, aggregates of these molecules may exhibit different geometries in n -heptane compared with in water or toluene. In this chapter, we report MD simulation results for the self-assembly of VO-78 based model compounds in n-heptane. The molecular models employed here, which have great potential use in organic photovoltaic devices, near-infrared OLEDs, and photodetectors,[39,40] possess the common features of PA compounds, and therefore the results may be applied to a broader class. Our simulation reveals that in n-heptane the PA molecules self-assemble into 1D rod-like

structures with long-range stacking order, which was not observed in our previous studies where water and toluene were the solvents,[25,27] suggesting aggregation mechanism in n-heptane may be very different from that in water or toluene. The remainder of this chapter is organized as follows: the molecular models and computational methods used in this study are introduced in section 5.2; in sections 5.3 and 5.4, simulation results allow us to examine and discuss the self-assembled structures in detail; final conclusion is given in section 5.5.

5.2. Methods

5.2.1. Molecular Models

Chemical structures of the 4 PA molecular models employed in this chapter are shown in Figure 5.2. These models were developed based on VO-78, which consists of nine fused aromatic rings, two aliphatic side chains and six oxygen atoms as heteroatoms. The hydrogen-saturated parts of the side chains (R_1 and R_2 in Figure 5.2) are completely uncharged, while the PA core region has certain polarity. The original VO-78 model has 16 interconnected aliphatic hydrocarbons on each of R_1 and R_2, and will be referred to as VO-16C. Because it is typically believed[41] that the $\pi - \pi$ interaction between PA cores promotes aggregation while the side chains interfere with it, three additional models were introduced by varying the length of the side chains relative to the PA core. The structure of VO-16C was constructed by Chem3D ultra 10.0 and structures of the other three models were obtained by manually removing a certain number of aliphatic hydrocarbons from each side chain of VO-16C. For instance, VO-12C in Figure 5.2 was developed by removing 4 aliphatic hydrocarbons from each chain. The aliphatic/aromatic ratio, defined as the ratio between the total number of interconnected aliphatic hydrocarbons on the side chains (R_1 and R_2) and the number of aromatic carbons in the PA core, are respectively 0.94, 0.71, 0.47 and

0.24 for VO-16C, VO-12C, VO-8C and VO-4C in Figure 5.2. n -Heptane, the solvent used in this chapter, is a linear chain alkane.

The topology for each PA model was validated in our previous work[25] and directly adopted here (functional groups, atom types and partial charges are given in Appendix C, section C.1). The topology for n -heptane was generated based on dipalmitoylphosphatidylcholine (DPPC) in the GROMOS96 force field parameter set 53A6[42] through the *pdb2gmx* routine in GROMACS.[43-46] The topology validation for n -heptane is available in Appendix C (section C.2).

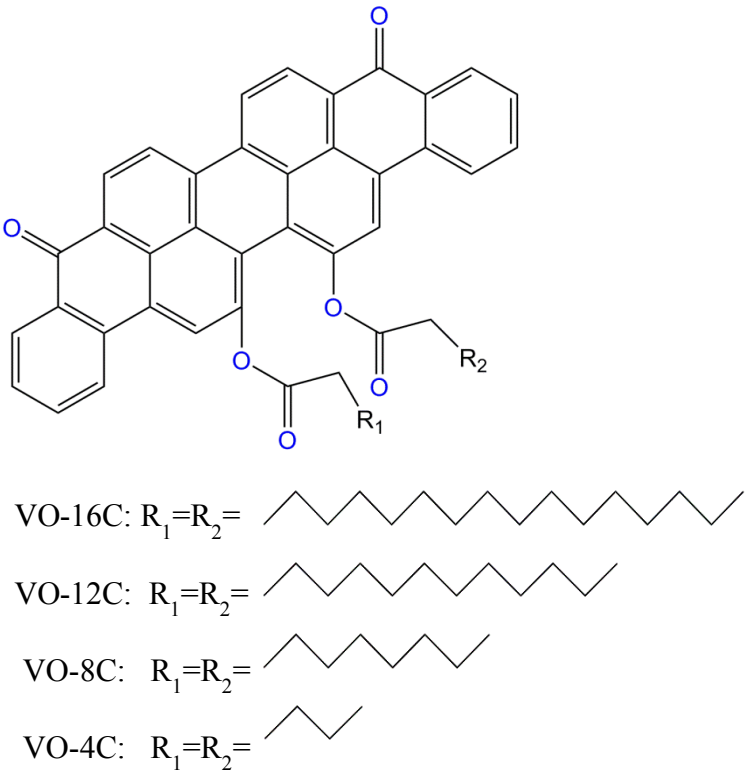

Figure 5.2: Chemical structures of the PA molecular models employed in this chapter.

5.2.2. Simulation Details

Four systems were simulated, named VO-16C, VO-12C, VO-8C and VO-4C, each containing a single type of molecular models described in section 5.2.1. In constructing the initial configuration of each system, an ordered $2 \times 3 \times 4$ array of 24 PA molecules was packed into a

cubic box of dimension $12 \times 12 \times 12$ nm^3, with the PA cores parallel with one another. The spacing between the mass centers of two neighboring PA molecules is respectively 5.2, 3 and 2.6 nm in the three directions, which is much larger than the characteristic length for $\pi - \pi$ stacking distance (~0.45 nm). Therefore although the PA cores are arranged in a parallel manner in the initial configuration, it should not lead to unrealistic trapping of the molecules in parallel stacked configurations. This was proven[25] in our earlier simulations for the same PA compounds in water, where initially parallel PA molecules form disordered sphere-like aggregates at the end of the simulation. Following this, the simulation boxes were randomly filled with n-heptane molecules, resulting in a solute mass concentration of ~3.8%, 3.4%, 3.0%, and 2.6% respectively for systems VO-16C, VO-12C, VO-8C and VO-4C. Inside each simulation box, the number of n-heptane molecules is ~6100 and its initial bulk density is ~650 g/L, close to the literature value[47] of 679 g/L.

All simulations were performed using the MD package GROMACS (version 4.0.7)[43-46] with periodic boundary conditions applied. During each simulation, static structure optimization was first performed, followed by 1 ns position restrained simulations at 300 K and 1 bar, where harmonic potential was applied on the non-hydrogen atoms of the solutes with a spring constant of 1000 kJ/(mol·nm^2) while the solvent molecules were allowed to relax around the solutes. The restraint was then removed and full dynamics simulation was performed in NPT ensemble for 180 ns. The pressure and temperature were controlled by Parrinello-Rahman barostat[48] and velocity rescaling thermostat[49] respectively; the latter is based on correctly producing the probability distribution of kinetic energy under constant temperature and differs from the isokinetic scheme[50] of maintaining constant temperature. For all dynamics simulations, the integration time step was 2 fs; intra-molecular bonds were constrained by LINCS algorithm;[51] full

electrostatics was treated by particle-mesh Ewald method;[52] and van der Waals interactions were evaluated by twin range cutoff approach.[53]

5.2.3. Data Analysis

Appropriate post-processing programs available in GROMACS were used for trajectory analysis and VMD[54] used for visualization. Unless otherwise specified, all analysis was based on average over the last 20 ns of the simulation. Demonstration for the achievement of dynamic equilibrium is available in Appendix C, section C.3.

A quantity useful for describing the geometry of a structure is the radius of gyration. Two types of radius of gyration have been employed in this chapter: radius of gyration about the center of mass and principal radii of gyration. Radius of gyration R_g about the center of mass is calculated by[55]:

$$R_g = \left(\frac{\sum_i m_i {r_i}^2}{\sum_i m_i}\right)^{0.5}, \tag{5.1}$$

where m_i and r_i are respectively the mass and distance from the center of mass for atom i; $\sum_i m_i$ is the total atomic mass; and $\sum_i m_i {r_i}^2$ is the mass moment of inertial. Passing through the center of mass, three principal axes can be found and will be denoted by x, y and z. Radii of gyration about these principal axes are calculated by:[55]

$$R_x = \left(\frac{\sum_i m_i (y_i^2 + z_i^2)}{\sum_i m_i}\right)^{0.5}, \tag{5.2}$$

$$R_y = \left(\frac{\sum_i m_i (x_i^2 + z_i^2)}{\sum_i m_i}\right)^{0.5}, \tag{5.3}$$

$$R_z = \left(\frac{\sum_i m_i (x_i^2 + y_i^2)}{\sum_i m_i}\right)^{0.5}, \tag{5.4}$$

where (x_i, y_i, z_i) are the coordinates for atom i and the summations are over all atoms in the molecular structure of interest. After $\{R_x, R_y, R_z\}$ are computed, we further denote R_0 as the minimum of $\{R_x, R_y, R_z\}$, R_2 as the maximum of $\{R_x, R_y, R_z\}$, and R_1 as the intermediate value.

For a 1D structure, the length scale in one direction will be much larger than the other two. Hence, $R_0 \ll R_1 \approx R_2$. In contrast, for a sphere-like structure, since the three dimensions are approximately equal, $R_0 \approx R_1 \approx R_2$. For structures that resemble short cylinders, $R_0 < R_1 \approx R_2$. Therefore, the relative magnitude of R_0, R_1 and R_2 is a good indicator for the dimension characteristics of the structure. Furthermore, these geometry descriptions can also be applied to a subset of the atoms in the structure. In this case, the summations in eqs. 5.2, 5.3 and 5.4 should be performed over atoms in the subset.

5.3. Results

Figure 5.3 shows the snapshots of the largest stable self-assemblies in the 4 systems, i.e., the ones that do not dissociate at the equilibrium stage of the simulations. All self-assemblies shown are formed by the molecules contained in the primitive simulation cells. In systems VO-4C, VO-8C and VO-12C, the largest stable self-assembly involves all 24 molecules, whereas in system VO-16C, the largest stable self-assembly contains 16 molecules. It can be clearly seen from Figure 5.3 that irrespective of the aliphatic/aromatic ratios, the dominant structures are formed by the parallel stacking of multiple PA cores, indicated by the blue arrows in Figure 5.3. For instance, there are three stacks of parallel aligned PA cores in the largest stable self-assembly formed in system VO-12C, labeled as (I), (II) and (III), respectively. More interestingly, there exists a clear axis in each self-assembly, depicted as blue curves in Figure 5.3, along which the stacking of the PA cores are propagated. This suggests the formation of 1D rod-like structures with a certain degree of bending flexibility. These structures found from our simulations show great similarities to SEM, TEM, AFM and fluorescence microscopy results[56,57] on organic semiconductors, where large PA cores with linear aliphatic side chain substitutions were observed to form 1D nanobelt. In addition, unlike the ideal parallel stacking shown in Figure

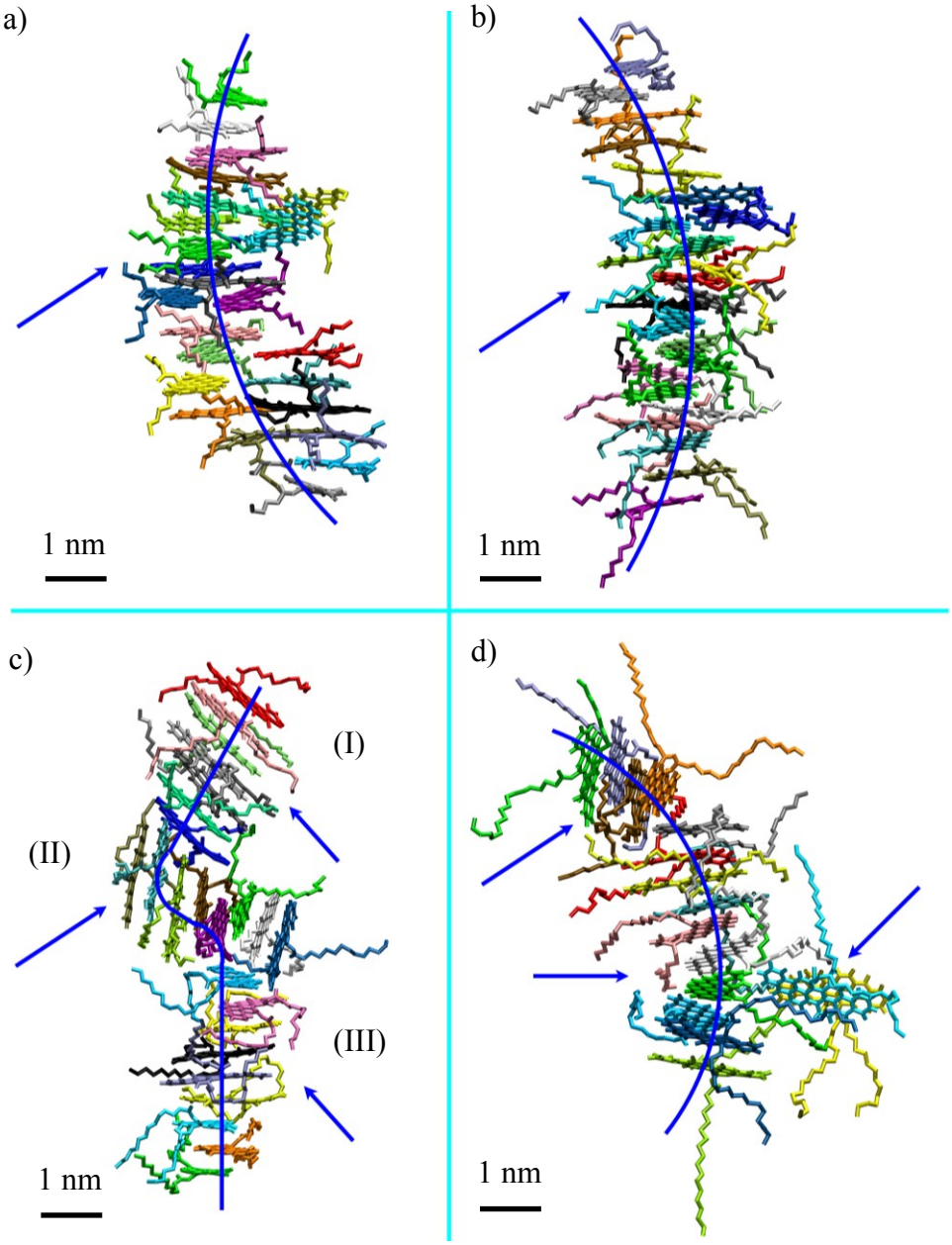

Figure 5.3: Snapshots of the largest stable self-assemblies formed at the equilibrium stage of the simulations in systems: (a) VO-4C, (b) VO-8C, (c) VO-12C, and (d) VO-16C. In the first 3 systems, the largest stable self-assembly involves all 24 molecules in the simulation box. In system VO-16C, besides the largest stable self-assembly, there are 2 additional small aggregates (not shown), each involving 4 molecules. (I), (II) and (III) in (c) show the three stacks of parallel PA cores in the largest stable self-assembly formed in system VO-12C.

5.1b, the self-assemblies obtained in our simulations all involve molecular tilting, slipping, and twisting along the stacking axis. The formation of a 1D ideal parallel stacking structure requires significant reduction in entropy, which can in turn increase the free energy of the system although such stacking also tends to reduce the free energy by decreasing enthalpy. Therefore it is entirely possible to have some titling, slipping and twisting, as resulted from the enthalpy/entropy competition.

To quantitatively confirm and describe the 1D self-assembly, we first plotted, in Figure 5.4, the RDFs for the COG distances r (nm) between any two PA cores. For each of the four systems, there exist multiple peaks in the RDFs, the first four located at approximately r = 0.45 nm, 0.75 nm, 1.1 nm and 1.5 nm, respectively. At these COG separations, to probe the relative orientation of PA cores, we calculated the cosine of angle σ ($cos\,\sigma$) between any two PA core planes. If two PA core planes are close to being parallel, it is expected that $cos\,\sigma$ will be near one. Figure 5.5 shows the PDFs for $cos\,\sigma$ at the first four RDF peaks. Clearly, in each subfigure, the PDFs have their sole and pronounced peaks at $cos\,\sigma \approx 1$, confirming the parallel stacking configuration of PA cores at these COG separations. The four curves in the subfigures are only distinguishable for r > 1 nm (Figures 5.5c and d). And even at r > 1 nm, they only differ quantitatively, suggesting similar parallel configurations regardless of the aliphatic/aromatic ratios. The parallel stacking at 0.45 nm (Figure 5.5a) corresponds to $\pi - \pi$ stacked PA cores where the COG of one core is directly on top of the other (inset in Figure 5.5a). The parallel stacking at 0.75 nm (Figure 5.5b) can correspond to 2 different configurations (insets in Figure 5.5b): in the first one PA core is still on top of the other but is shifted laterally so that the line connecting the two COGs is not perpendicular to the cores (left inset in Figure 5.5b); the second configuration results from the parallel alignment of two PA cores that have a third PA core

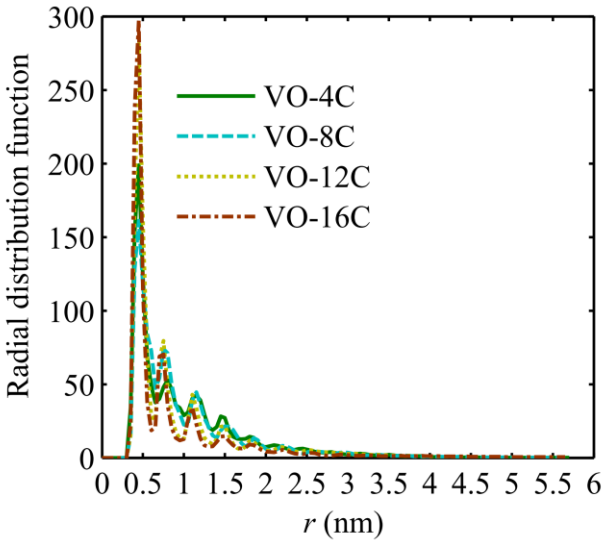

Figure 5.4: RDFs for the COG separation distance r (nm) between two PA cores. Each peak in the RDFs corresponds to high density of PA cores at this location. The first four peaks for the 4 systems are respectively located at: 0.45, 0.80, 1.15, and 1.45 nm for VO-4C, 0.45, 0.75, 1.15 and 1.50 nm for VO-8C, 0.45, 0.75, 1.10 and 1.50 nm for VO-12C and 0.45, 0.75, 1.10 and 1.50 nm for VO-16C.

sandwiched between them (right inset in Figure 5.5b). The PDF peaks at $r = 1.1$ nm and 1.5 nm (Figures 5.5c and d) correspond to parallel alignment of two PA cores when there are two or three other PA cores sandwiched in between (insets in Figures 5c and d, respectively). Therefore these plots confirm the parallel stacking of multiple PA cores visually observed from Figure 5.3.

Although the peaks in Figure 5.4 become considerably smaller after 1.5 nm, the parallel stacking of PA cores persists for a distance much longer than 1.5 nm. Figure 5.6 shows $cos\,\sigma$ vs. COG distance r for the largest stable self-assemblies formed in the four systems (snapshots shown in Figure 5.3). Each plot was generated by calculating the COG distance and $cos\,\sigma$ between any pair of PA cores in the largest stable self-assembly, averaged over the last 20 ns of

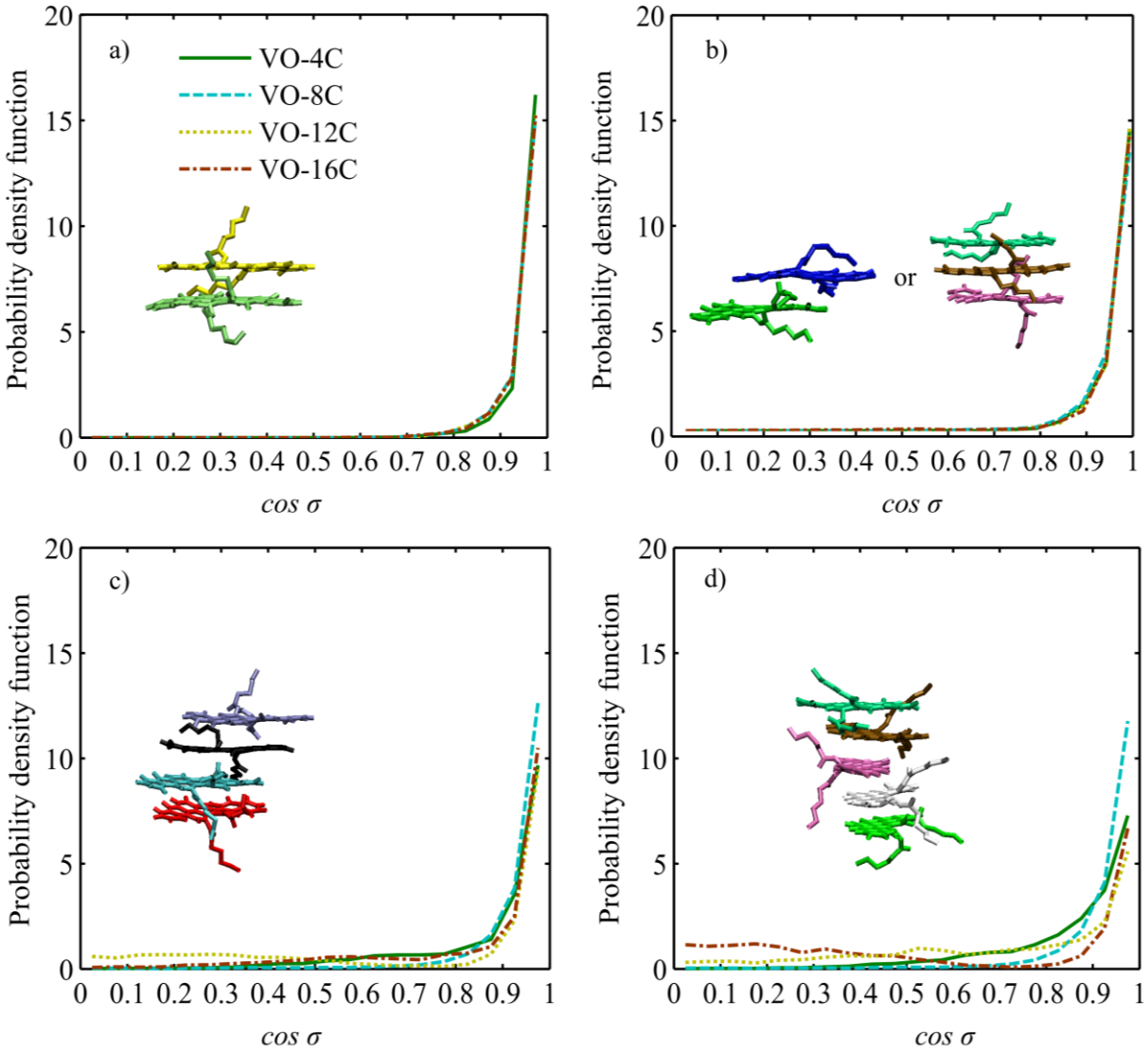

Figure 5.5: PDFs for $cos\,\sigma$ at COG separation distances of: (a) 0.45 nm, (b) 0.75 nm, (c) 1.1 nm and (d) 1.5 nm. The peak at $cos\,\sigma \sim 1$ in each subfigure corresponds to a parallel stacking configuration that is shown as the inset.

the simulation. In each of the three systems VO-4C, VO-8C and VO-12C, the largest stable self-assembly consists of all 24 molecules; hence there are in total $c_{24}^2 = \frac{24\times23}{2} = 276$ pairs of PA cores and 276 data points. There are 16 molecules in the largest stable self-assembly formed in system VO-16C, resulting in $c_{16}^2 = \frac{16\times15}{2} = 120$ data points in Figure 5.6d. Let us first consider

Figure 5.6a, for system VO-4C, where most data points are distributed around $cos\,\sigma = 0.88$. This is consistent with the nearly parallel stacking of all 24 PA cores shown in Figure 5.3a. A horizontal segment is drawn in Figure 5.6a to show the average $cos\,\sigma$ value (0.88). The start and end points of the segment are determined by first identifying data that differ from the average (0.88) by 10% or less. Within this group of data, the smallest r value was used as the leftmost point of the segment, and the largest r value as the rightmost point. The leftmost point is in fact located at r = 0.45 nm, corresponding to the direct parallel stacking of two neighboring PA cores, as shown in Figure 5.5a. The rightmost point of the segment is located at r = 5.5 nm, which corresponds to the COG distance between the lowest and highest PA cores shown in Figure 5.3a. This implies that the parallel stacking of PA cores persists for at least (given that only 24 molecules were simulated) 5.5 nm along the axis of the self-assembly. This length will be referred to as the persistence length of parallel stacking for the self-assembly, which quantifies the range of parallel stacking.

Similar segments are drawn in Figures 5.6b-d to show the location of data. Figure 5.6b exhibits great similarity to Figure 5.6a, and the persistence length for VO-8C is 5.6 nm. Unlike in Figures 5.6a and b, data in Figure 5.6c, for system VO-12C, can be separated into three different groups: (1) near $cos\,\sigma = 1$, (2) near $cos\,\sigma = 0.6$ and (3) near $cos\,\sigma = 0.3$. Thus three segments are drawn to show the average $cos\,\sigma$ value and the range of r for each group of data. Consistently, the self-assembly in Figure 5.3c also contains three stacks of parallel PA cores that are labeled as (I), (II) and (III), respectively. Data group (1) corresponds to parallel stacking within each stack (I), (II) or (III). Data in group (2) correspond to PA core pairs with one from stack (I) and the other from stack (III). The leftmost point (~2.4 nm) is the COG distance

between two closest molecules from stacks (I) and (III), and the rightmost point (~6.6 nm) is the COG distance between two furthest molecules from the two stacks. The average $cos\,\sigma$ value for

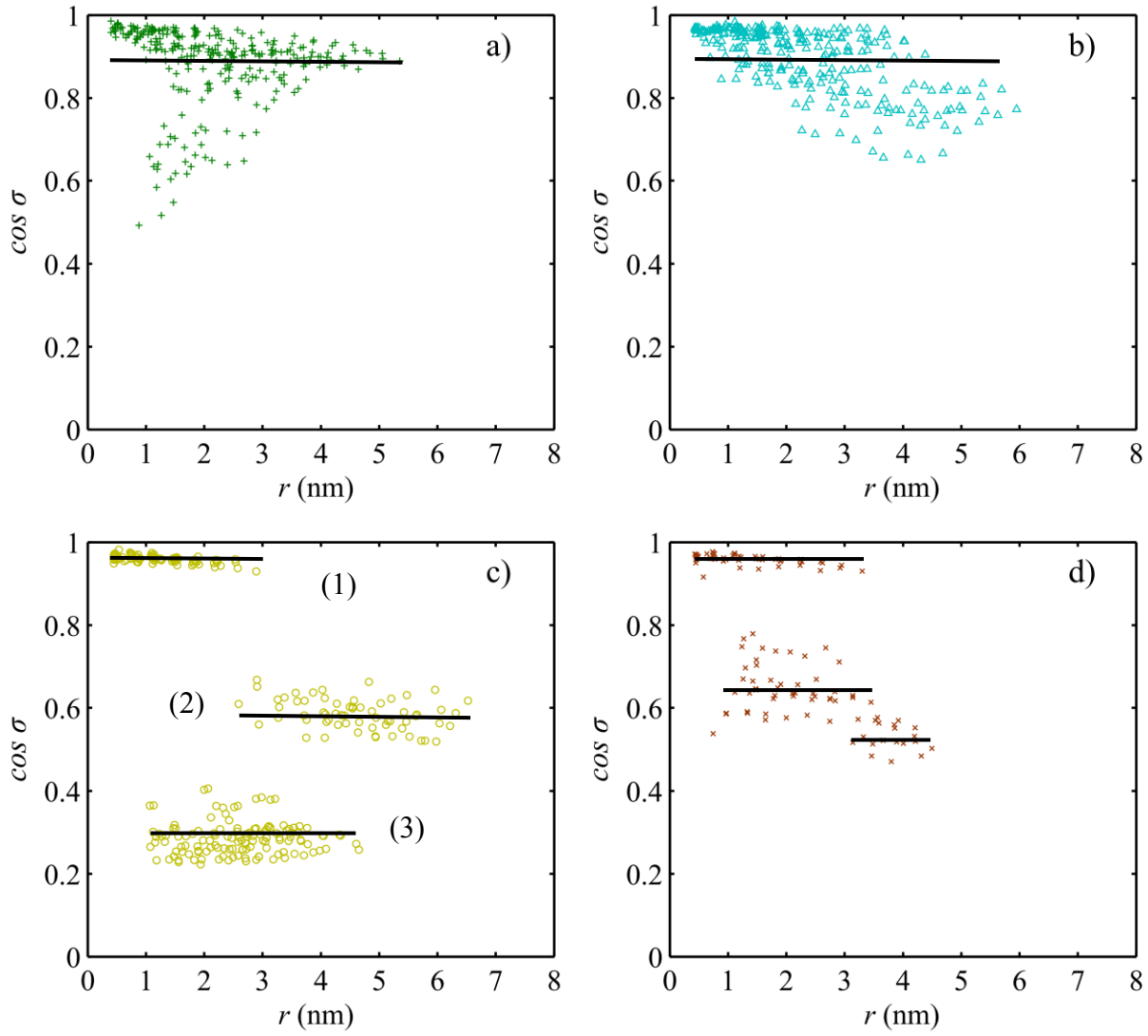

Figure 5.6: $cos\,\sigma$ vs. COG distance r for the largest stable assemblies in systems: (a) VO-4C, (b) VO-8C, (c) VO-12C and (d) VO-16C. A horizontal segment is drawn to show the average $cos\,\sigma$ value for each group of data, and the rightmost point of the segment for the $cos\,\sigma \approx 1$ group in each subfigure represents the persistence length of parallel stacking in n-heptane. The long persistence length for PA compounds in n-heptane is consistent with previous observation of 1D rod-like structure shown in Figure 5.3.

group (2), 0.59, implies that the angle between the two stacks is ~54°. Data in group (3) are obtained from PA core pairs with one from stack (I) and the other from stack (II), or with one from stack (II) and the other from stack (III). The average $\cos\sigma$ value is 0.29, indicating that the angle between neighboring stacks is ~73°. Since data group (1) represents parallel alignment within each stack, its range of r is the persistence length for VO-12C, evaluated to be 3 nm. Self-assembly in VO-16C is similar to that in VO-12C, and the data in Figure 5.6d can also be separated into 3 groups. The persistence length, calculated based on data near $cos\,\sigma = 1$, is about 3.4 nm. Comparing data in Figure 5.6, it can be learned that as the length of the side chains increases, the persistence length shows a decreasing trend. Nevertheless, the shortest persistence length found in our simulations is still ~3 nm, which, considering that the COG separation distance between directly parallel stacked PA cores is about 0.45 nm, corresponds to approximately 8 parallel-aligned PA cores.

The existence of 1D rod-like self-assembly strongly depends on the type of solvent. The same PA molecules were previously simulated in water and in toluene;[25,27] however, the formation of 1D rods is only observed in n-heptane. Figure 5.7 shows $cos\,\sigma$ vs. COG separation distance for the largest stable aggregates in water and in toluene. It can be clearly seen that data points in water are randomly distributed over the range of $cos\,\sigma = 0.2$ to 1, demonstrating the random orientation of PA cores with respect to one other inside the largest stable aggregates. That is, the PA compounds do not self-assemble into an ordered structure in water. For PA compounds in toluene, most of the data points are distributed between $cos\,\sigma = 0.8$ to 1, corresponding to the previous observation[27] that aggregates formed in toluene mainly consisted of nearly parallel stacked PA cores. However, compared with in n-heptane, the persistence length of parallel stacking in toluene is much smaller: ~2.2 nm for VO-4C, ~2 nm for VO-8C,

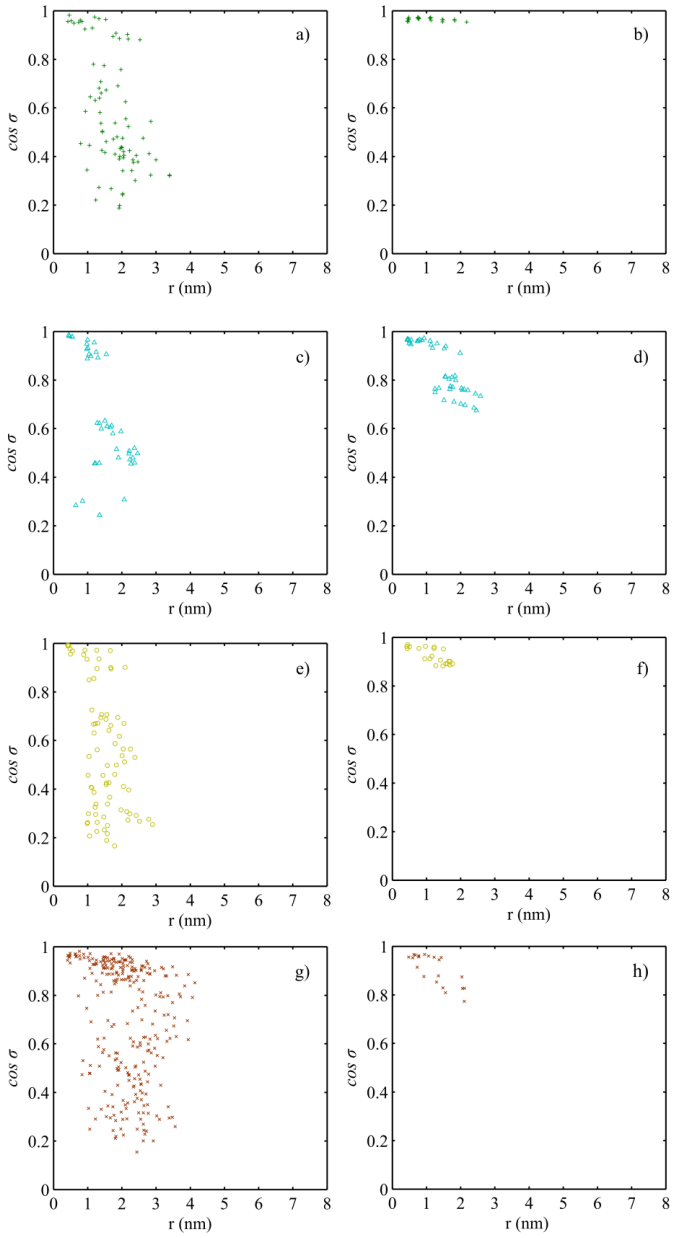

Figure 5.7: $cos\,\sigma$ vs. COG separation distance r for the largest stable aggregates in water (left panel) and toluene (right panel) formed by: (a) and (b) VO-4C, (c) and (d) VO-8C, (e) and (f) VO-12C, (g) and (h) VO-16C. The random distribution of the data points in water confirms the disordered orientation of PA cores inside the aggregate, and the short persistence lengths for PA compounds in toluene verify that the number of PA cores consecutively forming parallel stacking is small.

VO-12C and VO-16C. This suggests that[27] the largest number of PA cores that can consecutively form parallel stacking in toluene is approximately 6 in systems VO-4C, and 5 in systems VO-8C, VO-12C and VO-16C.

The lack of stacking order in water and lack of long-range order in toluene lead to very different geometries formed by the PA cores in these two solvents compared with in n-heptane. Figure 5.8 shows the three principal radii of gyration (from smallest to largest: R_0, R_1 and R_2) for the PA core regions of the largest stable aggregates in different solvents. It can be clearly seen that for each system in n-heptane R_0, R_1 and R_2 are of the following order: $R_0 << R_1 \approx R_2$. In fact, R_2/R_0 are respectively 2.05, 2.44, 2.61 and 2.33 for VO-4C, VO-8C, VO-12C and VO-16C, which is the characteristic of the 1D rod-like structures observed in Figures 5.3 and 5.6. For toluene, R_1 and R_2 are again close, but unlike in n-heptane they are not significantly larger than R_0 ($R_2/R_0 = 1.73$, 1.91, 1.88 and 1.90 respectively for VO-4C, VO-8C, VO-12C and VO-16C), confirming that the stacked PA cores in toluene resemble short-cylinders.[27] As for water, R_0, R_1 and R_2 are relatively close for VO-4C, VO-12C and VO-16C ($R_2/R_0 = 1.32$, 1.33 and 1.28, respectively), corresponding to sphere-like aggregates.[25] For VO-8C in water, although $R_2/R_0 = 1.71$, it is still smaller compared to those in toluene and n-heptane.

5.4. Discussion

Formation of aggregates' configurations and geometries is facilitated by specific driving forces that greatly depend on the solvent properties.[58] It has been observed in our previous work[25,27] that $\pi - \pi$ interaction between PA cores is of great importance for PA aggregation, which is confirmed by the prevalence of parallel stacking found in n-heptane. On the other hand, the very different structures formed by the same PA molecules in different solvents indicate the importance of interactions between solvent and solute. Firstly, longer side chains have been

suggested[25] to provide larger interference with $\pi - \pi$ stacking of PA cores. Although our simulation data in n-heptane show an overall decreasing trend in the persistence length as the side-chain length increases, the decrease is not strictly monotonic. For example, the persistence

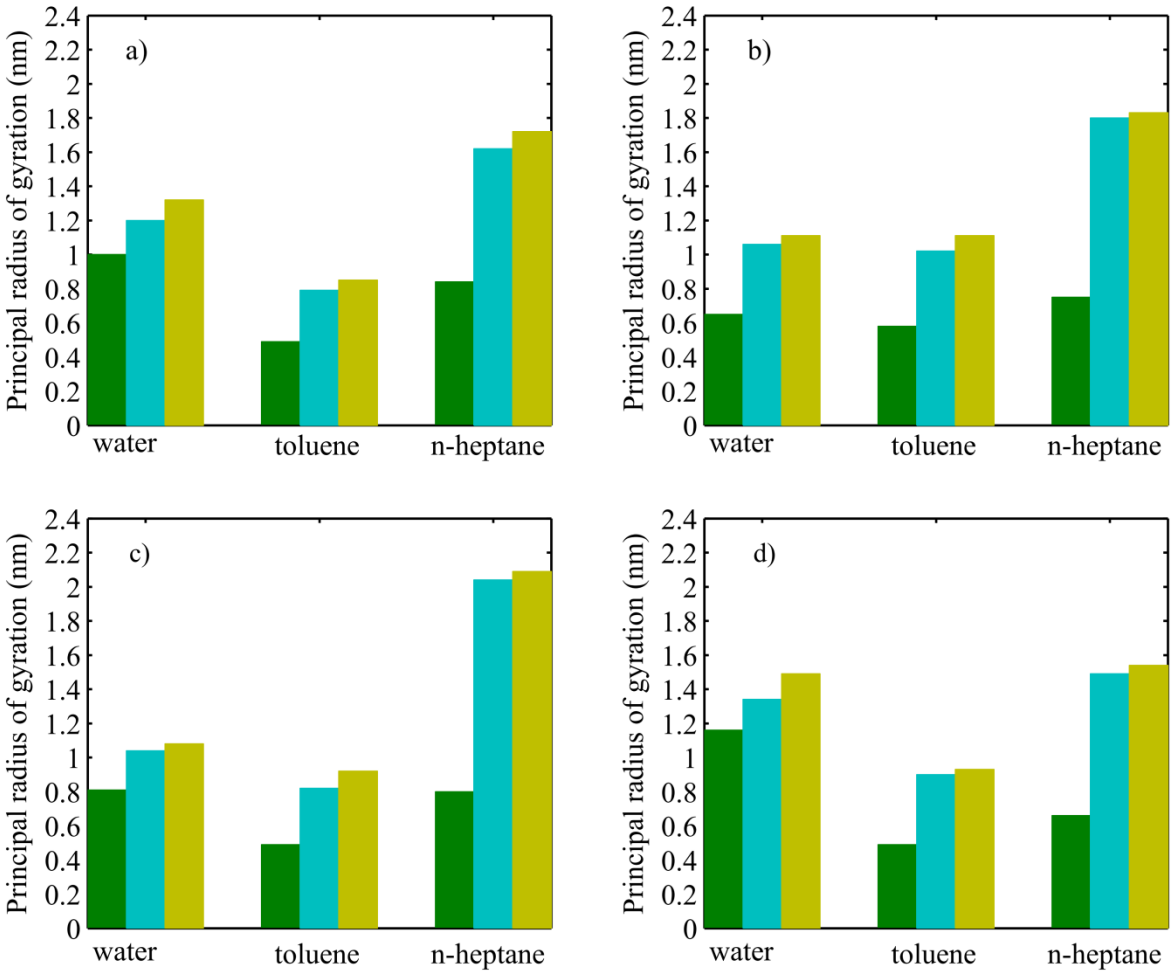

Figure 5.8: Principal radii of gyration for the PA core regions of the largest stable aggregates in: (a) VO-4C, (b) VO-8C, (c) VO-12C, (d) VO-16C. Each subfigure contains three groups of data, one for a specific solvent (water, toluene or n-heptane). For each group of data, from left to right: R_0, R_1 and R_2.

lengths of VO-4C and VO-8C are close to each other and the persistence length of systems VO-12C (~3 nm) is slightly smaller than that of system VO-16C (~3.4 nm). Our simulations further

show that for all four systems, the side chains are quite well solvated in n-heptane and do not strongly interfere with the stacking of PA cores (see evidence using radius of gyration, details in Appendix C, section C.4). The solvated side chains indicate the existence of attraction between solvent (n-heptane) molecules and side chains, which was also observed for PA compounds in toluene.[27] Contrarily, hydrophobic nature of the side chains results in their entanglement in water, especially for PA compounds with long side chains. These tangled side chains promote and enhance the stability of the aggregation. On the other hand, they prevent the PA cores from forming parallel stacking, leading to disordered and sphere-like aggregates in water.

Secondly, although similar solvent-side chain attraction was observed for PA compounds in toluene,[27] Figure 5.7 shows that the persistence length of parallel stacking is much smaller in toluene than in n-heptane. This can be attributed to the additional solvent-PA core attraction that exists in toluene. Indeed, the aromatic cores of toluene can form $\pi - \pi$ interaction with PA molecules and have a certain order around the PA cores.[27] This additional solvent-solute attraction competes with the attraction among solutes and reduces the number of molecules that can simultaneously form parallel stacking. In contrast, the absence of such solvent-PA core attraction in n-heptane favors the $\pi - \pi$ interaction among PA cores, leading to a larger number of PA cores stacked together. These observations are consistent with the solubility definition of asphaltenes these PA compounds represent.

The above comparison allows us to derive the conditions on the solvent under which 1D rod-like self-assembly can be formed from PA compounds. These conditions are expected to be associated with the solvent-solute interactions, and should strongly depend on the molecular structure of the solute. For PA compounds that only possess aromatic core region, the single role the solvent has to play is to optimize the parallel $\pi - \pi$ stacking of PA cores. This requires a

certain solubility so that the solutes can arrange themselves in a parallel manner along one direction. On the other hand, the solubility cannot be too high to disrupt the long-range parallel stacking. Therefore the size of the PA core, its polarity, and the polarity of the solvent must be tuned in order to achieve the optimal condition. When PA cores are accompanied by side chains, in order to self-assemble into 1D rod-like structure, the solvent must play two separate roles. Firstly, the solvent should be able to prevent the side-chains from mutual association and from interfering with parallel stacking of PA cores. This implies that there has to be sufficiently strong attraction between the solvent and the side chains of the PA compounds. Secondly, the attraction between the solvent and the PA cores should be limited so as not to disrupt the parallel stacking of PA cores. Depending on the nature of the side chains, different solvents can be chosen to achieve the 1D self-assembling of different PA compounds. For instance, for PTCDIs with hydrophilic imide substituents, water is a "good" solvent to interact with side chains; while for PTCDIs with hydrophobic imide substituents, apolar solvent such as methylcyclohexane can efficiently prevent the side-chain association.[18,59] In both solvents, the stacking of PA cores can be maintained,[18,59] and hence 1D self-assemblies can be obtained for these two PA compounds in different solvents.

Finally we point out that the simulations in this chapter were performed for 180 ns, which is longer than any existing MD simulations on PA molecules. Stacked parallel pairs were observed by Headen et al.[26] (mass concentration of PA compounds ~7%) and Teklebrhan et al.[24] (mass concentration ~3.5%) in their short MD simulations (~10 or 20 ns), but unlike the dominance of parallel stacking discussed here, tail-tail contact and tail-core contact were also reported as highly possible configurations between adjacent PA molecules. Sedghi et al.[60] conducted 80 ns MD simulations for 8 types of PA molecules in heptane at mass concentrations

of ~7%. For their A03 and A04 molecular models, parallel stacking of multiple PA cores was found, but 1D rod-like structure was only observed to start forming in the system of A04 molecules. With a short simulation time (~10 ns), self-assembly with long-range order, such as seen in the present study, was only observed at mass concentrations significantly higher than the ones used in this chapter (~3.8%, 3.4%, 3.0%, and 2.6% for systems VO-16C, VO-12C, VO-8C and VO-4C, respectively). For example, a decamer structure with PA cores facing each other was reported[61] to form in n-pentane within 10 ns, where the mass concentration of PA compounds was ~25%. Similarly, within 10 ns, long-ranged parallel stacking involving as many as 24 PA cores in n-heptane was found in the work by Kuznicki et al.,[22] where the mass concentration was ~38%. These results seem to suggest that at low mass concentrations, a sufficiently long simulation time is required in order to observe the formation of 1D rod-like self-assembly. We indeed performed a series of simulations for the same systems with different simulation time (see Appendix C section C.5), which confirms that simulation time longer than 120 ns is needed to observe the overall aggregation dynamics and the 1D self-assembly. The 1D self-assembling is therefore a process whose rate strongly depends on the concentration.

5.5. Conclusion

In this chapter, we report MD simulations which revealed the formation of 1D rod-like self-assembly for PA compounds in n-heptane. The self-assembly results from parallel stacking of multiple PA cores. The range of stacking, quantified by a persistence length, is 3 to 5.6 nm, significantly larger than the spacing between two neighboring $\pi-\pi$ stacked PA cores. Increasing the side chain length reduces the persistence length, but does not change the existence of the 1D structure. Formation of such 1D self-assembly is facilitated by two factors: (i) solvent-side chain attraction, which minimizes interference of side chains with core stacking; and (ii)

limited solvent-core interaction, which allows for long-ranged stacking. The results reported here help us to gain insight into conditions that favor the formation of 1D self-assembly (e.g., nanorod or nanobelt) that has great potential in optical and electronic nanodevices.

Bibliography

(1) Vo-Dinh, T.; Fetzer, J.; Campiglia, A. Monitoring and Characterization of Polyaromatic Compounds in the Environment. *Talanta* **1998,** *47*, 943-969.

(2) Liu, Z.; Laha, S.; Luthy, R. G. Surfactant Solubilization of Polycyclic Aromatic Hydrocarbon Compounds in Soil-Water Suspensions. *Water Sci. Techol.* **1991,** *23, 475-485.*

(3) Hoeben, F. J.; Jonkheijm, P.; Meijer, E.; Schenning, A. P. About Supramolecular Assemblies of π-Conjugated Systems. *Chem. Rev.* **2005,** *105*, 1491-1546.

(4) Groenzin, H.; Mullins, O. C. Asphaltene Molecular Size and Structure. *J Phys. Chem. A* **1999,** *103*, 11237-11245.

(5) Hippius, C.; Schlosser, F.; Vysotsky, M. O.; Böhmer, V.; Würthner, F. Energy Transfer in Calixarene-Based Cofacial-Positioned Perylene Bisimide Arrays. *J. Am. Chem. Soc.* **2006,** *128*, 3870-3871.

(6) Wong, W. W.; Khoury, T.; Vak, D.; Yan, C.; Jones, D. J.; Crossley, M. J.; Holmes, A. B. A Porphyrin-hexa-*peri*-hexabenzocoronene-porphyrin Triad: Synthesis, Photophysical Properties and Performance in a Photovoltaic Device. *J. Mater. Chem.* **2010,** *20*, 7005-7014.

(7) Facchetti, A. π-Conjugated Polymers for Organic Electronics and Photovoltaic Cell Applications. *Chem. Mater.* **2010,** *23*, 733-758.

(8) Wong, W. W.; Singh, T. B.; Vak, D.; Pisula, W.; Yan, C.; Feng, X.; Williams, E. L.; Chan, K. L.; Mao, Q.; Jones, D. J. Solution Processable Fluorenyl Hexa-peri-hexabenzocoronenes in Organic Field-Effect Transistors and Solar Cells. *Adv. Funct. Mater.* **2010,** *20*, 927-938.

(9) Mizoshita, N.; Tani, T.; Inagaki, S. Highly Conductive Organosilica Hybrid Films Prepared from a Liquid-Crystal Perylene Bisimide Precursor. *Adv. Funct. Mater.* **2011,** *21*, 3291-3296.

(10) Schmidt-Mende, L.; Fechtenkotter, A.; Mullen, K.; Moons, E.; Friend, R. H.; MacKenzie, J. D. Self-Organized Discotic Liquid Crystals for High-Efficiency Organic Photovoltaics. *Science* **2001,** *293*, 1119-1122.

(11) Díaz-García, M.; Calzado, E.; Villalvilla, J.; Boj, P.; Quintana, J.; Cespedes-Guirao, F.; Fernandez-Lazaro, F.; Sastre-Santos, A. Effect of Structural Modifications in the Laser Properties of Polymer Films Doped with Perylenebisimide Derivatives. *Synth. Met.* **2009,** *159*, 2293-2295.

(12) Choi, H.; Paek, S.; Song, J.; Kim, C.; Cho, N.; Ko, J. Synthesis of Annulated Thiophene Perylene Bisimide Analogues: Their Applications to Bulk Heterojunction Organic Solar Cells. *Chem. Commun.* **2011,** *47*, 5509-5511.

(13) Speight, J. Petroleum Asphaltenes-Part 1: Asphaltenes, Resins and the Structure of Petroleum. *Oil Gas Sci. Technol.* **2004,** *59*, 467-477.

(14) Spiecker, P. M.; Gawrys, K. L.; Trail, C. B.; Kilpatrick, P. K. Effects of Petroleum Resins on Asphaltene Aggregation and Water-in-Oil Emulsion Formation. *Colloids Surf., A* **2003,** *220*, 9-27.

(15) Kilpatrick, P. K. Water-in-Crude Oil Emulsion Stabilization: Review and Unanswered Questions. *Energy Fuels* **2012,** *26*, 4017-4026.

(16) Wang, C.; Dong, H.; Hu, W.; Liu, Y.; Zhu, D. Semiconducting π-Conjugated Systems in Field-Effect Transistors: A Material Odyssey of Organic Electronics. *Chem. Rev.* **2011,** *112*, 2208-2267.

(17) Figueira-Duarte, T. M.; Müllen, K. Pyrene-Based Materials for Organic Electronics. *Chem. Rev.* **2011,** *111*, 7260-7314.

(18) Chen, Z.; Stepanenko, V.; Dehm, V.; Prins, P.; Siebbeles, L. D.; Seibt, J.; Marquetand, P.; Engel, V.; Würthner, F. Photoluminescence and Conductivity of Self-Assembled π− π Stacks of Perylene Bisimide Dyes. *Chem. — Eur. J.* **2007***, 13*, 436-449.

(19) Würthner, F.; Chen, Z.; Dehm, V.; Stepanenko, V. One-Dimensional Luminescent Nanoaggregates of Perylene Bisimides. *Chem. Commun.* **2006,** 1188-1190.

(20) Yamamoto, T.; Fukushima, T.; Yamamoto, Y.; Kosaka, A.; Jin, W.; Ishii, N.; Aida, T. Stabilization of a Kinetically Favored Nanostructure: Surface ROMP of Self-Assembled Conductive Nanocoils from a Norbornene-Appended Hexa-*peri*-hexabenzocoronene. *J. Am. Chem. Soc.* **2006,** *128*, 14337-14340.

(21) Tan, X.; Fenniri, H.; Gray, M. R. Pyrene Derivatives of 2,2′-Bipyridine as Models for Asphaltenes: Synthesis, Characterization, and Supramolecular Organization. *Energy Fuels* **2007,** *22*, 715-720.

(22) Kuznicki, T.; Masliyah, J. H.; Bhattacharjee, S. Molecular Dynamics Study of Model Molecules Resembling Asphaltene-Like Structures in Aqueous Organic Solvent Systems. *Energy Fuels* **2008,** *22*, 2379-2389.

(23) Kuznicki, T.; Masliyah, J. H.; Bhattacharjee, S. Aggregation and Partitioning of Model Asphaltenes at Toluene−Water Interfaces: Molecular Dynamics Simulations. *Energy Fuels* **2009,** *23*, 5027-5035.

(24) Teklebrhan, R. B.; Ge, L.; Bhattacharjee, S.; Xu, Z.; Sjöblom, J. Probing Structure–Nanoaggregation Relations of Polyaromatic Surfactants: A Molecular Dynamics Simulation and Dynamic Light Scattering Study. *J. Phys. Chem. B* **2012,** *116*, 5907-5918.

(25) Jian, C.; Tang, T.; Bhattacharjee, S. Probing the Effect of Side-Chain Length on the Aggregation of a Model Asphaltene Using Molecular Dynamics Simulations. *Energy Fuels* **2013,** *27*, 2057-2067.

(26) Headen, T. F.; Boek, E. S.; Skipper, N. T. Evidence for Asphaltene Nanoaggregation in Toluene and Heptane from Molecular Dynamics Simulations. *Energy Fuels* **2009,** *23*, 1220-1229.

(27) Jian, C.; Tang, T.; Bhattacharjee, S. Molecular Dynamics Investigation on the Aggregation of Violanthrone78-Based Model Asphaltenes in Toluene. *Energy Fuels* **2014,** *28,* 3604–3613

(28) Liu, Y.; Li, Y.; Jiang, L.; Gan, H.; Liu, H.; Li, Y.; Zhuang, J.; Lu, F.; Zhu, D. Assembly and Characterization of Novel Hydrogen-Bond-Induced Nanoscale Rods. *J. Org. Chem.* **2004,** *69*, 9049-9054.

(29) Kastler, M.; Pisula, W.; Wasserfallen, D.; Pakula, T.; Müllen, K. Influence of Alkyl Substituents on the Solution- and Surface-Organization of Hexa-*peri*-hexabenzocoronenes. *J. Am. Chem. Soc.* **2005,** *127*, 4286-4296.

(30) Bunk, O.; Nielsen, M. M.; Sølling, T. I.; van de Craats, A. M; Stutzmann, N. Induced Alignment of a Solution-Cast Discotic Hexabenzocoronene Derivative for Electronic Devices Investigated by Surface X-ray Diffraction. *J. Am. Chem. Soc.* **2003,** *125*, 2252-2258.

(31) Bai, S.; Debnath, S.; Javid, N.; Frederix, P. W.; Fleming, S.; Pappas, C.; Ulijn, R. V. Differential Self-Assembly and Tunable Emission of Aromatic Peptide Bola-Amphiphiles Containing Perylene Bisimide in Polar Solvents Including Water. *Langmuir* **2014,** *30*, 7576-7584.

(32) Su, W.; Zhang, Y.; Zhao, C.; Li, X.; Jiang, J. Self-Assembled Organic Nanostructures: Effect of Substituents on the Morphology. *ChemPhysChem* **2007,** *8*, 1857-1862.

(33) Pisula, W.; Feng, X.; Müllen, K. Tuning the Columnar Organization of Discotic Polycyclic Aromatic Hydrocarbons. *Adv. Mater.* **2010,** *22*, 3634-3649.

(34) Ameen, M. Y.; Abhijith, T.; De, S.; Ray, S.; Reddy, V. Linearly Polarized Emission from PTCDI-C_8 One-Dimensional Microstructures. *Org. Electron.* **2013,** *14*, 554-559.

(35) Islam, M. R.; Sundararajan, P. Self-Assembly of a Set of Hydrophilic–Solvophobic–Hydrophobic Coil–Rod–Coil Molecules Based on Perylene Diimide. *Phys. Chem. Chem. Phys.* **2013,** *15*, 21058-21069.

(36) Jang, K.; Kinyanjui, J. M.; Hatchett, D. W.; Lee, D. Morphological Control of One-Dimensional Nanostructures of T-Shaped Asymmetric Bisphenazine. *Chem. Mater.* **2009,** *21*, 2070-2076.

(37) Buckley, J.; Hirasaki, G.; Liu, Y.; Von Drasek, S.; Wang, J.; Gill, B. Asphaltene Precipitation and Solvent Properties of Crude Oils. *Pet. Sci. Technol.* **1998,** *16*, 251-285.

(38) Mullins, O. C. The Asphaltenes. *Annu. Rev. Anal. Chem.* **2011,** *4*, 393-418.

(39) Shi, M.; Chen, Y.; Nan, Y.; Ling, J.; Zuo, L.; Qiu, W.; Wang, M.; Chen, H. π-π Interaction among Violanthrone Molecules: Observation, Enhancement, and Resulting Charge Transport Properties. *J. Phys. Chem. B* **2010,** *115*, 618-623.

(40) Shi, M.; Hao, F.; Zuo, L.; Chen, Y.; Nan, Y.; Chen, H. Effect of Substituents on the Aggregate Structure and Photovoltaic Property of Violanthrone Derivatives. *Dyes Pigm.* **2012,** *95*, 377-383.

(41) Buenrostro-Gonzalez, E.; Groenzin, H.; Lira-Galeana, C.; Mullins, O. C. The Overriding Chemical Principles that Define Asphaltenes. *Energy Fuels* **2001,** *15*, 972-978.

(42) Oostenbrink, C.; Villa, A.; Mark, A. E.; Van Gunsteren, W. F. A Biomolecular Force Field Based on the Free Enthalpy of Hydration and Solvation: The GROMOS Force-Field Parameter Sets 53A5 and 53A6. *J. Comput. Chem.* **2004,** *25*, 1656-1676.

(43) Hess, B.; Kutzner, C.; van der Spoel, D.; Lindahl, E. GROMACS 4: Algorithms for Highly Efficient, Load-Balanced, and Scalable Molecular Simulation. *J. Chem. Theory Comput.* **2008,** *4*, 435-447.

(44) van der Spoel, D.; Lindahl, E.; Hess, B.; Groenhof, G.; Mark, A. E.; Berendsen, H. J. GROMACS: Fast, Flexible, and Free. *J. Comput. Chem.* **2005,** *26*, 1701-1718.

(45) Lindahl, E.; Hess, B.; van der Spoel, D. GROMACS 3.0: A Package for Molecular Simulation and Trajectory Analysis. *J. Mol. Model.* **2001,** *7*, 306-317.

(46) Berendsen, H. J.; van der Spoel, D.; van Drunen, R. GROMACS: A Message-Passing Parallel Molecular Dynamics Implementation. *Comput. Phys. Commun.* **1995,** *91*, 43-56.

(47) Riddick, J. A.; Bunger, W. B.; Sakano, T. K. *Organic Solvents: Physical Properties and Methods of Purification,* 4th ed.; John Wiley & Sons Inc.: New York, 1986**.**

(48) Parrinello, M.; Rahman, A. Polymorphic Transitions in Single Crystals: A New Molecular Dynamics Method. *J. Appl. Phys.* **1981,** *52*, 7182-7190.

(49) Bussi, G.; Donadio, D.; Parrinello, M. Canonical Sampling through Velocity Rescaling. *J. Chem. Phys.* **2007,** 126, 014101.

(50) Evans, D. J.; Morriss, G. P. Non-Newtonian Molecular Dynamics. *Comput. Phys. Rep.* **1984,** *1*, 297-343.

(51) Hess, B. P-LINCS: A Parallel Linear Constraint Solver for Molecular Simulation. *J. Chem. Theory Comput.* **2008,** *4*, 116-122.

(52) Essmann, U.; Perera, L.; Berkowitz, M. L.; Darden, T.; Lee, H.; Pedersen, L. G. A Smooth Particle Mesh Ewald Method. *J. Chem. Phys.* **1995,** *103*, 8577.

(53) van der Spoel, D.; Lindahl, E.; Hess, B.; van Buuren, A. R.; Apol, E.; Meulenhoff, P. J.; Tieleman, D. P.; Sijbers, A. L. T. M.; Feenstra, K. A.; van Drunen, R.; Berendsen, H. J. C. *Gromacs User Manua*l, version 4.0. http://www.gromacs.org (2005).

(54) Humphrey, W.; Dalke, A.; Schulten, K. VMD: Visual Molecular Dynamics. *J. Mol. Graphics* **1996,** *14*, 33-38.

(55) Meriam, J. L.; Kraige, L. G. *Engineering Mechanics: Dynamics*, 6th ed.; John Wiley & Sons Inc.: New York, 2007.

(56) Balakrishnan, K.; Datar, A.; Oitker, R.; Chen, H.; Zuo, J.; Zang, L. Nanobelt Self-Assembly from an Organic n-Type Semiconductor: Propoxyethyl-PTCDI. *J. Am. Chem. Soc.* **2005,** *127*, 10496-10497.

(57) Balakrishnan, K.; Datar, A.; Naddo, T.; Huang, J.; Oitker, R.; Yen, M.; Zhao, J.; Zang, L. Effect of Side-Chain Substituents on Self-Assembly of Perylene Diimide Molecules: Morphology Control. *J. Am. Chem. Soc.* **2006,** *128*, 7390-7398.

(58) Israelachvili, J. N. *Intermolecular and Surface Forces;* Academic Press: San Diego, CA, 2011.

(59) Zhang, X.; Chen, Z.; Würthner, F. Morphology Control of Fluorescent Nanoaggregates by Co-Self-Assembly of Wedge-and Dumbbell-Shaped Amphiphilic Perylene Bisimides. *J. Am. Chem. Soc.* **2007,** *129*, 4886-4887.

(60) Sedghi, M.; Goual, L.; Welch, W.; Kubelka, J. Effect of Asphaltene Structure on Association and Aggregation Using Molecular Dynamics. *J. Phys. Chem. B* **2013,** *117*, 5765-5776.

(61) Frigerio, F.; Molinari, D. A Multiscale Approach to the Simulation of Asphaltenes. *Comput. Theor. Chem.* **2011,** *975*, 76-82.

Chapter 6: Inhomogeneity-Enhanced Stacking of Polyaromatic Compounds*

6.1. Introduction

The aggregation of PA compounds has gained an increasing interest, mainly due to their promising applications in the design of optical and electronic devices[1] as well as their serious effects in processing industrial materials.[2] For instance, 1D nanostructures, self-assembled via parallel stacking ($\pi-\pi$ stacking) of PA molecules, are finding their applications in organic photovoltaics, sensors, nanophotonics and nanoelectronics.[3] On the other hand, the highly stable aggregates formed by industrial PA compounds, such as asphaltenes, have caused many problems in heavy oil processing associated with well production and exploration, pipeline transport, oil refining, and emulsion stabilization.[4-6]

Many factors can influence the aggregated structures of PA compounds, such as their molecular structures,[7-10] type of solvents,[11] solution concentrations,[12,13] and external conditions including temperature as well as pressure.[10,14,15] Among these factors, the effect of solvents and solute molecular structures has been extensively investigated in literature for different types of PA compounds, such as the derivatives of PTCDI,[16] HBC,[16] pyrene,[17] and Violanthrone.[18-21] For instance, a series of studies by Zang et al.[1,22-25] have revealed the vital role played by solvents and the side-chain substituents of PTCDIs. It was found PTCDI molecules modified with acid groups could self-assemble into 1D nanostructure in aqueous solvent upon the adjustments of solution pH,[24] whereas in organic solvents, 1D nanostructures could be generated from PTCDIs

*A version of this chapter has been published. Reprinted with permission from Jian, C.; Tang, T. Molecular Dynamics Simulations Reveal Inhomogeneity-Enhanced Stacking of Violanthrone-78-Based Polyaromatic Compounds in n-Heptane–Toluene Mixtures. *J. Phys. Chem. B* **2015,** *119,* 8660–8668. Copyright 2015 American Chemical Society.

substituted with alkyl and alkyloxy side chains.[22,23,25] In addition, under the same conditions in organic solvents while PTCDIs modified with linear alkyl chains could form well-defined 1D nanobelt structures, PTCDI molecules modified with nonyldecyl groups could only generate irregular chunky aggregates.[21,22] For violanthrone derivatives, our previous work explored the effect of solvents on the geometry of the aggregates.[19-21] Given a particular type of PA molecules, results from MD simulations revealed[19-21] aggregates of distinct geometry characteristics in different solvents: while most PA cores were simply entangled together in water, leading to sphere-like aggregates,[19] the aggregated PA cores in n-hetpane resembled 1D rod-like geometry, self-assembled mainly via $\pi - \pi$ stacking.[21] In toluene, although $\pi - \pi$ stacking of PA cores was still widely observed, the range of the stacking was much smaller compared with that in n-hetpane, and hence a 1D geometry was absent.[20]

These previous studies mainly focused on the aggregated structures formed by a single type of PA compounds. However, impurity (inhomogeneity) in solute can exist in practical applications. For instance, asphaltenes are a mixture of different types of PA molecules.[26,27] Therefore, it is of interest to study the aggregation behavior of mixed PA compounds. In fact, some recent studies have reported interesting findings on the aggregation of a mixture of molecules possessing aromatic features. Shown by Ryan et al.,[28] equimolar mixtures of Fmoc-Phe and Fmoc-F5-Phe readily co-assembled to form two-component fibrils and hydrogels under conditions where Fmoc-Phe alone failed to self-assemble. Demonstrated by Shakai et al.,[29] mixing multiple types of amyloid peptides provides remarkable control over the self-assembled structures, which is very difficult to achieve by a single type of peptide. Recently, to enhance the photoconductivity of 1D nanostructure formed by PTCDIs, Hayward et al.[30,31] reported the coupled aggregation of poly(3-hexyl thiophene) (P3HT, polymerized thiophene) and dioctyl

substituted PTCDI in organic solvent 1,2-dichlorobenzene. It was found that the aggregates resembled "shish-kebab" type of structures consisting of central PTCDI 1D nanowires flanked by P3HT fibrils, where these fibrils were proposed to reduce the lateral association of PTCDI molecules.[30,31]

Despite these interesting works, theoretical study on the aggregation of mixed PA compounds has been quite limited. To mimic industrial asphaltenes, Kuznicki et al.[17] simulated the aggregation of mixed PA compounds in water, toluene, and heptane. The two types of PA compounds in their study have distinct structures: one possessing a single core with side-chain substituents and the other consisting of two small aromatic regions interconnected by aliphatic chains. The dominant structural feature of the aggregates was found to be the stacking of the PA rings, which could occur between the molecules of the same type or between molecules of different structures. In the work of Zhang et al.,[32] dissipative particle dynamics simulations were performed on model heavy crude oil systems. It was found that small PA compounds (with two hexa-particle rings), used to represent resins, did not participate in forming aggregates with large PA molecules (with at least three hexa-particle rings) which represented asphaltenes. While these two studies and a few other works[33-38] have probed the aggregation phenomena of their given mixtures, how mixing molecules of different structures may affect the overall aggregated morphologies was not investigated. In addition, no direct comparison was made between mixture and a pure type of PA compounds. Will different PA molecules in the mixture demonstrate any collective behaviors? And if so will such behaviors depend on the property of solvent? To answer these questions, in this Chapter, we performed MD simulations on the aggregation of two kinds of solutes: one involving a single type of PA molecule and the other containing a mixture of four types of systematically varied PA molecules. Comparison between these two kinds of

solutes provides direct information on the contribution of inhomogeneity to aggregation. Furthermore, these two kinds of solutes were solvated in several different organic solvents, which allows us to explore the role of solvents. The remainder of this chapter is organized as follows: the molecular models, systems simulated and computational methods are introduced in section 6.2; section 6.3 presents a detailed examination on the aggregates of the two kinds of solutes in different solvents; and final conclusions are given in section 6.4.

6.2. Methods

Four PA compounds (developed based on VO-78 and named VO-4C, VO-8C, VO-12C and VO-16C respectively), with different aromatic/aliphatic ratios, were used in this chapter, and their chemical structures are shown in Figure 6.1. As can be seen, these four PA compounds all consist of a fused PA core with peripheral side chains, similar to the island molecular model[2] proposed for asphaltenes in petroleum industry as well as many organic compounds used in optoelectronics devices.[1] The detailed design and construction schemes of these molecular models are available from our previous studies.[19-21]

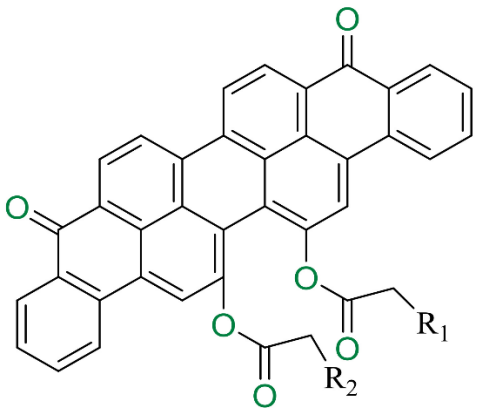

VO-16C: R_1=R_2= $C_{16}H_{33}$
VO-12C: R_1=R_2= $C_{12}H_{25}$
VO-8C: R_1=R_2= C_8H_{17}
VO-4C: R_1=R_2= C_4H_9

Figure 6.1: Chemical structures of the PA molecular models employed in this chapter.

Two sets of simulations were performed: (I) in which the 24 solute molecules were of a single type (VO-4C) and (II) where the solutes were a mixture of four types of molecules, containing 6 molecules of each model. In each case, toluene (a good solvent for the PA compounds),[20] n-heptane (a poor solvent for the PA compounds)[21] and heptol (a mixture of n-heptane and toluene) of different n-heptane/toluene ratios were chosen as the solvents. A total of 16 systems were simulated in this chapter, and their information is summarized in Table 6.1. Details of the simulated systems and the explanations on their designations are given below.

6.2.1. Systems Simulated

The first five systems shown in Table 6.1 involve only VO-4C as the solute. For each system, 24 VO-4C molecules were initially packed into a cubic box of dimensions $12 \times 12 \times 12$ nm^3, forming a $2 \times 3 \times 4$ array with their PA cores parallel to one another (see Figure 6.2a). These molecules were then solvated in different solvents: pure toluene in VO-4C-T, heptol with 25% n-heptane in VO-4C-HT25, heptol with 50% n-heptane in VO-4C-HT50, heptol with 75% n-heptane in VO-4C-HT75, and pure n-heptane in VO-4C-H.

Similar methods were used to build the systems involving a mixture of solutes. Particularly, for system Mixture-T, 6 molecules of each type of solute (VO-16C, VO-12C, VO-8C, or VO-4C) were arranged to form a 2×3 array in the $x - y$ plane (see Figure 6.2b), where VO-16C is colored purple, VO-12C pink, VO-8C cyan, and VO-4C green. These arrays were then aligned in the z-direction to form a $2 \times 3 \times 4$ matrix, followed by solvation in pure toluene. The mixture was also simulated in pure n-heptane (system Mixture-H) and in heptols at seven n-heptane/toluene ratios: 12.5:87.5 (system Mixture-HT12.5), 25:75 (system Mixture-HT25), 37.5:62.5 (system Mixture-HT37.5), 50:50 (system Mixture-HT50), 62.5:37.5 (system Mixture-HT62.5), 75:25 (system Mixture-HT75), and 87.5:12.5 (system Mixture-HT87.5).

Table 6.1: Information on the 16 Different Systems Simulated

system name	number of PA molecules	number of toluene molecules	number of n-heptane molecules	simulation time (ns)
VO-4C-T[19]	24	8857	0	80
VO-4C-HT25	24	7068	1684	200
VO-4C-HT50	24	4736	3365	200
VO-4C-HT75	24	2362	5053	200
VO-4C-H[20]	24	0	6233	180
VO-4C-TR	24	8857	0	220
Mixture-T	24	8751	0	200
Mixture-HT12.5	24	8126	834	200
Mixture-HT25	24	6999	1661	200
Mixture-HT37.5	24	5405	2370	200
Mixture-HT50	24	4671	3329	200
Mixture-HT62.5	24	3294	3825	200
Mixutre-HT75	24	2335	4990	200
Mixture-HT87.5	24	1163	5278	200
Mixture-H	24	0	6157	200
Mixture-TR	24	8751	0	220

For each of the system described above, standard MD simulations were performed (details given in section 6.2.2). As will be demonstrated later, at the late stage of the standard MD simulations, while in system VO-4C-T only short-range stacking was observed, a nearly 1D structure of long-range PA core stacking was formed by the mixture in toluene (system Mixture-T). To make sure such difference was not due to the systems being trapped in potential energy wells, we enhanced the sampling by performing additional replica-exchange MD (REMD) simulations in toluene (systems VO-4C-TR and Mixture-TR in Table 6.1). The starting configurations for these two systems were adopted from the final structures formed in systems VO-4C-T and Mixture-T.

6.2.2. Simulation Details

The topologies for VO molecules, toluene and n-heptane, which were developed based on GROMOS96 force field parameter set 53A6,[39] were validated in our previous work,[20,21,40] and

directly adopted here. Detailed information on the development of heptol solvent is available in Appendix D (section D.1).

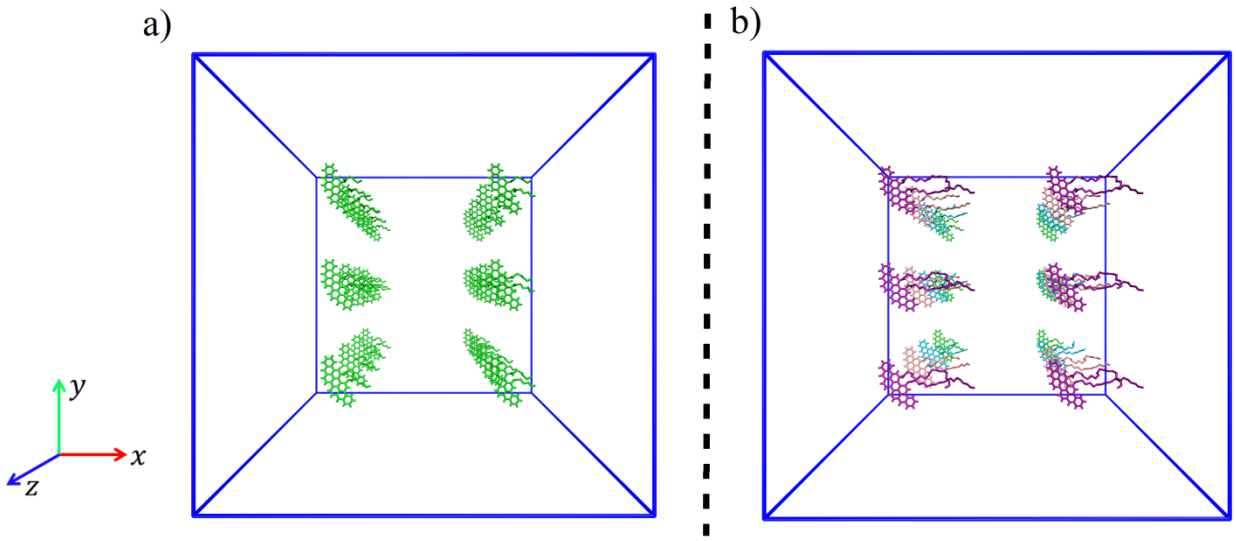

Figure 6.2: Initial solute configurations: (a) for systems VO-4C-T, VO-4C-HT25, VO-4C-HT50, VO-4C-HT75, and VO-4C-H; (b) for systems Mixture-T, Mixture-HT12.5, Mixture-HT25, Mixture-HT37.5, Mixture-HT50, Mixture-HT62.5, Mixture-HT75, Mixture-HT87.5, and Mixture-H, where different types of VO compounds are represented by different colors.

Both standard MD and REMD simulations were performed using the MD package GROMACS (version 4.0.7).[41-44] Periodic boundary conditions, full electrostatics with particle-mesh Ewald method,[45] cutoff distance 1.4 nm for van der Waals interactions and electrostatics pairwise calculations, LINCS algorithm to constraint all bonds,[46] and a time step of 2 fs were used in all simulations.

During each standard MD simulation, static structure optimization was first performed to minimize the total potential energy. Then the non-hydrogen atoms of the solutes were restrained with 1000 kJ/(mol·nm^2) harmonic potential for 1 ns at 300 K and 1 bar to relax the solvents around the solutes. The restraint was then removed and NPT ensemble simulation was performed for 80 ns for system VO-4C-T, 180 ns for system VO-4C-H, and 200 ns for the other systems.

REMD is an enhanced sampling technique by simulating copies (replicas) of the same systems to sample conformations at different temperatures, and attempting exchanges between neighboring replicas at a certain frequency.[47] By doing so, it helps with overcoming energy barrier on the potential energy surface, thus allowing the exploration of new conformational space. In this chapter, each run of the two REMD systems, VO-4C-TR and Mixture-TR in Table 6.1, is composed of 11 replicas at 300, 301.25, 302.5, 303.75, 305, 306.25, 307.5, 308.75, 310, 311.25, and 312.5 K. The temperature distribution was chosen such that an acceptance ratio of 21%-23% was achieved between all replicas. Each replica was run for 20 ns, resulting in a total of 220 ns integration time and 22000 configurations for each system. Performance of each REMD system was checked using a probability distribution of total potential energy of each replica, and this information is available in Appendix D (section D.2).

6.2.3. Data Analysis

Appropriate post-processing tools available in GROMACS were used for trajectory analysis and VMD[48] used for visualization.

To quantitatively describe the geometry of molecular aggregates in the standard MD simulations, a dimension map method[40] (see Chapter 7 of this thesis) was adopted here. Specifically, using heavy atoms in the PA cores of the molecules in an aggregate, three principal radii of gyration can be calculated, and are denoted by R_x, R_y and R_z. A pair of gyradius ratios (r_1 and r_2) were then defined as:

$$r_1 = \frac{R_1}{R_0}, r_2 = \frac{R_2}{R_0}, \tag{6.1}$$

where R_0 is the minimum of $\{R_x, R_y, R_z\}$, R_2 is the maximum of $\{R_x, R_y, R_z\}$, and R_1 is the intermediate value. For a 1D structure, as the length scale in one direction is much larger than that in the other two, $r_2 \approx r_1 \gg 1$. For a sphere-like structure, because the three dimensions are

approximately equal, $r_2 \approx r_1 \approx 1$. For a short-cylinder-like structure, the length of the cylinder is comparable to its diameter, thus $r_2 \approx r_1 > 1$. Therefore, gyradius ratios are a good indicator for the dimension characteristics of molecular aggregates, and examining the locations of the points on the dimension map provides an effective way to directly compare the geometries of molecular aggregates.

To evaluate the relative stability of the conformations formed in REMD, we calculated the free energy (potential of mean force) difference ΔW as a function of two reaction coordinates, number of aggregates (n) and size of the largest aggregate (s). Here, the size is defined as the number of molecules inside the largest aggregate. By counting the relative probability of the configurations with different n and s, ΔW is calculated using:[49,50]

$$\Delta W(n,s) = -kTln\frac{P(n,s)}{P_{max}} = -kTln\frac{N(n,s)}{N_{max}}. \quad (6.2)$$

In eq. 6.2, $P(n,s)$ is the probability density obtained from the REMD data, P_{max} is the maximum of $P(n,s)$, $N(n,s)$ is the number of configurations with the same n and s, and N_{max} is the largest of $N(n,s)$. Therefore, the ratio represents the relative probability, and by this definition, $\Delta W(n,s) \geq 0$.

6.3. Results and Discussions

6.3.1. Aggregation in Pure Toluene

Figure 6.3 shows the largest stable aggregates formed in systems VO-4C-T and Mixture-T at the equilibrium stage of the simulations, where different types of VO molecules are represented by different colors. Here, the largest stable aggregates are the ones that do not dissociate at the equilibrium stage of the simulations (the last 10 ns for VO-4C-T and the last 20 ns for Mixture-T). It can be seen from Figure 6.3 that irrespective of the solute kinds, the aggregates are mainly formed by the parallel stacking of multiple PA cores, demonstrating the dominant role of $\pi - \pi$

interaction.[19-21,51] In addition, for each of the two aggregates, there exists a clear axis, depicted as blue lines in Figure 6.3 for a guide to the eye, along which the stacking of PA cores is propagated. However, the parallel stacking formed by mixtures persists for a much longer distance. To be specific, in system VO-4C-T, the largest stable aggregate involves 7 molecules and resembles a short cylinder. Such structure is consistent with the well-known Yen-Mullins model[52-54] for asphaltene aggregation in toluene. On the contrary, in system Mixture-T, the largest stable assembly contains 15 molecules, leading to a 1D rod-like structure.

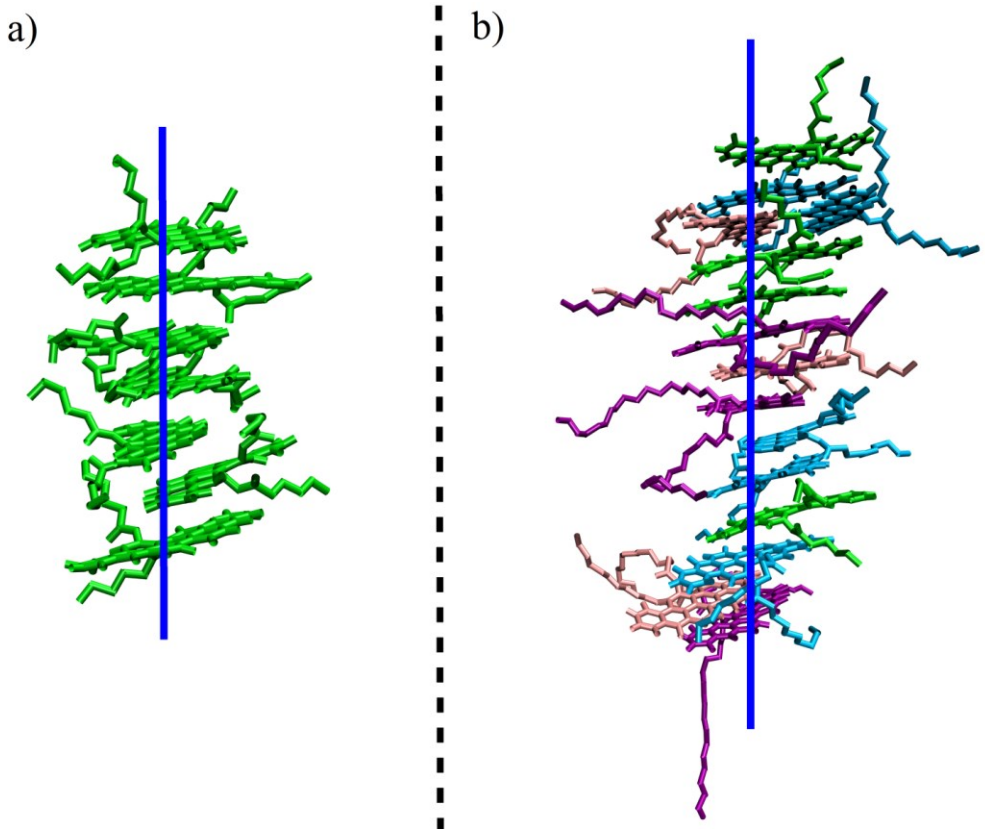

Figure 6.3: Snapshots of the largest stable aggregates formed at the equilibrium stage of the simulations in systems: (a) VO-4C-T, and (b) Mixture-T.

To quantitatively describe these geometry differences, we calculated the gyradius ratios of the PA core regions for the two aggregates shown in Figure 6.3 using the method described in section 6.2.3. The corresponding values are, respectively, $\{r_1 = 1.61, r_2 = 1.73\}$ for VO-4C-T

and $\{r_1 = 2.67, r_2 = 2.72\}$ for Mixture-T. These gyradius ratios apparently deviate from the case of $\{r_1 \approx 1, r_2 \approx 1\}$ which are the characteristics of a sphere-like structure. This is consistent with the ordered parallel stacking of PA cores observed. More importantly, the gyradius ratios of the aggregates formed in Mixture-T are much larger than those in VO-4C-T, quantitatively confirming that the parallel stacking is significantly enhanced by having a mixture of solute molecules.

One could argue that the above difference in configuration may be caused by poor sampling in standard MD techniques where the VO molecules are trapped in a potential energy well. To address this, REMD techniques were employed to enhance the configuration sampling of VO-4C and mixtures. Using the method described in section 6.2.2, in Figure 6.4, we reported the free energy landscape of aggregation for systems VO-4C-TR and Mixture-TR at 300 K as a function of two reaction coordinates, number of molecular aggregates (n) and size of the largest aggregate (s). If none of the PA molecules aggregate, the maximum possible value for *n* is 24. However, in both plots, *n* is limited to 10, as no data were found for *n* = 10-24. Figure 6.4 shows that for system VO-4C-TR, the free energy minimum is located at $n \approx 4{\sim}6$ and $s \approx 7$, whereas for system Mixture-TR, the most evident free energy minimum is located at $n \approx 3{\sim}4$ and $s \approx 15$. It clearly demonstrates that mixture tends to form larger aggregates, resulting in less number of molecular aggregates. As the free energy minimum represents the most probable configuration at a specific temperature, these results confirms previous results from standard MD simulations. To understand the physical meaning behind this interesting phenomenon, below we will take a detailed look at the aggregated structures.

Further inspection of Figure 6.3b shows that molecules of different types, denoted by different colors, appear in an alternating manner. If we "sequence" the aggregate from top to

bottom, then the 4 types of molecules appear in the following order (omitting "VO" for simplicity): 4C-8C-8C(12C)-4C-4C-16C-12C-16C-8C-8C-4C-8C-12C-16C, where 8C(12C) denotes the one VO-8C molecule and one VO-12C molecule that are located in a side-by-side

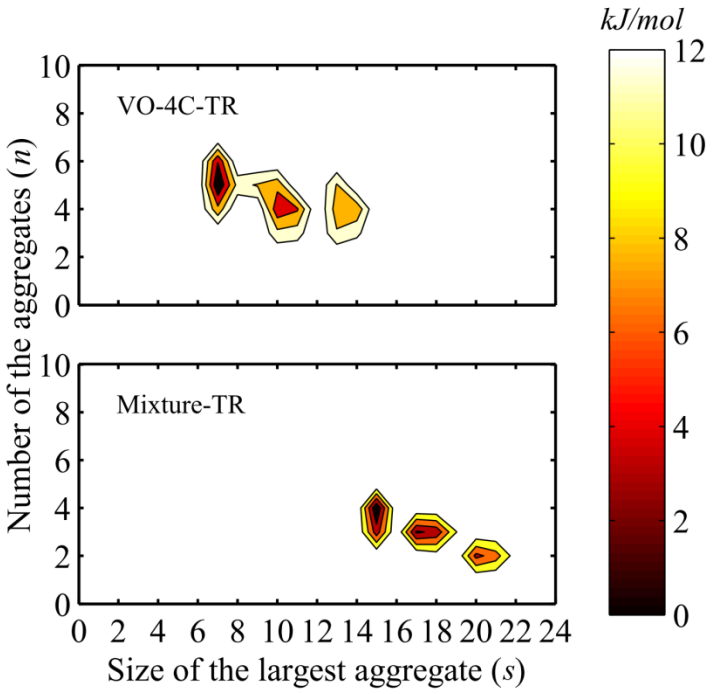

Figure 6.4: Free energy landscape versus number of the aggregates (n) and size of the largest aggregate (s) for systems VO-4C-TR and Mixture-TR.

manner. It seems that $\pi-\pi$ stacking in the aggregate is more likely to be formed between molecules of different types. To quantify the $\pi-\pi$ interaction among these PA molecules, we first introduced the molecule identification (ID) number and labeled the molecules in system Mixture-T by numbers 1-24. Specifically, number 1-6 was used to label the 6 VO-4C molecules, followed by number 7-12 for VO-8C molecules, 13-18 for VO-12C molecules, and 19-24 for VO-16C molecules. Then for each pair of PA cores, the minimum distance between their PA cores was calculated every 100 ps, resulting in 2000 data points during the 200 ns simulation run. A $\pi-\pi$ contact is counted if this minimum distance is $\leq$ 0.5 nm.[9,55] If out of the 2000 data points, the total number of $\pi-\pi$ contacts is $\geq$ 1000 over the whole simulation course, i.e., the

two PA cores are in $\pi-\pi$ contact for at least 50% of the simulation time, then we say the two PA cores are stably stacked. Figure 6.5 shows the pairwise stacking table, where the x and y axes represent the molecule ID number and a grid point will be marked with a blue square if a stable stacked pair is formed between molecules x and y. Because of symmetry, only the upper left half of the grid is utilized. Stacking that falls in the purple triangular region are the ones formed between the PA molecules of the same type. It can be clearly seen that in total, 6 stacking pairs are formed between PA molecules of the same type. On the other hand, there are 12 pairs outside the purple triangular regions, which demonstrates that the $\pi-\pi$ stacking is more likely to be formed between molecules of different types, consistent with previous observation in Figure 6.3b. As it has been reported[20] that for a single type of PA molecules, only short ranged stacking was found in pure toluene, the results shown here suggest that the alternating stacking manner of PA mixtures can introduce advantages to increasing the stacking range. These advantages are analyzed in detail below.

In toluene, longer side chains have been proposed to reduce the flexibility of PA molecules and provide larger steric hindrance to $\pi-\pi$ stacking, thus limiting the stacking range.[20] For instance, in our previous work,[20] it has been shown that long side chains prohibits the formation of large direct parallel stacking structures that involve more than three molecules. When multiple types of PA compounds co-aggregate, short-chained molecules can exist between long-chained ones. By having smaller molecules in-between, the steric hindrance of long side chains were decreased. This is the first advantage the mixture brings to promoting long-range stacking.

The second advantage lies in the "protection" long-chained molecules bring to the short-chained molecules. It has been proved[20] that toluene is a good solvent for the PA molecules

because they can have attractions with the PA cores. When short-chained molecules stack, toluene molecules can diffuse into the space between neighboring molecules and break the $\pi - \pi$

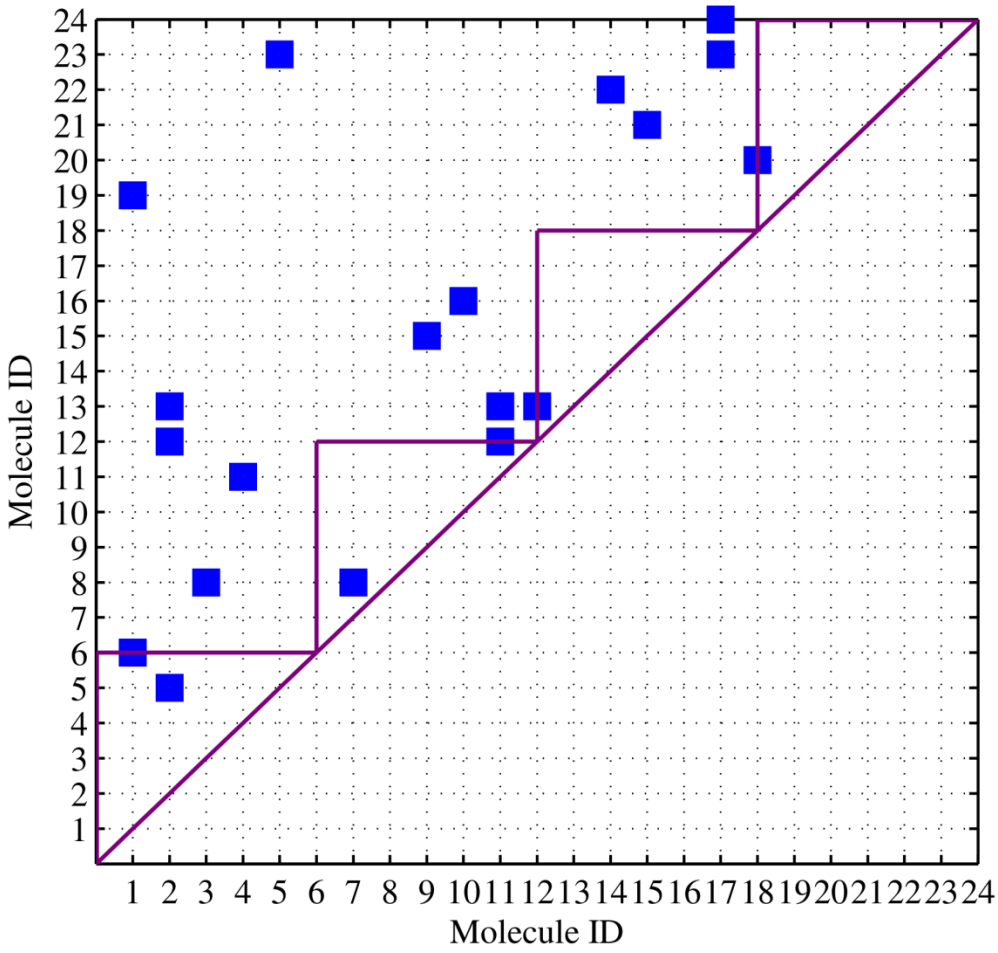

Figure 6.5: Pairwise stacking table for system Mixture-T. The x and y axes represent the molecule ID number (1 to 24, representing the 24 molecules in the simulation system), and the grid point marked with a blue square indicates that a stable stacked pair is formed between molecules x and y. Symbols in the purple triangular region correspond to the stable stacking formed between the VO molecules of the same type. Because of symmetry, only the upper left half of the grid is utilized.

stacking through their attraction with the PA cores. However, if these PA molecules with short side chains are sandwiched between molecules with longer side chains, the PA cores are better

"protected" and the solvent-solute attractions are reduced, thus helping with stacking. To clearly show the protection from the long side chains, we performed 3 additional simulations, each of which has three VO molecules forming parallel stacking in toluene. Specifically, 2 systems involves three VO molecules of a single type (VO-4C or VO-16C), and will be, respectively, referred to as systems 4C-4C-4C and 16C-16C-16C. The third system, referred to as 16C-4C-16C, contains a mixture of VO-4C and VO-16C types of molecules, where the parallel stacked structure is of the "sequence" 16C-4C-16C. Thus comparison for the toluene distribution around the PA core in the 3 systems can provide direct information about the "protection" roles of long-chained molecules. Figure 6.6 shows the RDF and the cumulative number (CN) of toluene atoms around the atoms on the PA core of the middle VO molecule (e.g., 4C in 16C-4C-16C). It can be seen that in the RDF and CN plots, the curve for system 16C-4C-16C nearly overlaps with the

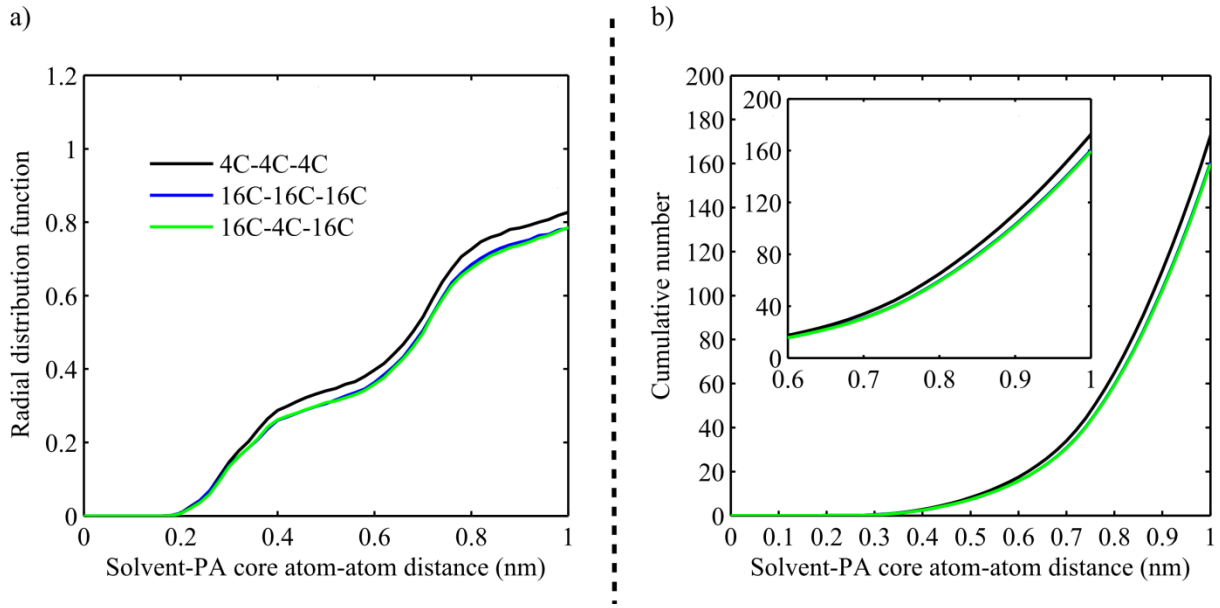

Figure 6.6: (a) RDF and (b) CN for the distance between toluene atoms and PA core atoms (middle molecule). The inset in (b) shows the enlarged CN for atom-atom distance from 0.6 to 1 nm.

one for system 16C-16C-16C, and is below the one for system 4C-4C-4C. The smaller values of RDF and CN here confirm that at a given distance there is less contact, hence less attraction, between toluene molecules and the VO molecule in the middle of the stacking in systems 16C-4C-16C and 16C-16C-16C.

6.3.2. Aggregation in Heptol

It has been shown in the previous section that in pure toluene, the stacking range and formation of 1D rod-like structure have been enhanced by having a mixture of PA molecules as solutes. As the property of the solvent is a crucial factor that can influence the structure of the aggregates,[11] it is of great interest to investigate the variation of aggregated structures with the change of solvents. It was shown in our previous work[20,21] that for a single type of PA molecules, while the stacked PA cores resemble short cylinders in toluene, a 1D rod-like structure of long-range stacked PA cores was formed in n-heptane. The enhanced aggregation/association of PA compounds in n-heptane, compared with that in toluene, has also been reported in the work of Headen et al.[56] and Sedghi et al.[57] Therefore we chose to vary the solvent from pure toluene to pure n-heptane by increasing the n-heptane ratio, and the results are shown below.

Figures 6.7 shows the dimension map generated using the PA core region of the aggregated structures formed by VO-4C in toluene, heptol (3 different heptol ratios), and n-heptane. The corresponding dimension map for the aggregates formed by the mixture of solutes is given by Figure 6.8, with 4 additional heptol ratios. There may be more than one aggregate in each system and each aggregate is represented by a separate symbol. As has been proved (see Chapter 7 of this dissertation),[40] all the data on the dimension map are bounded by two curves $r_2 = r_1$ and $r_2 = \sqrt{{r_1}^2 + 1}$, plotted as black dashed lines. To further investigate the distribution

of gyradius ratios, we divided each dimension map into three regimes, each corresponding to a particular group of structures:

(I) $r_2 \geq 1.90$, which represents 1D rod-like structures (the stacking range is much larger than the dimensions in the PA core plane).

(II) $1.40 < r_2 < 1.90$, which represents short-cylinder-like structures (the stacking range is comparable to the dimensions in the PA core plane).

(III) $r_2 \leq 1.40$, which represents three-dimensional sphere-like structures (PA cores entangled together without preferred stacking directions).

The boundary lines separating the three regimes were chosen based on the natural gaps found on the dimension map in Figure 6.7, and applied to Figure 6.8 as well.

The first observation made from Figures 6.7 and 6.8 is that in both figures, almost all of the data are located above $r_2 = 1.4$, below which aggregates of sphere-like shapes locate. This is consistent with the ordered structures visually observed earlier. Despite these similarities, detailed examination reveals that considerable differences can be found between the two dimension maps. Let's first consider Figure 6.7. Clearly, the gyradius ratios for the aggregates formed in system VO-4C-T, depicted as blue squares, are mainly located in regime (II), indicating that the aggregated PA cores are of short-range stacking. As n-heptane ratio increases in the solvent, the parallel stacking of PA cores is enhanced, and consequently the gyradius ratios show a trend of moving into regime (I). At sufficiently high n-heptane/toluene ratios (>25%), the gyradius ratios mostly lie in regime (I) and are well distinguished from those of system VO-4C-T, corresponding to the long-range stacking of PA cores. On the contrary, in Figure 6.8, aggregates in regime (I) are present for all types of solvents except when n-heptane/toluene ratio $= 25\%{:}\,75\%$. That is, given a mixture as the solutes, the existence of 1D rod-like structure

becomes insensitive to the type of solvent. Secondly, at the same n-heptane/toluene ratios, the largest gyradius ratio from a system involving mixtures is generally larger than its counterpart with VO-4C as the solute. For instance, at 75%:25% (n-heptane/toluene ratio), the largest pair of gyradius ratios for system Mixture-HT75 are $\{r_1 \approx 2.6, r_2 \approx 2.7\}$ while the corresponding values for VO-4C-HT75 are $\{r_1 \approx 2.1, r_2 \approx 2.2\}$. Finally, a nearly straight 1D structure with infinity curvature (hence the largest gyradius ratios) is formed in system Mixture-HT87.5, shown

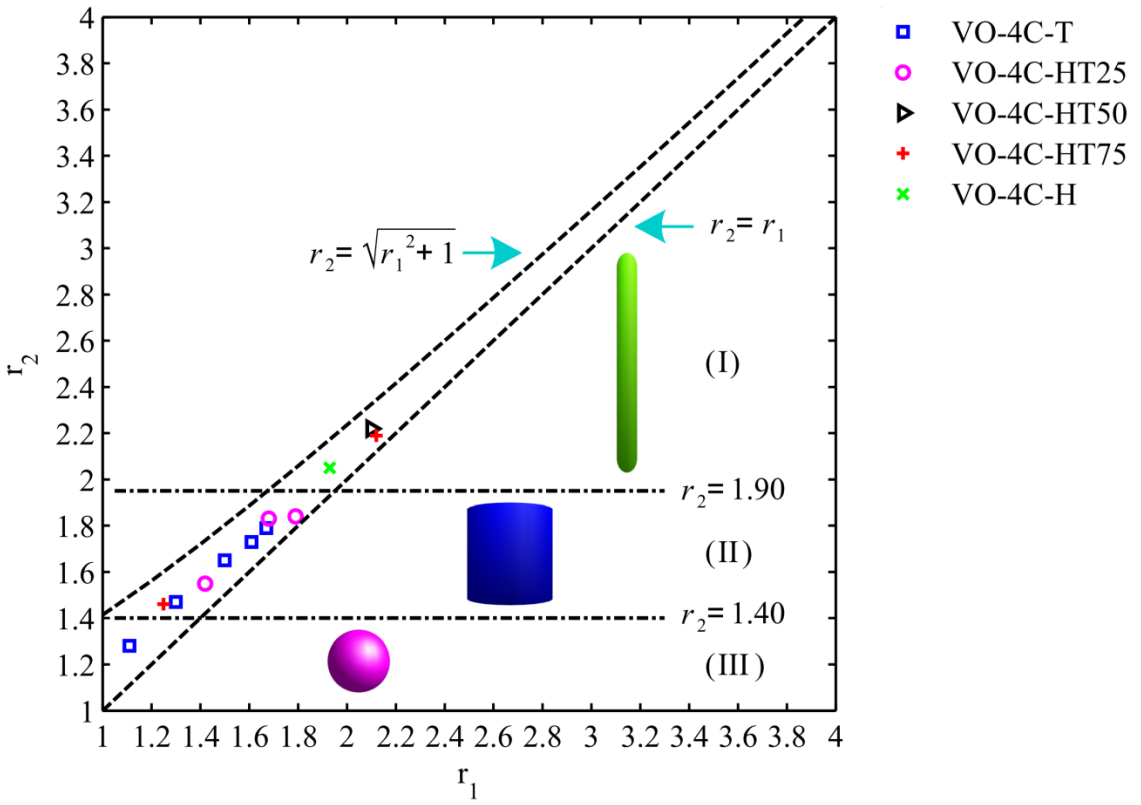

Figure 6.7: Dimension map for systems with VO-4C as solutes. Different symbols correspond to simulations with different solvents. There may be more than one aggregate in a particular system and each aggregate is represented by a separate point. Each of the three regimes (I), (II), and (III) corresponds to a particular group of structures: regime (I) represents 1D rod-like structures, regime (II) represents short-cylinder-like structures, and regime (III) represents three-dimensional sphere-like structures.

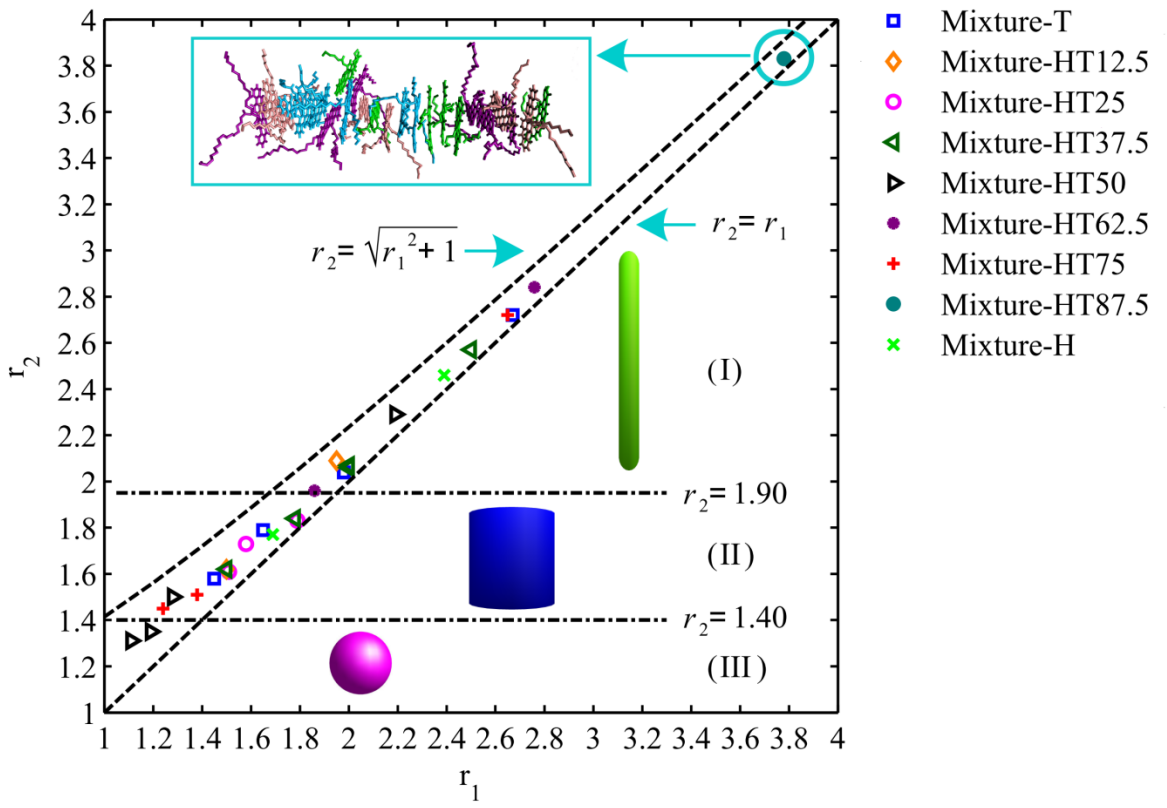

Figure 6.8: Dimension map for systems with a mixture of different PA molecules as solutes. Different symbols correspond to simulations with different solvents. There may be more than one aggregate in a particular system and each aggregate is represented by a separate point. Each of the three regimes (I), (II), and (III) corresponds to a particular group of structures: regime (I) represents 1D rod-like structures, regime (II) represents short-cylinder-like structures, and regime (III) represents three-dimensional sphere-like structures.

as the inset in Figure 6.8, which is not observed in systems involving solely VO-4C as solute. If we "sequence" this structure (see section D.3 in Appendix D), again, molecules of different types stack together in an alternating manner. All these observations further support previous conclusion that by having mixtures as solute, parallel stacking of PA cores is enhanced.

One interesting observation, as mentioned above, is that the largest gyradius ratios found in Figure 6.8 are not formed by mixture in pure *n*-heptane, but rather in heptol with 87.5% *n*-

heptane. Examination of Figure 6.7 also shows that the largest gyradius ratios for VO-4C are found in systems with heptol being the solvents (i.e. systems VO-4C-HT50 and VO-4C-HT75). While intuitively adding n-heptane should help with PA core stacking, the observation here seems to indicate that this effect is not monotonic. In other words, the longest range of stacking is achieved when a small amount of toluene is present. To understand this, it is necessary to take a detailed look at the aggregation mechanism.

It has been proved[20,21] that compared with n-heptane, toluene can form $\pi-\pi$ stacking with PA molecules, which reduces the interaction between PA cores ($\pi-\pi$ interaction), between PA core and side chain ($\pi-\theta$ interaction) and between side chains ($\theta-\theta$ interaction). Among these three types of solute-solute interactions, $\pi-\pi$ interaction is the main force driving the formation of 1D rod-like structure, while $\pi-\theta$ and $\theta-\theta$ interactions bring in adverse effect that interfere with the parallel stacking of PA cores. With the increase of the n-heptane ratio in the solvents, all three types of interactions are increased (see evidence using intermolecular contacts; details given in Appendix D, section D.4), thus resulting in a larger aggregate. On the other hand, when the n-heptane ratio is too high, for instance, in the case of pure n-heptane, the large amount of $\pi-\theta$ and $\theta-\theta$ interactions can introduce relative titling, slipping and twisting between neighboring PA cores. This reduces the likelihood of forming "perfect parallel stacking" where one PA core is parallel to another with the line connecting their centers perpendicular to the PA planes.[21] Therefore to maximize the stacking range in the 1D structure, the optimum solvent should simultaneously promote the $\pi-\pi$ interaction between solutes and avoid too much increase in the $\pi-\theta$ and $\theta-\theta$ interactions. This explains why the largest gyradius ratios in Figures 6.7 and 6.8 are from systems with heptol as solvents instead of pure n-heptane.

6.3.3. Implications

Obtaining 1D structure of parallel-stacked PA cores is of crucial importance in the design of optical and electrical nanodevices.[1,3] For the PA compounds studied here, the present work provides two potential methods that can be employed in practice. Firstly, for a given solute, the stacking of PA cores can be enhanced through selecting appropriate solvents. The optimal solvent is the one that can increase the $\pi - \pi$ interaction between PA cores without introducing too much association between side chains and between side chains and PA cores.

Secondly and also more importantly, for a given solvent, the stacking of PA cores can be enhanced by introducing inhomogeneity into the solutes. To obtain a 1D structure in a given solvent, a typical approach in literature is to synthesize new-functionalized PA molecules.[1,21-24] However, instead of looking for a new kind of solutes, our results suggest that simply mixing different types of PA molecules in hand may provide an additional approach to generate 1D structure, thus avoiding the design of new synthetic procedure. Furthermore, as shown earlier, for a mixture of solutes the existence of the 1D aggregates is not so sensitive to the solvents, although the composition of the solvent can affect the degrees of stacking inside the 1D structure. Therefore, having a solute mixture may allow more flexibility in choosing appropriate solvents.

Finally, it is of great importance to point out that although a particular type of PA compounds is studied here, these molecules possess the common features of PA compounds. Therefore, the results discussed in this chapter can be applied to a broader class. For instance, to precipitate industrial PA compounds, such as asphaltenes, precipitants ("bad" solvents) are usually added to heavy oil solutions.[58] The aggregation behaviors in heptol investigated here can provide information about the amount of precipitants needed for effective precipitation.

6.4. **Conclusions**

In this chapter, we investigated the effect of inhomogeneity in solute on the aggregation of our representative PA compounds using all-atom MD simulations. The PA compounds studied here are differentiated by their side-chain lengths. In toluene, we found that compared with a single type of PA compound, parallel stacking of PA cores were enhanced by having a mixture of four types of PA compounds. Specifically, PA compounds of different types organize themselves in an alternating manner. This alternating stacking manner reduces the steric hindrance of long side chains and shields the attractive interaction between toluene molecules and the PA cores, allowing the assembly of a 1D rod-like structure with long-range stacking. It was further shown that while for a single type of PA compound the 1D rod-like structure could only be formed in pure n-heptane or heptol of sufficiently large n-heptane/toluene ratio, the existence of the 1D structure formed by mixtures is insensitive to the composition of the solvents. However, solvents can tune the stacking manner of PA cores by affecting the intermolecular interactions among the solutes. To achieve "perfect" stacking, the solvent should simultaneously increase the interaction between PA cores, and avoid introducing too much association between PA core and side chain as well as between side chains. These results shed light on how one may control the aggregation of PA compounds by adjusting solute as well as solvent.

Bibliography

(1) Zang, L.; Che, Y.; Moore, J. S. One-Dimensional Self-Assembly of Planar π-Conjugated Molecules: Adaptable Building Blocks for Organic Nanodevices. *Acc. Chem. Res.* **2008,** *41*, 1596-1608.

(2) Groenzin, H.; Mullins, O. C. Asphaltene Molecular Size and Structure. *J. Phys. Chem. A* **1999,** *103*, 11237-11245.

(3) Kim, F. S.; Ren, G.; Jenekhe, S. A. One-Dimensional Nanostructures of π-Conjugated Molecular Systems: Assembly, Properties, and Applications from Photovoltaics, Sensors, and Nanophotonics to Nanoelectronics. *Chem. Mater.* **2010,** *23*, 682-732.

(4) Speight, J. Petroleum Asphaltenes-Part 1: Asphaltenes, Resins and the Structure of Petroleum. *Oil Gas Sci. Technol.* **2004,** *59*, 467-477.

(5) Spiecker, P. M.; Gawrys, K. L.; Trail, C. B.; Kilpatrick, P. K. Effects of Petroleum Resins on Asphaltene Aggregation and Water-in-Oil Emulsion Formation. *Colloids Surf., A* **2003,** *220*, 9-27.

(6) Kilpatrick, P. K. Water-in-Crude Oil Emulsion Stabilization: Review and Unanswered Questions. *Energy Fuels* **2012,** *26*, 4017-4026.

(7) Bai, S.; Debnath, S.; Javid, N.; Frederix, P. W.; Fleming, S.; Pappas, C.; Ulijn, R. V. Differential Self-Assembly and Tunable Emission of Aromatic Peptide Bola-Amphiphiles Containing Perylene Bisimide in Polar Solvents Including Water. *Langmuir* **2014,** *30*, 7576-7584.

(8) Su, W.; Zhang, Y.; Zhao, C.; Li, X.; Jiang, J. Self-Assembled Organic Nanostructures: Effect of Substituents on the Morphology. *ChemPhysChem* **2007,** *8*, 1857-1862.

(9) Pisula, W.; Feng, X.; Müllen, K. Tuning the Columnar Organization of Discotic Polycyclic Aromatic Hydrocarbons. *Adv. Mater.* **2010,** *22*, 3634-3649.

(10) Safont-Sempere, M. M.; Fernández, G.; Würthner, F. Self-Sorting Phenomena in Complex Supramolecular Systems. *Chem. Rev.* **2011,** *111*, 5784-5814.

(11) Ameen, M. Y.; Abhijith, T.; De, S.; Ray, S.; Reddy, V. Linearly Polarized Emission from PTCDI-C_8 One-Dimensional Microstructures. *Org. Electron.* **2013,** *14*, 554-559.

(12) Islam, M. R.; Sundararajan, P. Self-Assembly of a Set of Hydrophilic–Solvophobic

Hydrophobic Coil–Rod–Coil Molecules Based on Perylene Diimide. *Phys. Chem. Chem. Phys.* **2013,** *15*, 21058-21069.

(13) Jang, K.; Kinyanjui, J. M.; Hatchett, D. W.; Lee, D. Morphological Control of One Dimensional Nanostructures of T-Shaped Asymmetric Bisphenazine. *Chem. Mater.* **2009,** *21*, 2070-2076.

(14) Wu, H.; Xue, L.; Shi, Y.; Chen, Y.; Li, X. Organogels Based on J- and H-Type Aggregates of Amphiphilic Perylenetetracarboxylic Diimides. *Langmuir* **2011,** *27*, 3074-3082.

(15) Verdier, S.; Carrier, H.; Andersen, S. I.; Daridon, J. Study of Pressure and Temperature Effects on Asphaltene Stability in Presence of CO_2. *Energy Fuels* **2006,** *20*, 1584-1590.

(16) Wang, C.; Dong, H.; Hu, W.; Liu, Y.; Zhu, D. Semiconducting π-Conjugated Systems in Field-Effect Transistors: A Material Odyssey of Organic Electronics. *Chem. Rev.* **2011,** *112*, 2208-2267.

(17) Figueira-Duarte, T. M.; Müllen, K. Pyrene-Based Materials for Organic Electronics. *Chem. Rev.* **2011,** *111*, 7260-7314.

(18) Kuznicki, T.; Masliyah, J. H.; Bhattacharjee, S. Molecular Dynamics Study of Model Molecules Resembling Asphaltene-Like Structures in Aqueous Organic Solvent Systems. *Energy Fuels* **2008,** *22*, 2379-2389.

(19) Jian, C.; Tang, T.; Bhattacharjee, S. Probing the Effect of Side-Chain Length on the Aggregation of a Model Asphaltene Using Molecular Dynamics Simulations. *Energy Fuels* **2013,** *27*, 2057-2067.

(20) Jian, C.; Tang, T.; Bhattacharjee, S. Molecular Dynamics Investigation on the Aggregation of Violanthrone78-Based Model Asphaltenes in Toluene. *Energy Fuels* **2014,** *28*, 3604-3613.

(21) Jian, C.; Tang, T. One-Dimensional Self-Assembly of Polyaromatic Compounds Revealed by Molecular Dynamics Simulations. *J. Phys. Chem. B* **2014,** *118*, 12772–12780.

(22) Balakrishnan, K.; Datar, A.; Oitker, R.; Chen, H.; Zuo, J.; Zang, L. Nanobelt Self-Assembly from an Organic n-Type Semiconductor: Propoxyethyl-PTCDI. *J. Am. Chem. Soc.* **2005,** *127*, 10496-10497.

(23) Balakrishnan, K.; Datar, A.; Naddo, T.; Huang, J.; Oitker, R.; Yen, M.; Zhao, J.; Zang, L. Effect of Side-Chain Substituents on Self-Assembly of Perylene Diimide Molecules: Morphology Control. *J. Am. Chem. Soc.* **2006,** *128*, 7390-7398.

(24) Datar, A.; Balakrishnan, K.; Zang, L. One-Dimensional Self-Assembly of a Water Soluble Perylene Diimide Molecule by pH Triggered Hydrogelation. *Chem. Commun.* **2013,** *49*, 6894-6896.

(25) Che, Y.; Datar, A.; Balakrishnan, K.; Zang, L. Ultralong Nanobelts Self-Assembled from an Asymmetric Perylene Tetracarboxylic Diimide. *J. Am. Chem. Soc.* **2007,** *129*, 7234-7235.

(26) Klein, G. C.; Kim, S.; Rodgers, R. P.; Marshall, A. G.; Yen, A.; Asomaning, S. Mass Spectral Analysis of Asphaltenes. I. Compositional Differences between Pressure-Drop and Solvent-Drop Asphaltenes Determined by Electrospray Ionization Fourier Transform Ion Cyclotron Resonance Mass Spectrometry. *Energy Fuels* **2006,** *20*, 1965-1972.

(27) Klein, G. C.; Kim, S.; Rodgers, R. P.; Marshall, A. G.; Yen, A. Mass Spectral Analysis of Asphaltenes. II. Detailed Compositional Comparison of Asphaltenes Deposit to Its Crude Oil Counterpart for Two Geographically Different Crude Oils by ESI FT-ICR MS. *Energy Fuels* **2006,** *20*, 1973-1979.

(28) Ryan, D. M.; Doran, T. M.; Nilsson, B. L. Complementary π− π Interactions Induce Multicomponent Coassembly into Functional Fibrils. *Langmuir* **2011,** *27*, 11145-11156.

(29) Sakai, H.; Watanabe, K.; Asanomi, Y.; Kobayashi, Y.; Chuman, Y.; Shi, L.; Masuda, T.; Wyttenbach, T.; Bowers, M. T.; Uosaki, K. Formation of Functionalized Nanowires by Control of Self-Assembly Using Multiple Modified Amyloid Peptides. *Adv. Funct. Mater.* **2013,** *23*, 4881-4887.

(30) Bu, L.; Pentzer, E.; Bokel, F. A.; Emrick, T.; Hayward, R. C. Growth of Polythiophene/Perylene Tetracarboxydiimide Donor/Acceptor Shish-Kebab Nanostructures by Coupled Crystal Modification. *ACS Nano* **2012,** *6*, 10924-10929.

(31) Bu, L.; Dawson, T. J.; Hayward, R. C. Tailoring Ultrasound-Induced Growth of Perylene Diimide Nanowire Crystals from Solution by Modification with Poly (3-hexyl thiophene). *ACS Nano* **2015,** *9*, 1878-1885.

(32) Zhang, S.; Sun, L. L.; Xu, J.; Wu, H.; Wen, H. Aggregate Structure in Heavy Crude Oil: Using a Dissipative Particle Dynamics Based Mesoscale Platform. *Energy Fuels* **2010,** *24*, 4312-4326.

(33) Zhang, S.; Xu, J.; Wen, H.; Bhattacharjee, S. Integration of Rotational Algorithms into Dissipative Particle Dynamics: Modeling Polyaromatic Hydrocarbons on the Meso-Scale. *Mol. Phys.* **2011,** *109*, 1873-1888.

(34) Zhang, L.; Greenfield, M. L. Molecular Orientation in Model Asphalts using Molecular Simulation. *Energy Fuels* **2007,** *21*, 1102-1111.

(35) Ortega-Rodriguez, A.; Lira-Galeana, C.; Ruiz-Morales, Y.; Cruz, S. A. Interaction Energy in Maya-Oil Asphaltenes: A Molecular Mechanics Study. *Petrol. Sci. Technol.* **2001,** *19*, 245-256.

(36) Takanohashi, T.; Sato, S.; Saito, I.; Tanaka, R. Molecular Dynamics Simulation of the Heat-Induced Relaxation of Asphaltene Aggregates. *Energy Fuels* **2003,** *17*, 135-139.

(37) Aguilera-Mercado, B.; Herdes, C.; Murgich, J.; Müller, E. Mesoscopic Simulation of Aggregation of Asphaltene and Resin Molecules in Crude Oils. *Energy Fuels* **2006,** *20*, 327-338.

(38) Ortega-Rodríguez, A.; Cruz, S. A.; Gil-Villegas, A.; Guevara-Rodriguez, F.; Lira-Galeana, C. Molecular View of the Asphaltene Aggregation Behavior in Asphaltene-Resin Mixtures. *Energy Fuels* **2003,** *17*, 1100-1108.

(39) Oostenbrink, C.; Villa, A.; Mark, A. E.; Van Gunsteren, W. F. A Biomolecular Force Field Based on the Free Enthalpy of Hydration and Solvation: The GROMOS Force-Field Parameter Sets 53A5 and 53A6. *J. Comput. Chem.* **2004,** *25*, 1656-1676.

(40) Jian, C.; Tang, T.; Bhattacharjee, S. A Dimension Map for Molecular Aggregates. *J. Mol. Graphics Modell.* **2015,** *58*, 10-15.

(41) Hess, B.; Kutzner, C.; van der Spoel, D.; Lindahl, E. GROMACS 4: Algorithms for Highly Efficient, Load-Balanced, and Scalable Molecular Simulation. *J. Chem. Theory Comput.* **2008,** *4*, 435-447.

(42) van der Spoel, D.; Lindahl, E.; Hess, B.; Groenhof, G.; Mark, A. E.; Berendsen, H. J. GROMACS: Fast, Flexible, and Free. *J. Comput. Chem.* **2005,** *26*, 1701-1718.

(43) Lindahl, E.; Hess, B.; van der Spoel, D. GROMACS 3.0: A Package for Molecular Simulation and Trajectory Analysis. *J. Mol. Model.* **2001**, *7*, 306-317.

(44) Berendsen, H. J.; van der Spoel, D.; van Drunen, R. GROMACS: A Message-Passing Parallel Molecular Dynamics Implementation. *Comput. Phys. Commun.* **1995,** *91*, 43-56.

(45) Essmann, U.; Perera, L.; Berkowitz, M. L.; Darden, T.; Lee, H.; Pedersen, L. G. A Smooth Particle Mesh Ewald Method. *J. Chem. Phys.* **1995,** *103*, 8577.

(46) Hess, B. P-LINCS: A Parallel Linear Constraint Solver for Molecular Simulation. *J. Chem.*

Theory Comput. **2008,** *4*, 116-122.

(47) Sugita, Y.; Okamoto, Y. Replica-Exchange Molecular Dynamics Method for Protein Folding. *Chem. Phys. Lett.* **1999,** *314*, 141-151.

(48) Humphrey, W.; Dalke, A.; Schulten, K. VMD: Visual Molecular Dynamics. *J. Mol. Graphics* **1996,** *14*, 33-38.

(49) Sugita, Y.; Kitao, A.; Okamoto, Y. Multidimensional Replica-Exchange Method for Free Energy Calculations. *J. Chem. Phys.* **2000,** *113*, 6042-6051.

(50) Yu, T.; Schatz, G. C. Free-Energy Landscape for Peptide Amphiphile Self-Assembly: Stepwise versus Continuous Assembly Mechanisms. *J. Phys. Chem. B* **2013,** *117*, 14059-14064.

(51) Buenrostro-Gonzalez, E.; Groenzin, H.; Lira-Galeana, C.; Mullins, O. C. The Overriding Chemical Principles That Define Asphaltenes. *Energy Fuels* **2001,** *15*, 972-978.

(52) Mullins, O. C.; Sabbah, H.; Eyssautier, J.; Pomerantz, A. E.; Barre, L.; Andrews, A. B.; Ruiz-Morales, Y.; Mostowfi, F.; McFarlane, R.; Goual, L., et al. Advances in Asphaltene Science and the Yen–Mullins Model. *Energy Fuels* **2012,** *26*, 3986-4003.

(53) Mullins, O. C. The Modified Yen Model. *Energy Fuels* **2010,** *24*, 2179-2207.

(54) Mullins, O. C. The Asphaltenes. *Annu. Rev. Anal. Chem.* **2011,** *4*, 393-418.

(55) Pisula, W.; Tomovic, Z.; Simpson, C.; Kastler, M.; Pakula, T.; Müllen, K. Relationship between Core Size, Side Chain Length, and the Supramolecular Organization of Polycyclic Aromatic Hydrocarbons. *Chem. Mater.* **2005,** *17*, 4296-4303.

(56) Headen, T. F.; Boek, E. S.; Skipper, N. T. Evidence for Asphaltene Nanoaggregation in Toluene and Heptane from Molecular Dynamics Simulations. *Energy Fuels* **2009,** *23*, 1220-1229.

(57) Sedghi, M.; Goual, L.; Welch, W.; Kubelka, J. Effect of Asphaltene Structure on Association and Aggregation Using Molecular Dynamics. *J. Phys. Chem. B* **2013,** *117*, 5765-5776.

(58) Speight, J. G.; Long, R. B.; Trowbridge, T. D. Factors Influencing the Separation of Asphaltenes from Heavy Petroleum Feedstocks. *Fuel* **1984,** *63*, 616-620.

Chapter 7: A Dimension Map for Molecular Aggregates*

Aggregation of molecules is a universal phenomenon which occurs in many processes. For instance, proteins or peptides are associated together to form fibrils in a number of human diseases; phospholipid molecules in water can spontaneously aggregate into bilayer membranes; organic molecules possessing PA cores, such as perylene tetracarboxylic diimide, can assemble into semiconductors of nanobelt structures in solutions; heavy aromatics in crude oil known as asphaltenes aggregate during petroleum processing.[1-5] Depending on the aggregation driving forces, various shapes can be formed, examples including spherical micelles or rod-like micelles.[6-8] These structures have been revealed by imaging techniques such as SEM, AFM, TEM, circular dichroism, NMR, small-angle neutron scattering, as well as MD simulations.[4,6-11] Many parameters have been used to define the shapes of various aggregates, such as radii of curvature employed in the work of Israelachvili et al.[12] However, most of them are difficult to obtain numerically and/or experimentally, and hence, are not widely used. On the other hand, a consistent and generalized method quantifying dimension characteristics will facilitate direct comparison among different observations, which helps not only to track the morphology variations of molecular aggregates but also gain insight into the aggregation manner and driving forces. In this chapter, we introduce a dimension map based on a pair of unitless quantities, defined from the ratios between the principal radii of gyration of the aggregated structures, as a simple way to quantify their dimension characteristics. Applications of the dimension map are demonstrated using aggregates formed by biomolecules as well as PA compounds in water and organic solvents, obtained from MD simulations. Its potential use in experimental studies, such

*A version of this chapter has been published. Reprinted from J. *Mol. Graphics Modell. 58*, Jian, C.; Tang, T.; Bhattacharjee, S. A dimension map for molecular aggregates, 10-15.

as microscopic analysis of molecular aggregates, is discussed.

Seven different compounds selected from the categories of peptides, lipids and PA compounds were simulated using MD. Their chemical structures are shown in Figure 7.1. Tetra-peptide (TYR-TYR-TYR-TYR, TYR-4; Figure 7.1a) was selected as a representative for peptide. Dodecylphosphocholine (DPC; Figure 7.1b) and dipalmitoylphosphatidylcholine (DPPC; Figure 7.1c) were chosen as representatives for single- and double-chained lipids, respectively. Peptides and lipids are known to aggregate in aqueous environment;[1,2] hence they were simulated in water. PA compounds are often used as surrogates in petroleum engineering for probing the aggregation behaviors of asphaltenes,[13] which are defined as toluene soluble but n-heptane insoluble heavy aromatic compounds.[14-17] Four PA models, developed from VO-78,[18,19] were employed in the MD simulations. These four models have the same PA core but differ by the length of their aliphatic side chains. Based on the number of interconnected aliphatic hydrocarbons on each chain, the four models are respectively referred to as VO-4C (Figure 7.1d), VO-8C (Figure 7.1e), VO-12C (Figure 7.1f) and VO-16C (Figure 7.1g). Three solvents (water, toluene and n-heptane) were used in their MD simulations. In total, 15 systems were studied, all of which were simulated using GROMACS 4.0.7[20-23] based on the GROMOS96 force field parameter set 53A6.[24] Each system was subjected to an NPT simulation of length varying from 30 to 180 ns. Details on the MD simulations are available in Appendix E, section E.1.

Figure 7.2 shows snapshots of selected aggregated structures obtained at the equilibrium stage of the simulations. The achievement of dynamic equilibrium is demonstrated in Appendix E, section E.2. It can be clearly seen that these aggregates exhibit different geometries. For example, the stacked PA cores of VO-8C in n-heptane (Figure 7.2f) form a nearly 1D structure

not observed in other subfigures. In order to quantitatively describe the dimension of each aggregate, we define a pair of unitless quantities called gyradius ratios, based on the principal radii of gyration (gyradii).[25,26] Specifically, for an aggregate we denote the three principal axes that pass through its center of mass as x, y, z and the three principal mass moments of inertia as I_{xx}, I_{yy}, I_{zz}. The detailed procedure of determining the principal mass moments of

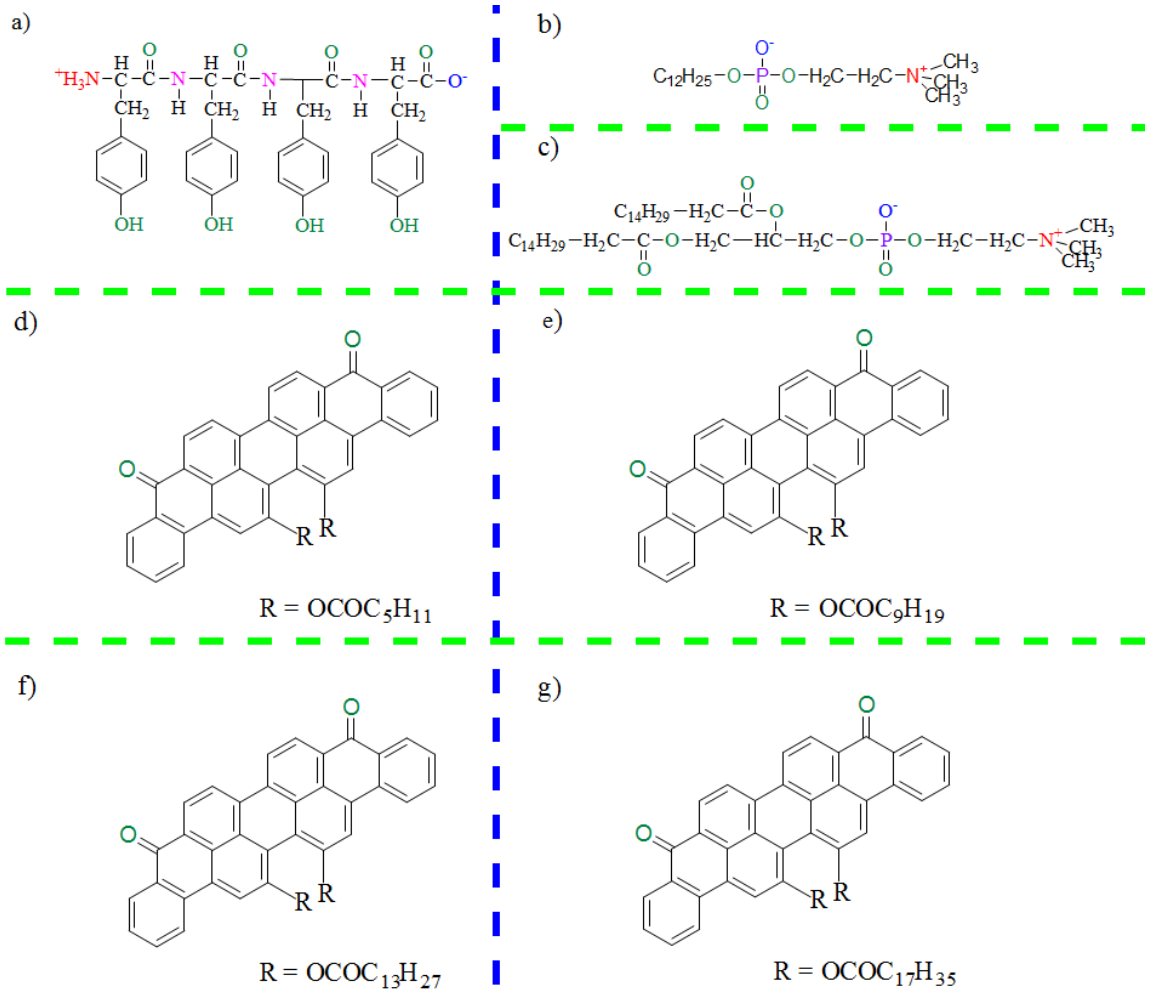

Figure 7.1: Molecular structures employed in this study: (a) TYR-4, (b) DPC, (c) DPPC, (d) VO-4C, (e) VO-8C, (f) VO-12C and (g) VO-16C.

inertia and principal axes are available in Appendix E, section E.3. The principal radii of gyration are defined by:[27-29]

$$R_x = \left(\frac{I_{xx}}{\sum_i m_i}\right)^{0.5} = \left(\frac{\sum_i m_i(y_i^2+z_i^2)}{\sum_i m_i}\right)^{0.5}, \quad (7.1)$$

$$R_y = \left(\frac{I_{yy}}{\sum_i m_i}\right)^{0.5} = \left(\frac{\sum_i m_i(x_i^2+z_i^2)}{\sum_i m_i}\right)^{0.5}, \quad (7.2)$$

$$R_z = \left(\frac{I_{zz}}{\sum_i m_i}\right)^{0.5} = \left(\frac{\sum_i m_i(x_i^2+y_i^2)}{\sum_i m_i}\right)^{0.5}, \quad (7.3)$$

where m_i and (x_i, y_i, z_i) are respectively the mass and coordinates for atom i and the summations are over all atoms in a given aggregate. One can always denote R_0 as the minimum of $\{R_x, R_y, R_z\}$, R_2 as the maximum of $\{R_x, R_y, R_z\}$, and R_1 as the intermediate value among $\{R_x, R_y, R_z\}$. The gyradius ratios r_1 and r_2 are then defined as:

$$r_1 = \frac{R_1}{R_0}, r_2 = \frac{R_2}{R_0}. \quad (7.4)$$

Clearly $r_1 \leq r_2$. Furthermore, it can be shown that for any structure, $1 \leq r_1 \leq r_2 \leq \sqrt{1+{r_1}^2}$ (see Appendix E, section E.4). Therefore, if we generate a dimension map with r_1 and r_2 being the horizontal and vertical axes respectively (Figure 7.3), any one aggregate will correspond to a point on this map, and all the points will be bounded by two curves of $r_2 = r_1$ and $r_2 = \sqrt{1+{r_1}^2}$. These two curves are plotted as black dashed lines in Figure 7.3. As r_1 increases, the two curves will approach each other, and eventually become indistinguishable when $r_1 \gg 1$. We now examine the gyradius ratios of the aggregates formed in our MD simulations and their locations on this dimension map

Examples of final aggregated structures formed by TYR-4 and DPC are shown in Figures 7.2a and b, respectively. In each system, the molecules formed 2 aggregates (one shown in Figure 7.2) and each aggregate is more or less isotropic, with approximately equal dimensions in all directions. The gyradius ratios (r_1, r_2) for these aggregates are depicted in Figure 7.3 as purple diamonds and purple plus signs, respectively for TYR-4 and DPC. All data points are

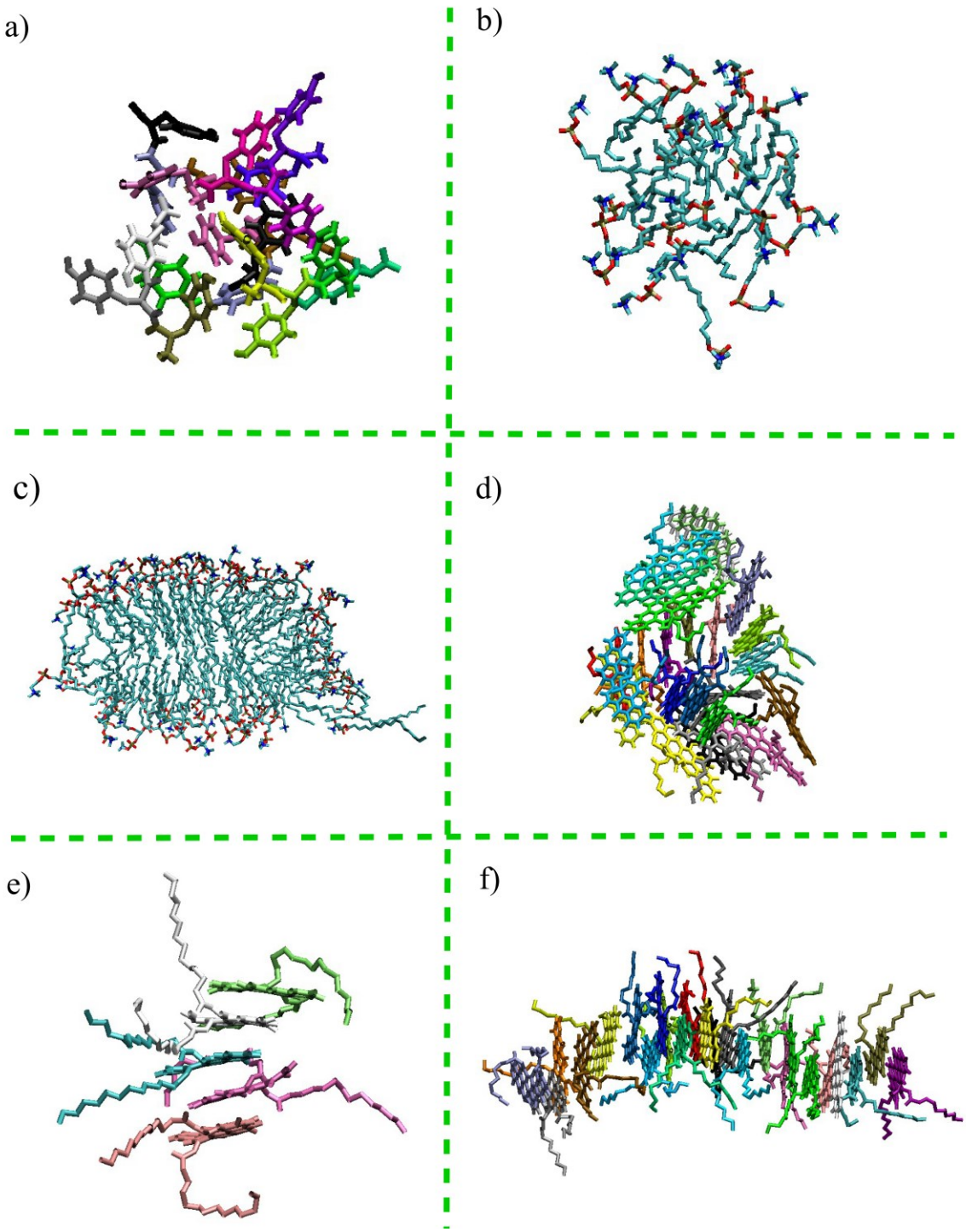

Figure 7.2: Snapshots of the final aggregates formed by: (a) TYR-4 in water, (b) DPC in water, (c) DPPC in water, (d) VO-4C in water, (e) VO-12C in toluene and (f) VO-8C in *n*-heptane. In all subfigures, solvent molecules are removed for clarity.

located in the lower left region of the dimension map and near the boundary line of $r_2 = r_1$. This corresponds to a geometry which has approximately equal principal axes and resembles a three-dimensional sphere-like structure. In the system of DPPC, on the other hand, a single bilayer structure was formed (Figure 7.2c) where the tail groups (colored cyan) are sandwiched between the head groups (colored red and blue). The point for the corresponding gyradius ratios, depicted by purple filled circle in Figure 7.3, is well distinguished from those of DPC aggregates (See more discussion on DPPC in Appendix E, section E.5) and lies in a region where some data of the PA compounds are located, as discussed below.

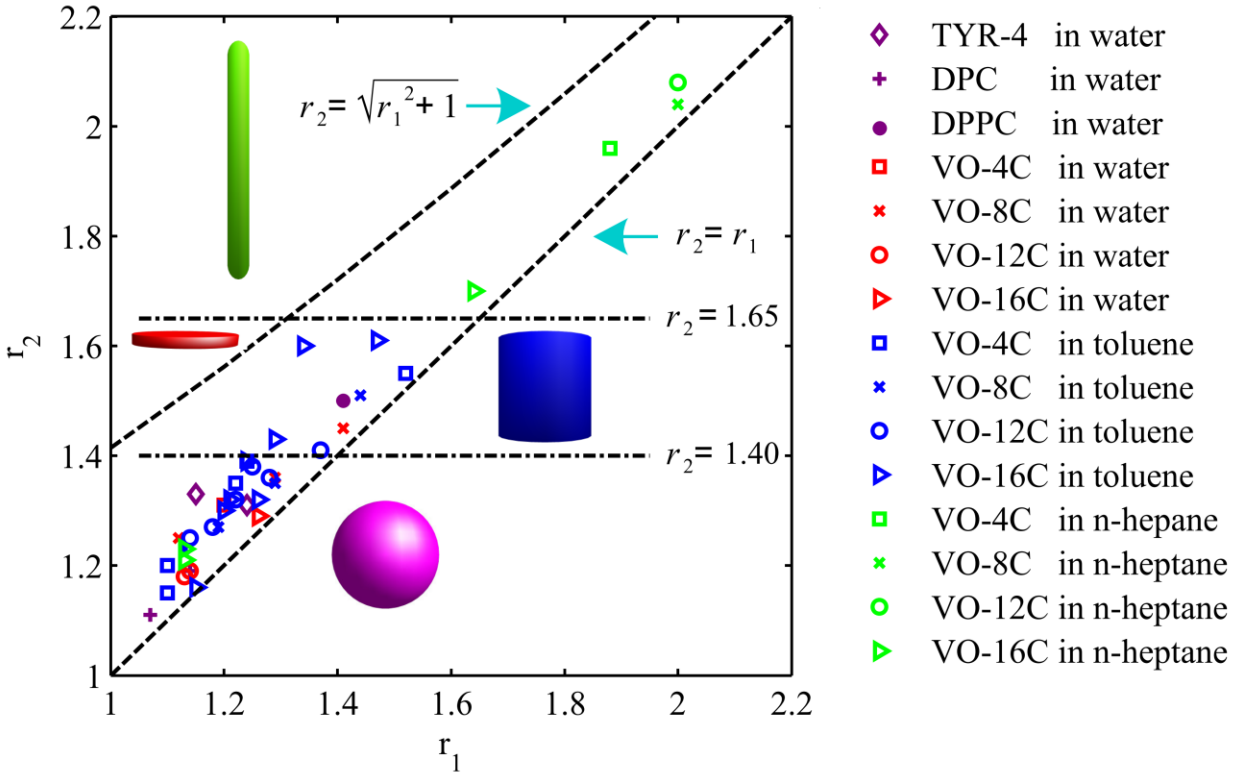

Figure 7.3: Dimension map for the aggregates formed in the MD simulations.

Selected final aggregated structures for PA compounds in water, toluene and *n*-heptane are shown in Figures 7.2d, e and f, respectively. Inside each system, more than one aggregate may be formed. Only one aggregate is shown in Figure 7.2 as a representative structure, whereas

in Figure 7.3 all the aggregates formed are represented by individual symbols. Because each PA molecule consists of a PA planar region, the PA cores from two molecules can stack in a parallel fashion due to the $\pi - \pi$ interaction between them.[30-32] For PA molecules in water (Figure 7.2d), while some PA core stacking is observed, most molecules are simply entangled together, without a clearly preferred orientation in the aggregate. The final structure shares some similarities with the aggregates formed by TYR-4 and DPC and is close to a three-dimensional sphere. This is reflected in Figure 7.3 where almost all the data for PA aggregates in water are located in the lower left region of the dimension map and near the boundary line of $r_2 = r_1$. Unlike in water, for PA molecules in n-heptane (Figure 7.2f), the majority of the aggregates consist of many molecules with their PA cores parallel stacked in interior and side chains solvated in exterior. The parallel stacking persists for a long distance, much larger than the length scale of each PA molecule. As a result, a nearly 1D rod-like structure is formed. Accordingly in Figure 7.3, the gyradius ratios for PA aggregates in n-heptane are mostly located in the upper right region of the dimension map. In this region, the difference between the two boundary curves becomes smaller; r_1 and r_2 are of similar magnitude and are much greater than one, which is exactly the characteristic of a 1D rod-like structure. The location of the PA aggregates in toluene on the dimension map is more puzzling. From Figure 7.2e, the aggregate clearly exhibits different characteristics compared with Figure 7.2d in water and Figure 7.2f in n-heptane: unlike the random entanglement in water, the PA cores form ordered one-on-one stacking in toluene, but compared with in n-heptane the parallel stacking persists for a much shorter distance. Similar structural arrangements as seen in Figure 7.2e were observed for all aggregates formed by PA compounds in toluene. On the other hand, their corresponding gyradius ratios on the dimension

map are distributed in a range: some located in the lower left region, while others located in the middle region with moderate r_1 and r_2 values.

To further investigate this, we first divide the dimension map into three regions, each representing a particular group of structures:

(I) $r_2 \geq 1.65$, which represents 1D rod-like structures (length of rod much larger than the diameter).

(II)$1.40 < r_2 < 1.65$, which represents short-cylinder-like structures (when the data are near the lower boundary of $r_2 = r_1$, length of rod comparable to the diameter) or two-dimensional planar structures (when the data are near the upper boundary of $r_2 = \sqrt{1 + {r_1}^2}$).

(III) $r_2 \leq 1.40$, which represents three-dimensional sphere-like structures.

The boundary lines of $r_2 = 1.40$ and $r_2 = 1.65$ were chosen based on the natural gaps found on the dimension map. Using PA compounds as an example, for each simulated system, we calculated the percentages of molecules that participated in each type of structure and summarized them in Table 7.1. For instance, for VO-16C in n-heptane, the formed type (I) aggregate involves 16 molecules, resulting in a percentage of 16/24 = 66.67%. It can be clearly seen that in water, sphere-like structures dominate, with 100% for VO-4C, VO-12C and VO-16C, and near 80% for VO-8C. In n-heptane, rod-like structures are of the largest percentage,

Table 7.1: Percentage of Molecules That Participated in Each Type of Aggregated Structures of PA Compounds in Different Solvents

criteria	$r_2 \geq 1.65$ (type I)			$1.40 < r_2 < 1.65$ (type II)			$r_2 \leq 1.40$ (type III)		
solvent	water	toluene	n-heptane	water	toluene	n-heptane	water	toluene	n-heptane
VO-4C			100%		29.17%		100%	70.83%	
VO-8C			100%	20.83%	43.48%		79.17%	56.52%	
VO-12C			100%		30.43%		100%	69.57%	
VO-16C			66.77%		25%		100%	75%	33.33%

with 100% for VO-4C, VO-8C and VO-12C, and close to 70% for VO-16C. In toluene, both type (II) and type (III) structures are found for all the four types of PA molecular models.

With the above calculation, we now re-examine the location of the PA aggregates in toluene on the dimension map. While type (III) aggregates are dominant for PA aggregates in both toluene and water, compared with in water where type (II) aggregates are only formed by VO-8C molecules, all the four PA compounds can form type (II) structures in toluene. In fact, if individual dimension maps are generated for VO-4C, VO-12C and VO-16C (see Appendix E, Figure E.2), the data associated with different solvents (water, toluene and n-heptane) can be easily distinguished on each map. This allows us to infer that the molecular arrangements in the PA aggregates should be different in the two different solvents (water and toluene). In addition, while for PA compounds with shorter side chains, their type (II) aggregates in toluene are all located close to the $r_2 = r_1$ curve, type (II) aggregates formed by VO-16C in toluene have shown the trend of moving towards the $r_2 = \sqrt{1 + {r_1}^2}$ boundary, which represents planar structures. If the PA molecules in toluene tend to form disordered aggregates like those in water through random entanglement of PA cores and side chains, such planar structures cannot be formed. Therefore one may suspect that, regardless of the side chain length, an ordered stacking structure of PA cores is formed for each aggregate in toluene with the side chains fully solvated. The stacking of the PA cores tends to promote the formation of a cylindrical structure, while the solvation and flexibility of side chains can make the overall geometry of an aggregate close to a sphere, if the stacking does not persist for a long distance as in n-heptane. These two competing factors are the reason why both type (II) and type (III) structures are present in toluene. In addition, if the side-chain length is so long that it exceeds the range of stacking in the aggregates, the dimension in the plane perpendicular to the stacking direction will be large enough to make

the aggregate resemble a planar structure; such a trend is observed for VO-16C. The aggregation manner inferred from the dimension map is consistent with previous visual observation in Figure 7.2, and can be further verified by plotting the gyradius ratios generated using the PA cores on the same dimension map (see Appendix E, section E.7).

What structure will be formed when certain molecules aggregate in a given solvent is related to the solubility of the molecules. For example, the PA aggregates in toluene (type (III) and type (II) structures) differ from those in n-heptane (mainly type (I) structure) by the range of stacking. The smaller distance over which stacking persists in toluene indicates better solubility of PA compounds in toluene, which is consistent with the fact for the same total number (24) of PA molecules simulated, toluene gives rise to the most number of aggregates (number of data points on the dimension map; see Figure 7.3) among the three solvents, and consistent with the definition of asphaltenes these PA compounds represent.[14-17] The structure of the aggregates is ultimately determined by the interaction between solutes, as well as the interaction between solute and solvent. Quantification and comparison of dimensional characteristics of the aggregates based on the dimension map helps us understand such interactions and hence the mechanisms of aggregation. For example, DPC molecules aggregate in water due to the hydrophobic interaction among them. The hydrophobic tails (depicted by cyan colors in Figure 7.2b) tend to associate together to minimize their contact with water while exposing the hydrophilic head groups (depicted by red and blue colors in Figure 7.2b) to water.[33] The sphere-like structure formed from the aggregation is consistent with such interaction. It is well-known that the shape of the aggregates formed by lipids depends on their molecular structure:[33] while single-chained lipids tend to form spherical micelles, double-chained lipids tend to form bilayer structures due to their large hydrocarbon volume. This is evident from the simulation and

dimension map. For PA compounds in toluene, the progression of aggregates from type (III) into type (II) and the trend of forming planar structures by VO-16C has allowed us to conclude that ordered short-ranged stacking is formed in toluene, which suggests that the main driving force for aggregation of PA compounds in toluene is the $\pi - \pi$ stacking between PA cores.[34] In comparison, the much larger range of stacking observed for PA compounds in n-heptane suggests that much greater solvent-solute attraction exists for the same PA molecules in toluene.[34,35] Almost all the aggregates formed by PA compounds in water are sphere-like. This indicates that $\pi - \pi$ stacking between PA cores is not the only mechanism driving aggregation in water. In fact, the hydrophobic associations among the aliphatic side chains played an important role in causing the aggregation, prohibiting the formation of ordered stacking structures.[18] Particularly, for VO-8C which has intermediate side-chain length, the decreased $\pi - \pi$ stacking and the insufficient hydrophobic association has led to the smallest percentage of sphere-like structure in water among all the PA compounds. Additionally, despite the very different size and molecular structure TYR-4, DPC and PA molecules have, their aggregates in water are located in the same region on the dimension map, suggesting that hydrophobic interaction as a common critical driving force in their aggregation.

Apart from its applications in MD studies, the dimension map proposed here can also be used for experimental structure characterization. For instance, in determining the size and shape of gas phase molecules, the three principal mass moments of inertial for a molecule can be obtained by spectroscopic measurements in the microwave region,[36] and according to their relationships, molecular shapes have been roughly classified into linear, symmetric top, spherical top and asymmetric top categories.[37] Since the gyradius ratios can be directly calculated from the principal mass moments of inertia, these molecules can be easily located onto the dimension

map, which helps to quantitatively compare molecular structures and further understand the structure-function relationship. Mathematically, gyradius ratios introduced in this chapter share some similarities with the asphericity defined for studying the shape of polymers,[38] which is also derived based on the principal moments of inertia. On the other hand, asphericity only describes the deviation of a geometry shape from spherical symmetry, while our dimension map further provides a more complete way to directly differentiate geometries. More importantly, adopting image analysis method described in the work by Maurstad et al.,[39] principal moments of inertia for molecular aggregates can be obtained from AFM topographs. Hence, gyradius ratios can be easily calculated to generate a comprehensive dimension map, where the direct morphology comparison between numerical simulations and experiments can be made to shed lights on understanding the aggregation process. Furthermore, accurate knowledge of the aggregates' geometries and hence the associated molecular aggregation manner can help us infer the chemical structures of aggregated molecules. For instance, in the petroleum field atomic structures of large asphalt compounds are often under debate.[5] By measuring the geometries of their aggregates in different solvents and locating them on the dimension map, their solubility behavior, potential aggregation driving forces and interaction with different solvents can be determined, which can provide new insight into their chemical structures.

In conclusion, we introduce a simple but effective way to quantify the geometry of molecular aggregates often seen in biology as well as in industrial complex fluids. A dimension map is generated based on a pair of unitless numbers named gyradius ratios. Aggregated structures can be categorized into different groups according to the locations of their gyradius ratios on the dimension map. Examining the location of the aggregates on the dimension map and how the location changes with solvent type and solute material parameter can help us infer

the aggregation manner and understand mechanisms driving aggregation in a given solvent, and it can be applied to both simulations and experiments. It should be noted that we focus on providing quantification for structures resulting from molecular aggregation of soft condensed matter, which typically do not have unusual geometries such as sharp corners. Description of all geometries (particularly crystalline structures) that can exist mathematically is out of the scope of this chapter.

Bibliography

(1) Wu, C.; Lei, H.; Duan, Y. Elongation of Ordered Peptide Aggregate of an Amyloidogenic Hexapeptide NFGAIL Observed in Molecular Dynamics Simulations with Explicit Solvent. *J. Am. Chem. Soc.* **2005,** *127*, 13530-13537.

(2) Marrink, S. J.; Lindahl, E.; Edholm, O.; Mark, A. E. Simulation of the Spontaneous Aggregation of Phospholipids into Bilayers. *J. Am. Chem. Soc.* **2001,** *123*, 8638-8639.

(3) Balakrishnan, K.; Datar, A.; Oitker, R.; Chen, H.; Zuo, J.; Zang, L. Nanobelt Self-Assembly from an Organic n-Type Semiconductor: Propoxyethyl-PTCDI. *J. Am. Chem. Soc.* **2005,** *127*, 10496-10497.

(4) Balakrishnan, K.; Datar, A.; Naddo, T.; Huang, J.; Oitker, R.; Yen, M.; Zhao, J.; Zang, L. Effect of Side-Chain Substituents on Self-Assembly of Perylene Diimide Molecules: Morphology Control. *J. Am. Chem. Soc.* **2006,** *128*, 7390-7398.

(5) Speight, J. G. *The Chemistry and Technology of Petroleum,* 4th ed.; CRC Press: Boca Raton, 2006.

(6) Sangwai, A. V.; Sureshkumar, R. Coarse-Grained Molecular Dynamics Simulations of the Sphere to Rod Transition in Surfactant Micelles. *Langmuir* **2011,** *27*, 6628-6638.

(7) Velinova, M.; Sengupta, D.; Tadjer, A. V.; Marrink, S. Sphere-to-Rod Transitions of Nonionic Surfactant Micelles in Aqueous Solution Modeled by Molecular Dynamics

Simulations. *Langmuir* **2011,** *27*, 14071-14077.

(8) Liu, Z.; Shang, Y.; Feng, J.; Peng, C.; Liu, H.; Hu, Y. Effect of Hydrophilicity or Hydrophobicity of Polyelectrolyte on the Interaction between Polyelectrolyte and Surfactants: Molecular Dynamics Simulations. *J. Phys. Chem. B* **2012,** *116*, 5516-5526.

(9) Benjwal, S.; Verma, S.; Röhm, K.; Gursky, O. Monitoring Protein Aggregation during Thermal Unfolding in Circular Dichroism Experiments. *Protein Sci.* **2006,** *15*, 635-639.

(10) Törnblom, M.; Henriksson, U. Effect of Solubilization of Aliphatic Hydrocarbons on Size and Shape of Rodlike C_{16}TABr Micelles Studied by ^{2}H NMR Relaxation. *J. Phys. Chem. B* **1997,** *101*, 6028-6035.

(11) Porte, G.; Marignan, J.; Bassereau, P.; May, R. Shape Transformations of the Aggregates in Dilute Surfactant Solutions : A Small-Angle Neutron Scattering Study. *J. Phys.* **1988,** *49*, 511-519.

(12) Israelachvili, J. N.; Mitchell, D. J.; Ninham, B. W. Theory of Self-Assembly of Hydrocarbon Amphiphiles into Micelles and Bilayers. *J. Chem. Soc., Faraday Trans.2* **1976,** *72*, 1525-1568.

(13) Breure, B.; Subramanian, D.; Leys, J.; Peters, C. J.; Anisimov, M. A. Modeling Asphaltene Aggregation with a Single Compound. *Energy Fuels* **2012,** *27*, 172-176.

(14) Speight, J. G.; Long, R. B.; Trowbridge, T. D. Factors Influencing the Separation of Asphaltenes from Heavy Petroleum Feedstocks. *Fuel* **1984,** *63*, 616-620.

(15) Groenzin, H.; Mullins, O. C. Asphaltene Molecular Size and Structure. *J. Phys. Chem. A* **1999,** *103*, 11237-11245.

(16) Yarranton, H. W.; Alboudwarej, H.; Jakher, R. Investigation of Asphaltene Association

with Vapor Pressure Osmometry and Interfacial Tension Measurements. *Ind. Eng. Chem. Res.* **2000,** *39*, 2916-2924.

(17) Headen, T. F.; Boek, E. S.; Skipper, N. T. Evidence for Asphaltene Nanoaggregation in Toluene and Heptane from Molecular Dynamics Simulations. *Energy Fuels* **2009,** *23*, 1220-1229.

(18) Jian, C.; Tang, T.; Bhattacharjee, S. Probing the Effect of Side-Chain Length on the Aggregation of a Model Asphaltene Using Molecular Dynamics Simulations. *Energy Fuels* **2013,** *27*, 2057-2067.

(19) Andrews, A. B.; McClelland, A.; Korkeila, O.; Demidov, A.; Krummel, A.; Mullins, O. C.; Chen, Z. Molecular Orientation of Asphaltenes and PAH Model Compounds in Langmuir−Blodgett Films Using Sum Frequency Generation Spectroscopy. *Langmuir* **2011,** *27*, 6049-6058.

(20) Hess, B.; Kutzner, C.; van der Spoel, D.; Lindahl, E. GROMACS 4: Algorithms for Highly Efficient, Load-Balanced, and Scalable Molecular Simulation *J. Chem. Theory Comput.* **2008,** *4*, 435-447.

(21) van der Spoel, D.; Lindahl, E.; Hess, B.; Groenhof, G.; Mark, A. E.; Berendsen, H. J. GROMACS: Fast, Flexible, and Free. *J. Comput. Chem.* **2005,** *26*, 1701-1718.

(22) Lindahl, E.; Hess, B.; van der Spoel, D. GROMACS 3.0: A Package for Molecular Simulation and Trajectory Analysis. *Mol. Model.* **2001,** *7*, 306-317.

(23) Berendsen, H. J.; van der Spoel, D.; van Drunen, R. GROMACS: A Message-Passing Parallel Molecular Dynamics Implementation. *Comput. Phys. Commun.* **1995,** *91*, 43-56.

(24) Oostenbrink, C.; Villa, A.; Mark, A. E.; Van Gunsteren, W. F. A Biomolecular Force Field Based on the Free Enthalpy of Hydration and Solvation: The GROMOS Force-Field Parameter Sets 53A5 and 53A6. *J. Comput. Chem.* **2004,** *25*, 1656-1676.

(25) Rigo, P. Roll Motion of a Floating Storm Surge Barrier. *J. Hydrosci. Hydr. Eng.* **1992,** *10*, 27-36.

(26) Allen III, J. H. *Mechanics of Materials for Dummies;* Wiley Publishing, Inc.: Hoboken, 2011.

(27) Meriam, J. L.; Kraige, L. G. *Engineering Mechanics: Dynamics,* 6th ed.; John Wiley & Sons Inc.: New York 2007.

(28) Wittenburg, J. *Dynamics of Multibody Systems;* Springer: Berlin, 2007.

(29) Pytel, A.; Kiusalaas, J. *Engineering Mechanics: Dynamics,* 3rd ed.; Cengage Learning: Stamford, 2010.

(30) Dickie, J. P.; Yen, T. F. Macrostructures of the Asphaltic Fractions by Various Instrumental Methods. *Anal. Chem.* **1967,** *39*, 1847-1852.

(31) Yen, T. Structure of Petroleum Asphaltene and Its Significance. *Energy Sources* **1974,** *1*, 447-463.

(32) Murgich, J. Intermolecular Forces in Aggregates Of Asphaltenes and Resins. *Pet. Sci. Technol.* **2002,** *20*, 983-997.

(33) Israelachvili, J. N. *Intermolecular and Surface Forces;* Academic Press: San Diego, CA, 2011.

(34) Jian, C.; Tang, T.; Bhattacharjee, S. Molecular Dynamics Investigation on the Aggregation of Violanthrone78-Based Model Asphaltenes in Toluene. *Energy Fuels* **2014,** *28*, 3604-3613.

(35) Jian, C.; Tang, T. One-Dimensional Self-Assembly of Polyaromatic Compounds Revealed by Molecular Dynamics Simulations. *J. Phys. Chem. B* **2014,** *118,* 12772–12780.

(36) Kraitchman, J. Determination of Molecular Structure from Microwave Spectroscopic Data. *Am. J. Phys.* **1953,** *21*, 17-25.

(37) Gupta, M. C. *Atomic and Molecular Spectroscopy;* New Age International (P) Ltd.: New Delhi, 2007.

(38) Rudnick, J.; Gaspari, G. The Asphericity of Random Walks. *J. Phys. A: Math. Gen.* **1986,** *19*, L191-L193.

(39) Maurstad, G.; Danielsen, S.; Stokke, B. T. Analysis of Compacted Semiflexible Polyanions Visualized by Atomic Force Microscopy: Influence of Chain Stiffness on the Morphologies of Polyelectrolyte Complexes. *J. Phys. Chem. B* **2003,** *107*, 8172-8180.

Chapter 8: Conclusions and Future Perspectives

8.1. Conclusions

Motivated from the serious problems encountered in petroleum processing, a series of MD simulations were performed in this dissertation to investigate the aggregation behaviors of model PA compounds in water and organic solvents. Through these studies, the effect of solvents, side-chain length of PA compounds, and the inhomogeneity in solutes on the aggregated structures and aggregation mechanisms of these representative PA compounds were clarified from atomic level.

As the first step, we developed a series of molecular models based on VO-78, which are of the same PA cores but possess systematically varied side chains. Following this, Chapters 3-5 investigated the aggregation behaviors of a single type of PA compound in water, toluene and n-heptane. Our results revealed that aggregates of distinct sizes, stabilities and geometry characteristics were formed in different solvents: large stable spherical aggregates were formed in water while 1D structures mainly of parallel stacked PA cores were only observed in n-heptane. In toluene, the majority of the aggregates were small with the stacked PA cores resembling the shape of short cylinders, and the size of these aggregates fluctuated to the largest extent among the three solvents. The effect of side-chain length on the aggregation was also found to be greatly dependent on the solvent property. While long side chains interfered with the π-π stacking of PA cores, there is a non-monotonic relation between side-chain lengths and the degree of aggregation in water. That is, PA molecules with very long or very short side chains could fully aggregate but those with intermediate side chains could not. Contrarily, in toluene and n-heptane, side-chain length was shown to have little effect on the aggregation extent.

Regardless of the solvents and side-chain lengths, the most favorable configurations formed by two neighboring PA molecules were the parallel stacking of their PA cores.

What aggregated structure will be formed depends on the aggregation mechanism. The preference of parallel stacking between neighboring PA cores in the three solvents confirms the importance of $\pi - \pi$ interaction for the aggregation. However, the sphere-like aggregate formed in water, as well as the non-monotonic relation between side-chain lengths and the degree of aggregation, indicates that $\pi - \pi$ stacking between PA cores is not the only driving force in water. Indeed, the side-chain association, due to hydrophobic interaction, provides an additional mechanism for the aggregation of PA molecules in water, contributes to the much enhanced stability of the aggregates, and leads to the non-monotonic dependence of the aggregation extent on the side-chain length. Contrarily, the ordered aggregates formed in toluene and n-heptane are facilitated by the attraction between the solvents and the aliphatic regions of PA molecules, which reduced the steric hindrance of side chains and helped with stacking. Compared with n-heptane, the aromatic ring of toluene can have additional attractions with the core regions of PA molecules, thus resulting in the smallest and most unstable aggregates observed in toluene. n-Heptane, on the other hand, is completely apolar, thus leading to the formation of 1D rod-like aggregate mainly composed of parallel stacked PA cores.

As solvents demonstrated important effect on the aggregation of PA compounds, in Chapter 6, we performed additional simulations on a single type of PA compound in mixed solvents (heptol) and varied its composition. Also explored were the aggregation behaviors of a solute mixture of different types of PA compounds in toluene, n-heptane and heptol. It was found that for both kinds of solutes, the longest range of PA core stacking was achieved from systems with heptol as solvents instead of pure n-heptane. Detailed analysis on the

intermolecular interaction confirms that to achieve "perfect" stacking, the optimum solvent should simultaneously increase the interaction between PA cores of the solutes, and avoid introducing too much association between PA core and side chain as well as between side chains. More interestingly, in toluene, contrary to the short-range stacking formed by a single type of PA compound (shown in Chapter 4), a 1D rod-like structure containing many parallel stacked PA cores was formed by the mixture. In addition, while for a single type of PA compound the 1D rod-like structure could only be formed in pure n-heptane or heptol of sufficiently large n-heptane/toluene ratio, no clear dependence on the solvent was found for the existence of 1D structure from the mixture. Detailed examination on the aggregated structures formed by mixed PA compounds showed that different types of molecules tended to stack in an alternating manner, which reduced the steric hindrance of long side chains and shielded the attractive interaction between toluene and the PA cores.

To quantitatively describe the different geometries of PA molecular aggregates, we developed a dimension map in chapter 7, which can be applied in MD studies as well as experimental structure characterization. It was shown that on the dimension map, molecular aggregate data were bounded by two boundary curves, and that the map could be separated into three regions representing three groups of structures: three-dimensional sphere-like structures (e.g. aggregates shown in Chapter 3); two-dimensional planar structures or short-cylinder-like structures; and 1D rod-like structures (e.g. aggregates shown in Chapter 5). Further applications of the dimension map were demonstrated by analyzing the aggregates formed by PA compounds as well as biomolecules in solution.

The results reported here can advance our knowledge in understanding the aggregation behaviors of PA compounds from atomic level. The molecular models studied here, apart from

representing certain features of petroleum asphaltenes, possess the common characteristics of PA compounds. Therefore, it's expected that the conclusions from this dissertation can be of promising applications in many areas, where controlling and utilizing the aggregation of PA molecules is desired. For instance, the analysis performed on the formation of 1D rod-like structure in Chapters 5 and 6 can be very helpful in the design of optical and electronic nanodevices.

8.2. Future Perspectives

Based on the scope of this dissertation, the following three perspectives are suggested for future consideration:

8.2.1. Developing New PA Molecular Models

The side chains of the PA molecules employed in this dissertation are of aliphatic nature and none of the oxygen atoms present is connected to hydrogen. In practice, other polar functional groups, such as carboxylic acid and alcohol, can be attached to the aliphatic side chains. It's expected that these polar structural components can influence the aggregation activities of PA compounds. For instance, carboxylic acid functional groups may provide additional driving forces to PA aggregation through the formation of hydrogen bonding. Therefore, incorporating polar functional groups into side chains and further probing their effects with the variation of side-chain length can help with proposing novel methods to achieve certain aggregated structures, such as 1D rod-like aggregates. In addition, as reviewed in Chapter 2, chemical structures of industrial asphaltenes often contain heteroatoms, e.g. nitrogen, oxygen, and sulfur, associated with different functional groups. Hence these studies can also provide more fundamental information on understanding the solution behaviors of petroleum molecules.

8.2.2. Designing Comprehensive Simulation Systems

In Chapter 6, the "inhomogeneity" in solute was shown to enhance the stacking of PA compounds in organic solvents, where only the aliphatic side-chain length of these PA compounds was varied. It is thus anticipated that mixtures of diverse molecular structures may possess collective behaviors that is absent in a single type of compound. Furthermore, petroleum asphaltenes are a mixture of different types of molecules. Hence, studies on mixed PA molecules of other structural variations are of great importance for clarifying experimental observations on asphaltenes as well as generating novel aggregated structures as potential functional materials.

As has been demonstrated in this dissertation, solvent property is an important factor that can influence the solubility behaviors of PA compounds. While the organic solvents employed here are either of little polarity (toluene) or nonpolar (n-heptane), for PA compounds with polar functional groups, it's highly recommended to include other organic solvents of higher polarity. The polar interaction between solvents and solutes may bring in additional effects on the aggregation behaviors of PA compounds.

8.2.3. Adopting Advanced MD Techniques

Standard MD techniques were mainly adopted in this dissertation for the purpose of understanding the aggregation of PA compounds through structural analysis. With the development of computational capacities, force fields, and sophisticated numerical algorithms, advanced MD techniques can be employed to provide further information from free energy perspectives. For instance, as discussed in Chapter 6, REMD simulations can help with overcoming energy barriers encountered in standard MD simulations, thus allowing the exploration of more configurations. However in the current study of PA compounds, the temperature range used in the REMD simulations is limited, which is resulted from the fact that

small temperature difference between neighboring replicas must be adopted to ensure sufficient overlapping of potential energy. Therefore, it's expected that with the further advancement of computational technologies, large number of replicas can be simultaneously simulated for a longer time to further improve sampling and more accurately evaluate the stability of the aggregates formed by PA compounds.

Grand Unified Bibliography

(1.1) Hall, C. A.; Day Jr, J. W. Revisiting the Limits to Growth After Peak Oil. *Am. Sci.* **2009,** *97,* 230-237.

(1.2) Speight, J. G. *The Chemistry and Technology of Petroleum,* 4th ed.; CRC Press: Boca Raton, 2006.

(1.3) Hemmingsen, P.; Kim, S.; Pettersen, H. E.; Rodgers, R. P.; Sjöblom, J.; Marshall, A. G. Structural Characterization and Interfacial Behavior of Acidic Compounds Extracted from a North Sea Oil. *Energy Fuels* **2006,** *20,* 1980–1987.

(1.4) Mansoori, G. A. Modeling of Asphaltene and Other Heavy organic Depositions. *J. Pet. Sci. Eng.* **1997,** *17,* 101-111.

(1.5) Gaspar, A.; Zellermann, E.; Lababidi, S.; Reece, J.; Schrader, W. Characterization of Saturates, Aromatics, Resins, and Asphaltenes Heavy Crude Oil Fractions by Atmospheric Pressure Laser Ionization Fourier Transform Ion Cyclotron Resonance Mass Spectrometry. *Energy Fuels* **2012,** *26,* 3481-3487.

(1.6) Jewell, D.; Weber, J.; Bunger, J.; Plancher, H.; Latham, D. Ion-Exchange, Coordination, and Adsorption Chromatographic Separation of Heavy-End Petroleum Distillates. *Anal. Chem.* **1972,** *44,* 1391-1395.

(1.7) Mitchell, D. L.; Speight, J. G. The Solubility of Asphaltenes in Hydrocarbon Solvents. *Fuel* **1973,** *52,* 149-152.

(1.8) Permsukarome, P.; Chang, C.; Fogler, H. S. Kinetic Study of Asphaltene Dissolution in Amphiphile/Alkane Solutions. *Ind. Eng. Chem. Res.* **1997,** *36,* 3960-3967.

(1.9) Speight, J. G.; Long, R. B.; Trowbridge, T. D.; Linden, N. On the Definition of Asphaltenes. *Am. Chem. Soc., Div. Pet. Chem., Prepr.* **1982,** *27,* 268-275.

(1.10) Kokal, S. L.; Sayegh, S. G.Asphaltenes: The Cholesterol of Petroleum. Presented at SPE Middle East Oil Show, Manama, Bahrain, March 11−14, **1995;** Paper SPE 29787.

(1.11) Mendoza de la Cruz, José L; Argüelles-Vivas, F. J.; Matías-Pérez, V.; Durán-Valencia, Cecilia de los A; López-Ramírez, S. Asphaltene-Induced Precipitation and Deposition During Pressure Depletion on a Porous Medium: An Experimental Investigation and Modeling Approach. *Energy Fuels* **2009,** *23,* 5611-5625.

(1.12) Vafaie-Sefti, M.; Mousavi-Dehghani, S. Application of Association Theory to the Prediction of Asphaltene Deposition: Deposition due to Natural Depletion and Miscible Gas Injection Processes in Petroleum Reservoirs. *Fluid Phase Equilib.* **2006,** *247,* 182-189.

(1.13) Cosultchi, A.; Rossbach, P.; Hernández-Calderon, I. XPS Analysis of Petroleum Well Tubing Adherence. *Surf. Interface Anal.* **2003,** *35,* 239-245.

(1.14) Bartholomew, C. H. Mechanisms of Catalyst Deactivation. *Appl. Catal. A* **2001,** *212, 17-60.*

(1.15) Gawel, I.; Bociarska, D.; Biskupski, P. Effect of Asphaltenes on Hydroprocessing of Heavy Oils and Residua. *Appl. Catal. A* **2005,** *295,* 89-94.

(1.16) Park, S. J.; Ali Mansoori, G. Aggregation and Deposition of Heavy Organics in Petroleum Crudes. *Energy Sources* **1988,** *10,* 109-125.

(1.17) Andersen, S. I.; Birdi, K. S. Aggregation of Asphaltenes as Determined by Calorimetry. *J. Colloid Interface Sci.* **1991,** *142,* 497-502.

(1.18) Leon, O.; Rogel, E.; Espidel, J.; Torres, G. Asphaltenes: Structural Characterization, Self Association, and Stability Behavior. *Energy Fuels* **2000,** *14,* 6-10.

(1.19) Breure, B.; Subramanian, D.; Leys, J.; Peters, C. J.; Anisimov, M. A. Modeling Asphaltene Aggregation with a Single Compound. *Energy Fuels* **2012,** *27*, 172-176.

(1.20) Kim, F. S.; Ren, G.; Jenekhe, S. A. One-Dimensional Nanostructures of π-Conjugated Molecular Systems: Assembly, Properties, and Applications from Photovoltaics, Sensors, and Nanophotonics to Nanoelectronics. *Chem. Mater.* **2010,** *23,* 682-732

(2.1) Speight, J.; Wernick, D.; Gould, K.; Overfield, R.; Rao, B. Molecular Weight and Association of Asphaltenes: A Critical Review. *Rev. Inst. Fr. Pet.* **1985,** *40*, 51-61.

(2.2) Strausz, O. P.; Safarik, I.; Lown, E.; Morales-Izquierdo, A. A Critique of Asphaltene Fluorescence Decay and Depolarization-Based Claims about Molecular Weight and Molecular Architecture. *Energy Fuels* **2008,** *22*, 1156-1166.

(2.3) Strausz, O. P.; Mojelsky, T. W.; Faraji, F.; Lown, E. M.; Peng, P. Additional Structural Details on Athabasca Asphaltene and Their Ramifications. *Energy Fuels* **1999,** *13*, 207-227.

(2.4) Mullins, O. C.; Sabbah, H.; Eyssautier, J.; Pomerantz, A. E.; Barré, L.; Andrews, A. B.; Ruiz-Morales, Y.; Mostowfi, F.; McFarlane, R.; Goual, L. Advances in Asphaltene Science and the Yen–Mullins Model. *Energy Fuels* **2012,** *26*, 3986-4003.

(2.5) Strausz, O. P.; Mojelsky, T. W.; Lown, E. M. The Molecular Structure of Asphaltene: an Unfolding Story. *Fuel* **1992,** *71*, 1355-1363.

(2.6) Dickie, J. P.; Yen, T. F. Macrostructures of the Asphaltic Fractions by Various Instrumental Methods. *Anal. Chem.* **1967,** *39*, 1847-1852.

(2.7) Mullins, O. C. The Asphaltenes. *Annu. Rev. Anal. Chem.* **2011,** *4*, 393-418.

(2.8) Leon, O.; Rogel, E.; Espidel, J.; Torres, G. Asphaltenes: Structural Characterization, Self-Association, and Stability Behavior. *Energy Fuels* **2000,** *14*, 6-10.

(2.9) Sabbah, H.; Morrow, A. L.; Pomerantz, A. E.; Mullins, O. C.; Tan, X.; Gray, M. R.; Azyat, K.; Tykwinski, R. R.; Zare, R. N. Comparing Laser Desorption/Laser Ionization

Mass Spectra of Asphaltenes and Model Compounds. *Energy Fuels* **2010,** *24*, 3589-3594.

(2.10) Sabbah, H.; Morrow, A. L.; Pomerantz, A. E.; Zare, R. N. Evidence for Island Structures as the Dominant Architecture of Asphaltenes. *Energy Fuels* **2011,** *25*, 1597-1604.

(2.11) Hortal, A. R.; Hurtado, P.; Martínez-Haya, B.; Mullins, O. C. Molecular-Weight Distributions of Coal and Petroleum Asphaltenes from Laser Desorption/Ionization Experiments. *Energy Fuels* **2007,** *21*, 2863-2868.

(2.12) Groenzin, H.; Mullins, O. C. Asphaltene Molecular size and Structure. *J. Phys. Chem. A* **1999,** *103*, 11237-11245.

(2.13) Groenzin, H.; Mullins, O. C. Molecular Size and Structure of Asphaltenes from Various Sources. *Energy Fuels* **2000,** *14*, 677-684.

(2.14) Andrews, A. B.; Guerra, R. E.; Mullins, O. C.; Sen, P. N. Diffusivity of Asphaltene Molecules by Fluorescence Correlation Spectroscopy. *J. Phys. Chem. A* **2006,** *110*, 8093-8097.

(2.15) Bergmann, U.; Groenzin, H.; Mullins, O. C.; Glatzel, P.; Fetzer, J.; Cramer, S. Carbon K-Edge X-ray Raman Spectroscopy Supports Simple, yet Powerful Description of Aromatic Hydrocarbons and Asphaltenes. *Chem. Phys. Lett.* **2003,** *369*, 184-191.

(2.16) Pinkston, D. S.; Duan, P.; Gallardo, V. A.; Habicht, S. C.; Tan, X.; Qian, K.; Gray, M.; Mullen, K.; Kenttamaa, H. I. Analysis of Asphaltenes and Asphaltene Model Compounds by Laser-Induced Acoustic Desorption/Fourier Transform Ion Cyclotron Resonance Mass Spectrometry. *Energy Fuels* **2009,** *23*, 5564-5570.

(2.17) Qian, K.; Edwards, K. E.; Siskin, M.; Olmstead, W. N.; Mennito, A. S.; Dechert, G. J.;

Hoosain, N. E. Desorption and Ionization of Heavy Petroleum Molecules and Measurement of Molecular Weight Distributions. *Energy Fuels* **2007,** *21*, 1042-1047.

(2.18) Lisitza, N. V.; Freed, D. E.; Sen, P. N.; Song, Y. Study of Asphaltene Nanoaggregation by Nuclear Magnetic Resonance (NMR). *Energy Fuels* **2009,** *23*, 1189-1193.

(2.19) Bouhadda, Y.; Bormann, D.; Sheu, E.; Bendedouch, D.; Krallafa, A.; Daaou, M. Characterization of Algerian Hassi-Messaoud Asphaltene Structure Using Raman Spectrometry and X-ray Diffraction. *Fuel* **2007,** *86*, 1855-1864.

(2.20) Payzant, J.; Rubinstein, I.; Hogg, A.; Strausz, O. Field-Ionization Mass Spectrometry: Application to Geochemical Analysis. *Geochim. Cosmochim. Acta* **1979,** *43*, 1187-1193.

(2.21) Rubinstein, I.; Strausz, O. Thermal Treatment of the Athabasca Oil Sand Bitumen and Its Component Parts. *Geochim. Cosmochim. Acta* **1979,** *43*, 1887-1893.

(2.22) Rubinstein, I.; Spyckerelle, C.; Strausz, O. Pyrolysis of Asphaltenes: A Source of Geochemical Information. *Geochim. Cosmochim. Acta* **1979,** *43*, 1-6.

(2.23) Calemma, V.; Rausa, R.; D'Anton, P.; Montanari, L. Characterization of Asphaltenes Molecular Structure. *Energy Fuels* **1998,** *12*, 422-428.

(2.24) Ferris, S.; Black, E.; Clelland, J. Aromatic Structure in Asphalt Fractions. *Ind. Eng. Chem. Prod. Res. Dev.* **1967,** *6*, 127-132.

(2.25) Su, Y.; Artok, L.; Murata, S.; Nomura, M. Structural Analysis of the Asphaltene Fraction of an Arabian Mixture by a Ruthenium-Ion-Catalyzed Oxidation Reaction. *Energy Fuels* **1998,** *12*, 1265-1271.

(2.26) Murgich, J.; Abanero, J. A.; Strausz, O. P. Molecular Recognition in Aggregates Formed by Asphaltene and Resin Molecules from the Athabasca Oil Sand. *Energy Fuels* **1999,** *13*, 278-286.

(2.27) Artok, L.; Su, Y.; Hirose, Y.; Hosokawa, M.; Murata, S.; Nomura, M. Structure and Reactivity of Petroleum-Derived Asphaltene. *Energy Fuels* **1999,** *13*, 287-296.

(2.28) Siskin, M.; Kelemen, S.; Eppig, C.; Brown, L.; Afeworki, M. Asphaltene Molecular Structure and Chemical Influences on the Morphology of Coke Produced in Delayed Coking. *Energy Fuels* **2006,** *20*, 1227-1234.

(2.29) Gray, M. R. Consistency of Asphaltene Chemical Structures with Pyrolysis and Coking Behavior. *Energy Fuels* **2003,** *17*, 1566-1569.

(2.30) Karimi, A.; Qian, K.; Olmstead, W. N.; Freund, H.; Yung, C.; Gray, M. R. Quantitative Evidence for Bridged Structures in Asphaltenes by Thin Film Pyrolysis. *Energy Fuels* **2011,** *25*, 3581-3589.

(2.31) Ralston, C. Y.; Mitra-Kirtley, S.; Mullins, O. C. Small Population of One to Three Fused-Aromatic Ring Moieties in Asphaltenes. *Energy Fuels* **1996,** *10*, 623-630.

(2.32) Buenrostro-Gonzalez, E.; Groenzin, H.; Lira-Galeana, C.; Mullins, O. C. The Overriding Chemical Principles that Define Asphaltenes. *Energy Fuels* **2001,** *15*, 972-978.

(2.33) Groenzin, H.; Mullins, O. C.; Eser, S.; Mathews, J.; Yang, M.; Jones, D. Molecular Size of Asphaltene Solubility Fractions. *Energy Fuels* **2003,** *17*, 498-503.

(2.34) Badre, S.; Carla Goncalves, C.; Norinaga, K.; Gustavson, G.; Mullins, O. C. Molecular Size and Weight of Asphaltene and Asphaltene Solubility Fractions from Coals, Crude Oils and Bitumen. *Fuel* **2006,** *85*, 1-11.

(2.35) Mullins, O. C. Rebuttal to Strausz et al. Regarding Time-Resolved Fluorescence Depolarization of Asphaltenes. *Energy Fuels* **2009,** *23*, 2845-2854.

(2.36) Nalwaya, V.; Tantayakom, V.; Piumsomboon, P.; Fogler, S. Studies on Asphaltenes

Through Analysis of Polar Fractions. *Ind. Eng. Chem. Res.* **1999,** *38*, 964-972.

(2.37) Kaminski, T. J.; Fogler, H. S.; Wolf, N.; Wattana, P.; Mairal, A. Classification of Asphaltenes via Fractionation and the Effect of Heteroatom Content on Dissolution Kinetics. *Energy Fuels* **2000,** *14*, 25-30.

(2.38) Fish, R. H.; Komlenic, J. J.; Wines, B. K. Characterization and Comparison of Vanadyl and Nickel Compounds in Heavy Crude Petroleums and Asphaltenes by Reverse-Phase and Size- Exclusion Liquid Chromatography/Graphite Furnace Atomic Absorption Spectrometry. *Anal. Chem.* **1984,** *56*, 2452-2460.

(2.39) Ancheyta, J.; Centeno, G.; Trejo, F.; Marroquin, G.; Garcia, J.; Tenorio, E.; Torres, A. Extraction and Characterization of Asphaltenes from Different Crude Oils and Solvents. *Energy Fuels* **2002,** *16*, 1121-1127.

(2.40) George, G. N.; Gorbaty, M. L. Sulfur K-Edge X-ray Absorption Spectroscopy of Petroleum Asphaltenes and Model Compounds. *J. Am. Chem. Soc.* **1989,** *111*, 3182-3186.

(2.41) Waldo, G. S.; Mullins, O. C.; Penner-Hahn, J. E.; Cramer, S. Determination of the Chemical Environment of Sulphur in Petroleum Asphaltenes by X-ray Absorption Spectroscopy. *Fuel* **1992,** *71*, 53-57.

(2.42) Kelemen, S.; George, G.; Gorbaty, M. Direct Determination and Quantification of Sulphur Forms in Heavy Petroleum and Coals: 1. The X-ray Photoelectron Spectroscopy (XPS) Approach. *Fuel* **1990,** *69*, 939-944.

(2.43) Mitra-Kirtley, S.; Mullins, O. C.; Van Elp, J.; George, S. J.; Chen, J.; Cramer, S. P. Determination of the Nitrogen Chemical Structures in Petroleum Asphaltenes Using XANES Spectroscopy. *J. Am. Chem. Soc.* **1993,** *115*, 252-258.

(2.44) Desando, M. A.; Ripmeester, J. A. Chemical Derivatization of Athabasca Oil Sand Asphaltene for Analysis of Hydroxyl and Carboxyl Groups via Nuclear magnetic Resonance Spectroscopy. *Fuel* **2002,** *81*, 1305-1319.

(2.45) Moschopedis, S. E.; Speight, J. G. Oxygen Functions in Asphaltenes. *Fuel* **1976,** *55*, 334-336.

(2.46) Ignasiak, T.; Strausz, O. P.; Montgomery, D. S. Oxygen Distribution and Hydrogen Bonding in Athabasca Asphaltene. *Fuel* **1977,** *56*, 359-365.

(2.47) Mullins, O. C. The Modified Yen Model. *Energy Fuels* **2010,** *24*, 2179-2207.

(2.48) Yen, T. Structure of Petroleum Asphaltene and Its Significance. *Energy Sources* **1974,** *1*, 447-463.

(2.49) Andreatta, G.; Goncalves, C. C.; Buffin, G.; Bostrom, N.; Quintella, C. M.; Arteaga-Larios, F.; Pérez, E.; Mullins, O. C. Nanoaggregates and Structure−Function Relations in Asphaltenes. *Energy Fuels* **2005,** *19*, 1282-1289.

(2.50) Zeng, H.; Song, Y.; Johnson, D. L.; Mullins, O. C. Critical Nanoaggregate Concentration of Asphaltenes by Direct-Current (DC) Electrical Conductivity. *Energy Fuels* **2009,** *23*, 1201-1208.

(2.51) Andersen, S. I.; del Rio, J. M.; Khvostitchenko, D.; Shakir, S.; Lira-Galeana, C. Interaction and Solubilization of Water by Petroleum Asphaltenes in Organic Solution. *Langmuir* **2001,** *17*, 307-313.

(2.52) Evdokimov, I.; Eliseev, N. Y.; Akhmetov, B. Assembly of Asphaltene Molecular as Studied by Near-UV/Visible Spectroscopy Aggregates, I. Structure of the Absorbance Spectrum. *J. Petrol. Sci. Eng.* **2003,** *37*, 135-143.

(2.53) Evdokimov, I.; Eliseev, N. Y.; Akhmetov, B. Assembly of Asphaltene Molecular

Aggregates as Studied by Near-UV/Visible Spectroscopy: II. Concentration Dependencies of Absorptivities. *J. Pet. Sci. Eng.* **2003,** *37*, 145-152.

(2.54) Hoepfner, M. P.; Fogler, H. S. Multiscale Scattering Investigations of Asphaltene Cluster Breakup, Nanoaggregate Dissociation, and Molecular Ordering. *Langmuir* **2013,** *29*, 15423-15432.

(2.55) Tanaka, R.; Hunt, J. E.; Winans, R. E.; Thiyagarajan, P.; Sato, S.; Takanohashi, T. Aggregates Structure Analysis of Petroleum Asphaltenes with Small-Angle Neutron Scattering. *Energy Fuels* **2003,** *17*, 127-134.

(2.56) Gawrys, K. L.; Kilpatrick, P. K. Asphaltenic Aggregates are Polydisperse Oblate Cylinders. *J. Colloid Interface Sci.* **2005,** *288*, 325-334.

(2.57) Eyssautier, J.; Levitz, P.; Espinat, D.; Jestin, J.; Gummel, J.; Grillo, I.; Barré, L. Insight into Asphaltene Nanoaggregate Structure Inferred by Small Angle Neutron and X-ray Scattering. *J. Phys. Chem. B* **2011,** *115*, 6827-6837.

(2.58) Seki, H.; Kumata, F. Structural Change of Petroleum Asphaltenes and Resins by Hydrodemetallization. *Energy Fuels* **2000,** *14*, 980-985.

(2.59) Soorghali, F.; Zolghadr, A.; Ayatollahi, S. Effect of Resins on Asphaltene Deposition and the Changes of Surface Properties at Different Pressures: A Microstructure Study. *Energy Fuels* **2014,** *28*, 2415-2421.

(2.60) González, G.; Neves, G. B.; Saraiva, S. M.; Lucas, E. F.; dos Anjos de Sousa, M. Electrokinetic Characterization of Asphaltenes and the Asphaltenes−Resins Interaction. *Energy Fuels* **2003,** *17*, 879-886.

(2.61) Mullins, O. C.; Betancourt, S. S.; Cribbs, M. E.; Dubost, F. X.; Creek, J. L.; Andrews, A. B.; Venkataramanan, L. The Colloidal Structure of Crude Oil and the Structure of

Oil Reservoirs. *Energy Fuels* **2007,** *21*, 2785-2794.

(2.62) Sedghi, M.; Goual, L. Role of Resins on Asphaltene Stability. *Energy Fuels* **2009,** *24*, 2275- 2280.

(2.63) Breure, B.; Subramanian, D.; Leys, J.; Peters, C. J.; Anisimov, M. A. Modeling Asphaltene Aggregation with a Single Compound. *Energy Fuels* **2012,** *27*, 172-176.

(2.64) Tan, X.; Fenniri, H.; Gray, M. R. Pyrene Derivatives of 2, 2′-Bipyridine as Models for Asphaltenes: Synthesis, Characterization, and Supramolecular Organization. *Energy Fuels* **2007,** *22*, 715-720.

(2.65) Gray, M. R.; Tykwinski, R. R.; Stryker, J. M.; Tan, X. Supramolecular Assembly Model for Aggregation of Petroleum Asphaltenes. *Energy Fuels* **2011,** *25*, 3125-3134.

(2.66) Murgich, J. Intermolecular Forces in Aggregates of Asphaltenes and Resins. *Petrol. Sci. Technol.* **2002,** *20*, 983-997.

(2.67) Tan, X.; Fenniri, H.; Gray, M. R. Water Enhances the Aggregation of Model Asphaltenes in Solution via Hydrogen Bonding. *Energy Fuels* **2009,** *23*, 3687-3693.

(2.68) Stoyanov, S. R.; Yin, C.; Gray, M. R.; Stryker, J. M.; Gusarov, S.; Kovalenko, A. Computational and Experimental Study of the Structure, Binding Preferences, and Spectroscopy of Nickel(II) and Vanadyl Porphyrins in Petroleum. *J. Phys. Chem. B* **2010,** *114*, 2180-2188.

(2.69) Rogel, E. Asphaltene Aggregation: A Molecular Thermodynamic Approach. *Langmuir* **2002,** *18*, 1928-1937.

(2.70) Rogel, E. Thermodynamic Modeling of Asphaltene Aggregation. *Langmuir* **2004,** *20*, 1003-1012.

(2.71) Rogel, E. Molecular Thermodynamic Approach to the Formation of Mixed

Asphaltene-Resin Aggregates. *Energy Fuels* **2008,** *22*, 3922-3929.

(2.72) Agrawala, M.; Yarranton, H. W. An Asphaltene Association Model Analogous to Linear Polymerization. *Ind. Eng. Chem. Res.* **2001,** *40*, 4664-4672.

(2.73) Zhang, L.; Shi, Q.; Zhao, C.; Zhang, N.; Chung, K. H.; Xu, C.; Zhao, S. Hindered Stepwise Aggregation Model for Molecular Weight Determination of Heavy Petroleum Fractions by Vapor Pressure Osmometry (VPO). *Energy Fuels* **2013,** *27*, 1331-1336.

(2.74) Zhang, L.; Zhao, S.; Xu, Z.; Chung, K. H.; Zhao, C.; Zhang, N.; Xu, C.; Shi, Q. Molecular Weight and Aggregation of Heavy Petroleum Fractions Measured by Vapor Pressure Osmometry and Hindered Stepwise Aggregation Model. *Energy Fuels* **2014,** *28,* 6179-6187.

(2.75) Acevedo, S.; Caetano, M.; Ranaudo, M. A.; Jaimes, B. Simulation of Asphaltene Aggregation and Related Properties Using an Equilibrium-Based Mathematical Model. *Energy Fuels* **2011,** *25*, 3544-3551.

(2.76) Andersen, S. I.; Speight, J. G. Thermodynamic Models for Asphaltene Solubility and Precipitation. *J. Pet. Sci. Eng.* **1999,** *22*, 53-66.

(2.77) Hirschberg, A.; DeJong, L.; Schipper, B.; Meijer, J. Influence of Temperature and Pressure on Asphaltene Flocculation. *Soc. Pet. Eng. J.* **1984,** *24*, 283-293.

(2.78) Leontaritis, K.; Mansoori, G. Asphaltene Flocculation During Oil Production and Processing: A Thermodynamic Colloidal model. Presented at the SPE International Symposium on Oil field Chemistry, San Antonio, TX, Feb. 4–6, 1987; Paper SPE 16258.

(2.79) Flory, P. J. Thermodynamics of High Polymer Solutions. *J. Chem. Phys.* **1942,** *10*, 51-61.

(2.80) Huggins, M. L. Solutions of Long Chain Compounds. *J. Chem. Phys.* **1941,** *9*, 440-440.

(2.81) Victorov, A. I.; Firoozabadi, A. Thermodynamic Micellization Model of Asphaltene Precipitation from Petroleum Fluids. *AIChE J.* **1996,** *42*, 1753-1764.

(2.82) Pan, H.; Firoozabadi, A. Thermodynamic Micellization Model for Asphaltene Aggregation and Precipitation in Petroleum Fluids. *SPE Prod. Facil.* **1998,** *13*, 118-127.

(2.83) Hinze, W. L.; Pramauro, E. A Critical Review of Surfactant-Mediated Phase Separations (Cloud-Point Extractions): Theory and Applications. *Crit. Rev. Anal. Chem.* **1993,** *24*, 133-177.

(2.84) Peng, D.; Robinson, D. B. A New Two-Constant Equation of State. *Ind. Eng. Chem. Fundam.* **1976,** *15*, 59-64.

(2.85) Ashoori, S.; Shahsavani, B.; Ahmadi, M. A.; Rezaei, A. Developing Thermodynamic Micellization Approach to Model Asphaltene Precipitation Behavior. *J. Dispersion Sci. Technol.* **2013**, *35,* 1325-1338.

(2.86) Wu, J.; Prausnitz, J. M.; Firoozabadi, A. Molecular-Thermodynamic Framework for Asphaltene-Oil Equilibria. *AIChE J.* **1998,** *44*, 1188-1199.

(2.87) Victorov, A. I.; Smirnova, N. A. Thermodynamic Model of Petroleum Fluids Containing Polydisperse Asphaltene Aggregates. *Ind. Eng. Chem. Res.* **1998,** *37*, 3242-3251.

(2.88) Victorov, A. I.; Smirnova, N. A. Description of Asphaltene Polydispersity and Precipitation by Means of Thermodynamic Model of Self-Assembly. *Fluid Phase Equilib.* **1999,** *158*, 471-480.

(2.89) Hildebrand, J.; Scott, R. *Solubility of Nonelectrolytes;* Reinhold Pub. Corp.: New York 1950.

(2.90) Correra, S.; Donaggio, F. OCCAM: Onset-constrained colloidal asphaltene model.

Presented at the SPE International Symposium on Formation Damage, Lafayette, LA, Feb. 23-24, 2000; Paper SPE 58724.

(2.91) Correra, S.; Merino-Garcia, D. Simplifying the Thermodynamic Modeling of Asphaltenes in Upstream Operations. *Energy Fuels* **2007,** *21*, 1243-1247.

(2.92) Merino-Garcia, D.; Correra, S. A Shortcut Application of a Flory-Like Model to Asphaltene Precipitation. *J. Dispersion Sci. Technol.* **2007,** *28*, 339-347.

(2.93) Burke, N. E.; Hobbs, R. E.; Kashou, S. F. Measurement and Modeling of Asphaltene Precipitation (includes associated paper 23831). *J. Pet. Technol.* **1990,** *42*, 1,440-1,446.

(2.94) Novosad, Z.; Costain, T. G. Experimental and Modeling Studies of Asphaltene Equilibria for a Reservoir Under CO_2 Injection. Presented at the Annual Technical Conference and Exhibition of the Society of Petroleum Engineers, New Orleans, LA, Sept. 23-26, 1990; Paper SPE 20530.

(2.95) Hirschberg, A.; Hermans, L. Hirschberg, A.; Hermans, L. Asphaltene Phase Behavior: A Molecular Thermodynamic Model. Characterization of Heavy Crude Oils and Petroleum Residues, Symposium Internationale, Lyon June 25−27, 1984, Editions Technip, 492-497.

(2.96) Kawanaka, S.; Park, S.; Mansoori, G. A. Organic Deposition from Reservoir Fluids: A Thermodynamic Predictive. *SPE Reservoir Eng.* **1991,** *6*, 185-192.

(2.97) Scott, R. L.; Magat, M. The Thermodynamics of High-Polymer Solutions: I. The Free Energy of Mixing of Solvents and Polymers of Heterogeneous Distribution. *J. Chem. Phys.* **1945,** *13*, 172-177.

(2.98) Manshad, A. K.; Edalat, M. Application of Continuous Polydisperse Molecular Thermodynamics for Modeling Asphaltene Precipitation in Crude Oil Systems. *Energy*

Fuels **2008,** *22*, 2678-2686.

(2.99) Browarzik, D.; Laux, H.; Rahimian, I. Asphaltene Flocculation in Crude Oil Systems. *Fluid Phase Equilib.* **1999,** *154*, 285-300.

(2.100) Browarzik, C.; Browarzik, D. Modeling the Onset of Asphaltene Flocculation at High Pressure by an Association Model. *Pet. Sci. Technol.* **2005,** *23*, 795-810.

(2.101) Browarzik, D.; Kabatek, R.; Kahl, H.; Laux, H. Flocculation of Asphaltenes at High Pressure. II. Calculation of the Onset of Flocculation. *Pet. Sci. Technol.* **2002,** *20*, 233-249.

(2.102) Yarranton, H. W.; Masliyah, J. H. Molar Mass Distribution and Solubility Modeling of Asphaltenes. *AIChE J.* **1996,** *42*, 3533-3543.

(2.103) Nor-Azlan, N.; Adewumi, M. Development of Asphaltene Phase Equilibria Predictive Model. Present at SPE Eastern Regional Meeting: Pittsburgh, PA, 2−4 Nov. 1993; Paper SPE 26905.

(2.104) Alboudwarej, H.; Akbarzadeh, K.; Beck, J.; Svrcek, W. Y.; Yarranton, H. W. Regular Solution Model for Asphaltene Precipitation from Bitumens and Solvents. *AIChE J.* **2003,** *49*, 2948-2956.

(2.105) Akbarzadeh, K.; Dhillon, A.; Svrcek, W. Y.; Yarranton, H. W. Methodology for the Characterization and Modeling of Asphaltene Precipitation from Heavy Oils Diluted with *n*-Alkanes. *Energy Fuels* **2004,** *18*, 1434-1441.

(2.106) Wiehe, I. A.; Yarranton, H. W.; Akbarzadeh, K.; Rahimi, P. M.; Teclemariam, A. The Paradox of Asphaltene Precipitation with Normal Paraffins. *Energy Fuels* **2005,** *19*, 1261-1267.

(2.107) Tharanivasan, A. K.; Yarranton, H. W.; Taylor, S. D. Application of a Regular

Solution-Based Model to Asphaltene Precipitation from Live Oils. *Energy Fuels* **2010,** *25*, 528-538.

(2.108) Cimino, R.; Correra, S.; Sacomani, P. A.; Carniani, C. Thermodynamic Modelling for Prediction of Asphaltene Deposition in Live Oils. Presented at the SPE International Symposium on Oilfield Chemistry, San Antonio, TX, Feb 14–17, 1995; Paper SPE 28993.

(2.109) Wang, J.; Buckley, J. A Two-Component Solubility Model of the Onset of Asphaltene Flocculation in Crude Oils. *Energy Fuels* **2001,** *15*, 1004-1012.

(2.110) Buckley, J.; Hirasaki, G.; Liu, Y.; Von Drasek, S.; Wang, J.; Gill, B. Asphaltene Precipitation and Solvent Properties of Crude oils. *Pet. Sci. Technol.* **1998,** *16*, 251-285.

(2.111) Mohammadi, A. H.; Richon, D. A Monodisperse Thermodynamic Model for Estimating Asphaltene Precipitation. *AIChE J.* **2007,** *53*, 2940-2947.

(2.112) Mohammadi, A. H.; Eslamimanesh, A.; Richon, D. Monodisperse Thermodynamic Model Based on Chemical Flory–Huggins Polymer Solution Theories for Predicting Asphaltene Precipitation. *Ind. Eng. Chem. Res.* **2012,** *51*, 4041-4055.

(2.113) Pazuki, G.; Nikookar, M. A Modified Flory-Huggins Model for Prediction of Asphaltenes Precipitation in Crude Oil. *Fuel* **2006,** *85*, 1083-1086.

(2.114) Mofidi, A. M.; Edalat, M. A Simplified Thermodynamic Modeling Procedure for Predicting Asphaltene Precipitation. *Fuel* **2006,** *85*, 2616-2621.

(2.115) Nourbakhsh, H.; Yazdizadeh, M.; Esmaeilzadeh, F. Prediction of Asphaltene Precipitation by the Extended Flory–Huggins Model using the Modified Esmaeilzadeh–Roshanfekr Equation of State. *J. Pet. Sci. Eng.* **2011,** *80*, 61-68.

(2.116) Orangi, H. S.; Modarress, H.; Fazlali, A.; Namazi, M. Phase Behavior of Binary Mixture of Asphaltene + Solvent and Ternary Mixture of Asphaltene + Solvent + Precipitant. *Fluid Phase Equilib.* **2006,** *245*, 117-124.

(2.117) Mousavi-Dehghani, S.; Mirzayi, B.; Mousavi, S. M. H.; Fasih, M. An Applied and Efficient Model for Asphaltene Precipitation in Production and Miscible Gas Injection Processes. *Pet. Sci. Technol.* **2010,** *28*, 113-124.

(2.118) Miller A. R. The Vapor-Pressure Equations of Solutions and The Osmotic Pressure of Rubber. *Proc. Cambridge Philos. Soc.* **1943,** *39*, 131-131.

(2.119) Yang, Z.; Ma, C.; Lin, X.; Yang, J.; Guo, T. Experimental and Modeling Studies on the Asphaltene Precipitation in Degassed and Gas-Injected Reservoir Oils. *Fluid Phase Equilib.* **1999,** *157*, 143-158.

(2.120) Akbarzadeh, K.; Ayatollahi, S.; Moshfeghian, M.; Alboudwarej, H.; Yarranton, H. Estimation of SARA Fraction Properties with the SRK EOS. *J. Can. Pet. Technol.* **2004,** *43*, 31-39.

(2.121) Du, J. L.; Zhang, D. A Thermodynamic Model for the Prediction of Asphaltene Precipitation. *Pet. Sci. Technol.* **2004,** *22*, 1023-1033.

(2.122) Anderko, A. Extension of the AEOS Model to Systems Containing Any Number of Associating and Inert Components. *Fluid Phase Equilib.* **1989,** *50*, 21-52.

(2.123) Ikonomou, G.; Donohue, M. D. Thermodynamics of Hydrogen-Bonded Molecules: The Associated Perturbed Anisotropic Chain theory. *AIChE J.* **1986,** *32*, 1716-1725.

(2.124) Ikonomou, G. D.; Donohue, M. D. Extension of the Associated Perturbed Anisotropic Chain Theory to Mixtures with More than One Associating Component. *Fluid Phase Equilib.* **1988,** *39*, 129-159.

(2.125) Vafaie-Sefti, M.; Mousavi-Dehghani, S. A.; Mohammad-Zadeh, M. A Simple Model for Asphaltene Deposition in Petroleum Mixtures. *Fluid Phase Equilib.* **2003,** *206*, 1-11.

(2.126) Sabbagh, O.; Akbarzadeh, K.; Badamchi-Zadeh, A.; Svrcek, W.; Yarranton, H. Applying the PR-EoS to Asphaltene Precipitation from n-Alkane Diluted Heavy Oils and Bitumens. *Energy Fuels* **2006,** *20*, 625-634.

(2.127) Agrawal, P.; Schoeggl, F.; Satyro, M.; Taylor, S.; Yarranton, H. Measurement and Modeling of the Phase Behavior of Solvent Diluted Bitumens. *Fluid Phase Equilib.* **2012,** *334*, 51-64.

(2.128) Li, Z.; Firoozabadi, A. Modeling Asphaltene Precipitation by n-Alkanes from Heavy Oils and Bitumens Using Cubic-Plus-Association Equation of State. *Energy Fuels* **2010,** *24*, 1106-1113.

(2.129) Kontogeorgis, G. M.; Voutsas, E. C.; Yakoumis, I. V.; Tassios, D. P. An Equation of State for Associating Fluids. *Ind. Eng. Chem. Res.* **1996,** *35*, 4310-4318.

(2.130) Wertheim, M. Fluids with Highly Directional Attractive Forces. I. Statistical Thermodynamics. *J. Stat. Phys.* **1984,** *35*, 19-34.

(2.131) Wertheim, M. Fluids with Highly Directional Attractive Forces. II. Thermodynamic Perturbation Theory and Integral Equations. *J. Stat. Phys.* **1984,** *35*, 35-47.

(2.132) Wertheim, M. Fluids of Dimerizing Hard Spheres, and Fluid Mixtures of Hard Spheres and Dispheres. *J. Chem. Phys.* **1986,** *85*, 2929-2936.

(2.133) Wertheim, M. Fluids with Highly Directional Attractive Forces. III. Multiple Attraction Sites. *J. Stat. Phys.***1986,** *42*, 459-476.

(2.134) Wertheim, M. Fluids with Highly Directional Attractive Forces. IV. Equilibrium

Polymerization. *J. Stat. Phys.* **1986,** *42*, 477-492.

(2.135) Wertheim, M. Thermodynamic Perturbation Theory of Polymerization. *J. Chem. Phys.* **1987,** *87*, 7323-7331.

(2.136) Li, Z.; Firoozabadi, A. Cubic-Plus-Association Equation of State for Asphaltene Precipitation in Live Oils. *Energy Fuels* **2010,** *24*, 2956-2963.

(2.137) Saeedi Dehaghani, A.; Sefti, M. V.; Amerighasrodashti, A. The Application of a New Association Equation of State (AEOS) for Prediction of Asphaltenes and Resins Deposition During CO_2 Gas Injection. *Pet. Sci. Technol.* **2012,** *30*, 1548-1561.

(2.138) Chapman, W. G.; Jackson, G.; Gubbins, K. E. Phase Equilibria of Associating Fluids. Chain Molecules with Multiple Bonding Sites. *Mol. Phys.* **1988,** *65*, 1057-1079.

(2.139) Chapman, W. G.; Gubbins, K. E.; Jackson, G.; Radosz, M. New Reference Equation of State for Associating Liquids. *Ind. Eng. Chem. Res.* **1990,** *29*, 1709-1721.

(2.140) David Ting, P.; Hirasaki, G. J.; Chapman, W. G. Modeling of Asphaltene Phase Behavior with the SAFT Equation of State. *Pet. Sci. Technol.* **2003,** *21*, 647-661.

(2.141) Gross, J.; Sadowski, G. Perturbed-Chain SAFT: An Equation of State Based on a Perturbation Theory for Chain Molecules. *Ind. Eng. Chem. Res.* **2001,** *40*, 1244-1260.

(2.142) Barker, J. A.; Henderson, D. Perturbation Theory and Equation of State for Fluids: The Square-Well Potential. *J. Chem. Phys.* **1967,** *47*, 2856-2861.

(2.143) Barker, J. A.; Henderson, D. Perturbation Theory and Equation of State for Fluids. II. A Successful Theory of Liquids. *J. Chem. Phys.* **1967,** *47*, 4714-4721.

(2.144) Vargas, F. M.; Gonzalez, D. L.; Hirasaki, G. J.; Chapman, W. G. Modeling Asphaltene Phase Behavior in Crude Oil Systems Using the Perturbed Chain Form of the Statistical Associating Fluid Theory (PC-SAFT) Equation of State. *Energy Fuels*

2009, *23*, 1140-1146.

(2.145) Panuganti, S. R.; Tavakkoli, M.; Vargas, F. M.; Gonzalez, D. L.; Chapman, W. G. SAFT Model for Upstream Asphaltene Applications. *Fluid Phase Equilib.* **2013,** *359*, 2-16.

(2.146) Panuganti, S. R.; Vargas, F. M.; Gonzalez, D. L.; Kurup, A. S.; Chapman, W. G. PC-SAFT Characterization of Crude Oils and Modeling of Asphaltene Phase Behavior. *Fuel* **2012,** *93*, 658-669.

(2.147) Gonzalez, D. L.; Hirasaki, G. J.; Creek, J.; Chapman, W. G. Modeling of Asphaltene Precipitation Due to Changes in Composition Using the Perturbed Chain Statistical Associating Fluid Theory Equation of State. *Energy Fuels* **2007,** *21*, 1231-1242.

(2.148) Tavakkoli, M.; Panuganti, S. R.; Taghikhani, V.; Pishvaie, M. R.; Chapman, W. G. Understanding the Polydisperse Behavior of Asphaltenes during Precipitation. *Fuel* **2014,** *117*, 206-217.

(2.149) Zúñiga-Hinojosa, M. A.; Justo-García, D. N.; Aquino-Olivos, M. A.; Román-Ramírez, L. A.; García-Sánchez, F. Modeling of Asphaltene Precipitation from n-Alkane Diluted Heavy Oils and Bitumens Using the PC-SAFT Equation of State. *Fluid Phase Equilib.* **2014,** *376*, 210-224.

(2.150) Gil-Villegas, A.; Galindo, A.; Whitehead, P. J.; Mills, S. J.; Jackson, G.; Burgess, A. N. Statistical Associating Fluid Theory for Chain Molecules with Attractive Potentials of Variable Range. *J. Chem. Phys.* **1997,** *106*, 4168-4186.

(2.151) Artola, P.; Pereira, F. E.; Adjiman, C. S.; Galindo, A.; Müller, E. A.; Jackson, G.; Haslam, A. J. Understanding the Fluid Phase Behaviour of Crude Oil: Asphaltene Precipitation. *Fluid Phase Equilib.* **2011,** *306*, 129-136.

(2.152) Wu, J.; Prausnitz, J. M.; Firoozabadi, A. Molecular Thermodynamics of Asphaltene Precipitation in Reservoir Fluids. *AIChE J.* **2000,** *46*, 197-209.

(2.153) Buenrostro-Gonzalez, E.; Lira-Galeana, C.; Gil-Villegas, A.; Wu, J. Asphaltene Precipitation in Crude Oils: Theory and Experiments. *AIChE J.* **2004,** *50*, 2552-2570.

(2.154) Aquino-Olivos, M. A.; Grolier, J. E.; Randzio, S. L.; Aguirre-Gutiérrez, A. J.; García-Sánchez, F. Determination of the Asphaltene Precipitation Envelope and Bubble Point Pressure for a Mexican Crude Oil by Scanning Transitiometry. *Energy Fuels* **2013,** *27*, 1212-1222.

(2.155) Rassamdana, H.; Dabir, B.; Nematy, M.; Farhani, M.; Sahimi, M. Asphalt Flocculation and Deposition: I. The Onset of Precipitation. *AIChE J.* **1996,** *42*, 10-22.

(2.156) Rassamdana, H.; Sahimi, M. Asphalt Flocculation and Deposition: II. Formation and Growth of Fractal Aggregates. *AIChE J.* **1996,** *42*, 3318-3332.

(2.157) Hu, Y.; Chen, G.; Yang, J.; Guo, T. A Study on the Application of Scaling Equation for Asphaltene Precipitation. *Fluid Phase Equilib.* **2000,** *171*, 181-195.

(2.158) Duda, Y.; Lira-Galeana, C. Thermodynamics of Asphaltene Structure and Aggregation. *Fluid Phase Equilib.* **2006,** *241*, 257-267.

(2.159) Zahedi, G.; Fazlali, A.; Hosseini, S.; Pazuki, G.; Sheikhattar, L. Prediction of Asphaltene Precipitation in Crude Oil. *J. Pet. Sci. Eng.* **2009,** *68*, 218-222.

(2.160) Na'imi, S. R.; Gholami, A.; Asoodeh, M. Prediction of Crude Oil Asphaltene Precipitation Using Support Vector Regression. *J. Dispersion Sci. Technol.* **2014,** *35*, 518-523.

(2.161) Alvarez-Ramirez, F.; Ramirez-Jaramillo, E.; Ruiz-Morales, Y. Calculation of the Interaction Potential Curve between Asphaltene−Asphaltene, Asphaltene−Resin, and

Resin−Resin Systems Using Density Functional Theory. *Energy Fuels* **2006,** *20*, 195-204.

(2.162) Harris, J. Simplified Method for Calculating the Energy of Weakly Interacting Fragments. *Physical Review B* **1985,** *31*, 1770.

(2.163) Vosko, S.; Wilk, L.; Nusair, M. Accurate Spin-Dependent Electron Liquid Correlation Energies for Local Spin Density Calculations: A Critical Analysis. *Can. J. Phys.* **1980,** *58*, 1200-1211.

(2.164) Perdew, J. P.; Wang, Y. Accurate and Simple Analytic Representation of the Electron-Gas Correlation Energy. *Phys. Rev. B* **1992,** *45,* 13244– 13249.

(2.165) Delley, B. An All-Electron Numerical Method for Solving the Local Density Functional for Polyatomic Molecules. *J. Chem. Phys.* **1990,** *92*, 508-517.

(2.166) Moreira da Costa, L.; Stoyanov, S. R.; Gusarov, S.; Seidl, P. R.; Walkimar de M. Carneiro, José; Kovalenko, A. Computational Study of the Effect of Dispersion Interactions on the Thermochemistry of Aggregation of Fused Polycyclic Aromatic Hydrocarbons as Model Asphaltene Compounds in Solution. *J. Phys. Chem. A* **2014,** *118*, 896-908.

(2.167) Grimme, S. Improved Second-Order Møller–Plesset Perturbation Theory by Separate Scaling of Parallel- and Antiparallel-Spin Pair Correlation Energies. *J. Chem. Phys.* **2003,** *118*, 9095-9102.

(2.168) Takatani, T.; Hohenstein, E. G.; Sherrill, C. D. Improvement of the Coupled-Cluster Singles and Doubles Method via Scaling Same- and Opposite-Spin Components of the Double Excitation Correlation Energy. *J. Chem. Phys.* **2008,** *128*, 124111.

(2.169) Frisch, M. J.; Head-Gordon, M.; Pople, J. A. A Direct MP2 Gradient Method. *Chem.*

Phys. Lett. **1990,** *166*, 275-280.

(2.170) Head-Gordon, M.; Head-Gordon, T. Analytic MP2 Frequencies without Fifth-Order Storage. Theory and Application to Bifurcated Hydrogen Bonds in the Water Hexamer. *Chem. Phys. Lett.* **1994,** *220*, 122-128.

(2.171) Frisch, M. J.; Pople, J. A.; Binkley, J. S. Self-Consistent Molecular Orbital Methods 25. Supplementary Functions for Gaussian Basis Sets. *J. Chem. Phys.* **1984,** *80*, 3265-3269.

(2.172) Rassolov, V. A.; Ratner, M. A.; Pople, J. A.; Redfern, P. C.; Curtiss, L. A. 6-31G* Basis Set for Third-Row Atoms. *J. Comput. Chem.* **2001,** *22*, 976-984.

(2.173) Barone, V.; Cossi, M. Quantum Calculation of Molecular Energies and Energy Gradients in Solution by a Conductor Solvent Model. *J. Phys. Chem. A* **1998,** *102*, 1995-2001.

(2.174) Cossi, M.; Rega, N.; Scalmani, G.; Barone, V. Energies, Structures, and Electronic Properties of Molecules in Solution with the C-PCM Solvation Model. *J. Comput. Chem.* **2003,** *24*, 669-681.

(2.175) da Costa, L. M.; Stoyanov, S. R.; Gusarov, S.; Tan, X.; Gray, M. R.; Stryker, J. M.; Tykwinski, R.; de M. Carneiro, J Walkimar; Seidl, P. R.; Kovalenko, A. Density Functional Theory Investigation of the Contributions of $\pi-\pi$ Stacking and Hydrogen-Bonding Interactions to the Aggregation of Model Asphaltene Compounds. *Energy Fuels* **2012,** *26*, 2727-2735.

(2.176) Chai, J.; Head-Gordon, M. Long-Range Corrected Hybrid Density Functionals with Damped Atom–Atom Dispersion Corrections. *Phys. Chem. Chem. Phys.* **2008,** *10*, 6615-6620.

(2.177) Tomasi, J.; Mennucci, B.; Cammi, R. Quantum Mechanical Continuum Solvation

Models. *Chem. Rev.* **2005,** *105*, 2999-3094.

(2.178) da Costa, L. M.; Hayaki, S.; Stoyanov, S. R.; Gusarov, S.; Tan, X.; Gray, M. R.; Stryker, J. M.; Tykwinski, R.; Carneiro, J. d. M.; Sato, H. 3D-RISM-KH Molecular Theory of Solvation and Density Functional Theory Investigation of the Role of Water in the Aggregation of Model Asphaltenes. *Phys. Chem. Chem. Phys.* **2012,** *14*, 3922-3934.

(2.179) Carauta, A. N.; Correia, J. C.; Seidl, P. R.; Silva, D. M. Conformational Search and Dimerization Study of Average Structures of Asphaltenes. *J. Mol. Struct. (Theochem)* **2005,** *755*, 1-8.

(2.180) Castellano, O.; Gimon, R.; Soscun, H. Theoretical Study of the $\sigma - \pi$ and $\pi - \pi$ Interactions in Heteroaromatic Monocyclic Molecular Complexes of Benzene, Pyridine, and Thiophene Dimers: Implications on the Resin Asphaltene Stability in Crude Oil. *Energy Fuels* **2011,** *25*, 2526-2541.

(2.181) Brandt, H.; Hendriks, E.; Michels, M.; Visser, F. Thermodynamic Modeling of Asphaltene Stacking. *J. Phys. Chem.* **1995,** *99*, 10430-10432.

(2.182) Ortega-Rodriguez, A.; Lira-Galeana, C.; Ruiz-Morales, Y.; Cruz, S. A. Interaction Energy in Maya-Oil Asphaltenes: A Molecular Mechanics Study. *Pet. Sci. Technol.* **2001,** *19*, 245-256.

(2.183) Pacheco-Sánchez, J. H.; Alvarez-Ramírez, F.; Martínez-Magadán, J. Aggregate Asphaltene Structural Models. *Prepr. Am. Chem. Soc., Div. Pet. Chem.* **2003,** *48*, 71-73.

(2.184) Pacheco-Sánchez, J. H.; Alvarez-Ramirez, F.; Martínez-Magadán, J. Morphology of Aggregated Asphaltene Structural Models. *Energy Fuels* **2004,** *18*, 1676-1686.

(2.185) Murgich, J.; Merino-Garcia, D.; Andersen, S. I.; Manuel del Río, J.; Galeana, C. L. Molecular Mechanics and Microcalorimetric Investigations of the Effects of Molecular Water on the Aggregation of Asphaltenes in Solutions. *Langmuir* **2002,** *18*, 9080-9086.

(2.186) Murgich, J.; Rodríguez, J.; Aray, Y. Molecular Recognition and Molecular Mechanics of Micelles of Some Model Asphaltenes and Resins. *Energy Fuels* **1996,** *10*, 68-76.

(2.187) Murgich, J.; Strausz, O. P. Molecular Mechanics of Aggregates of Asphaltenes and Resins of the Athabasca Oil. *Pet. Sci. Technol.* **2001,** *19*, 231-243.

(2.188) Murgich, J. Molecular Simulation and the Aggregation of the Heavy Fractions in Crude Oils. *Mol. Simul.* **2003,** *29*, 451-461.

(2.189) Rogel, E. Simulation of Interactions in Asphaltene Aggregates. *Energy Fuels* **2000,** *14*, 566-574.

(2.190) Pacheco-Sánchez, J. H.; Zaragoza, I.; Martinez-Magadan, J. Asphaltene Aggregation under Vacuum at Different Temperatures by Molecular Dynamics. *Energy Fuels* **2003,** *17*, 1346-1355.

(2.191) Takanohashi, T.; Sato, S.; Saito, I.; Tanaka, R. Molecular Dynamics Simulation of the Heat-Induced Relaxation of Asphaltene Aggregates. *Energy Fuels* **2003,** *17*, 135-139.

(2.192) Mitchell, D. L.; Speight, J. G. The Solubility of Asphaltenes in Hydrocarbon Solvents. *Fuel* **1973,** *52*, 149-152.

(2.193) Permsukarome, P.; Chang, C.; Fogler, H. S. Kinetic Study of Asphaltene Dissolution in Amphiphile/Alkane Solutions. *Ind. Eng. Chem. Res.* **1997,** *36*, 3960-3967.

(2.194) Speight, J. G.; Long, R. B.; Trowbridge, T. D.; Linden, N. On the Definition of Asphaltenes. *Am. Chem. Soc., Div. Pet. Chem., Prepr.* **1982,** *27*, 268-275.

(2.195) Boek, E. S.; Yakovlev, D. S.; Headen, T. F. Quantitative Molecular Representation of

Asphaltenes and Molecular Dynamics Simulation of Their Aggregation. *Energy Fuels* **2009,** *23*, 1209-1219.

(2.196) Rogel, E. Studies on Asphaltene Aggregation via Computational Chemistry. *Colloids Surf., A.* **1995,** *104*, 85-93.

(2.197) Headen, T. F.; Boek, E. S.; Skipper, N. T. Evidence for Asphaltene Nanoaggregation in Toluene and Heptane from Molecular Dynamics Simulations. *Energy Fuels* **2009,** *23*, 1220-1229.

(2.198) Ungerer, P.; Rigby, D.; Leblanc, B.; Yiannourakou, M. Sensitivity of the Aggregation Behaviour of Asphaltenes to Molecular Weight and Structure Using Molecular Dynamics. *Mol. Simul.* **2014,** *40*, 115-122.

(2.199) Kuznicki, T.; Masliyah, J. H.; Bhattacharjee, S. Molecular Dynamics Study of Model Molecules Resembling Asphaltene-Like Structures in Aqueous Organic Solvent Systems. *Energy Fuels* **2008,** *22*, 2379-2389.

(2.200) Sedghi, M.; Goual, L.; Welch, W.; Kubelka, J. Effect of Asphaltene Structure on Association and Aggregation Using Molecular Dynamics. *J. Phys. Chem. B* **2013,** *117*, 5765-5776.

(2.201) Teklebrhan, R. B.; Ge, L.; Bhattacharjee, S.; Xu, Z.; Sjöblom, J. Probing Structure–Nanoaggregation Relations of Polyaromatic Surfactants: A Molecular Dynamics Simulation and Dynamic Light Scattering Study. *J. Phys. Chem. B* **2012,** *116*, 5907-5918.

(2.202) Carauta, A. N.; Seidl, P. R.; Chrisman, E. C.; Correia, J. C.; Menechini, P. d. O.; Silva, D. M.; Leal, K. Z.; de Menezes, S. M.; de Souza, W. F.; Teixeira, M. A. Modeling Solvent Effects on Asphaltene Dimers. *Energy Fuels* **2005,** *19*, 1245-1251.

(2.203) Frigerio, F.; Molinari, D. A Multiscale Approach to the Simulation of Asphaltenes. *Comput. Theor. Chem.* **2011,** *975*, 76-82.

(2.204) Takanohashi, T.; Sato, S.; Tanaka, R. Molecular Dynamics Simulation of Structural Relaxation of Asphaltene Aggregates. *Pet. Sci. Technol.* **2003,** *21*, 491-505.

(2.205) Pacheco-Sánchez, J. H.; Zaragoza, I.; Martínez-Magadán, J. Preliminary Study of the Effect of Pressure on Asphaltene Disassociation by Molecular Dynamics. *Pet. Sci. Technol.* **2004,** *22*, 927-942.

(2.206) Headen, T. F.; Boek, E. S. Molecular Dynamics Simulations of Asphaltene Aggregation in Supercritical Carbon Dioxide with and without Limonene. *Energy Fuels* **2010,** *25*, 503-508.

(2.207) Hu, M.; Shao, C.; Dong, L.; Zhu, J. Molecular Dynamics Simulation of Asphaltene Deposition During CO_2 Miscible Flooding. *Pet. Sci. Technol.* **2011,** *29*, 1274-1284.

(2.208) Zhang, L.; Greenfield, M. L. Molecular Orientation in Model Asphalts Using Molecular Simulation. *Energy Fuels* **2007,** *21*, 1102-1111.

(2.209) Diallo, M. S.; Strachan, A.; Faulon, J.; Goddard III, W. A. Thermodynamic Properties of Asphaltenes Through Computer Assisted Structure Elucidation and Atomistic Simulations. 1. Bulk Arabian Light asphaltenes. *Pet. Sci. Technol.* **2004,** *22*, 877-899.

(2.210) Aray, Y.; Hernández-Bravo, R.; Parra, J. G.; Rodríguez, J.; Coll, D. S. Exploring the Structure–Solubility Relationship of Asphaltene Models in Toluene, Heptane, and Amphiphiles Using a Molecular Dynamic Atomistic Methodology. *J. Phys. Chem. A* **2011,** *115*, 11495-11507.

(2.211) Hansen, C. M. *Hansen Solubility Parameters: A User's Handbook;* 2nd ed.; CRC press: Hoboken, 2007.

(2.212) Aguilera-Mercado, B.; Herdes, C.; Murgich, J.; Müller, E. Mesoscopic Simulation of Aggregation of Asphaltene and Resin Molecules in Crude Oils. *Energy Fuels* **2006,** *20*, 327-338.

(2.213) Ortega-Rodríguez, A.; Cruz, S. A.; Gil-Villegas, A.; Guevara-Rodriguez, F.; Lira-Galeana, C. Molecular View of the Asphaltene Aggregation Behavior in Asphaltene−Resin Mixtures. *Energy Fuels* **2003,** *17*, 1100-1108.

(2.214) Zhang, S.; Sun, L. L.; Xu, J.; Wu, H.; Wen, H. Aggregate Structure in Heavy Crude Oil: Using a Dissipative Particle Dynamics Based Mesoscale Platform. *Energy Fuels* **2010,** *24*, 4312-4326.

(2.215) Zhang, S.; Xu, J.; Wen, H.; Bhattacharjee, S. Integration of Rotational Algorithms into Dissipative Particle Dynamics: Modeling Polyaromatic Hydrocarbons on the Meso-Scale. *Mol. Phys.* **2011,** *109*, 1873-1888.

(2.216) Wang, S.; Xu, J.; Wen, H. The Aggregation and Diffusion of Asphaltenes Studied by GPU-Accelerated Dissipative Particle dynamics. *Comput. Phys. Commun.* **2014,** *185*, 3069-3078.

(3.1) Groenzin, H.; Mullins, O. C. Asphaltene Molecular Size and Structure. *J. Phys. Chem. A* **1999,** *103*, 11237-11245.

(3.2) Mansoori, G. A. Modeling of Asphaltene and Other Heavy Organic Depositions. *J. Petr. Sci. Eng.* **1997,** *17*, 101-111.

(3.3) Escobedo, J.; Mansoori, G. A. Heavy Organic Deposition and Plugging of Wells (Analysis of Mexico's experience). Presented at the SPE Latin America Petroleum Engineering Conference, Caracas, Venezuela, March 8–11, 1992; Paper SPE 23696.

(3.4) Kokal, S. L.; Sayegh, S. G. Asphaltenes: The Cholesterol of Petroleum. Presented at the SPE Middle East Oil Show, Bahrain, March 11–14, 1995; Paper SPE 29787.

(3.5) Spiecker, P. M.; Gawrys, K. L.; Kilpatrick, P. K. Aggregation and Solubility Behavior of Asphaltenes and Their Subfractions. *J. Colloid Interface Sci.* **2003,** *267*, 178-193.

(3.6) Yarranton, H. W.; Alboudwarej, H.; Jakher, R. Investigation of Asphaltene Association with Vapor Pressure Osmometry and Interfacial Tension Measurements. *Ind. Eng. Chem. Res.* **2000,** *39*, 2916-2924.

(3.7) Ho, B.; Briggs, D. E. Small Angle X-Ray Scattering from Coal-Derived Liquids. *Colloids Surf.* **1982,** *4*, 271-284.

(3.8) Ravey, J. C.; Ducouret, G.; Espinat, D. Asphaltene Macrostructure by Small Angle Neutron Scattering. *Fuel* **1988,** *67*, 1560-1567.

(3.9) Andersen, S. I.; Birdi, K. S. Aggregation of Asphaltenes as Determined by Calorimetry. *J. Colloid Interface Sci.* **1991,** *142*, 497-502.

(3.10) Anisimov, M. A.; Yudin, I. K.; Nikitin, V.; Nikolaenko, G.; Chernoutsan, A.; Toulhoat, H.; Frot, D.; Briolant, Y. Asphaltene Aggregation in Hydrocarbon Solutions Studied by Photon Correlation Spectroscopy. *J. Phys. Chem.* **1995,** *99*, 9576-9580.

(3.11) Sjöblom, J.; Aske, N.; Auflem, I. H.; Brandal, Ø; Havre, T. E.; Sæther, Ø; Westvik, A.; Johnsen, E. E.; Kallevik, H. Our current Understanding of Water-in-Crude Oil Emulsions.: Recent Characterization Techniques and High Pressure Performance. *Adv. Colloid Interface Sci.* **2003,** *100-102*, 399-473.

(3.12) Lisitza, N. V.; Freed, D. E.; Sen, P. N.; Song, Y. Q. Study of Asphaltene Nanoaggregation by Nuclear Magnetic Resonance (NMR). *Energy Fuels* **2009,** *23*, 1189-1193.

(3.13) Mullins, O. C.; Sabbah, H.; Eyssautier, J.; Pomerantz, A. E.; Barré, L.; Andrews, A. B.; Ruiz-Morales, Y.; Mostowfi, F.; McFarlane, R.; Goual, L., et al. Advances in Asphaltene Science and the Yen–Mullins Model. *Energy Fuels* **2012,** *26*, 3986-4003.

(3.14) Mullins, O. C. The Modified Yen Model. *Energy Fuels* **2010,** *24*, 2179-2207.

(3.15) Mullins, O. C. The Asphaltenes. *Annu. Rev. Anal. Chem.* **2011,** *4*, 393-418.

(3.16) Kuznicki, T.; Masliyah, J. H.; Bhattacharjee, S. Molecular Dynamics Study of Model Molecules Resembling Asphaltene-Like Structures in Aqueous Organic Solvent Systems. *Energy Fuels* **2008,** *22*, 2379-2389.

(3.17) Badre, S.; Carla Goncalves, C.; Norinaga, K.; Gustavson, G.; Mullins, O. C. Molecular Size and Weight of Asphaltene and Asphaltene Solubility Fractions from Coals, Crude Oils and Bitumen. *Fuel* **2006,** *85*, 1-11.

(3.18) Karimi, A.; Qian, K.; Olmstead, W. N.; Freund, H.; Yung, C.; Gray, M. R. Quantitative Evidence for Bridged Structures in Asphaltenes by Thin Film Pyrolysis. *Energy Fuels* **2011,** *25*, 3581-3589.

(3.19) Tan, X.; Fenniri, H.; Gray, M. R. Pyrene Derivatives of 2,2'-Bipyridine as Models for Asphaltenes: Synthesis, Characterization, and Supramolecular Organization. *Energy Fuels* **2008,** *22*, 715-720.

(3.20) Zeng, H.; Song, Y. Q.; Johnson, D. L.; Mullins, O. C. Critical Nanoaggregate Concentration of Asphaltenes by Direct-Current (DC) Electrical Conductivity. *Energy Fuels* **2009,** *23*, 1201-1208.

(3.21) Kuznicki, T.; Masliyah, J. H.; Bhattacharjee, S. Aggregation and Partitioning of Model Asphaltenes at Toluene−Water Interfaces: Molecular Dynamics Simulations. *Energy Fuels* **2009,** *23*, 5027-5035.

(3.22) Aray, Y.; Hernández-Bravo, R.; Parra, J. G.; Rodríguez, J.; Coll, D. S. Exploring the Structure–Solubility Relationship of Asphaltene Models in Toluene, Heptane, and Amphiphiles Using a Molecular Dynamic Atomistic Methodology. *J. Phys. Chem. A* **2011,** *115*, 11495-11507.

(3.23) Spiecker, P. M.; Gawrys, K. L.; Trail, C. B.; Kilpatrick, P. K. Effects of Petroleum Resins on Asphaltene Aggregation and Water-in-Oil Emulsion Formation. *Colloids Surf. A* **2003,** *220*, 9-27.

(3.24) Ortega-Rodríguez, A.; Cruz, S. A.; Gil-Villegas, A.; Guevara-Rodríguez, F.; Lira-Galeana, C. Molecular View of the Asphaltene Aggregation Behavior in Asphaltene−Resin Mixtures. *Energy Fuels* **2003,** *17*, 1100-1108.

(3.25) Speight, J. G.; Long, R. B.; Trowbridge, T. D. Factors Influencing the Separation of Asphaltenes from Heavy Petroleum Feedstocks. *Fuel* **1984,** *63*, 616-620.

(3.26) Tan, X.; Fenniri, H.; Gray, M. R. Water Enhances the Aggregation of Model Asphaltenes in Solution via Hydrogen Bonding. *Energy Fuels* **2009,** *23*, 3687-3693.

(3.27) Gray, M. R.; Tykwinski, R. R.; Stryker, J. M.; Tan, X. Supramolecular Assembly Model for Aggregation of Petroleum Asphaltenes. *Energy Fuels* **2011,** *25*, 3125-3134.

(3.28) Yen, T. F. Structure of Petroleum Asphaltene and Its Significance. *Energy Sources* **1974,** *1*, 447-463.

(3.29) Buenrostro-Gonzalez, E.; Groenzin, H.; Lira-Galeana, C.; Mullins, O. C. The Overriding Chemical Principles that Define Asphaltenes. *Energy Fuels* **2001,** *15*, 972-978.

(3.30) Andreatta, G.; Goncalves, C. C.; Buffin, G.; Bostrom, N.; Quintella, C. M.; Arteaga-Larios, F.; Pérez, E.; Mullins, O. C. Nanoaggregates and Structure−Function Relations in Asphaltenes. *Energy Fuels* **2005,** *19*, 1282-1289.

(3.31) Stachowiak, C.; Viguié, J. R..; Grolier, J. P. E.; Rogalski, M. Effect of n-Alkanes on Asphaltene Structuring in Petroleum Oils. *Langmuir* **2005,** *21*, 4824-4829.

(3.32) Takanohashi, T.; Sato, S.; Saito, I.; Tanaka, R. Molecular Dynamics Simulation of the Heat-Induced Relaxation of Asphaltene Aggregates. *Energy Fuels* **2003,** *17*, 135-139.

(3.33) Pacheco-Sánchez, J. H.; Álvarez-Ramírez, F.; Martínez-Magadán, J. M. Morphology of Aggregated Asphaltene Structural Models. *Energy Fuels* **2004,***18*, 1676-1686.

(3.34) Groenzin, H.; Mullins, O. C. Molecular Size and Structure of Asphaltenes from Various Sources. *Energy Fuels* **2000,** *14*, 677-684.

(3.35) Speight, J. G.; Moschopedis, S. E. Some Observations on the Molecular "Nature" of Petroleum Asphaltenes. *Am. Chem. Soc., Div. Pet. Chem. Prepr.* **1979,** *24*, 910-923.

(3.36) Speight, J. G. *The Chemistry and Technology of Petroleum,* 4th ed.; CRC Press: Boca Raton, 2006.

(3.37) Zajac, G. W.; Sethi, N. K.; Joseph, J. T.; Thomson, D. J.; Weiss, P. S. Molecular Imaging of Petroleum Asphaltenes by Scanning Tunneling Microscopy: Verification of Structure from ^{13}C and Proton Nuclear Magnetic Resonance Data. *Scanning Microscopy* **1994,** *8*, 463-470.

(3.38) Murgich, J.; Jesús Rodríguez, M.; Aray, Y. Molecular Recognition and Molecular Mechanics of Micelles of Some Model Asphaltenes and Resins. *Energy Fuels* **1996,** *10*, 68-76.

(3.39) Headen, T. F.; Boek, E. S.; Skipper, N. T. Evidence for Asphaltene Nanoaggregation in Toluene and Heptane from Molecular Dynamics Simulations. *Energy Fuels* **2009,** *23*, 1220-1229.

(3.40) Teklebrhan, R. B.; Ge, L.; Bhattacharjee, S.; Xu, Z.; Sjöblom, J. Probing Structure–

Nanoaggregation Relations of Polyaromatic Surfactants: A Molecular Dynamics Simulation and Dynamic Light Scattering Study. *J. Phys. Chem. B* **2012,** *116*, 5907-5918.

(3.41) Zhang, L.; Greendfield, M. L. Molecular Orientation in Model Asphalts Using Molecular Simulation. *Energy Fuels* **2007,** *21*, 1102-1111.

(3.42) Andrews, A. B.; McClelland, A.; Korkeila, O.; Demidov, A.; Krummel, A.; Mullins, O. C.; Chen, Z. Molecular Orientation of Asphaltenes and PAH Model Compounds in Langmuir−Blodgett Films Using Sum Frequency Generation Spectroscopy. *Langmuir* **2011,** *27*, 6049-6058.

(3.43) González, M. F.; Stull, C. S.; López-Linares, F.; Pereira-Almao, P. Comparing Asphaltene Adsorption with Model Heavy Molecules over Macroporous Solid Surfaces. *Energy Fuels* **2007,** *21*, 234-241.

(3.44) Jarne, C.; Cebolla, V. L.; Membrado, L.; Le Mapihan, K.; Giusti, P. High-Performance Thin-Layer Chromatography Using Automated Multiple Development for the Separation of Heavy Petroleum Products According to Their Number of Aromatic Rings. *Energy Fuels* **2011,** *25*, 4586-4594.

(3.45) Schüttelkopf, A. W.; Van Aalten, D. M. F. PRODRG: A Tool for High-Throughput Crystallography of Protein-Ligand Complexes. *Acta Crystallogr. Sect. D: Biol. Crystallogr.* **2004,** *60*, 1355-1363.

(3.46) Oostenbrink, C.; Villa, A.; Mark, A. E.; Van Gunsteren, W. F. A Biomolecular Force Field Based on the Free Enthalpy of Hydration and Solvation: The GROMOS Force-Field Parameter Sets 53A5 and 53A6. *J. Comput. Chem.* **2004,** *25*, 1656-1676.

(3.47) Lemkul, J. A.; Allen, W. J.; Bevan, D. R. Practical Considerations for Building

GROMOS-Compatible Small-Molecule Topologies. *J. Chem. Inf. Model.* **2010,** *50*, 2221-2235.

(3.48) Hess, B.; Kutzner, C.; van der Spoel, D.; Lindahl, E. GROMACS 4: Algorithms for Highly Efficient, Load-Balanced, and Scalable Molecular Simulation. *J. Chem. Theory Comput.* **2008,** *4*, 435-447.

(3.49) van der Spoel, D.; Lindahl, E.; Hess, B.; Groenhof, G.; Mark, A. E.; Berendsen, H. J. C. GROMACS: Fast, Flexible, and Free. *J. Comput. Chem.* **2005,** *26*, 1701-1718.

(3.50) Lindahl, E.; Hess, B.; van der Spoel, D. GROMACS 3.0: A Package for Molecular Simulation and Trajectory Analysis. *J. Mol. Model.* **2001,** *7*, 306-317.

(3.51) Berendsen, H. J. C.; van der Spoel, D.; van Drunen, R. GROMACS: A Message-Passing Parallel Molecular Dynamics Implementation. *Comput. Phys. Commun.* **1995,** *91*, 43-56.

(3.52) Berendsen, H. J. C.; Postma, J. P. M.; van Gunsteren, W.; Hermans, J. In *Intermolecular Forces*; Pullman, B., Ed.; Reidel: Dordrecht, The Netherlands, 1981.

(3.53) Essmann, U.; Perera, L.; Berkowitz, M. L.; Darden, T.; Lee, H.; Pedersen, L. G. A Smooth Particle Mesh Ewald Method. *J. Chem. Phys.* **1995,** *103*, 8577-8593.

(3.54) Miyamoto, S.; Kollman, P. A. Settle: An Analytical Version of the SHAKE and RATTLE Algorithm for Rigid Water Models. *J. Comput. Chem.* **1992,** *13*, 952-962.

(3.55) Hess, B. P-LINCS: A Parallel Linear Constraint Solver for Molecular Simulation. *J. Chem. Theory Comput.* **2008,** *4*, 116-122.

(3.56) van der Spoel, D.; van Maaren, P. J.; Berendsen, H. J. A Systematic Study of Water Models for Molecular Simulation: Derivation of Water Models Optimized for Use with a Reaction Field. *J. Chem. Phys.* **1998,** *108*, 10220-10230.

(3.57) Zielkiewicz, J. Structural Properties of Water: Comparison of the SPC, SPCE, TIP4P, and TIP5P Models of Water. *J. Chem. Phys.* **2005,** *123*, 104501.

(3.58) Humphrey, W.; Dalke, A.; Schulten, K. VMD: Visual Molecular Dynamics. *J. Mol. Graphics* **1996,** *14*, 33-38.

(3.59) Hunter, C. A.; Sanders, J. K. The Nature of $\pi - \pi$ Interactions. *J. Am. Chem. Soc.* **1990***, 112*, 5525-5534.

(3.60) Pisula, W.; Tomović, Ž; Simpson, C.; Kastler, M.; Pakula, T.; Müllen, K. Relationship between Core Size, Side Chain Length, and the Supramolecular Organization of Polycyclic Aromatic Hydrocarbons. *Chem. Mater.* **2005,** *17*, 4296-4303.

(3.61) Cussler, E. L. *Diffusion: Mass Transfer in Liquid Systems,* 2nd ed.; Cambridge University Press: Cambridge, U.K., 1997.

(3.62) Frenkel, D.; Smit, B. *Understanding Molecular Simulation: From Algorithms to Applications,*2nd ed.; Academic Press: San Diego, 2002.

(3.63) Balakrishnan, K.; Datar, A.; Naddo, T.; Huang, J.; Oitker, R.; Yen, M.; Zhao, J.; Zang, L. Effect of Side-Chain Substituents on Self-Assembly of Perylene Diimide Molecules: Morphology Control. *J. Am. Chem. Soc.* **2006,** *128*, 7390-7398.

(4.1) Spiecker, P. M.; Gawrys, K. L.; Kilpatrick, P. K. Aggregation and Solubility Behavior of Asphaltenes and Their Subfractions. *J. Colloid Interface Sci.* **2003,** *267*, 178-193.

(4.2) Ho, B.; Briggs, D. E. Small Angle X-ray Scattering from Coal-Derived Liquids. *Colloids Surf.* **1982,** *4*, 271-284.

(4.3) Ravey, J. C.; Ducouret, G.; Espinat, D. Asphaltene Macrostructure by Small Angle Neutron Scattering. *Fuel* **1988,** *67*, 1560-1567.

(4.4) Andersen, S. I.; Birdi, K. S. Aggregation of Asphaltenes as Determined by Calorimetry. *J. Colloid Interface Sci.* **1991,** *142*, 497-502.

(4.5) Anisimov, M. A.; Yudin, I. K.; Nikitin, V.; Nikolaenko, G.; Chernoutsan, A.; Toulhoat, H.; Frot, D.; Briolant, Y. Asphaltene Aggregation in Hydrocarbon Solutions Studied by Photon Correlation Spectroscopy. *J. Phys. Chem.* **1995,** *99*, 9576-9580.

(4.6) Sjöblom, J.; Aske, N.; Auflem, I. H.; Brandal, Ø.; Havre, T. E.; Sæther, Ø.; Westvik, A.; Johnsen, E. E.; Kallevik, H. Our Current Understanding of Water-in-Crude Oil Emulsions.: Recent Characterization Techniques and High Pressure Performance. *Adv. Colloid Interface Sci.* **2003,** *100-102*, 399-473.

(4.7) Lisitza, N. V.; Freed, D. E.; Sen, P. N.; Song, Y. Study of Asphaltene Nanoaggregation by Nuclear Magnetic Resonance (NMR). *Energy Fuels* **2009,** *23*, 1189-1193.

(4.8) Groenzin, H.; Mullins, O. C. Asphaltene Molecular Size and Structure. *J. Phys. Chem. A* **1999,** *103*, 11237-11245.

(4.9) Mansoori, G. A. Modeling of Asphaltene and Other Heavy Organic Depositions. *J. Pet. Sci. Eng.* **1997,** *17*, 101-111.

(4.10) Escobedo, J.; Mansoori, G. A. Heavy Organic Deposition and Plugging of Wells (Analysis of Mexico's Experience). Presented at the SPE Latin America Petroleum Engineering Conference, Caracas, Venezuela, March 8−11, **1992;** Paper SPE 23696.

(4.11) Kokal, S. L.; Sayegh, S. G. Asphaltenes: The Cholesterol of Petroleum. Presented at the SPE Middle East Oil Show, Bahrain, March 11−14, 1995; Paper SPE 29787.

(4.12) Ruiz-Morales, Y. HOMO−LUMO Gap as an Index of Molecular Size and Structure for Polycyclic Aromatic Hydrocarbons (PAHs) and Asphaltenes: A Theoretical Study. I. *J. Phys. Chem. A* **2002,** *106*, 11283-11308.

(4.13) Buenrostro-Gonzalez, E.; Groenzin, H.; Lira-Galeana, C.; Mullins, O. C. The Overriding Chemical Principles that Define Asphaltenes. *Energy Fuels* **2001,** *15*, 972-978.

(4.14) Dickie, J. P.; Yen, T. F. Macrostructures of the Asphaltic Fractions by Various Instrumental Methods. *Anal. Chem.* **1967,** *39*, 1847-1852.

(4.15) Yen, T. F. Structure of Petroleum Asphaltene and Its Significance. *Energy Sources* **1974,** *1*, 447-463.

(4.16) Murgich, J. Intermolecular Forces in Aggregates of Asphaltenes and Resins. *Pet. Sci. Technol.* **2002,** *20*, 983-997.

(4.17) Breure, B.; Subramanian, D.; Leys, J.; Peters, C. J.; Anisimov, M. A. Modeling Asphaltene Aggregation with a Single Compound. *Energy Fuels* **2012,** *27*, 172-176.

(4.18) Sharma, A.; Groenzin, H.; Tomita, A.; Mullins, O. C. Probing Order in Asphaltenes and Aromatic Ring Systems by HRTEM. *Energy Fuels* **2002,** *16*, 490-496.

(4.19) Tanaka, R.; Sato, E.; Hunt, J. E.; Winans, R. E.; Sato, S.; Takanohashi, T. Characterization of Asphaltene Aggregates Using X-ray Diffraction and Small-Angle X-ray Scattering. *Energy Fuels* **2004,** *18*, 1118-1125.

(4.20) Kuznicki, T.; Masliyah, J. H.; Bhattacharjee, S. Molecular Dynamics Study of Model Molecules Resembling Asphaltene-Like Structures in Aqueous Organic Solvent Systems. *Energy and Fuels* **2008,** *22*, 2379-2389.

(4.21) Headen, T. F.; Boek, E. S.; Skipper, N. T. Evidence for Asphaltene Nanoaggregation in Toluene and Heptane from Molecular Dynamics Simulations. *Energy and Fuels* **2009,** *23*, 1220-1229.

(4.22) Kuznicki, T.; Masliyah, J. H.; Bhattacharjee, S. Aggregation and Partitioning of Model Asphaltenes at Toluene−Water Interfaces: Molecular Dynamics Simulations. *Energy Fuels*

2009, *23*, 5027-5035.

(4.23) Teklebrhan, R. B.; Ge, L.; Bhattacharjee, S.; Xu, Z.; Sjöblom, J. Probing Structure–Nanoaggregation Relations of Polyaromatic Surfactants: A Molecular Dynamics Simulation and Dynamic Light Scattering Study. *J Phys. Chem. B* **2012,** *116*, 5907-5918.

(4.24) Boek, E. S.; Yakovlev, D. S.; Headen, T. F. Quantitative Molecular Representation of Asphaltenes and Molecular Dynamics Simulation of Their Aggregation. *Energy Fuels* **2009,** *23*, 1209-1219.

(4.25) Murgich, J.; Rodríguez, J.; Aray, Y. Molecular Recognition and Molecular Mechanics of Micelles of Some Model Asphaltenes and Resins. *Energy Fuels* **1996,** *10*, 68-76.

(4.26) Zhang, L.; Greendfield, M. L. Molecular Orientation in Model Asphalts Using Molecular Simulation. *Energy Fuels* **2007,** *21*, 1102-1111.

(4.27) Andreatta, G.; Goncalves, C. C.; Buffin, G.; Bostrom, N.; Quintella, C. M.; Arteaga-Larios, F.; Pérez, E.; Mullins, O. C. Nanoaggregates and Structure−Function Relations in Asphaltenes. *Energy Fuels* **2005,** *19*, 1282-1289.

(4.28) Zeng, H.; Song, Y. -.; Johnson, D. L.; Mullins, O. C. Critical Nanoaggregate Concentration of Asphaltenes by Direct-Current (DC) Electrical Conductivity. *Energy Fuels* **2009,** *23*, 1201-1208.

(4.29) Trejo, F.; Ancheyta, J.; Rana, M. S. Structural Characterization of Asphaltenes Obtained from Hydroprocessed Crude Oils by SEM and TEM. *Energy Fuels* **2009,** *23*, 429-439.

(4.30) Pacheco-Sánchez, J. H.; Álvarez-Ramírez, F.; Martínez-Magadán, J. M. Morphology of Aggregated Asphaltene Structural Models. *Energy Fuels* **2004,** *18*, 1676-1686.

(4.31) Takanohashi, T.; Sato, S.; Saito, I.; Tanaka, R. Molecular Dynamics Simulation of the Heat-Induced Relaxation of Asphaltene Aggregates. *Energy Fuels* **2003,** *17*, 135-139.

(4.32) Stachowiak, C.; Viguie, J. R.; Grolier, J. P. E.; Rogalski, M. Effect of n-Alkanes on Asphaltene Structuring in Petroleum Oils. *Langmuir* **2005***, 21*, 4824-4829.

(4.33) Yarranton, H. W.; Alboudwarej, H.; Jakher, R. Investigation of Asphaltene Association with Vapor Pressure Osmometry and Interfacial Tension Measurements. *Ind. Eng. Chem. Res.* **2000,** *39*, 2916-2924.

(4.34) Speight, J. G.; Long, R. B.; Trowbridge, T. D. Factors Iinfluencing the Separation of Asphaltenes from Heavy Petroleum Feedstocks. *Fuel* **1984,** *63*, 616-620.

(4.35) Murgich, J.; Merino-Garcia, D.; Andersen, S. I.; Manuel del Río, J.; Galeana, C. L. Molecular Mechanics and Microcalorimetric Investigations of the Effects of Molecular Water on the Aggregation of Asphaltenes in Solutions. *Langmuir* **2002,** *18*, 9080-9086.

(4.36) Andersen, S. I.; del Rio, J. M.; Khvostitchenko, D.; Shakir, S.; Lira-Galeana, C. Interaction and Solubilization of Water by Petroleum Asphaltenes in Organic Solution. *Langmuir.* **2001,** *17*, 307-313.

(4.37) Jian, C.; Tang, T.; Bhattacharjee, S. Probing the Effect of Side-Chain Length on the Aggregation of a Model Asphaltene Using Molecular Dynamics Simulations. *Energy Fuels* **2013,** *27*, 2057-2067.

(4.38) Wang, S.; Liu, J.; Zhang, L.; Masliyah, J.; Xu, Z. Interaction Forces between Asphaltene Surfaces in Organic Solvents. *Langmuir* **2009,** *26*, 183-190.

(4.39) Durand, E.; Clemancey, M.; Lancelin, J.; Verstraete, J.; Espinat, D.; Quoineaud, A. Effect of Chemical Composition on Asphaltenes Aggregation. *Energy Fuels* **2010,** *24*, 1051-1062.

(4.40) Andrews, A. B.; McClelland, A.; Korkeila, O.; Demidov, A.; Krummel, A.; Mullins, O. C.; Chen, Z. Molecular Orientation of Asphaltenes and PAH Model Compounds in Langmuir−Blodgett Films Using Sum Frequency Generation Spectroscopy. *Langmuir* **2011,**

27, 6049-6058.

(4.41) González, M. F.; Stull, C. S.; López-Linares, F.; Pereira-Almao, P. Comparing Asphaltene Adsorption with Model Heavy Molecules over Macroporous Solid Surfaces. *Energy Fuels* **2007,** *21*, 234-241.

(4.42) Jarne, C.; Cebolla, V. L.; Membrado, L.; Le Mapihan, K.; Giusti, P. High-Performance Thin-Layer Chromatography Using Automated Multiple Development for the Separation of Heavy Petroleum Products According to Their Number of Aromatic Rings. *Energy Fuels* **2011,** *25*, 4586-4594.

(4.43) Mullins, O. C.; Sabbah, H.; Eyssautier, J.; Pomerantz, A. E.; Barré, L.; Andrews, A. B.; Ruiz-Morales, Y.; Mostowfi, F.; McFarlane, R.; Goual, L, et al. Advances in Asphaltene Science and the Yen–Mullins Model. *Energy Fuels* **2012,** *26*, 3986-4003.

(4.44) Hess, B.; Kutzner, C.; van der Spoel, D.; Lindahl, E. GROMACS 4: Algorithms for Highly Efficient, Load-Balanced, and Scalable Molecular Simulation. *J. Chem. Theory Comput.* **2008,** *4*, 435-447.

(4.45) van der Spoel, D.; Lindahl, E.; Hess, B.; Groenhof, G.; Mark, A. E.; Berendsen, H. J. GROMACS: Fast, Flexible, and Free. *J. Comput. Chem.* **2005,** *26*, 1701-1718.

(4.46) Lindahl, E.; Hess, B.; van der Spoel, D. GROMACS 3.0: A Package for Molecular Simulation and Trajectory Analysis. *J. Mol. Model.* **2001,** *7*, 306-317.

(4.47) Berendsen, H. J.; van der Spoel, D.; van Drunen, R. GROMACS: A Message-Passing Parallel Molecular Dynamics Implementation. *Comput. Phys. Commun.* **1995,** *91*, 43-56.

(4.48) Oostenbrink, C.; Villa, A.; Mark, A. E.; Van Gunsteren, W. F. A Biomolecular Force Field Based on the Free Enthalpy of Hydration and Solvation: The GROMOS Force-Field Parameter Sets 53A5 and 53A6. *J. Comput. Chem.* **2004,** *25*, 1656-1676.

(4.49) Parrinello, M.; Rahman, A. Polymorphic Transitions in Single Crystals: A New Molecular Dynamics Method. *J. Appl. Phys.* **1981,** *52*, 7182-7190.

(4.50) Bussi, G.; Donadio, D.; Parrinello, M. Canonical Sampling through Velocity Rescaling. *J. Chem. Phys.* **2007,** 126, 014101.

(4.51) Evans, D. J.; Morriss, G. P. Non-Newtonian Molecular Dynamics. *Comput. Phys. Rep.* **1984,** *1*, 297-343.

(4.52) Essmann, U.; Perera, L.; Berkowitz, M. L.; Darden, T.; Lee, H.; Pedersen, L. G. A Smooth Particle Mesh Ewald Method. *J. Chem. Phys.* **1995,** *103*, 8577.

(4.53) Hess, B. P-LINCS: A Parallel Linear Constraint Solver for Molecular Simulation. *J. Chem. Theory Comput.* **2008,** *4*, 116-122.

(4.54) Humphrey, W.; Dalke, A.; Schulten, K. VMD: Visual Molecular Dynamics. *J. Mol. Graphics* **1996,** *14*, 33-38.

(4.55) Gravetter, F. J. *Essentials of Statistics for the Behavioral Sciences,* 7th ed.; Wadsworth, Cengage Learning: Belmont, CA, 2009.

(4.56) Allen, M. P.; Tildesley, D. J. *Computer Simulation of Liquids;* Oxford university press: New York, 1989.

(4.57) Pisula, W.; Tomovic, Z.; Simpson, C.; Kastler, M.; Pakula, T.; Müllen, K. Relationship between Core Size, Side Chain Length, and the Supramolecular Organization of Polycyclic Aromatic Hydrocarbons. *Chem. Mater.* **2005,** *17*, 4296-4303.

(4.58) Mullins, O. C. The Modified Yen Model. *Energy Fuels* **2010,** *24*, 2179-2207.

(4.59) Mullins, O. C. The Asphaltenes. *Annu. Rev. Anal. Chem.* **2011,** *4*, 393-418.

(4.60) Tan, X.; Fenniri, H.; Gray, M. R. Water Enhances the Aggregation of Model Asphaltenes in Solution via Hydrogen Bonding. *Energy Fuels* **2009,** *23*, 3687-3693.

(4.61) Aslan, S.; Firoozabadi, A. Effect of Water on Deposition, Aggregate Size, and Viscosity of Asphaltenes. *Langmuir* **2014,** *30*, 3658-3664.

(4.62) Gray, M. R.; Tykwinski, R. R.; Stryker, J. M.; Tan, X. Supramolecular Assembly Model for Aggregation of Petroleum Asphaltenes. *Energy Fuels* **2011,** *25*, 3125-3134.

(5.1) Vo-Dinh, T.; Fetzer, J.; Campiglia, A. Monitoring and Characterization of Polyaromatic Compounds in the Environment. *Talanta* **1998,** *47*, 943-969.

(5.2) Liu, Z.; Laha, S.; Luthy, R. G. Surfactant Solubilization of Polycyclic Aromatic Hydrocarbon Compounds in Soil-Water Suspensions. *Water Sci. Techol.* **1991,** *23, 475-485.*

(5.3) Hoeben, F. J.; Jonkheijm, P.; Meijer, E.; Schenning, A. P. About Supramolecular Assemblies of π-Conjugated Systems. *Chem. Rev.* **2005,** *105*, 1491-1546.

(5.4) Groenzin, H.; Mullins, O. C. Asphaltene Molecular Size and Structure. *J Phys. Chem. A* **1999,** *103*, 11237-11245.

(5.5) Hippius, C.; Schlosser, F.; Vysotsky, M. O.; Böhmer, V.; Würthner, F. Energy Transfer in Calixarene-Based Cofacial-Positioned Perylene Bisimide Arrays. *J. Am. Chem. Soc.* **2006,** *128*, 3870-3871.

(5.6) Wong, W. W.; Khoury, T.; Vak, D.; Yan, C.; Jones, D. J.; Crossley, M. J.; Holmes, A. B. A Porphyrin-hexa-*peri*-hexabenzocoronene-porphyrin Triad: Synthesis, Photophysical Properties and Performance in a Photovoltaic Device. *J. Mater. Chem.* **2010,** *20*, 7005-7014.

(5.7) Facchetti, A. π-Conjugated Polymers for Organic Electronics and Photovoltaic Cell Applications. *Chem. Mater.* **2010,** *23*, 733-758.

(5.8) Wong, W. W.; Singh, T. B.; Vak, D.; Pisula, W.; Yan, C.; Feng, X.; Williams, E. L.; Chan,

K. L.; Mao, Q.; Jones, D. J. Solution Processable Fluorenyl Hexa-peri-hexabenzocoronenes In Organic Field-Effect Transistors and Solar Cells. *Adv. Funct. Mater.* **2010,** *20*, 927-938.

(5.9) Mizoshita, N.; Tani, T.; Inagaki, S. Highly Conductive Organosilica Hybrid Films Prepared from a Liquid-Crystal Perylene Bisimide Precursor. *Adv. Funct. Mater.* **2011,** *21*, 3291-3296.

(5.10) Schmidt-Mende, L.; Fechtenkotter, A.; Mullen, K.; Moons, E.; Friend, R. H.; MacKenzie, J. D. Self-Organized Discotic Liquid Crystals for High-Efficiency Organic Photovoltaics. *Science* **2001,** *293*, 1119-1122.

(5.11) Díaz-García, M.; Calzado, E.; Villalvilla, J.; Boj, P.; Quintana, J.; Cespedes-Guirao, F.; Fernandez-Lazaro, F.; Sastre-Santos, A. Effect of Structural Modifications in the Laser Properties of Polymer Films Doped with Perylenebisimide Derivatives. *Synth. Met.* **2009,** *159*, 2293-2295.

(5.12) Choi, H.; Paek, S.; Song, J.; Kim, C.; Cho, N.; Ko, J. Synthesis of Annulated Thiophene Perylene Bisimide Analogues: Their Applications to Bulk Heterojunction Organic Solar Cells. *Chem. Commun.* **2011,** *47*, 5509-5511.

(5.13) Speight, J. Petroleum Asphaltenes-Part 1: Asphaltenes, Resins and the Structure of Petroleum. *Oil Gas Sci. Technol.* **2004,** *59*, 467-477.

(5.14) Spiecker, P. M.; Gawrys, K. L.; Trail, C. B.; Kilpatrick, P. K. Effects of Petroleum Resins on Asphaltene Aggregation and Water-in-Oil Emulsion Formation. *Colloids Surf., A* **2003,** *220*, 9-27.

(5.15) Kilpatrick, P. K. Water-in-Crude Oil Emulsion Stabilization: Review and Unanswered Questions. *Energy Fuels* **2012,** *26*, 4017-4026.

(5.16) Wang, C.; Dong, H.; Hu, W.; Liu, Y.; Zhu, D. Semiconducting π-Conjugated Systems in

Field-Effect Transistors: A Material Odyssey of Organic Electronics. *Chem. Rev.* **2011,** *112*, 2208-2267.

(5.17) Figueira-Duarte, T. M.; Müllen, K. Pyrene-Based Materials for Organic Electronics. *Chem. Rev.* **2011,** *111*, 7260-7314.

(5.18) Chen, Z.; Stepanenko, V.; Dehm, V.; Prins, P.; Siebbeles, L. D.; Seibt, J.; Marquetand, P.; Engel, V.; Würthner, F. Photoluminescence and Conductivity of Self-Assembled $\pi-\pi$ Stacks of Perylene Bisimide Dyes. *Chem.— Eur. J.* **2007***, 13*, 436-449.

(5.19) Würthner, F.; Chen, Z.; Dehm, V.; Stepanenko, V. One-Dimensional Luminescent Nanoaggregates of Perylene Bisimides. *Chem. Commun.* **2006,** 1188-1190.

(5.20) Yamamoto, T.; Fukushima, T.; Yamamoto, Y.; Kosaka, A.; Jin, W.; Ishii, N.; Aida, T. Stabilization of a Kinetically Favored Nanostructure: Surface ROMP of Self-Assembled Conductive Nanocoils from a Norbornene-Appended Hexa-*peri*-hexabenzocoronene. *J. Am. Chem. Soc.* **2006,** *128*, 14337-14340.

(5.21) Tan, X.; Fenniri, H.; Gray, M. R. Pyrene Derivatives of 2,2′-Bipyridine as Models for Asphaltenes: Synthesis, Characterization, and Supramolecular Organization. *Energy Fuels* **2007,** *22*, 715-720.

(5.22) Kuznicki, T.; Masliyah, J. H.; Bhattacharjee, S. Molecular Dynamics Study of Model Molecules Resembling Asphaltene-Like Structures in Aqueous Organic Solvent Systems. *Energy Fuels* **2008,** *22*, 2379-2389.

(5.23) Kuznicki, T.; Masliyah, J. H.; Bhattacharjee, S. Aggregation and Partitioning of Model Asphaltenes at Toluene−Water Interfaces: Molecular Dynamics Simulations. *Energy Fuels* **2009,** *23*, 5027-5035.

(5.24) Teklebrhan, R. B.; Ge, L.; Bhattacharjee, S.; Xu, Z.; Sjöblom, J. Probing Structure–

Nanoaggregation Relations of Polyaromatic Surfactants: A Molecular Dynamics Simulation and Dynamic Light Scattering Study. *J. Phys. Chem. B* **2012,** *116*, 5907-5918.

(5.25) Jian, C.; Tang, T.; Bhattacharjee, S. Probing the Effect of Side-Chain Length on the Aggregation of a Model Asphaltene Using Molecular Dynamics Simulations. *Energy Fuels* **2013,** *27*, 2057-2067.

(5.26) Headen, T. F.; Boek, E. S.; Skipper, N. T. Evidence for Asphaltene Nanoaggregation in Toluene and Heptane from Molecular Dynamics Simulations. *Energy Fuels* **2009,** *23*, 1220-1229.

(5.27) Jian, C.; Tang, T.; Bhattacharjee, S. Molecular Dynamics Investigation on the Aggregation of Violanthrone78-Based Model Asphaltenes in Toluene. *Energy Fuels* **2014,** *28,* 3604– 3613

(5.28) Liu, Y.; Li, Y.; Jiang, L.; Gan, H.; Liu, H.; Li, Y.; Zhuang, J.; Lu, F.; Zhu, D. Assembly and Characterization of Novel Hydrogen-Bond-Induced Nanoscale Rods. *J. Org. Chem.* **2004,** *69*, 9049-9054.

(5.29) Kastler, M.; Pisula, W.; Wasserfallen, D.; Pakula, T.; Müllen, K. Influence of Alkyl Substituents on the Solution- and Surface-Organization of Hexa-*peri*-hexabenzocoronenes. *J. Am. Chem. Soc.* **2005,** *127*, 4286-4296.

(5.30) Bunk, O.; Nielsen, M. M.; Sølling, T. I.; van de Craats, A. M; Stutzmann, N. Induced Alignment of a Solution-Cast Discotic Hexabenzocoronene Derivative for Electronic Devices Investigated by Surface X-ray Diffraction. *J. Am. Chem. Soc.* **2003,** *125*, 2252-2258.

(5.31) Bai, S.; Debnath, S.; Javid, N.; Frederix, P. W.; Fleming, S.; Pappas, C.; Ulijn, R. V. Differential Self-Assembly and Tunable Emission of Aromatic Peptide Bola-Amphiphiles

Containing Perylene Bisimide in Polar Solvents Including Water. *Langmuir* **2014,** *30*, 7576-7584.

(5.32) Su, W.; Zhang, Y.; Zhao, C.; Li, X.; Jiang, J. Self-Assembled Organic Nanostructures: Effect of Substituents on the Morphology. *ChemPhysChem* **2007,** *8*, 1857-1862.

(5.33) Pisula, W.; Feng, X.; Müllen, K. Tuning the Columnar Organization of Discotic Polycyclic Aromatic Hydrocarbons. *Adv. Mater.* **2010,** *22*, 3634-3649.

(5.34) Ameen, M. Y.; Abhijith, T.; De, S.; Ray, S.; Reddy, V. Linearly Polarized Emission from PTCDI-C_8 One-Dimensional Microstructures. *Org. Electron.* **2013,** *14*, 554-559.

(5.35) Islam, M. R.; Sundararajan, P. Self-Assembly of a Set of Hydrophilic–Solvophobic–Hydrophobic Coil–Rod–Coil Molecules Based on Perylene Diimide. *Phys. Chem. Chem. Phys.* **2013,** *15*, 21058-21069.

(5.36) Jang, K.; Kinyanjui, J. M.; Hatchett, D. W.; Lee, D. Morphological Control of One-Dimensional Nanostructures of T-Shaped Asymmetric Bisphenazine. *Chem. Mater.* **2009,** *21*, 2070-2076.

(5.37) Buckley, J.; Hirasaki, G.; Liu, Y.; Von Drasek, S.; Wang, J.; Gill, B. Asphaltene Precipitation and Solvent Properties of Crude Oils. *Pet. Sci. Technol.* **1998,** *16*, 251-285.

(5.38) Mullins, O. C. The Asphaltenes. *Annu. Rev. Anal. Chem.* **2011,** *4*, 393-418.

(5.39) Shi, M.; Chen, Y.; Nan, Y.; Ling, J.; Zuo, L.; Qiu, W.; Wang, M.; Chen, H. $\pi - \pi$ Interaction among Violanthrone Molecules: Observation, Enhancement, and Resulting Charge Transport Properties. *J. Phys. Chem. B* **2010,** *115*, 618-623.

(5.40) Shi, M.; Hao, F.; Zuo, L.; Chen, Y.; Nan, Y.; Chen, H. Effect of Substituents on the Aggregate Structure and Photovoltaic Property of Violanthrone Derivatives. *Dyes Pigm.* **2012,** *95*, 377-383.

(5.41) Buenrostro-Gonzalez, E.; Groenzin, H.; Lira-Galeana, C.; Mullins, O. C. The Overriding Chemical Principles that Define Asphaltenes. *Energy Fuels* **2001,** *15*, 972-978.

(5.42) Oostenbrink, C.; Villa, A.; Mark, A. E.; Van Gunsteren, W. F. A Biomolecular Force Field Based on the Free Enthalpy of Hydration and Solvation: The GROMOS Force-Field Parameter Sets 53A5 and 53A6. *J. Comput. Chem.* **2004,** *25*, 1656-1676.

(5.43) Hess, B.; Kutzner, C.; van der Spoel, D.; Lindahl, E. GROMACS 4: Algorithms for Highly Efficient, Load-Balanced, and Scalable Molecular Simulation. *J. Chem. Theory Comput.* **2008,** *4*, 435-447.

(5.44) van der Spoel, D.; Lindahl, E.; Hess, B.; Groenhof, G.; Mark, A. E.; Berendsen, H. J. GROMACS: Fast, Flexible, and Free. *J. Comput. Chem.* **2005,** *26*, 1701-1718.

(5.45) Lindahl, E.; Hess, B.; van der Spoel, D. GROMACS 3.0: A Package for Molecular Simulation and Trajectory Analysis. *J. Mol. Model.* **2001,** *7*, 306-317.

(5.46) Berendsen, H. J.; van der Spoel, D.; van Drunen, R. GROMACS: A Message-Passing Parallel Molecular Dynamics Implementation. *Comput. Phys. Commun.* **1995,** *91*, 43-56.

(5.47) Riddick, J. A.; Bunger, W. B.; Sakano, T. K. *Organic Solvents: Physical Properties and Methods of Purification,* 4th ed.; John Wiley & Sons Inc.: New York, 1986**.**

(5.48) Parrinello, M.; Rahman, A. Polymorphic Transitions in Single Crystals: A New Molecular Dynamics Method. *J. Appl. Phys.* **1981,** *52*, 7182-7190.

(5.49) Bussi, G.; Donadio, D.; Parrinello, M. Canonical Sampling through Velocity Rescaling. *J. Chem. Phys.* **2007,** 126, 014101.

(5.50) Evans, D. J.; Morriss, G. P. Non-Newtonian Molecular Dynamics. *Comput. Phys. Rep.* **1984,** *1*, 297-343.

(5.51) Hess, B. P-LINCS: A Parallel Linear Constraint Solver for Molecular Simulation. *J. Chem.*

Theory Comput. **2008,** *4*, 116-122.

(5.52) Essmann, U.; Perera, L.; Berkowitz, M. L.; Darden, T.; Lee, H.; Pedersen, L. G. A Smooth Particle Mesh Ewald Method. *J. Chem. Phys.* **1995,** *103*, 8577.

(5.53) van der Spoel, D.; Lindahl, E.; Hess, B.; van Buuren, A. R.; Apol, E.; Meulenhoff, P. J.; Tieleman, D. P.; Sijbers, A. L. T. M.; Feenstra, K. A.; van Drunen, R.; Berendsen, H. J. C. *Gromacs User Manua*l, version 4.0. http://www.gromacs.org (2005).

(5.54) Humphrey, W.; Dalke, A.; Schulten, K. VMD: Visual Molecular Dynamics. *J. Mol. Graphics* **1996,** *14*, 33-38.

(5.55) Meriam, J. L.; Kraige, L. G. *Engineering Mechanics: Dynamics*, 6th ed.; John Wiley & Sons Inc.: New York, 2007.

(5.56) Balakrishnan, K.; Datar, A.; Oitker, R.; Chen, H.; Zuo, J.; Zang, L. Nanobelt Self-Assembly from an Organic n-Type Semiconductor: Propoxyethyl-PTCDI. *J. Am. Chem. Soc.* **2005,** *127*, 10496-10497.

(5.57) Balakrishnan, K.; Datar, A.; Naddo, T.; Huang, J.; Oitker, R.; Yen, M.; Zhao, J.; Zang, L. Effect of Side-Chain Substituents on Self-Assembly of Perylene Diimide Molecules: Morphology Control. *J. Am. Chem. Soc.* **2006,** *128*, 7390-7398.

(5.58) Israelachvili, J. N. *Intermolecular and Surface Forces;* Academic Press: San Diego, CA, 2011.

(5.59) Zhang, X.; Chen, Z.; Würthner, F. Morphology Control of Fluorescent Nanoaggregates by Co-Self-Assembly of Wedge-and Dumbbell-Shaped Amphiphilic Perylene Bisimides. *J. Am. Chem. Soc.* **2007,** *129*, 4886-4887.

(5.60) Sedghi, M.; Goual, L.; Welch, W.; Kubelka, J. Effect of Asphaltene Structure on Association and Aggregation Using Molecular Dynamics. *J. Phys. Chem. B* **2013,** *117*,

5765-5776.

(5.61) Frigerio, F.; Molinari, D. A Multiscale Approach to the Simulation of Asphaltenes. *Comput. Theor. Chem.* **2011,** *975*, 76-82.

(6.1) Zang, L.; Che, Y.; Moore, J. S. One-Dimensional Self-Assembly of Planar π-Conjugated Molecules: Adaptable Building Blocks for Organic Nanodevices. *Acc. Chem. Res.* **2008,** *41*, 1596-1608.

(6.2) Groenzin, H.; Mullins, O. C. Asphaltene Molecular Size and Structure. *J. Phys. Chem. A* **1999,** *103*, 11237-11245.

(6.3) Kim, F. S.; Ren, G.; Jenekhe, S. A. One-Dimensional Nanostructures of π-Conjugated Molecular Systems: Assembly, Properties, and Applications from Photovoltaics, Sensors, and Nanophotonics to Nanoelectronics. *Chem. Mater.* **2010,** *23*, 682-732.

(6.4) Speight, J. Petroleum Asphaltenes-Part 1: Asphaltenes, Resins and the Structure of Petroleum. *Oil Gas Sci. Technol.* **2004,** *59*, 467-477.

(6.5) Spiecker, P. M.; Gawrys, K. L.; Trail, C. B.; Kilpatrick, P. K. Effects of Petroleum Resins on Asphaltene Aggregation and Water-in-Oil Emulsion Formation. *Colloids Surf., A* **2003,** *220*, 9-27.

(6.6) Kilpatrick, P. K. Water-in-Crude Oil Emulsion Stabilization: Review and Unanswered Questions. *Energy Fuels* **2012,** *26*, 4017-4026.

(6.7) Bai, S.; Debnath, S.; Javid, N.; Frederix, P. W.; Fleming, S.; Pappas, C.; Ulijn, R. V. Differential Self-Assembly and Tunable Emission of Aromatic Peptide Bola-Amphiphiles Containing Perylene Bisimide in Polar Solvents Including Water. *Langmuir* **2014,** *30*, 7576-7584.

(6.8) Su, W.; Zhang, Y.; Zhao, C.; Li, X.; Jiang, J. Self-Assembled Organic Nanostructures: Effect of Substituents on the Morphology. *ChemPhysChem* **2007,** *8*, 1857-1862.

(6.9) Pisula, W.; Feng, X.; Müllen, K. Tuning the Columnar Organization of Discotic Polycyclic Aromatic Hydrocarbons. *Adv. Mater.* **2010,** *22*, 3634-3649.

(6.10) Safont-Sempere, M. M.; Fernández, G.; Würthner, F. Self-Sorting Phenomena in Complex Supramolecular Systems. *Chem. Rev.* **2011,** *111*, 5784-5814.

(6.11) Ameen, M. Y.; Abhijith, T.; De, S.; Ray, S.; Reddy, V. Linearly Polarized Emission from PTCDI-C_8 One-Dimensional Microstructures. *Org. Electron.* **2013,** *14*, 554-559.

(6.12) Islam, M. R.; Sundararajan, P. Self-Assembly of a Set of Hydrophilic–Solvophobic Hydrophobic Coil–Rod–Coil Molecules Based on Perylene Diimide. *Phys. Chem. Chem. Phys.* **2013,** *15*, 21058-21069.

(6.13) Jang, K.; Kinyanjui, J. M.; Hatchett, D. W.; Lee, D. Morphological Control of One Dimensional Nanostructures of T-Shaped Asymmetric Bisphenazine. *Chem. Mater.* **2009,** *21*, 2070-2076.

(6.14) Wu, H.; Xue, L.; Shi, Y.; Chen, Y.; Li, X. Organogels Based on J- and H-Type Aggregates of Amphiphilic Perylenetetracarboxylic Diimides. *Langmuir* **2011,** *27*, 3074-3082.

(6.15) Verdier, S.; Carrier, H.; Andersen, S. I.; Daridon, J. Study of Pressure and Temperature Effects on Asphaltene Stability in Presence of CO_2. *Energy Fuels* **2006,** *20*, 1584-1590.

(6.16) Wang, C.; Dong, H.; Hu, W.; Liu, Y.; Zhu, D. Semiconducting π-Conjugated Systems in Field-Effect Transistors: A Material Odyssey of Organic Electronics. *Chem. Rev.* **2011,** *112*, 2208-2267.

(6.17) Figueira-Duarte, T. M.; Müllen, K. Pyrene-Based Materials for Organic Electronics. *Chem.*

Rev. **2011,** *111*, 7260-7314.

(6.18) Kuznicki, T.; Masliyah, J. H.; Bhattacharjee, S. Molecular Dynamics Study of Model Molecules Resembling Asphaltene-Like Structures in Aqueous Organic Solvent Systems. *Energy Fuels* **2008,** *22*, 2379-2389.

(6.19) Jian, C.; Tang, T.; Bhattacharjee, S. Probing the Effect of Side-Chain Length on the Aggregation of a Model Asphaltene Using Molecular Dynamics Simulations. *Energy Fuels* **2013,** *27*, 2057-2067.

(6.20) Jian, C.; Tang, T.; Bhattacharjee, S. Molecular Dynamics Investigation on the Aggregation of Violanthrone78-Based Model Asphaltenes in Toluene. *Energy Fuels* **2014,** *28*, 3604-3613.

(6.21) Jian, C.; Tang, T. One-Dimensional Self-Assembly of Polyaromatic Compounds Revealed by Molecular Dynamics Simulations. *J. Phys. Chem. B* **2014,** *118*, 12772–12780.

(6.22) Balakrishnan, K.; Datar, A.; Oitker, R.; Chen, H.; Zuo, J.; Zang, L. Nanobelt Self-Assembly from an Organic n-Type Semiconductor: Propoxyethyl-PTCDI. *J. Am. Chem. Soc.* **2005,** *127*, 10496-10497.

(6.23) Balakrishnan, K.; Datar, A.; Naddo, T.; Huang, J.; Oitker, R.; Yen, M.; Zhao, J.; Zang, L. Effect of Side-Chain Substituents on Self-Assembly of Perylene Diimide Molecules: Morphology Control. *J. Am. Chem. Soc.* **2006,** *128*, 7390-7398.

(6.24) Datar, A.; Balakrishnan, K.; Zang, L. One-Dimensional Self-Assembly of a Water Soluble Perylene Diimide Molecule by pH Triggered Hydrogelation. *Chem. Commun.* **2013,** *49*, 6894-6896.

(6.25) Che, Y.; Datar, A.; Balakrishnan, K.; Zang, L. Ultralong Nanobelts Self-Assembled from an Asymmetric Perylene Tetracarboxylic Diimide. *J. Am. Chem. Soc.* **2007,** *129*, 7234-

7235.

(6.26) Klein, G. C.; Kim, S.; Rodgers, R. P.; Marshall, A. G.; Yen, A.; Asomaning, S. Mass Spectral Analysis of Asphaltenes. I. Compositional Differences between Pressure-Drop and Solvent-Drop Asphaltenes Determined by Electrospray Ionization Fourier Transform Ion Cyclotron Resonance Mass Spectrometry. *Energy Fuels* **2006,** *20*, 1965-1972.

(6.27) Klein, G. C.; Kim, S.; Rodgers, R. P.; Marshall, A. G.; Yen, A. Mass Spectral Analysis of Asphaltenes. II. Detailed Compositional Comparison of Asphaltenes Deposit to Its Crude Oil Counterpart for Two Geographically Different Crude Oils by ESI FT-ICR MS. *Energy Fuels* **2006,** *20*, 1973-1979.

(6.28) Ryan, D. M.; Doran, T. M.; Nilsson, B. L. Complementary π– π Interactions Induce Multicomponent Coassembly into Functional Fibrils. *Langmuir* **2011,** *27*, 11145-11156.

(6.29) Sakai, H.; Watanabe, K.; Asanomi, Y.; Kobayashi, Y.; Chuman, Y.; Shi, L.; Masuda, T.; Wyttenbach, T.; Bowers, M. T.; Uosaki, K. Formation of Functionalized Nanowires by Control of Self-Assembly Using Multiple Modified Amyloid Peptides. *Adv. Funct. Mater.* **2013,** *23*, 4881-4887.

(6.30) Bu, L.; Pentzer, E.; Bokel, F. A.; Emrick, T.; Hayward, R. C. Growth of Polythiophene/Perylene Tetracarboxydiimide Donor/Acceptor Shish-Kebab Nanostructures by Coupled Crystal Modification. *ACS Nano* **2012,** *6*, 10924-10929.

(6.31) Bu, L.; Dawson, T. J.; Hayward, R. C. Tailoring Ultrasound-Induced Growth of Perylene Diimide Nanowire Crystals from Solution by Modification with Poly (3-hexyl thiophene). *ACS Nano* **2015,** *9*, 1878-1885.

(6.32) Zhang, S.; Sun, L. L.; Xu, J.; Wu, H.; Wen, H. Aggregate Structure in Heavy Crude Oil: Using a Dissipative Particle Dynamics Based Mesoscale Platform. *Energy Fuels* **2010,** *24*,

4312-4326.

(6.33) Zhang, S.; Xu, J.; Wen, H.; Bhattacharjee, S. Integration of Rotational Algorithms into Dissipative Particle Dynamics: Modeling Polyaromatic Hydrocarbons on the Meso-Scale. *Mol. Phys.* **2011,** *109*, 1873-1888.

(6.34) Zhang, L.; Greenfield, M. L. Molecular Orientation in Model Asphalts using Molecular Simulation. *Energy Fuels* **2007,** *21*, 1102-1111.

(6.35) Ortega-Rodriguez, A.; Lira-Galeana, C.; Ruiz-Morales, Y.; Cruz, S. A. Interaction Energy in Maya-Oil Asphaltenes: A Molecular Mechanics Study. *Petrol. Sci. Technol.* **2001,** *19*, 245-256.

(6.36) Takanohashi, T.; Sato, S.; Saito, I.; Tanaka, R. Molecular Dynamics Simulation of the Heat-Induced Relaxation of Asphaltene Aggregates. *Energy Fuels* **2003,** *17*, 135-139.

(6.37) Aguilera-Mercado, B.; Herdes, C.; Murgich, J.; Müller, E. Mesoscopic Simulation of Aggregation of Asphaltene and Resin Molecules in Crude Oils. *Energy Fuels* **2006,** *20*, 327-338.

(6.38) Ortega-Rodríguez, A.; Cruz, S. A.; Gil-Villegas, A.; Guevara-Rodriguez, F.; Lira-Galeana, C. Molecular View of the Asphaltene Aggregation Behavior in Asphaltene-Resin Mixtures. *Energy Fuels* **2003,** *17*, 1100-1108.

(6.39) Oostenbrink, C.; Villa, A.; Mark, A. E.; Van Gunsteren, W. F. A Biomolecular Force Field Based on the Free Enthalpy of Hydration and Solvation: The GROMOS Force-Field Parameter Sets 53A5 and 53A6. *J. Comput. Chem.* **2004,** *25*, 1656-1676.

(6.40) Jian, C.; Tang, T.; Bhattacharjee, S. A Dimension Map for Molecular Aggregates. *J. Mol. Graphics Modell.* **2015,** *58*, 10-15.

(6.41) Hess, B.; Kutzner, C.; van der Spoel, D.; Lindahl, E. GROMACS 4: Algorithms for

Highly Efficient, Load-Balanced, and Scalable Molecular Simulation. *J. Chem. Theory Comput.* **2008,** *4*, 435-447.

(6.42) van der Spoel, D.; Lindahl, E.; Hess, B.; Groenhof, G.; Mark, A. E.; Berendsen, H. J. GROMACS: Fast, Flexible, and Free. *J. Comput. Chem.* **2005,** *26*, 1701-1718.

(6.43) Lindahl, E.; Hess, B.; van der Spoel, D. GROMACS 3.0: A Package for Molecular Simulation and Trajectory Analysis. *J. Mol. Model.* **2001**, *7*, 306-317.

(6.44) Berendsen, H. J.; van der Spoel, D.; van Drunen, R. GROMACS: A Message-Passing Parallel Molecular Dynamics Implementation. *Comput. Phys. Commun.* **1995,** *91*, 43-56.

(6.45) Essmann, U.; Perera, L.; Berkowitz, M. L.; Darden, T.; Lee, H.; Pedersen, L. G. A Smooth Particle Mesh Ewald Method. *J. Chem. Phys.* **1995,** *103*, 8577.

(6.46) Hess, B. P-LINCS: A Parallel Linear Constraint Solver for Molecular Simulation. *J. Chem. Theory Comput.* **2008,** *4*, 116-122.

(6.47) Sugita, Y.; Okamoto, Y. Replica-Exchange Molecular Dynamics Method for Protein Folding. *Chem. Phys. Lett.* **1999,** *314*, 141-151.

(6.48) Humphrey, W.; Dalke, A.; Schulten, K. VMD: Visual Molecular Dynamics. *J. Mol. Graphics* **1996,** *14*, 33-38.

(6.49) Sugita, Y.; Kitao, A.; Okamoto, Y. Multidimensional Replica-Exchange Method for Free Energy Calculations. *J. Chem. Phys.* **2000,** *113*, 6042-6051.

(6.50) Yu, T.; Schatz, G. C. Free-Energy Landscape for Peptide Amphiphile Self-Assembly: Stepwise versus Continuous Assembly Mechanisms. *J. Phys. Chem. B* **2013,** *117*, 14059-14064.

(6.51) Buenrostro-Gonzalez, E.; Groenzin, H.; Lira-Galeana, C.; Mullins, O. C. The Overriding Chemical Principles That Define Asphaltenes. *Energy Fuels* **2001,** *15*, 972-978.

(6.52) Mullins, O. C.; Sabbah, H.; Eyssautier, J.; Pomerantz, A. E.; Barre, L.; Andrews, A. B.; Ruiz-Morales, Y.; Mostowfi, F.; McFarlane, R.; Goual, L., et al. Advances in Asphaltene Science and the Yen–Mullins Model. *Energy Fuels* **2012,** *26*, 3986-4003.

(6.53) Mullins, O. C. The Modified Yen Model. *Energy Fuels* **2010,** *24*, 2179-2207.

(6.54) Mullins, O. C. The Asphaltenes. *Annu. Rev. Anal. Chem.* **2011,** *4*, 393-418.

(6.55) Pisula, W.; Tomovic, Z.; Simpson, C.; Kastler, M.; Pakula, T.; Müllen, K. Relationship between Core Size, Side Chain Length, and the Supramolecular Organization of Polycyclic Aromatic Hydrocarbons. *Chem. Mater.* **2005,** *17*, 4296-4303.

(6.56) Headen, T. F.; Boek, E. S.; Skipper, N. T. Evidence for Asphaltene Nanoaggregation in Toluene and Heptane from Molecular Dynamics Simulations. *Energy Fuels* **2009,** *23*, 1220-1229.

(6.57) Sedghi, M.; Goual, L.; Welch, W.; Kubelka, J. Effect of Asphaltene Structure on Association and Aggregation Using Molecular Dynamics. *J. Phys. Chem. B* **2013,** *117*, 5765-5776.

(6.58) Speight, J. G.; Long, R. B.; Trowbridge, T. D. Factors Influencing the Separation of Asphaltenes from Heavy Petroleum Feedstocks. *Fuel* **1984,** *63*, 616-620.

(7.1) Wu, C.; Lei, H.; Duan, Y. Elongation of Ordered Peptide Aggregate of an Amyloidogenic Hexapeptide NFGAIL Observed in Molecular Dynamics Simulations with Explicit Solvent. *J. Am. Chem. Soc.* **2005,** *127*, 13530-13537.

(7.2) Marrink, S. J.; Lindahl, E.; Edholm, O.; Mark, A. E. Simulation of the Spontaneous Aggregation of Phospholipids into Bilayers. *J. Am. Chem. Soc.* **2001,** *123*, 8638-8639.

(7.3) Balakrishnan, K.; Datar, A.; Oitker, R.; Chen, H.; Zuo, J.; Zang, L. Nanobelt Self-

Assembly from an Organic n-Type Semiconductor: Propoxyethyl-PTCDI. *J. Am. Chem. Soc.* **2005,** *127*, 10496-10497.

(7.4) Balakrishnan, K.; Datar, A.; Naddo, T.; Huang, J.; Oitker, R.; Yen, M.; Zhao, J.; Zang, L. Effect of Side-Chain Substituents on Self-Assembly of Perylene Diimide Molecules: Morphology Control. *J. Am. Chem. Soc.* **2006,** *128*, 7390-7398.

(7.5) Speight, J. G. *The Chemistry and Technology of Petroleum,* 4th ed.; CRC Press: Boca Raton, 2006.

(7.6) Sangwai, A. V.; Sureshkumar, R. Coarse-Grained Molecular Dynamics Simulations of the Sphere to Rod Transition in Surfactant Micelles. *Langmuir* **2011,** *27*, 6628-6638.

(7.7) Velinova, M.; Sengupta, D.; Tadjer, A. V.; Marrink, S. Sphere-to-Rod Transitions of Nonionic Surfactant Micelles in Aqueous Solution Modeled by Molecular Dynamics Simulations. *Langmuir* **2011,** *27*, 14071-14077.

(7.8) Liu, Z.; Shang, Y.; Feng, J.; Peng, C.; Liu, H.; Hu, Y. Effect of Hydrophilicity or Hydrophobicity of Polyelectrolyte on the Interaction between Polyelectrolyte and Surfactants: Molecular Dynamics Simulations. *J. Phys. Chem. B* **2012,** *116*, 5516-5526.

(7.9) Benjwal, S.; Verma, S.; Röhm, K.; Gursky, O. Monitoring Protein Aggregation during Thermal Unfolding in Circular Dichroism Experiments. *Protein Sci.* **2006,** *15*, 635-639.

(7.10) Törnblom, M.; Henriksson, U. Effect of Solubilization of Aliphatic Hydrocarbons on Size and Shape of Rodlike C_{16}TABr Micelles Studied by ^{2}H NMR Relaxation. *J. Phys. Chem. B* **1997,** *101*, 6028-6035.

(7.11) Porte, G.; Marignan, J.; Bassereau, P.; May, R. Shape Transformations of the Aggregates in Dilute Surfactant Solutions : A Small-Angle Neutron Scattering Study. *J. Phys.* **1988,** *49*, 511-519.

(7.12) Israelachvili, J. N.; Mitchell, D. J.; Ninham, B. W. Theory of Self-Assembly of Hydrocarbon Amphiphiles into Micelles and Bilayers. *J. Chem. Soc., Faraday Trans.2* **1976,** *72*, 1525-1568.

(7.13) Breure, B.; Subramanian, D.; Leys, J.; Peters, C. J.; Anisimov, M. A. Modeling Asphaltene Aggregation with a Single Compound. *Energy Fuels* **2012,** *27*, 172-176.

(7.14) Speight, J. G.; Long, R. B.; Trowbridge, T. D. Factors Influencing the Separation of Asphaltenes from Heavy Petroleum Feedstocks. *Fuel* **1984,** *63*, 616-620.

(7.15) Groenzin, H.; Mullins, O. C. Asphaltene Molecular Size and Structure. *J. Phys. Chem. A* **1999,** *103*, 11237-11245.

(7.16) Yarranton, H. W.; Alboudwarej, H.; Jakher, R. Investigation of Asphaltene Association with Vapor Pressure Osmometry and Interfacial Tension Measurements. *Ind. Eng. Chem. Res.* **2000,** *39*, 2916-2924.

(7.17) Headen, T. F.; Boek, E. S.; Skipper, N. T. Evidence for Asphaltene Nanoaggregation in Toluene and Heptane from Molecular Dynamics Simulations. *Energy Fuels* **2009,** *23*, 1220-1229.

(7.18) Jian, C.; Tang, T.; Bhattacharjee, S. Probing the Effect of Side-Chain Length on the Aggregation of a Model Asphaltene Using Molecular Dynamics Simulations. *Energy Fuels* **2013,** *27*, 2057-2067.

(7.19) Andrews, A. B.; McClelland, A.; Korkeila, O.; Demidov, A.; Krummel, A.; Mullins, O. C.; Chen, Z. Molecular Orientation of Asphaltenes and PAH Model Compounds in Langmuir−Blodgett Films Using Sum Frequency Generation Spectroscopy. *Langmuir* **2011,** *27*, 6049-6058.

(7.20) Hess, B.; Kutzner, C.; van der Spoel, D.; Lindahl, E. GROMACS 4: Algorithms for

Highly Efficient, Load-Balanced, and Scalable Molecular Simulation *J. Chem. Theory Comput.* **2008,** *4*, 435-447.

(7.21) van der Spoel, D.; Lindahl, E.; Hess, B.; Groenhof, G.; Mark, A. E.; Berendsen, H. J. GROMACS: Fast, Flexible, and Free. *J. Comput. Chem.* **2005,** *26*, 1701-1718.

(7.22) Lindahl, E.; Hess, B.; van der Spoel, D. GROMACS 3.0: A Package for Molecular Simulation and Trajectory Analysis. *Mol. Model.* **2001,** *7*, 306-317.

(7.23) Berendsen, H. J.; van der Spoel, D.; van Drunen, R. GROMACS: A Message-Passing Parallel Molecular Dynamics Implementation. *Comput. Phys. Commun.* **1995,** *91*, 43-56.

(7.24) Oostenbrink, C.; Villa, A.; Mark, A. E.; Van Gunsteren, W. F. A Biomolecular Force Field Based on the Free Enthalpy of Hydration and Solvation: The GROMOS Force-Field Parameter Sets 53A5 and 53A6. *J. Comput. Chem.* **2004,** *25*, 1656-1676.

(7.25) Rigo, P. Roll Motion of a Floating Storm Surge Barrier. *J. Hydrosci. Hydr. Eng.* **1992,** *10*, 27-36.

(7.26) Allen III, J. H. *Mechanics of Materials for Dummies;* Wiley Publishing, Inc.: Hoboken, 2011.

(7.27) Meriam, J. L.; Kraige, L. G. *Engineering Mechanics: Dynamics,* 6th ed.; John Wiley & Sons Inc.: New York 2007.

(7.28) Wittenburg, J. *Dynamics of Multibody Systems;* Springer: Berlin, 2007.

(7.29) Pytel, A.; Kiusalaas, J. *Engineering Mechanics: Dynamics,* 3rd ed.; Cengage Learning: Stamford, 2010.

(7.30) Dickie, J. P.; Yen, T. F. Macrostructures of the Asphaltic Fractions by Various Instrumental Methods. *Anal. Chem.* **1967,** *39*, 1847-1852.

(7.31) Yen, T. Structure of Petroleum Asphaltene and Its Significance. *Energy Sources* **1974,** *1*, 447-463.

(7.32) Murgich, J. Intermolecular Forces in Aggregates Of Asphaltenes and Resins. *Pet. Sci. Technol.* **2002,** *20*, 983-997.

(7.33) Israelachvili, J. N. *Intermolecular and Surface Forces; Academic Press: San Diego, CA, 2011.*

(7.34) Jian, C.; Tang, T.; Bhattacharjee, S. Molecular Dynamics Investigation on the Aggregation of Violanthrone78-Based Model Asphaltenes in Toluene. *Energy Fuels* **2014,** *28*, 3604-3613.

(7.35) Jian, C.; Tang, T. One-Dimensional Self-Assembly of Polyaromatic Compounds Revealed by Molecular Dynamics Simulations. *J. Phys. Chem. B* **2014,** *118,* 12772–12780.

(7.36) Kraitchman, J. Determination of Molecular Structure from Microwave Spectroscopic Data. *Am. J. Phys.* **1953,** *21*, 17-25.

(7.37) Gupta, M. C. *Atomic and Molecular Spectroscopy;* New Age International (P) Ltd.: New Delhi, 2007.

(7.38) Rudnick, J.; Gaspari, G. The Asphericity of Random Walks. *J. Phys. A: Math. Gen.* **1986,** *19*, L191-L193.

(7.39) Maurstad, G.; Danielsen, S.; Stokke, B. T. Analysis of Compacted Semiflexible Polyanions Visualized by Atomic Force Microscopy: Influence of Chain Stiffness on the Morphologies of Polyelectrolyte Complexes. *J. Phys. Chem. B* **2003,** *107*, 8172-8180.

Appendix A: Supporting Information for Chapter 3

A.1. Initial configurations for the four systems

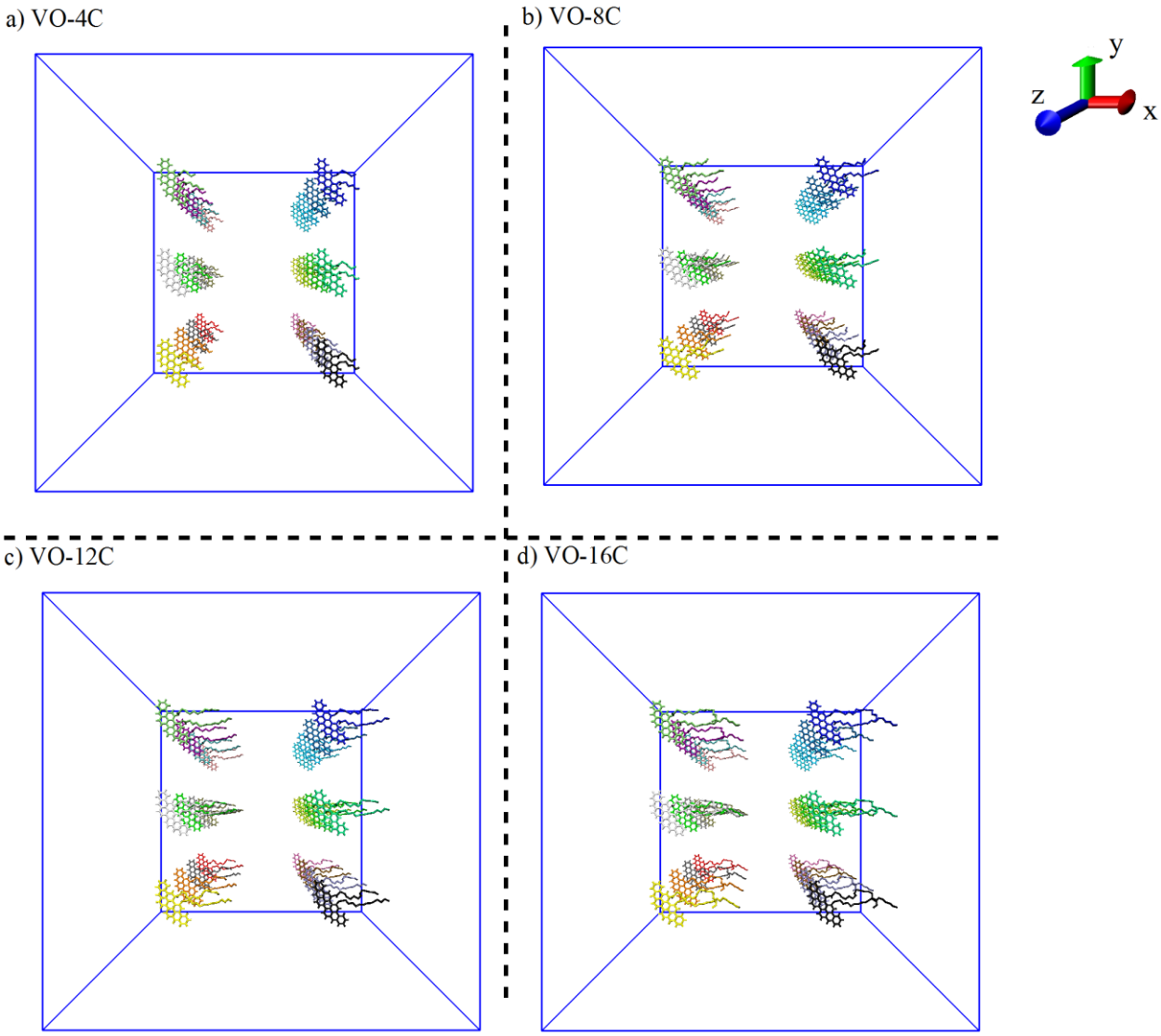

Figure A.1: Initial configurations for the four systems. The blue lines show the simulation box. For clarity, water molecules are not shown. The 24 asphaltene molecules in each system form a $2 \times 3 \times 4$ array (see section 3.2.1 in Chapter 3).

A.2. Details on the development of asphaltene topology

The topologies for the asphaltene model molecules were developed based on the default topology obtained from GlycoBioChem PRODRG2 server.[1] Bonded parameters for each atom were kept unchanged while the partial charges were manually modified according to similar functional groups in GROMOS96 force field parameter set 53A6.[2] The partial charges for united aliphatic carbons and ester groups in the side chains, aromatic carbons as well as hydrogens in the PA cores, and ketone groups in the PA cores were respectively adopted from existing parameters for analogue atom groups in residues dipalmitoylphosphatidylcholine (DPPC), phenylalanine (Phe) and peptide bond. All van der Waals parameters in the topologies were also adopted from GROMOS96 force field parameter set 53A6.

The reason why the partial charges were changed from the default values generated using PRODRG is that it has been reported in literature[3] that the default partial charges from PRODRG can lead to unphysical results. On the contrary, using analogous functional group existing in GROMOS96 force field has proven to be a more reliable approach.[3] To test this for our systems, we performed two simulations using two different topologies: (i) the default topology generated by PRODRG with van der Waals parameters adopted from the GROMOS96 force field parameter set 43A1 (this simulation will be referred to as the PRODRG simulation);[4] and (ii) the topology with partial charged adjusted and van der Waals parameters adopted from the GROMOS96 force field parameter set 53A6 (this simulation will be referred to as the 53A6 simulation). Different van der Waals parameters were used in the two simulations because the default topology obtained from PRODRG was designed to be consistent with parameter set 43A1.[3] The van der Waals parameters in parameter set 53A6 were re-parameterized to reproduce the free energy of hydration in conjunction with SPC water model,[2] and are more suitable when

the partial charges are derived from parameter set 53A6. For each of these two simulations, 8 asphaltene model molecules of VO-16C type were contained in a cubic box with an edge dimension of 6 nm and the total simulation time for the production stage was 20 ns. The rest of the simulation procedure was the same as that described in Chapter 3.

As shown in Figures A.2a and b, we found that aliphatic side chains can lie between parallel PA cores in the PRODRG simulation, which causes the mean separation between neighboring parallel PA cores to be ~ 0.7 nm. This is almost twice the expected separation for $\pi - \pi$ stacking (~0.35 nm).[5] This unphysical phenomenon can be attributed to the unreasonable charges assigned by PRODRG, which results in large electrostatic attraction between the aliphatic side chains and the PA cores. When the partial charges are adjusted in the 53A6 simulation, as shown in Figures A.2c and d, the PA cores form parallel pairs without side chains lying between them and the mean separation is ~0.35 nm, as expected for $\pi - \pi$ stacking.[5] Therefore, it is confirmed that the use of the default partial charges from PRODRG is problematic, and they should be adjusted to be more compatible with the GROMOS96 force field.

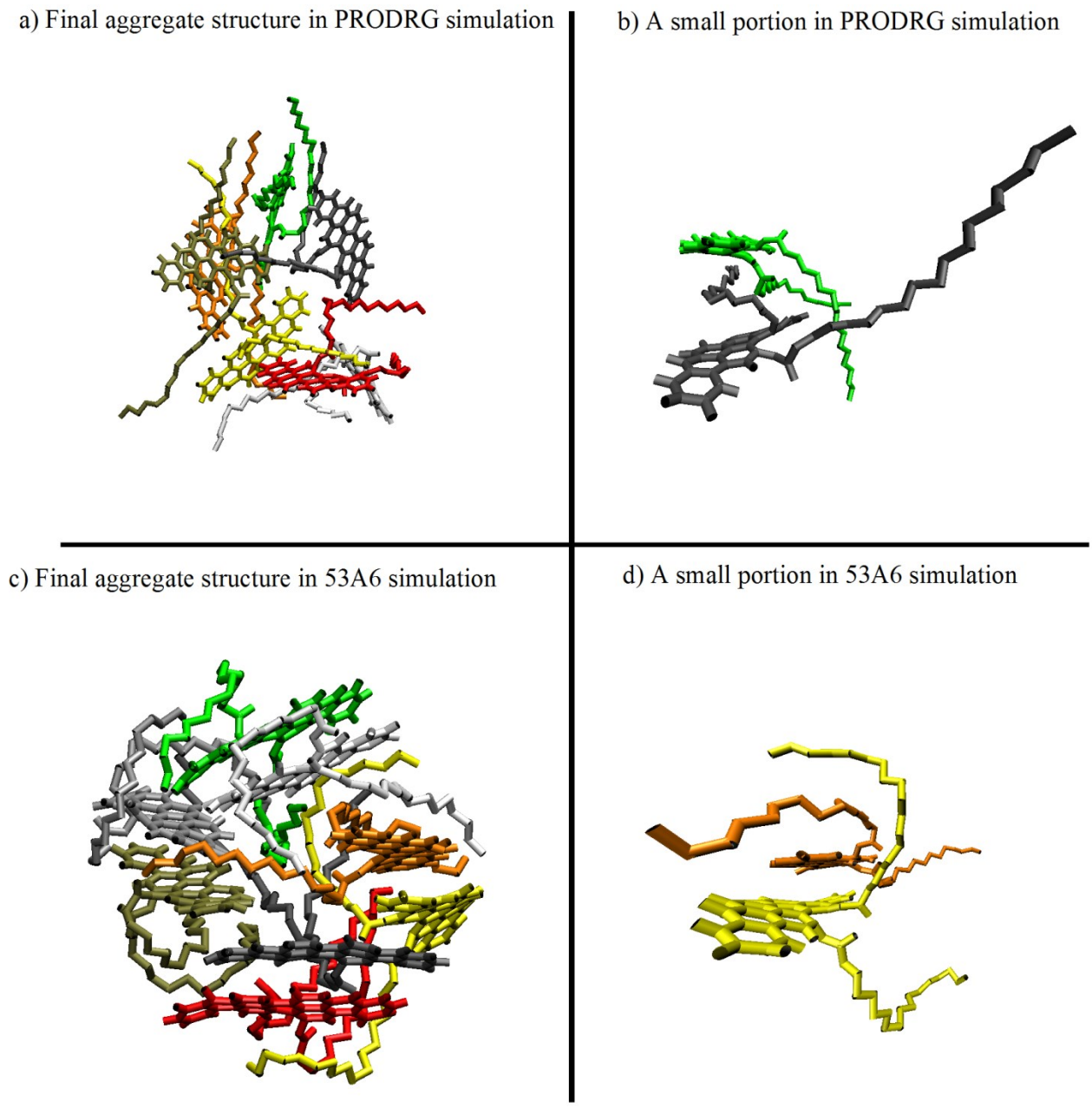

Figure A.2: Snapshots from the final stage of the simulations. (a) and (c) show the final aggregate structures in the two simulations; (b) and (d) show the parallel pairs formed by asphaltene model molecules. It can be clearly seen that the side chain can lie between parallel PA cores in PRODRG simulation, which is unphysical.

A.3. Representations of the PA plane, PA core group and aliphatic side-chain group

Figure A.3 shows representation of the PA plane for the calculations of COG distance and cosine of angle ($\cos\sigma$) between two PA cores (see section 3.2.3 in Chapter 3). Three carbon atoms marked by the three black circles were used to define the plane that approximates the PA core.

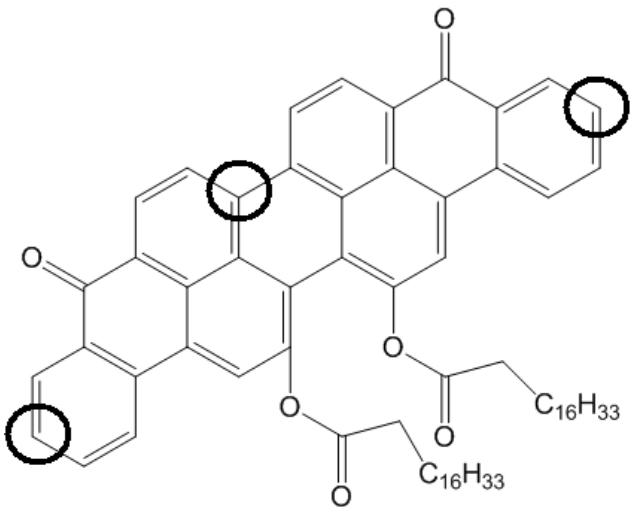

Figure A.3: PA plane representation (illustrated for VO-16C).

Figure A.4 shows the definition of PA core group and aliphatic side-chain group for the calculations of MIN distance between the two groups (see section 3.2.3 in Chapter 3). The top left box contains the atoms that belong to the PA core group and the bottom right box contains the atoms that belong to the aliphatic side-chain group. To calculate the MIN distance between the two groups, the distances between any one atom from one group and any one atom from the other group were calculated, and the minimum of those distances was defined as the MIN distance between the corresponding two groups. It should be mentioned that only the coordinates of the heavy atoms (i.e. carbon and oxygen atoms) were considered in the MIN distance calculations.

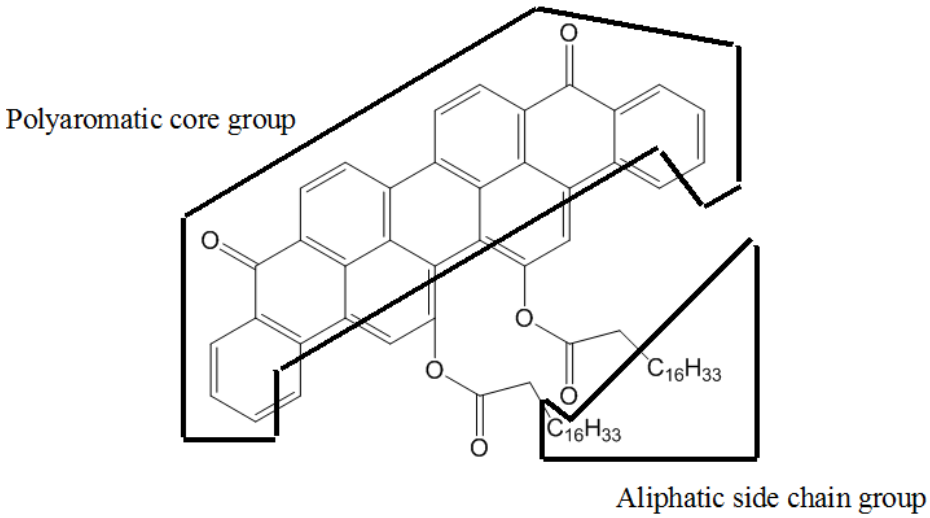

Figure A.4: Definitions of PA core group and aliphatic side-chain group (illustrated for VO-16C).

A.4. MIN distance between adjacent PA cores that become parallel at the final stage of the simulations

Figure A.5 shows the MIN distance between adjacent PA cores that become parallel at the final stage of the simulations. The MIN distance is plotted as a function of simulation time, and the four subfigures are respectively for the four simulated systems. Each subfigure contains different curves, each of which describes the MIN distance between a pair of adjacent PA cores that become parallel at the final stage of the simulations. The explanation for these figures is given in Chapter 3 (see section 3.3.1).

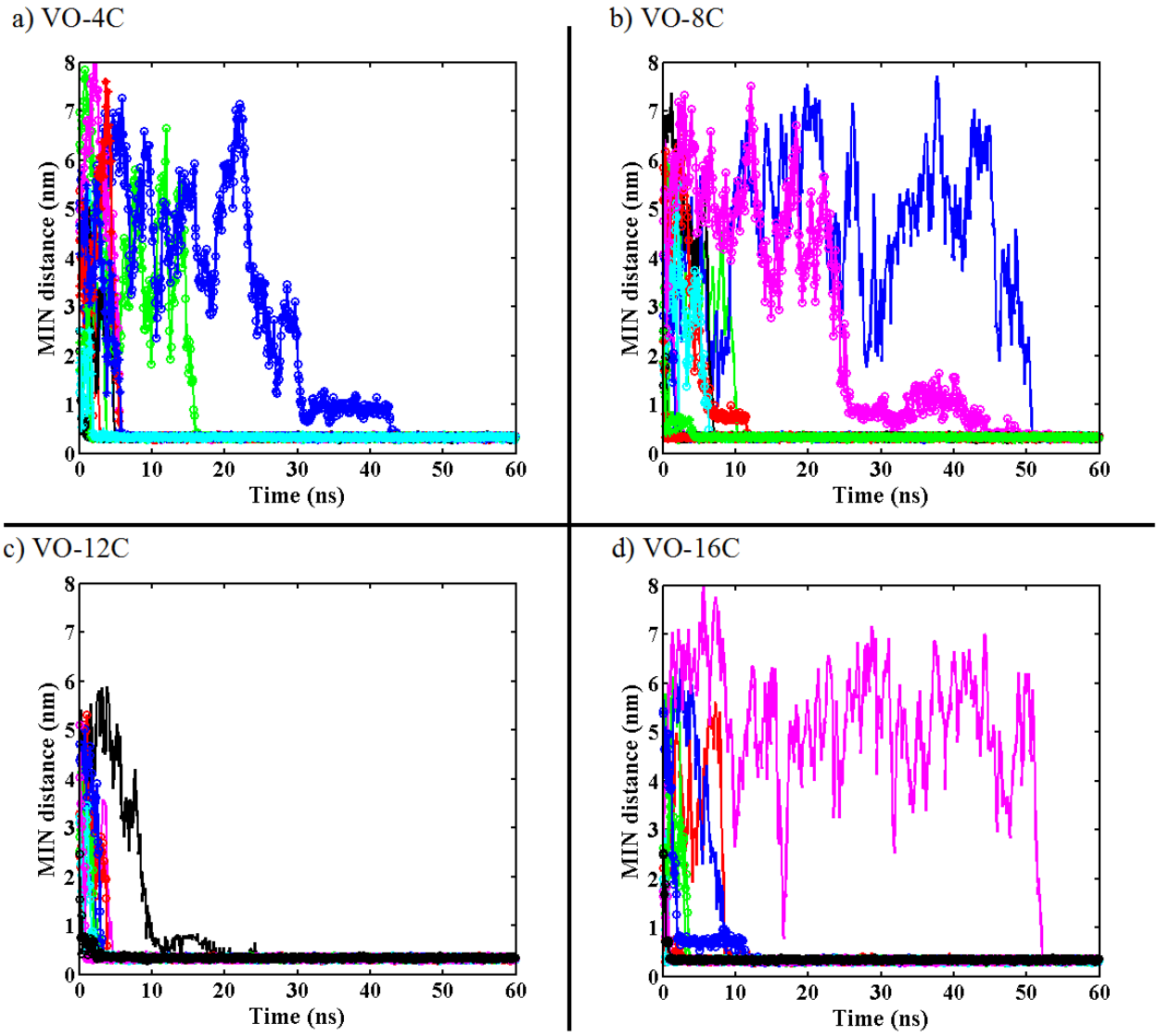

Figure A.5: MIN distance between adjacent PA cores that become parallel at the final stage of the simulations. The MIN distance is plotted as a function of simulation time, and each subfigure is for one of the four simulated systems.

A.5. PDF of $cos\,\sigma$ at COG separation > 0.75 nm

Figures A.6-A.11 shows the PDF of $cos\,\sigma$ of PA cores at COG separation > 0.75 nm for the four systems. The COG separations chosen here correspond to the locations of peaks in the RDF curves of PA cores (see Figure 3.5 in section 3.3.3 of Chapter 3).

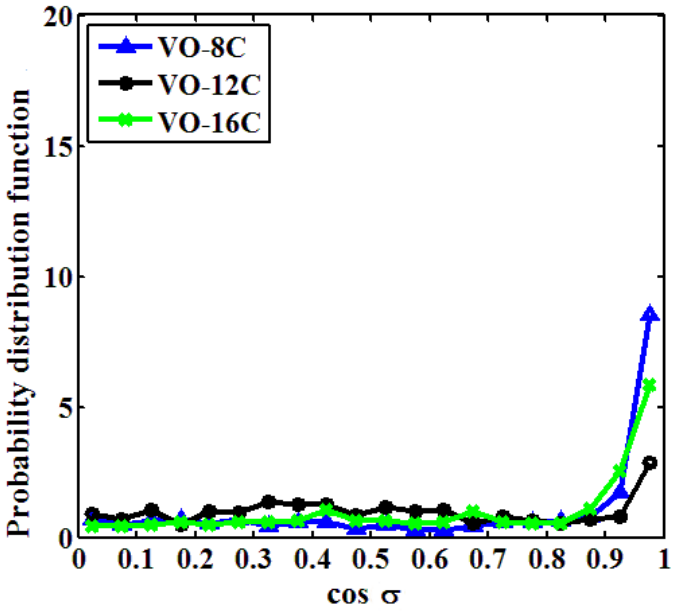

Figure A.6: PDF of $cos\,\sigma$ at COG distance ~ 1 nm for systems VO-8C, VO-12C and VO-16C.

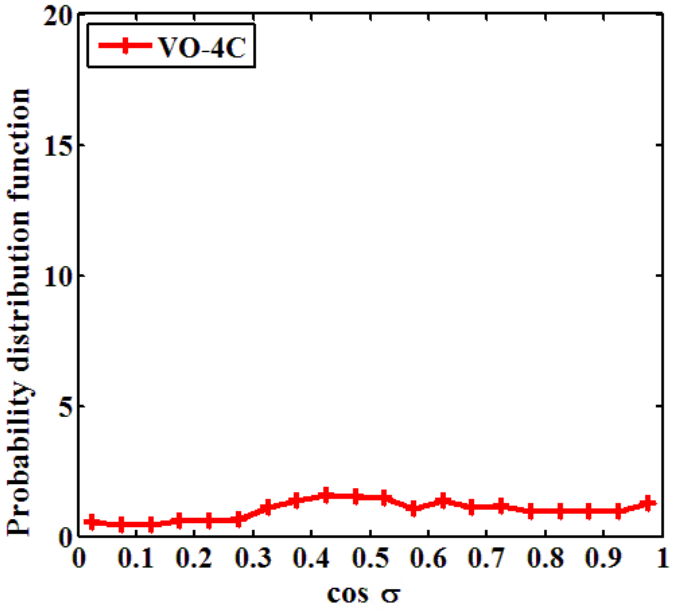

Figure A.7: PDF of $cos\,\sigma$ at COG distance ~1.1 nm for system VO-4C.

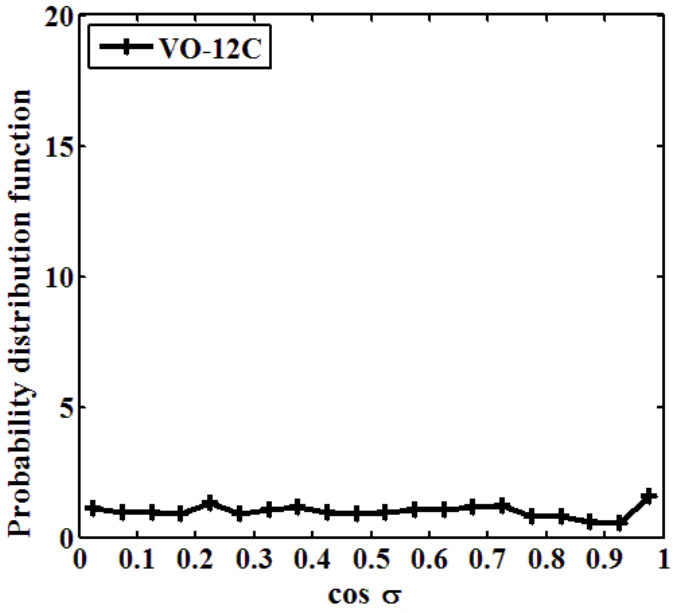

Figure A.8: PDF of $cos\,\sigma$ at COG distance ~1.25 nm for system VO-12C.

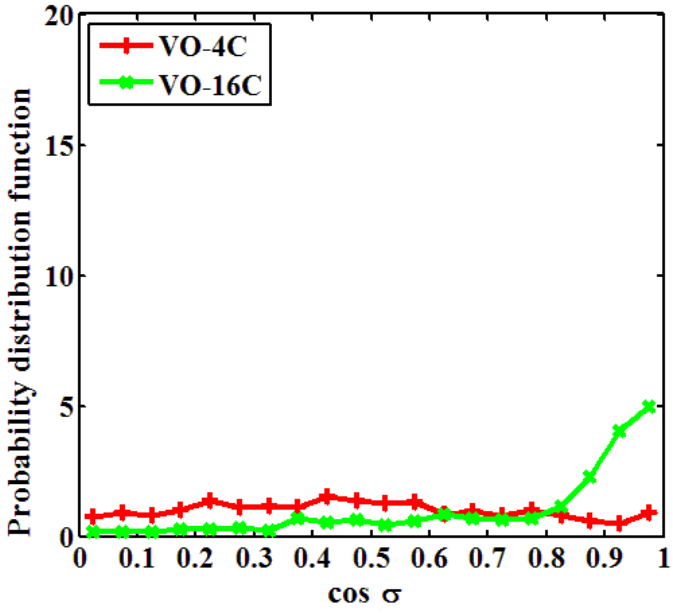

Figure A.9: PDF of $cos\,\sigma$ at COG distance ~1.4 nm for systems VO-4C and VO-16C.

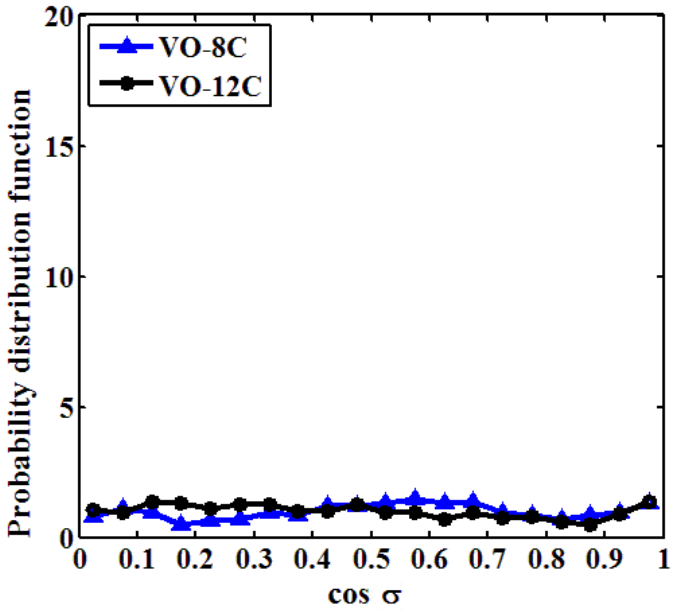

Figure A.10: PDF of $cos\,\sigma$ at COG distance ~1.5 nm for systems VO-8C and VO-12C.

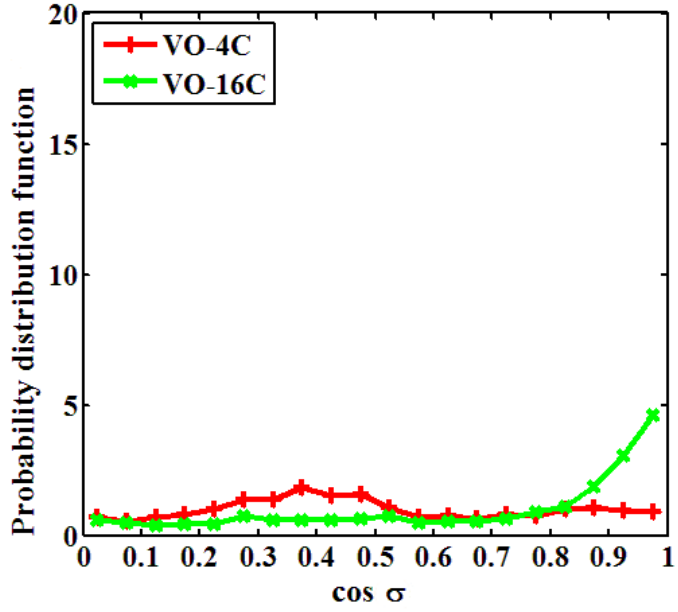

Figure A.11: PDF of $cos\,\sigma$ at COG distance ~1.75 nm for systems VO-4C and VO-16C.

A.6. Parallel configurations formed by asphaltenes involved in different m-MPS structures

Figure A.12 shows the parallel configuration formed by asphaltenes involved in different m-MPS structures. This configuration contains two 2-MPS structures indicated by the two blue

circles. The PA cores from the four asphaltene molecules are considered to be parallel by using the criterion of $\cos(\sigma) \geq 0.90$ (see section 3.3.3 in Chapter 3), although the two 2-MPS structures are sufficiently apart and do not form a single 4-MPS structure. The $\pi - \theta$ and $\theta - \theta$ contacts between the two 2-MPS structures are respectively indicated by the red and black arrows and circles.

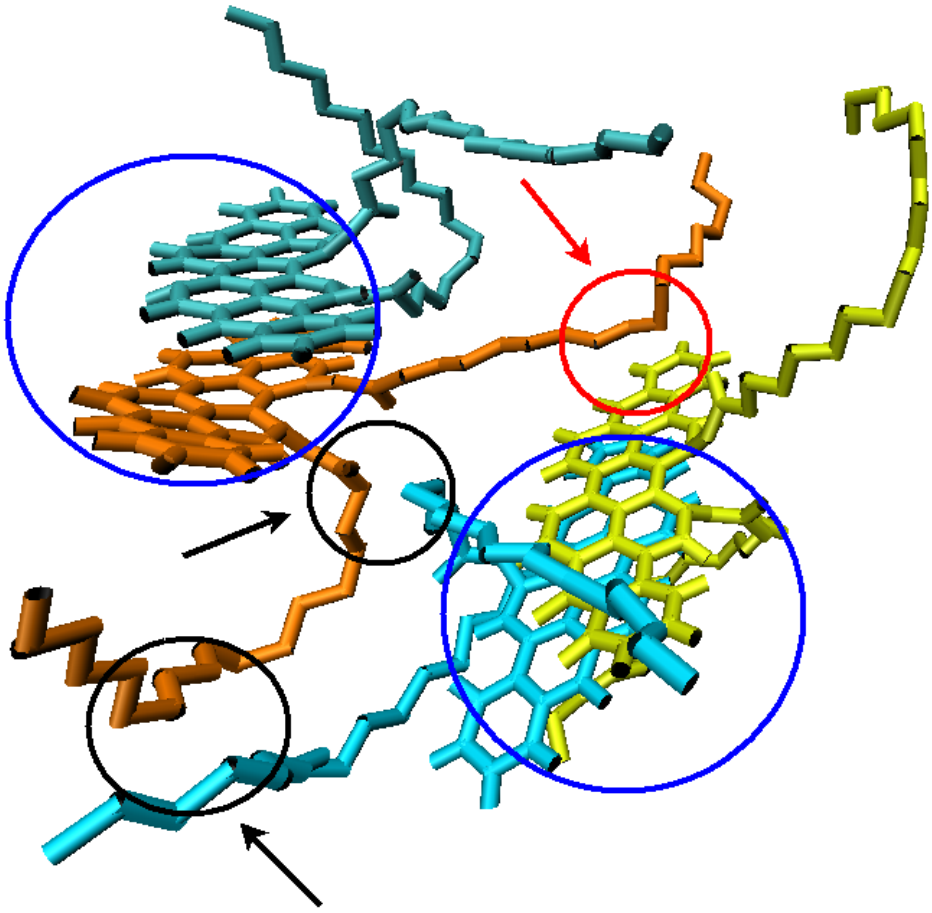

Figure A.12: Parallel configuration formed by asphaltenes involved in different m-MPS structures.

Bibliography

(1) Schüttelkopf, A. W.; Van Aalten, D. M. F. PRODRG: A Tool for High-Throughput Crystallography of Protein-Ligand Complexes. *Acta Crystallogr. Sect. D: Biol.*

Crystallogr. **2004,** *60*, 1355-1363.

(2) Oostenbrink, C.; Villa, A.; Mark, A. E.; Van Gunsteren, W. F. A Biomolecular Force Field Based on the Free Enthalpy of Hydration and Solvation: The GROMOS Force-Field Parameter Sets 53A5 and 53A6. *J. Comput. Chem.* **2004,** *25*, 1656-1676.

(3) Lemkul, J. A.; Allen, W. J.; Bevan, D. R. Practical Considerations for Building GROMOS-Compatible Small-Molecule Topologies. *J. Chem. Inf. Model.* **2010,** *50*, 2221-2235.

(4) van Gunsteren, W. F.; Billeter, S. R.; Eising, A. A.; Hünenberger, P. H.; Krüger, P.; Mark, A. E.; Scott, W. R. P.; Tironi, I. G. *Biomolecular Simulation: The GROMOS96 Manual and User Guide;* Vdf Hochschulverlag Ag an der ETH Zürich: Zürich, Switzerland, 1996.

(5) Pisula, W.; Tomović, Ž.; Simpson, C.; Kastler, M.; Pakula, T.; Müllen, K. Relationship between Core Size, Side Chain Length, and the Supramolecular Organization of Polycyclic Aromatic Hydrocarbons. *Chem. Mater.* **2005,** *17*, 4296-4303.

Appendix B: Supporting Information for Chapter 4

B.1. Details of the systems studied

Table B.1 shows the information of the eight systems simulated in Chapter 4 (toluene) and in Ref. 37 of Chapter 4 (water, see section 4.3.3). Table B.2 shows the partial charges for functional groups used in this chapter.

Table B.1: Information of the Eight Systems Simulated in Chapter 4 and in Ref. 37

systems		number of solvent molecules	initial size of simulation box (nm^3)	simulation time (ns)
in toluene	VO-4C	8857	12×12×12	80
	VO-8C	8789	12×12×12	80
	VO-12C	8715	12×12×12	80
	VO-16C	8673	12×12×12	80
in water	VO-4C	56833	12×12×12	60
	VO-8C	56620	12×12×12	60
	VO-12C	56465	12×12×12	60
	VO-16C	56269	12×12×12	60

Table B.2: Partial Charges for Functional Groups Used in This Chapter

functional groups	aliphatic carbon	aromatic carbon and hydrogen (C-H)	ketone carbon and oxygen (C=O)	ester group C-O-(C=O) (from left to right)
partial charges	0	-0.140, 0.140	0.450, -0.450	0.160 -0.360 0.580 -0.380

B.2. Demonstration for the achievement of dynamic equilibrium

Figure B.1a shows the RDFs for the COG distance r (nm) between PA cores of VO-16C in toluene. Different curves in the figure were plotted using data from different time windows. It can be seen that after 30 ns, the change in the RDF curves becomes quite small, and after 60 ns, they essentially overlap with one another, suggesting the attainment of equilibrium. As a

comparison, Figure B.1b shows the corresponding RDFs for water, which suggests that equilibrium has been attained at 55 ns.

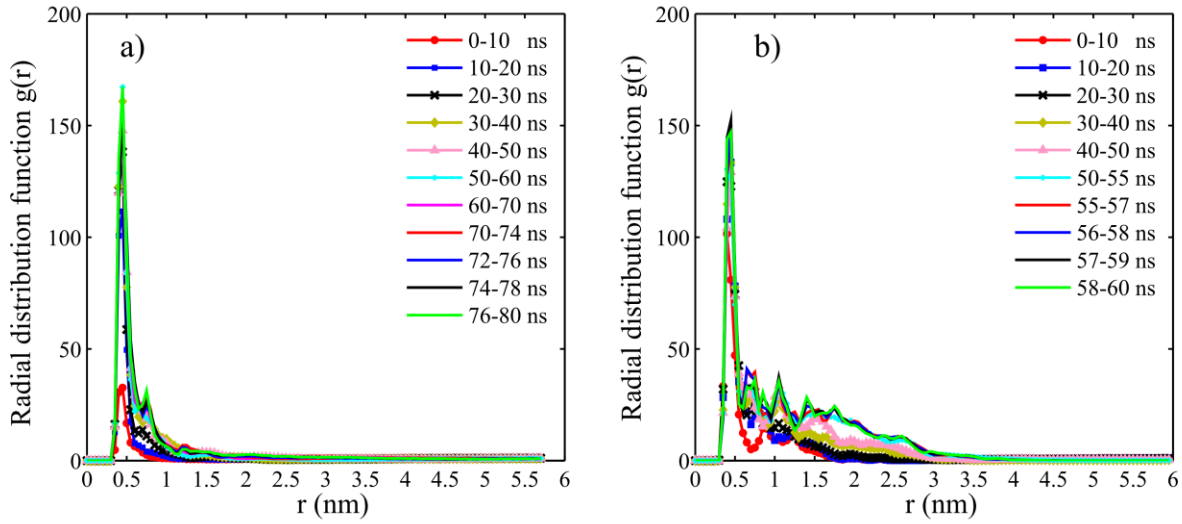

Figure B.1: RDFs for the COG distance r (nm) between PA cores of VO-16C: (a) in toluene and (b) in water.

B.3. Evidence for the stability of DPS pairs

Figure B.2 shows the MIN distance between adjacent PA cores that became directly parallel at the final stage of the simulations (from 70 to 80 ns) as a function of simulation time. Each subfigure corresponds to one of the four systems simulated, and it contains several curves, each describing the MIN distance between one pair of adjacent PA cores that became directly parallel at the final stage of the simulations. For all the pairs, the MIN distances first decrease to a plateau value (~ 0.35 nm) and remain unchanged afterwards. This shows that the DPS pairs, once formed, are very stable.

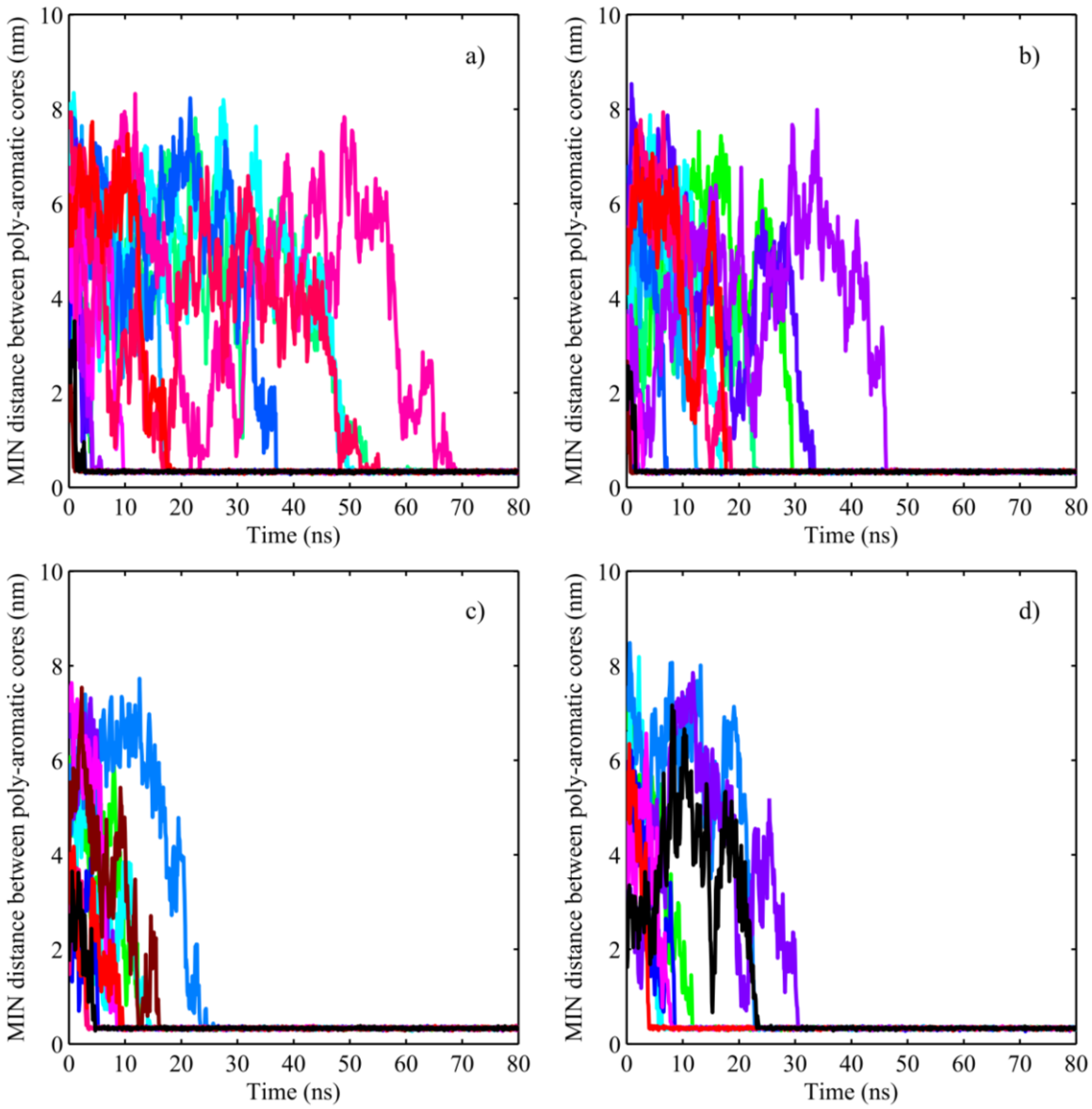

Figure B.2: MIN distance between adjacent PA cores that became directly parallel at the final stage of the simulations (from 70 to 80 ns): (a) VO-4C, (b) VO-8C, (c) VO-12C and (d) VO-16C. Each subfigure contains several curves (with different colors), each describing the MIN distance between one DPS pair.

B.4. RDFs for water molecules around oxygen atoms of model asphaltenes

The RDFs for the hydrogen and oxygen atoms of water around asphaltene oxygen are shown in Figure B.3. Each plot contains two curves: one for RDF between the oxygen of asphaltene and hydrogen of water (g_{O-H}), whereas the other for RDF between oxygen of asphaltene and oxygen of water (g_{O-O}). It can be seen that the first peaks of g_{O-H} and g_{O-O} are located at distance r_{O-H} ~0.2 nm and r_{O-O} ~0.3 nm, respectively. The difference between these two distances is ~0.1 nm, close to OH bond length in water molecules,[1] suggesting that hydrogen bond is formed between oxygen of model asphaltene and water molecules.

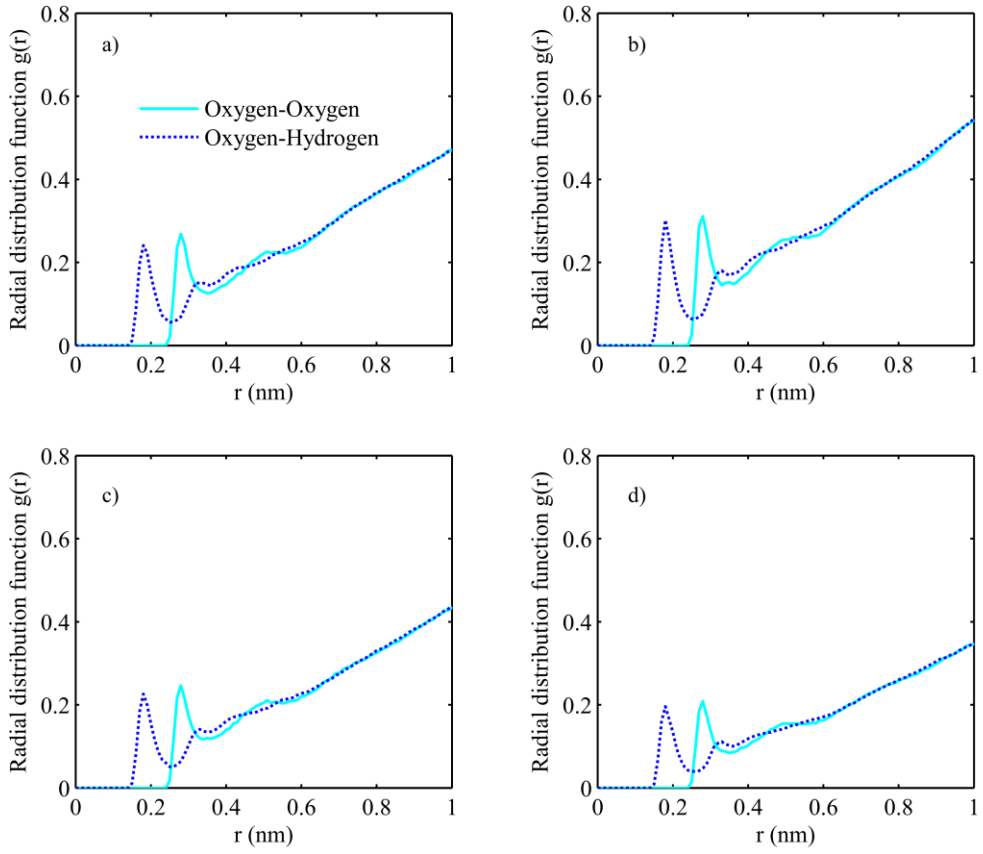

Figure B.3: RDFs of hydrogen and oxygen atoms in water around oxygen atoms in model asphaltenes: (a) VO-4C, (b) VO-8C, (c) VO-12C and (d) VO-16C.

Bibliography

(1) Kunieda, M.; Nakaoka, K.; Liang, Y.; Miranda, C. R.; Ueda, A.; Takahashi, S.; Okabe, H.; Matsuoka, T. Self-Accumulation of Aromatics at the Oil−Water Interface through Weak Hydrogen Bonding. *J. Am. Chem. Soc.* **2010,** *132,* 18281-18286.

Appendix C: Supporting Information for Chapter 5

C.1. Topology details

Table C.1 shows the atom types and partial charges used for the functional groups of the PA compounds.

Table C.1: Functional Groups, Atom Types and Their Partial Charges Used in Chapter 5

functional groups	aliphatic carbon	aromatic carbon and hydrogen (C-H)	ketone carbon and oxygen (C=O)	ester group C-O-(C=O) (from left to right)
atom types	CH2 CH3	CR1-HC	C=O	C-OA-(C=O)
partial charges	0	-0.140, 0.140	0.450, -0.450	0.160 -0.360 0.580 -0.380

C.2. Topology validation for n-heptane

To validate the topology of n-heptane molecules generated in this chapter (see section 5.2.1 in Chapter 5), simulation was first performed on pure n-heptane in liquid phase. One thousand n-heptane molecules were first randomly placed into a simulation box of dimension $10 \times 10 \times 10$ nm^3. Static structure optimization was then performed followed by 10 ns full dynamics simulation at 300 K and 1 bar with periodic boundary conditions applied. The density of n-heptane was then calculated from the final equilibrated volume. Furthermore, the enthalpy of vaporization was evaluated by performing one additional simulation in the gas phase. To do so, one n-heptane molecule was placed in vacuum. Static structure optimization and full dynamics simulation at 300 K were performed without periodic boundary conditions. Finally, the molar enthalpy of vaporization ΔH_{vap} was calculated using equation (C.1):[1]

$$\Delta H_{vap} = U_g - U_l + RT, \quad \text{(C.1)}$$

where U_g and U_l are respectively the molar potential energies in the gas phase and liquid phase, evaluated from the two sets of simulations above; R is the gas constant and T is the temperature (300 K). The density and enthalpy of vaporization determined from the simulations are listed in Table C.2. It can be seen that these values are very close to experimental results, demonstrating the accuracy of the n-heptane topology.

Table C.2: Density and Enthalpy of Vaporization of n-Heptane: Comparison between Simulation and Experiment

quantities	density (g/L)	enthalpy of vaporization (kJ/mol)
this Chapter	679.11	36.38
reference[2]	679.46	36.55

C.3 Demonstration for the achievement of dynamic equilibrium

To demonstrate the achievement of dynamic equilibrium during the last 20 ns of the simulation, root mean square deviation (*RMSD*) is computed as a function of simulation time for each aggregate that does not dissociate during this time period using the following equation:[3]

$$RMSD(t) = \left[\frac{1}{N^2}\sum_{i=1}^{N}\sum_{j=1}^{N}\left\|r_{ij}(t) - r_{ij}(0)\right\|^2\right]^{0.5}, \quad \text{(C.2)}$$

where the distance $r_{ij}(t)$ between two atoms i and j in an aggregate at time t is compared with the distance $r_{ij}(0)$ between the same atoms at time 0. In each of systems VO-4C, VO-8C and VO-12C, a single aggregate is formed, which is represented by one curve in Figure C.1. In system VO-16C, three aggregates exist, and their *RMSD* are shown by three individual curves in Figure C.1. For each aggregate, the *RMSD* first increased to a plateau value, and afterwards stayed near this value with small fluctuations, demonstrating that dynamic equilibrium has been achieved in each system.

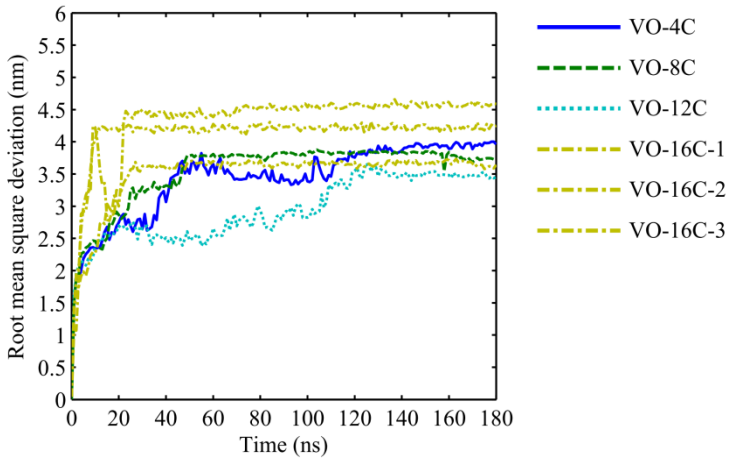

Figure C.1: *RMSD* as a function of simulation time for the four systems studied. In each of systems VO-4C, VO-8C and VO-12C, a single aggregate is formed, which is represented by one curve in the figure. In system VO-16C, three aggregates exist, and their *RMSD* are shown by three individual curves: VO-16C-1, VO-16C-2 and VO-16C-3.

C.4. Evidence for the solvation of side chains in n-heptane

The radius of gyration of individual PA molecule about its center of mass, averaged over all 24 molecules in each system, is plotted as a function of simulation time in Figure C.2. In the initial configurations (t = 0 ns in Figure C.2), each PA molecule has an extended structure as shown in Figure 5.2 of Chapter 5, where the aliphatic side chains are fully solvated in n-heptane. From Figure C.2, it can be seen that the radius of gyration in each system is almost constant during the entire simulation course, suggesting that the side chains remain fully solvated in n-heptane.

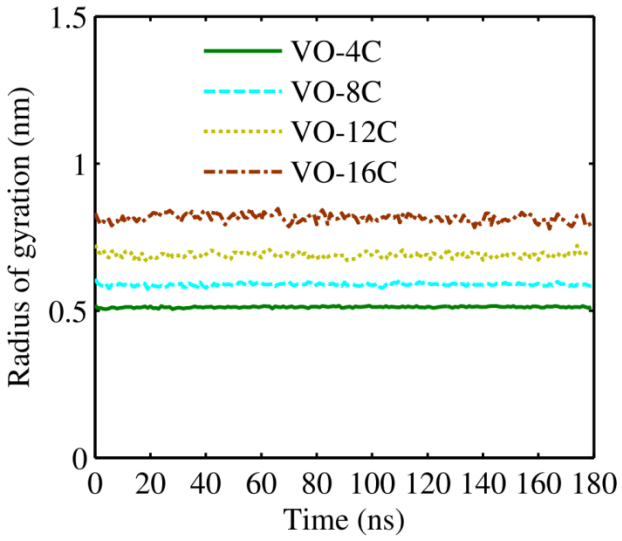

Figure C.2: Radius of gyration as a function of simulation time for the four systems studied.

C.5. Discussion on the length of simulation time

Four sets of simulations, with different simulation time, were performed to demonstrate that sufficiently long simulation time (> 120 ns) is required to observe the formation of 1D self-assembly. Figure C.3 shows the size of the largest aggregate as a function of simulation time in each set of the simulations. Here, the size is quantified by the number of PA molecules involved in the largest aggregate in each system. In each set of the simulations, the numbers for the 4 systems exhibit an overall increasing trend at the beginning, corresponding to the growth of the largest aggregate. In Figures C.3a-c, some of the curves reach their final plateau values after a certain time. For instance, the number for system VO-8C reaches 24 at ~40 ns in Figure C.3a; the number for system VO-4C reaches 20 at ~50 ns in Figure C.3b; and the number for system VO-16C reaches 24 at ~75 ns in Figure C.3c. However, the other curves still undergo large fluctuations at the end of these 3 sets of simulations. Only in Figure C.3d and after 120 ns, the numbers for all the 4 systems reach their plateau values with small fluctuations. The plateau values reflect the final sizes of the aggregates formed. Hence, sufficient long simulation time

(> 120 ns) is needed for each system to reach equilibrium configuration. To further demonstrate this, Figure C.4 shows snapshots for system VO-4C at the end of each set of the simulations. It can be seen that small aggregates formed during the short simulation (Figure C.4a) progressively clustered into larger aggregates (Figures C.4b and C.4c), but their re-organization into the 1D self-assembly was only achieved in Figure C.4d.

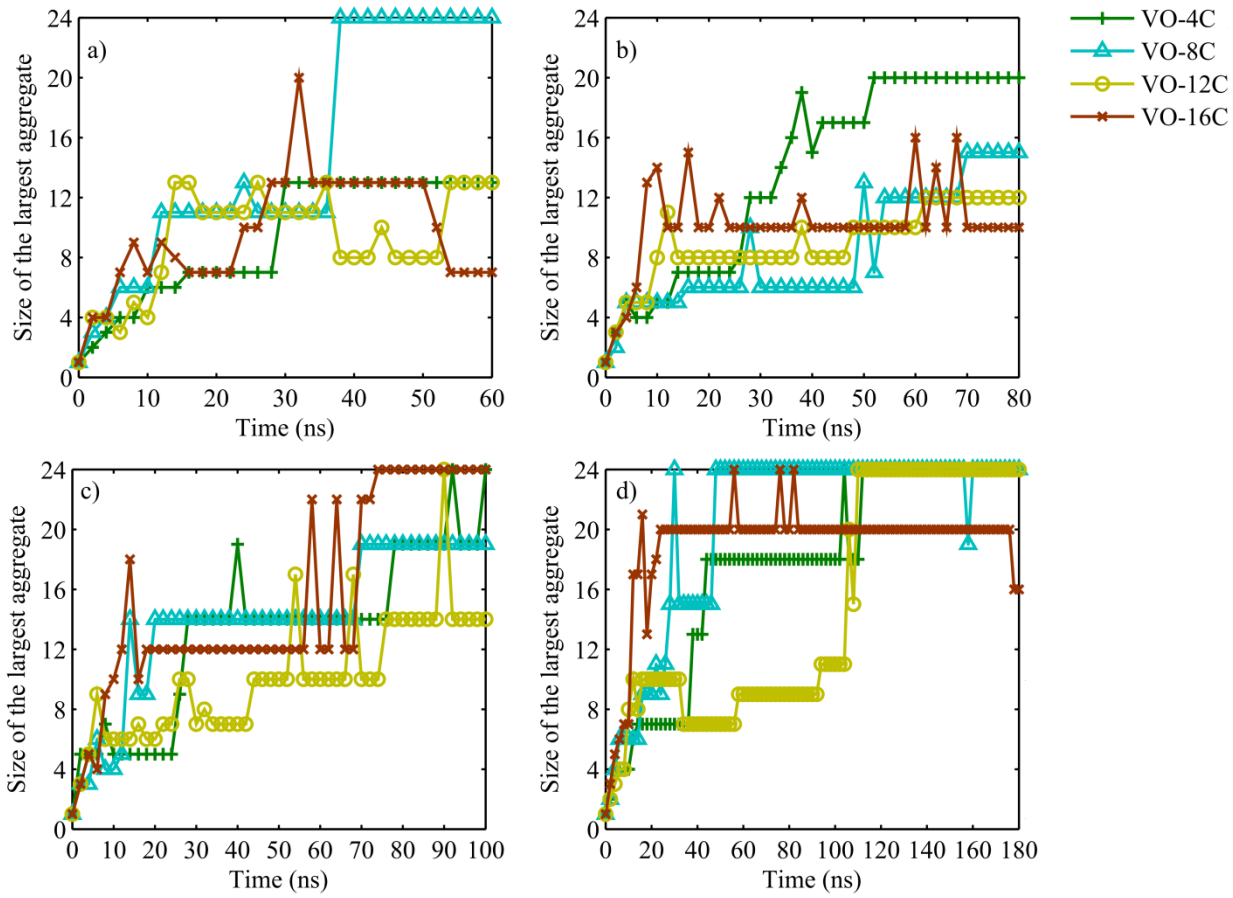

Figure C.3: Sizes of the largest aggregates as a function of simulation time in each set of simulations: (a) Set 1 performed for 60 ns; (b) Set 2 performed for 80 ns; (c) Set 3 performed for 100 ns; (d) Set 4 performed for 180 ns.

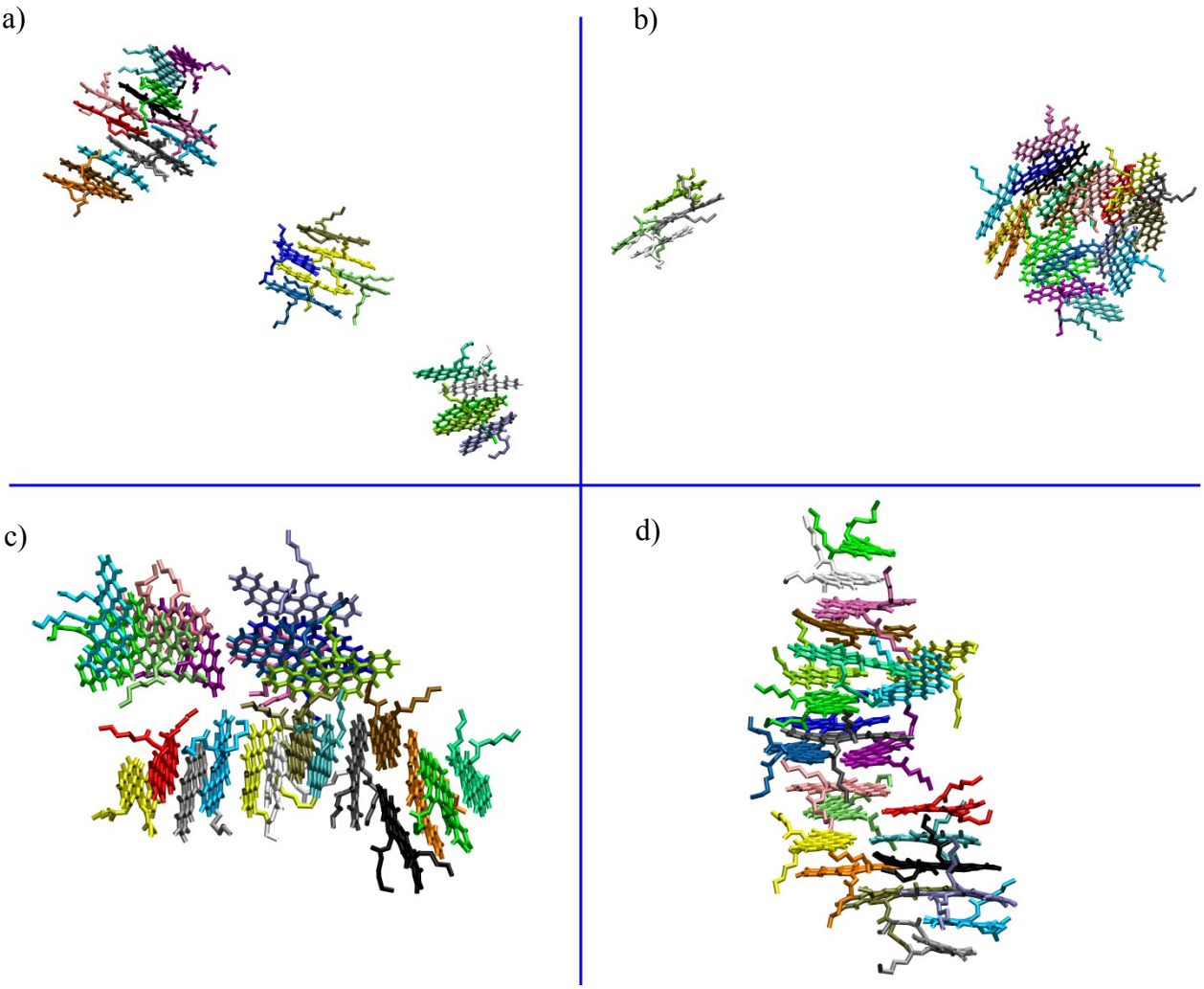

Figure C.4: Snapshots for system VO-4C at the end of each set of the simulations: (a) Set 1; (b) Set 2; (c) Set 3; (d) Set 4.

Bibliography

(1) Caleman, C.; van Maaren, P. J.; Hong, M.; Hub, J. S.; Costa, L. T.; van der Spoel, D. Force Field Benchmark of Organic Liquids: Density, Enthalpy of Vaporization, Heat Capacities, Surface Tension, Isothermal Compressibility, Volumetric Expansion Coefficient, and Dielectric Constant. *J. Chem. Theory. Comput.* **2011,** *8*, 61-74.

(2) Riddick, J. A.; Bunger, W. B.; Sakano, T. K. *Organic Solvents: Physical Properties and Methods of Purification,* 4th ed.; John Wiley & Sons Inc.: New York, 1986**.**

(3) van der Spoel, D.; Lindahl, E.; Hess, B.; van Buuren, A. R.; Apol, E.; Meulenhoff, P. J.; Tieleman, D. P.; Sijbers, A. L. T. M.; Feenstra, K. A.; van Drunen, R.; Berendsen, H. J. C. Gromacs User Manual, version 4.0. http://www.gromacs.org (2005).

Appendix D: Supporting Information for Chapter 6

D.1. Development of heptol solvent

In constructing heptol of different n-heptane/toluene volume ratios, we first generated the bulk liquid phases of pure n-heptane and pure toluene, and validated them by reproducing their experimental mass density and self-diffusivity.[1-3] Then, we converted the volume ratio into molecular number ratio, and determined the amount of n-heptane and toluene molecules that need to be placed in the simulation box of dimensions $12 \times 12 \times 12$ nm^3. These numbers of n-heptane and toluene molecules were respectively extracted from their pre-equilibrated liquid phases and merged together in the simulation box. The merged system was subjected to static structure minimization and dynamic equilibration. In the end of the equilibration process, the n-heptane and toluene molecules were found to be well-mixed and the mixtures were used as heptol solvents in the simulations of PA compounds as described in Chapter 6.

D.2. Probability distribution of total potential energy in the REMD simulations

Figure D.1 shows the probability density function for the total potential energy in systems VO-4C-TR and Mixture-TR. In each subfigure, there are 11 replicas, each simulated at a particular temperature and represented by a specific color. It can be seen that the potential energy has sufficient overlapping between neighboring replicas, ensuring uniform acceptance ratios between neighboring replicas.[4]

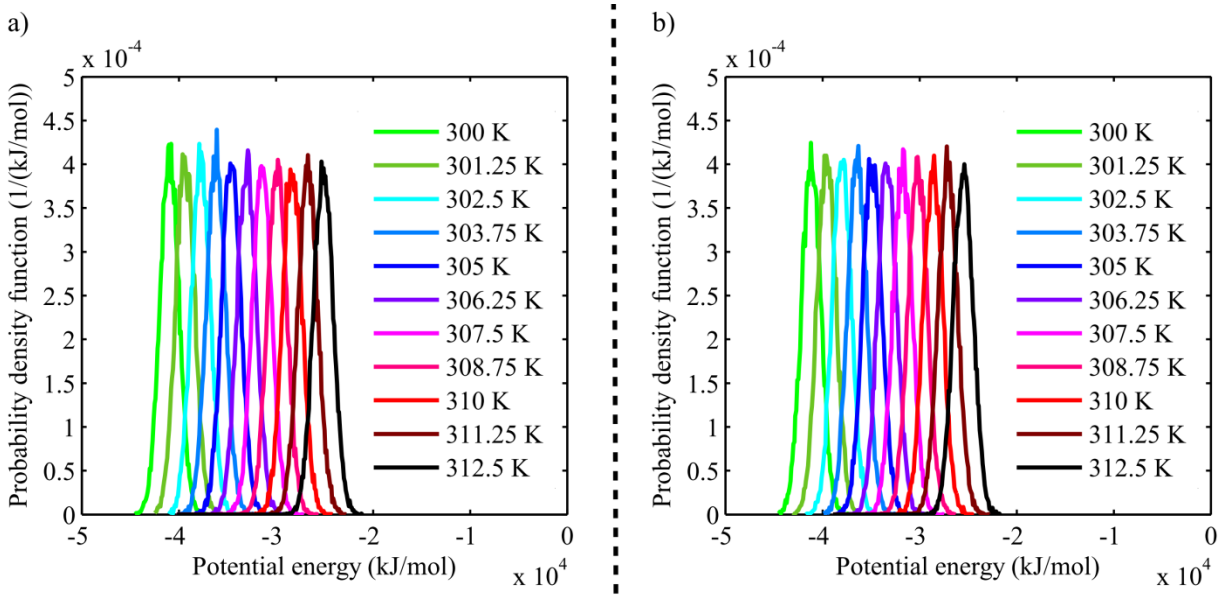

Figure D.1: Potential energy distribution for systems: (a) VO-4C-TR, and (b) Mixture-TR. In each system, different replicas are depicted using different colors.

D.3. Structural "sequence" of the aggregate formed in system Mixture-HT87.5

Figure D.2 shows the final aggregate formed in system Mixture-HT87.5, where VO-16C is colored purple, VO-12C pink, VO-8C cyan and VO-4C green. As it can be seen, its structural "sequence", from top to bottom, is: 16C-12C-12C-8C-8C-8C-16C(4C)-8C(16C)-12C-4C-12C-8C-8C-4C-4C-4C-16C-16C-12C-16C-12C-4C, where 16C(4C) and 8C(16C) denote two molecules that are located in a side-by-side manner. Again, different types of PA molecules appear in an alternating manner.

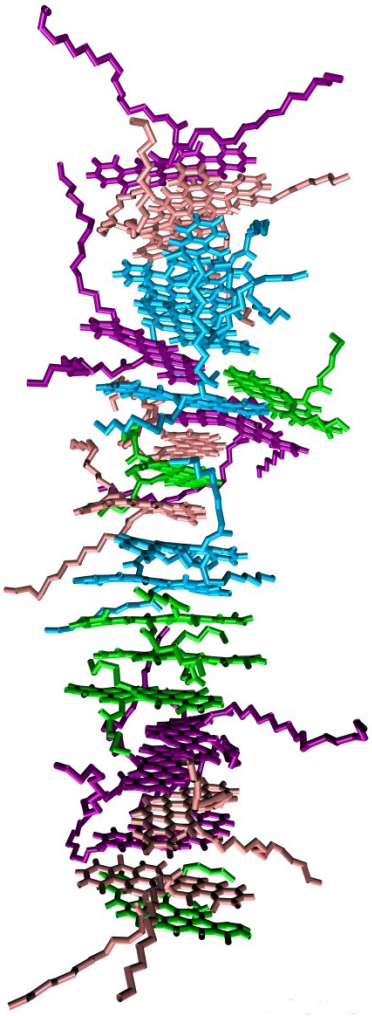

Figure D.2: Final aggregate formed in system Mixutre-HT87.5, where different types of PA molecules are represented by different colors.

D.4. Intermolecular contacts formed between PA compounds

Table D.1 summarizes the average numbers of intermolecular $\pi - \pi$, $\pi - \theta$ and $\theta - \theta$ contacts in systems of a single of PA compounds studied in Chapters 4 and 5. Clearly, for the four PA compounds, all three types of contacts are higher in n-heptane compared to toluene, demonstrating that n-heptane increases $\pi - \pi$ interaction as well as $\pi - \theta$ and $\theta - \theta$ interactions between PA compounds.

Table D.1: Intermolecular Contacts Formed between PA Compounds

solutes	VO-4C		VO-8C		VO-12C		VO-16C	
solvents	toluene[1]	n-heptane	toluene[1]	n-heptane	toluene[1]	n-heptane	toluene[1]	n-heptane
$\pi-\pi$	21	42	24	36	22	29	19	27
$\pi-\theta$	47	70	49	77	36	78	38	70
$\theta-\theta$	6	17	12	24	11	29	14	28

Bibliography

(1) Jian, C.; Tang, T.; Bhattacharjee, S. Molecular Dynamics Investigation on the Aggregation of Violanthrone78-Based Model Asphaltenes in Toluene. *Energy Fuels* **2014,** *28*, 3604-3613.

(2) Jian, C.; Tang, T. One-Dimensional Self-Assembly of Polyaromatic Compounds Revealed by Molecular Dynamics Simulations. *J. Phys. Chem. B* **2014,** *118*, 12772–12780.

(3) Jian, C.; Tang, T.; Bhattacharjee, S. A Dimension Map for Molecular Aggregates. *J. Mol. Graphics Modell.* **2015,** *58*, 10-15.

(4) Sugita, Y.; Okamoto, Y. Replica-Exchange Molecular Dynamics Method for Protein Folding. *Chem. Phys. Lett.* **1999,** *314*, 141-151.

Appendix E: Supporting Information for Chapter 7

E.1. Simulation details

Molecular structure for TYR-4 was built using AmberTools13.[1] For DPC and DPPC, their structures were adopted from literature.[2,3] The structure of VO-16C was obtained using Chem3D ultra 10.0 software, and the structures of the other three PA compounds were obtained by manually removing certain number of terminal aliphatic hydrocarbons from the side chains of VO-16C. Molecular topologies for the TYR-4 model, toluene and n-heptane molecules were generated using appropriate routine in GROMACS 4.0.7,[4-7] and were based on GROMOS96 force field parameter set 53A6,[8] which has been extensively used in literature for peptide and PA compound simulations.[9-12] Validation of the force field parameters for toluene and n-heptane was performed by comparing their bulk physical properties (density and diffusion constant) obtained from pure solvent MD simulations (at 300 K and 1 bar) with results reported in literature (see Table E.1). As can be seen from Table E.1, our simulations reproduced literature values fairly well, verifying the accuracy of the generated topologies. For the DPC and DPPC models, their molecular topologies were adopted from literature,[3,13] which were respectively constructed in GROMOS 54A7[14] and GROMOS96 53A6[8] force fields with partial charges of lipid headgroups re-parameterized according to the work by Chiu et al.[15] Topologies for PA compounds were initially obtained by submitting their structures to the GlycoBioChem PRODRG2 server,[16] after which the partial charge was manually adjusted, according to the approach suggested in literature,[17] to be compatible with GROMOS96 53A6 force field parameters. The so-generated topology has been tested and validated in our previous work (see Chapter 3 and Appendix A of this dissertation),[18] and Table E.2 shows the atom types and partial charges used for the functional groups of the PA compounds.

Table E.1: Comparison of Density and Diffusion Constant Obtained from MD Simulations with Literature

solvent	toluene		*n*-heptane	
	density (g/L)	diffusion constant (cm^2/s)	density (g/L)	diffusion constant(cm^2/s)
this chapter	866.6	2.31×10^{-5}	679.1	3.93×10^{-5}
literature[19-23]	862.3	2.40×10^{-5}	679.5	4.02×10^{-5}

Table E.2: Functional Groups, Atom Types and Their Partial Charges Used for PA Compounds

functional groups	aliphatic carbon	aromatic carbon and hydrogen (C-H)	ketone carbon and oxygen (C=O)	ester group C-O-(C=O) (from left to right)
atom types	CH2 CH3	CR1-HC	C=O	C-OA-(C=O)
partial charges	0	-0.140, 0.140	0.450, -0.450	0.160 -0.360 0.580 -0.380

In constructing the initial configurations, the solute molecules were arranged to form ordered arrays in the cases of TYR-4 and PA compounds. For DPC and DPPC, the solute molecules were randomly placed, following the procedure for lipid simulations in literature.[13,24] It should be pointed out here given sufficiently long simulation time, dynamic equilibrium can be arrived from any reasonable initial configurations and the choice of initial configuration should not be of any concern. Details of the 15 systems are listed in Table E.3. All simulations were conducted using MD package GROMACS 4.0.7.[4-7] For each system, static energy minimization was first conducted to ensure that the maximum force on any atom was less than 1000 kJ/(mol·nm). Then, heavy atoms of the solutes were restrained (except DPPC molecules in water, for which solute-solvent mass ratio was extremely high, ~1:1) with a 1000 kJ/(mol·nm^2) harmonic potential, while the solvent atoms were allowed to freely move for 1 ns at 300 K and 1 bar. Finally, the restraints were removed and dynamic simulations in NPT ensemble were

performed for the amount of time given in Table E.3. Periodic boundary conditions, full electrostatics with particle-mesh Ewald method,[25] a cutoff distance of 1.4 nm for van der Waals and electrostatics pairwise calculations, LINCS algorithm[26] to constrain all bonds for solute and organic solvent molecules, SETTLE algorithm[27] to constraint all bonds for water molecules, semi-isotropic (for DPPC) or isotropic (for other systems) Parrinello-Rahman barostat[28] to keep the average pressure at 1 bar, a velocity rescaling thermostat[29] to keep the average temperature at 323K (for DPPC, so that it is above the phase transition temperature of 315K[24]) or 300 K (for all other systems), and a time step of 2 fs were used. It should be mentioned that the velocity rescaling coupling method used here is based on correctly producing the probability distribution of kinetic energy under constant temperature, which differs from the isokinetic scheme[30] of maintaining constant temperature. Therefore it is an accurate method.

Table E.3: Details of the 15 Systems Studied

systems		number of solute molecules	number of solvent molecules	initial size of simulation box (nm^3)	simulation time (ns)
in water	TYR-4	12	16732	$8 \times 8 \times 8$	30
	DPC	54	15980	$8 \times 8 \times 8$	45
	DPPC	64	3000	$10 \times 10 \times 10$	40
	VO-4C	24	56833	$12 \times 12 \times 12$	60
	VO-8C	24	56620	$12 \times 12 \times 12$	60
	VO-12C	24	56465	$12 \times 12 \times 12$	60
	VO-16C	24	56269	$12 \times 12 \times 12$	60
in toluene	VO-4C	24	8857	$12 \times 12 \times 12$	80
	VO-8C	24	8789	$12 \times 12 \times 12$	80
	VO-12C	24	8715	$12 \times 12 \times 12$	80
	VO-16C	24	8673	$12 \times 12 \times 12$	80
in *n*-heptane	VO-4C	24	6233	$12 \times 12 \times 12$	180
	VO-8C	24	6175	$12 \times 12 \times 12$	180
	VO-12C	24	6125	$12 \times 12 \times 12$	180
	VO-16C	24	6073	$12 \times 12 \times 12$	180

E.2. Demonstration for the achievement of dynamic equilibrium

The data analysis was based on the last 5 ns of the simulations for TYR-4, DPC, DPPC and PA compounds in water, the last 10 ns for PA compounds in toluene, and the last 20 ns for PA compounds in n-heptane. To demonstrate the achievement of dynamic equilibrium during these periods, root mean square deviation (*RMSD*) is computed as a function of simulation time for each aggregate using the following equation:[31]

$$RMSD(t) = \left[\frac{1}{N^2}\sum_{i=1}^{N}\sum_{j=1}^{N}\left\|r_{ij}(t) - r_{ij}(0)\right\|^2\right]^{0.5}, \quad \text{(E.1)}$$

where the distance $r_{ij}(t)$ between atoms i and j in an aggregate at time t is compared with the distance $r_{ij}(0)$ between the same atoms at time 0, i.e. in the initial configuration before the full dynamic simulation. By definition, an aggregate involves at least two molecules. One or more aggregates may be found in each simulated system, and their *RMSD* are represented by individual lines in Figure E.1. For each aggregate, the *RMSD* first increased to a plateau value, and afterwards stayed near this value with small fluctuations. This demonstrates that dynamic equilibrium has been achieved in each system. For aggregate 4 formed in the system of VO-12C in toluene (VO-12C-4 in Figure E.1e), RMSD decreases to ~3.5 nm from ~40 to ~70 ns, caused by the detaching of two molecules from the aggregate. This is because, as discussed in Chapter 7, toluene is a good solvent for PA compounds, and aggregates formed by PA compounds in toluene are not rigidly stable. It should be pointed out that the *RMSD* curves plotted here were generated based on the data collected every 1 ns. We also checked the *RMSD* curves if data were collected every 100 ps, and the same observations were obtained. In addition, the achievement of dynamic equilibrium in the systems of PA compounds was also confirmed using radial distribution functions.[32]

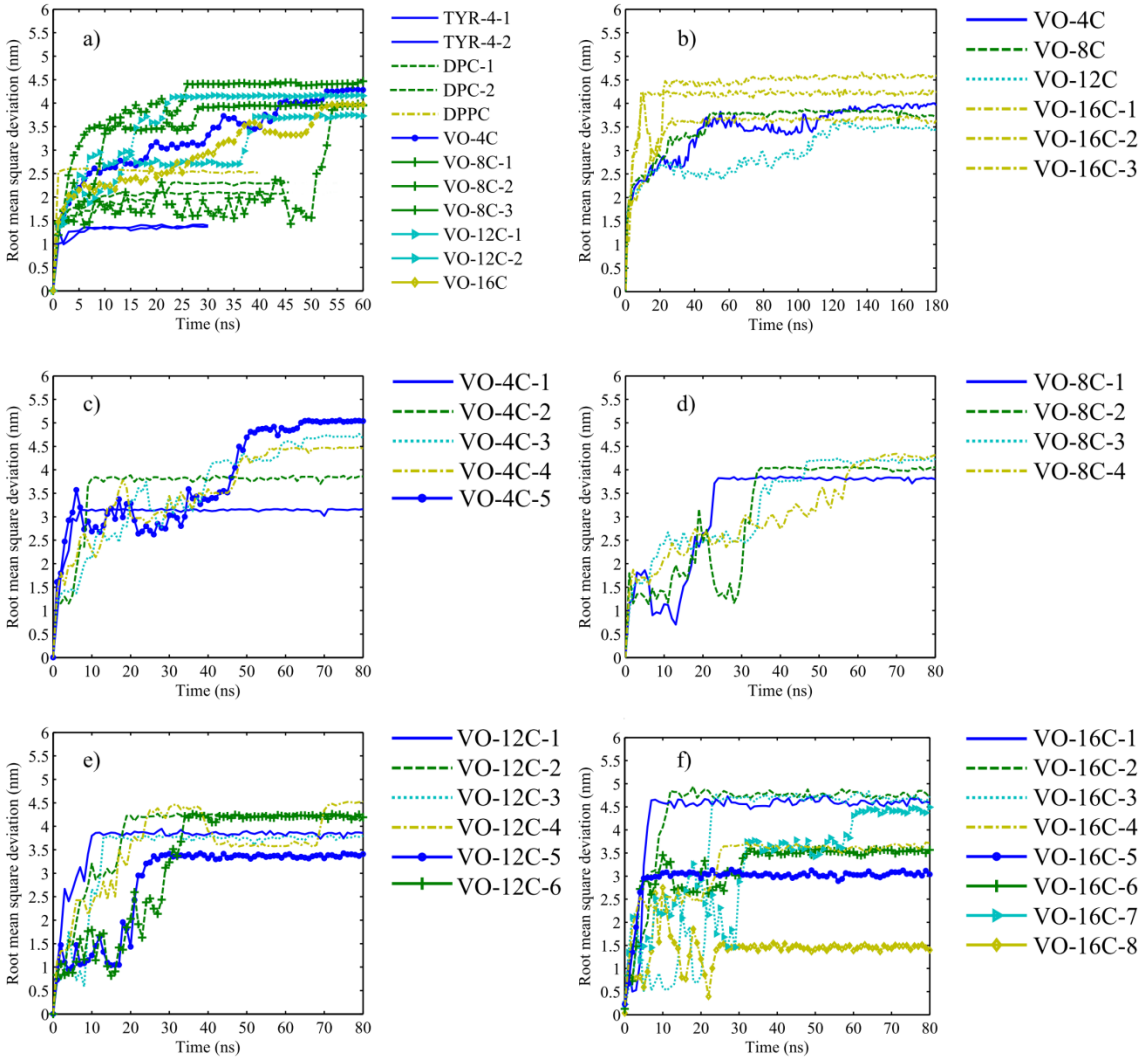

Figure E.1: *RMSD* as a function of simulation time for (a) TYR-4, DPC, DPPC and PA compounds in water, (b) PA compounds in *n*-heptane, (c) VO-4C in toluene, (d) VO-8C in toluene, (e) VO-12C in toluene, and (f) VO-16C in toluene. There may be more than one aggregate in a particular system and each aggregate is represented by a separate curve. For example, DPC-1 and DPC-2 refer to the two aggregates formed in the system of DPC in water.

E.3. Procedures of determining principal moments of inertia and principal axes

For a Cartesian coordinate system of x', y',and z' axes that pass through the mass center of an aggregate, the mass moment of inertia tensor I for the aggregate is given by:[33,34]

$$I = \begin{bmatrix} I_{x'x'} & I_{x'y'} & I_{x'z'} \\ I_{y'x'} & I_{y'y'} & I_{y'z'} \\ I_{z'x'} & I_{z'y'} & I_{z'z'} \end{bmatrix}. \quad \text{(E.2)}$$

The elements of I are respectively the moments of inertia about x', y', z':

$$I_{x'x'} = \sum m_i[(y_i')^2 + (z_i')^2], \quad \text{(E.3)}$$

$$I_{y'y'} = \sum m_i[(x_i')^2 + (z_i')^2], \quad \text{(E.4)}$$

$$I_{z'z'} = \sum m_i[(x_i')^2 + (y_i')^2], \quad \text{(E.5)}$$

and the products of inertia:

$$I_{x'y'} = I_{y'x'} = -\sum m_i x_i' y_i', \quad \text{(E.6)}$$

$$I_{x'z'} = I_{z'x'} = -\sum m_i x_i' z_i', \quad \text{(E.7)}$$

$$I_{y'z'} = I_{z'y'} = -\sum m_i z_i' y_i', \quad \text{(E.8)}$$

where m_i is the mass of atom i, (x_i', y_i', z_i') are its coordinates, and the summation is over all atoms in the aggregate. The eigenvalues of tensor I correspond to the principal moments of inertia (denoted by I_{xx}, I_{yy} and I_{zz} in Chapter 7), and the principal axes x, y and z, about which products of inertia vanish can be found, using the eigenvectors of tensor I.[33,34] Therefore, the principal axes x, y and z, and the principal moments of inertia I_{xx}, I_{yy} and I_{zz} can be determined from the diagonalization of I. Afterwards, principal radii of gyration can be calculated from eqs. 7.1-7.3 in Chapter 7.

The diagonalization procedure has been implemented in GROMACS 4.0.7 (routine *g_gyrate*) as well as VMD[35] (command *measure*). It should be noted that *g_gyrate* and *measure* do not properly treat boundary conditions. For example, in some cases there exist several

seemingly separated aggregates at the edges of the primitive simulation cell, but they actually belong to the same aggregate because of the periodic boundary condition. In those cases, the principal radii of gyration were calculated using our in-house developed *VMD* scripts. These post-processing tools were used in Chapter 7 to calculate the principal radii of gyration for the aggregates.

E.4. Proof of $1 \le r_1 \le r_2 \le \sqrt{1 + {r_1}^2}$

Since the principal radii of gyration R_0 , R_1 and R_2 follow the order of $R_0 \le R_1 \le R_2$, we have $1 \le r_1 \le r_2$. Further, from the definitions of R_x, R_y and R_z (eqs. 7.1-7.3 in Chapter 7), it can be seen that:

$$R_x = \left(\frac{I_{xx}}{\sum_i m_i}\right)^{0.5} = \left(\frac{\sum_i m_i(y_i^2+z_i^2)}{\sum_i m_i}\right)^{0.5} \le \left(\frac{\sum_i m_i(x_i^2+z_i^2)}{\sum_i m_i} + \frac{\sum_i m_i(x_i^2+y_i^2)}{\sum_i m_i}\right)^{0.5} = \sqrt{{R_y}^2 + {R_z}^2}, \quad \text{(E.9)}$$

$$R_y = \left(\frac{I_{yy}}{\sum_i m_i}\right)^{0.5} = \left(\frac{\sum_i m_i(x_i^2+z_i^2)}{\sum_i m_i}\right)^{0.5} \le \left(\frac{\sum_i m_i(y_i^2+z_i^2)}{\sum_i m_i} + \frac{\sum_i m_i(x_i^2+y_i^2)}{\sum_i m_i}\right)^{0.5} = \sqrt{{R_x}^2 + {R_z}^2}, \quad \text{(E.10)}$$

$$R_z = \left(\frac{I_{zz}}{\sum_i m_i}\right)^{0.5} = \left(\frac{\sum_i m_i(x_i^2+y_i^2)}{\sum_i m_i}\right)^{0.5} \le \left(\frac{\sum_i m_i(y_i^2+z_i^2)}{\sum_i m_i} + \frac{\sum_i m_i(x_i^2+z_i^2)}{\sum_i m_i}\right)^{0.5} = \sqrt{{R_x}^2 + {R_y}^2}, \quad \text{(E.11)}$$

suggesting that $R_2 \le \sqrt{{R_0}^2 + {R_1}^2}$. Hence, $r_2 = \frac{R_2}{R_0} \le \sqrt{1 + (\frac{R_1}{R_0})^2} = \sqrt{1 + {r_1}^2}$. In conclusion, $1 \le r_1 \le r_2 \le \sqrt{1 + {r_1}^2}$.

E.5. Discussion on DPPC aggregate

For an ideal bilayer that resembles an infinite two-dimensional plane, $R_0 = R_1$ and $R_2 = \sqrt{{R_0}^2 + {R_1}^2} = \sqrt{2}\,R_0$. The corresponding point on the dimension map should therefore be located on the line of $r_2 = \sqrt{1 + {r_1}^2}$ at $r_1 = 1$, which is not the case for the DPPC aggregate formed in our MD simulation. This is because in the calculation of gyradius ratios, periodic boundary condition was not taken into consideration (numerically impossible to calculate the

infinite sum) for the bilayer formed by DPPC in water, and hence the aggregate has finite dimension in all three directions.

E.6. Individual dimension maps generated for each type of PA compounds

In order to better examine the effect of solvent on the aggregation of PA compounds, Figure E.2 shows individual dimension maps generated for each type of PA compounds. It can be seen that the locations of gyradius ratios associated with different solvents (water, toluene and n-heptane) can be easily distinguished on each map for VO-4C, VO-12C and VO-16C, suggesting different molecular arrangements in different solvents. For instance, on the dimension map for VO-12C (see Figure E.2d), the aggregates in toluene give rise to gyradius ratios, for which the locations are clearly different from those in water or in n-heptane. As for VO-8C, short-cylinder-like aggregate is also formed in water (see Table 7.1 in Chapter 7). Therefore a relatively large overlap of gyradius ratios in water and toluene is observed.

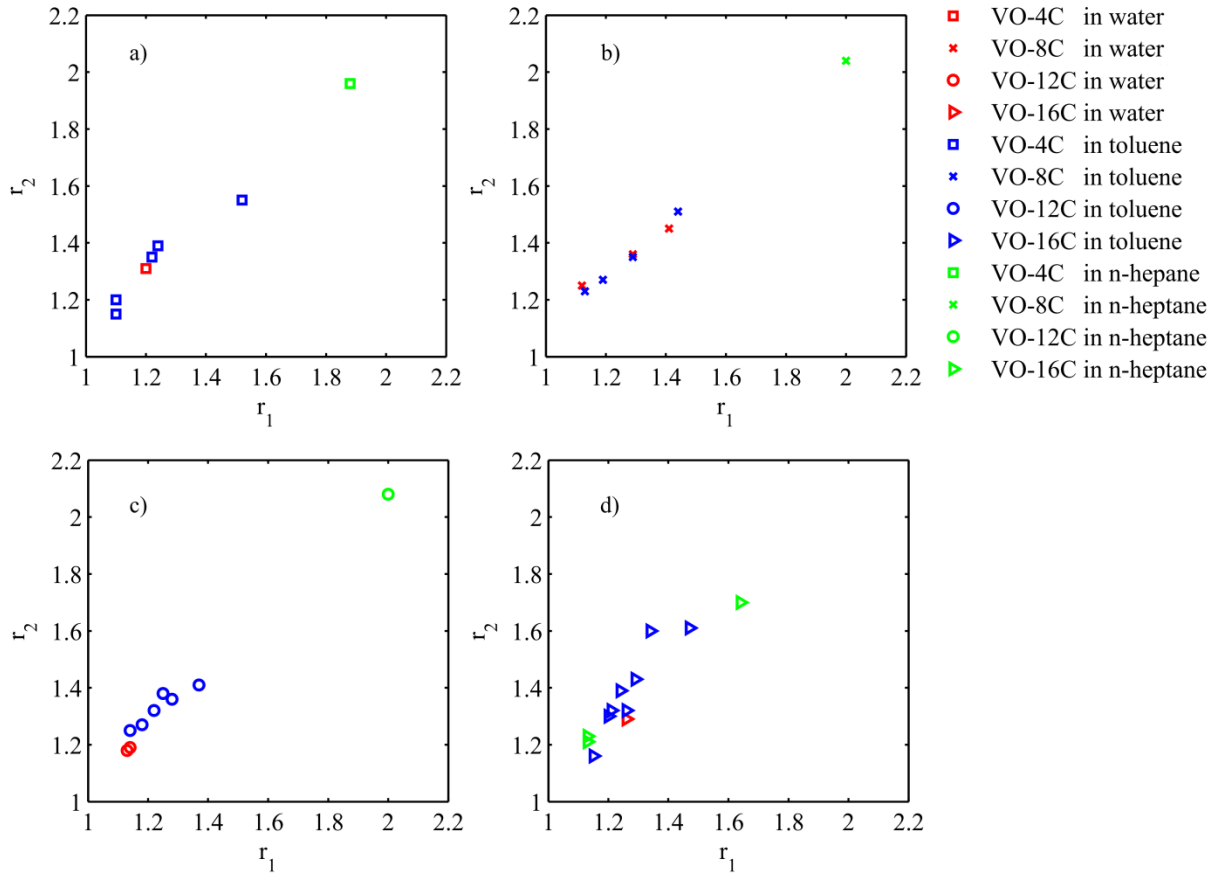

Figure E.2: Individual dimension maps for (a) VO-4C, (b) VO-8C, (c) VO-12C, and (d) VO-16C.

E.7. Dimension map generated by calculating the gyradius ratios for the PA cores

From the dimension map Figure 7.3 in Chapter 7, it is inferred that regardless of the side-chain length, the PA molecules are randomly entangled in water, while forming short-ranged stacking in toluene and long-ranged stacking in n-heptane. In order to further verify this, we calculated the gyradius ratios by using only the heavy atoms in the PA core region and generated a dimension map as shown in Figure E.3. It can be seen the data are clearly separated into three regions: lower left region for water, upper right region for n-heptane and middle region for toluene. As data on this map represent the arrangement of PA cores in the aggregates, they further demonstrate that the PA cores do not form ordered stacking in water, the stacking in

toluene resembles short-cylinder-like structures, and the stacking in n-heptane is of longer range and resembles rod-like structures.

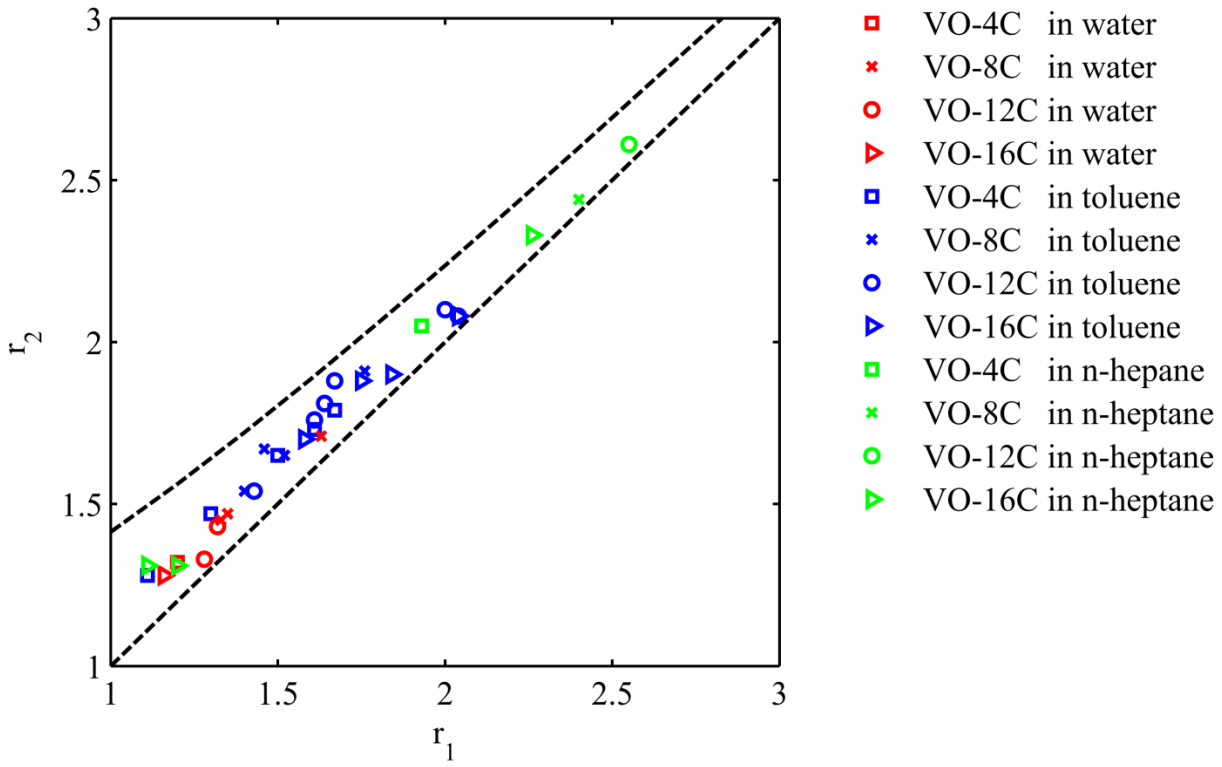

Figure E.3: Dimension map generated for PA cores.

Bibliography

(1) Case, D. A.; Darden, T. A.; Cheatham, III, T. E.; Simmerling, C. L.; Wang, J.; Duke, R. E.; Luo, R.; Walker, R. C.; Zhang, W., Merz, K. M., et al. *AMBER 13;* University of California, San Francisco. CA, 2012.

(2) Tieleman, D.; Van der Spoel, D.; Berendsen, H. Molecular Dynamics Simulations of Dodecylphosphocholine Micelles at Three Different Aggregate Sizes: Micellar Structure and Chain Relaxation. *J. Phys. Chem. B* **2000,** *104*, 6380-6388.

(3) Kukol, A. Lipid Models for United-Atom Molecular Dynamics Simulations of Proteins. *J. Chem. Theory .Comput.* **2009,** *5*, 615-626.

(4) Hess, B.; Kutzner, C.; van der Spoel, D.; Lindahl, E. GROMACS 4: Algorithms for Highly

Efficient, Load-Balanced, and Scalable Molecular Simulation. *J. Chem. Theory Comput.* **2008,** *4*, 435-447.

(5) van der Spoel, D.; Lindahl, E.; Hess, B.; Groenhof, G.; Mark, A. E.; Berendsen, H. J. GROMACS: Fast, Flexible, and Free. *J. Comput. Chem.* **2005,** *26*, 1701-1718.

(6) Lindahl, E.; Hess, B.; van der Spoel, D. GROMACS 3.0: A Package for Molecular Simulation and Trajectory Analysis. *J. Mol. Model.***2001,** *7*, 306-317.

(7) Berendsen, H. J.; van der Spoel, D.; van Drunen, R. GROMACS: A Message-Passing Parallel Molecular Dynamics Implementation. *Comput. Phys. Commun.* **1995,** *91*, 43-56.

(8) Oostenbrink, C.; Villa, A.; Mark, A. E.; Van Gunsteren, W. F. A Biomolecular Force Field Based on the Free Enthalpy of Hydration and Solvation: The GROMOS Force-Field Parameter Sets 53A5 and 53A6. *J. Comput. Chem.* **2004,** *25*, 1656-1676.

(9) Wang, L.; Middleton, C. T.; Zanni, M. T.; Skinner, J. L. Development and Validation of Transferable Amide I Vibrational Frequency Maps for Peptides. *J. Phys. Chem. B* **2011,** *115*, 3713-3724.

(10) Reddy, A. S.; Wang, L.; Singh, S.; Ling, Y. L.; Buchanan, L.; Zanni, M. T.; Skinner, J. L.; De Pablo, J. J. Stable and Metastable States of Human Amylin in Solution. *Biophys. J.* **2010,** *99*, 2208-2216.

(11) Reddy, A. S.; Wang, L.; Lin, Y.; Ling, Y.; Chopra, M.; Zanni, M. T.; Skinner, J. L.; De Pablo, J. J. Solution Structures of Rat Amylin Peptide: Simulation, Theory, and Experiment. *Biophys. J.* **2010,** *98*, 443-451.

(12) Teklebrhan, R. B.; Ge, L.; Bhattacharjee, S.; Xu, Z.; Sjöblom, J. Probing Structure–Nanoaggregation Relations of Polyaromatic Surfactants: A Molecular Dynamics Simulation and Dynamic Light Scattering Study. *J. Phys. Chem. B* **2012,** *116*, 5907-5918.

(13) Abel, S.; Dupradeau, F.; Marchi, M. Molecular Dynamics Simulations of a Characteristic DPC Micelle in Water. *J. Chem. Theory Comput.***2012,** *8*, 4610-4623.

(14) Schmid, N.; Eichenberger, A. P.; Choutko, A.; Riniker, S.; Winger, M.; Mark, A. E.; van Gunsteren, W. F. Definition and Testing of the GROMOS Force-Field Versions 54A7 and 54B7. *Eur. Biophys. J.* **2011,** *40*, 843-856.

(15) Chiu, S.; Clark, M.; Balaji, V.; Subramaniam, S.; Scott, H. L.; Jakobsson, E. Incorporation of Surface Tension into Molecular Dynamics Simulation of an Interface: A Fluid Phase Lipid Bilayer Membrane. *Biophys. J.* **1995,** *69*, 1230-1245.

(16) Schüttelkopf, A. W.; Van Aalten, D. M. PRODRG: A Tool for High-Throughput Crystallography of Protein-Ligand Complexes. *Acta Crystallogr. Sect. D: Biol. Crystallogr.* **2004,** *60*, 1355-1363.

(17) Lemkul, J. A.; Allen, W. J.; Bevan, D. R. Practical Considerations for Building GROMOS-Compatible Small-Molecule Topologies. *J. Chem. Inf. Model.* **2010,** *50*, 2221-2235.

(18) Jian, C.; Tang, T.; Bhattacharjee, S. Probing the Effect of Side-Chain Length on the Aggregation of a Model Asphaltene Using Molecular Dynamics Simulations. *Energy Fuels* **2013,** *27*, 2057-2067.

(19) Kashiwagi, H.; Hashimoto, T.; Tanaka, Y.; Kubota, H.; Makita, T. Thermal Conductivity and Density of Toluene in the Temperature Range 273–373 K at Pressures up to 250 MPa. *Int. J. Thermophys.* **1982,** *3*, 201-215.

(20) Lindman, B.; Stilbs, P.; Moseley, M. E. Fourier Transform NMR Self-Diffusion and Microemulsion Structure. *J. Colloid Interface Sci.* **1981,** *83*, 569-582.

(21) Riddick, J. A.; Bunger, W. B.; Sakano, T. K. *Organic Solvents: Physical Properties and Methods of Purification,* 4th ed.; John Wiley & Sons Inc.: New York, 1986.

(22) Zhao, L.; Choi, P. Molecular Dynamics Simulation of the Coalescence of Nanometer-Sized Water Droplets in n-Heptane. *J. Chem. Phys.* **2004,** *120*, 1935-1942.

(23) Lee, H.; Pak, H. Molecular Dynamics Simulation of Liquid Alkanes III. Thermodynamic, Structural, and Dynamic Properties of Branched-Chain Alkanes. *Bull. Korean Chem. Soc.* **1997,** *18*, 501-509.

(24) Marrink, S. J.; Lindahl, E.; Edholm, O.; Mark, A. E. Simulation of the Spontaneous Aggregation of Phospholipids into Bilayers. *J. Am. Chem. Soc.* **2001,** *123*, 8638-8639.

(25) Essmann, U.; Perera, L.; Berkowitz, M. L.; Darden, T.; Lee, H.; Pedersen, L. G. A Smooth Particle Mesh Ewald Method. *J. Chem. Phys.* **1995**, *103*, 8577-8593.

(26) Hess, B. P-LINCS: A Parallel Linear Constraint Solver for Molecular Simulation. *J. Chem. Theory Comput.* **2008,** *4*, 116-122.

(27) Miyamoto, S.; Kollman, P. A. An Analytical Version of the SHAKE and RATTLE Algorithm for Rigid Water Models. *J. Comput. Chem.* **1992,** *13*, 952-962.

(28) Parrinello, M.; Rahman, A. Polymorphic Transitions in Single Crystals: A New Molecular Dynamics Method. *J. Appl. Phys.* **1981,** *52*, 7182-7190.

(29) Bussi, G.; Donadio, D.; Parrinello, M. Canonical Sampling through Velocity Rescaling. *J. Chem. Phys.* **2007,** 126, 014101.

(30) Evans, D. J.; Morriss, G. P. Non-Newtonian Molecular Dynamics. *Comput. Phys. Rep.* **1984,** *1*, 297-343.

(31) van der Spoel, D.; Lindahl, E.; Hess, B.; van Buuren, A. R.; Apol, E.; Meulenhoff, P. J.; Tieleman, D. P.; Sijbers, A. L. T. M.; Feenstra, K. A.; van Drunen, R.; Berendsen, H. J. C. Gromacs User Manual, version 4.0. http://www.gromacs.org (2005).

(32) Jian, C.; Tang, T.; Bhattacharjee, S. Molecular Dynamics Investigation on the Aggregation of Violanthrone78-Based Model Asphaltenes in Toluene. *Energy Fuels* **2014,** *28*, 3604-3613.

(33) Wittenburg, J. *Dynamics of Multibody Systems;* Springer: Berlin, 2007.

(34) Pytel, A.; Kiusalaas, J. *Engineering Mechanics: Dynamics,* 3rd ed.; Cengage Learning: Stamford, 2010.

(35) Humphrey, W.; Dalke, A.; Schulten, K. VMD: Visual Molecular Dynamics. *J. Mol. Graphics* **1996,** *14*, 33-38.